NASA CONTRACTOR REPORT

NASA CR-

NASA CR-2539

2.4/4

THEORETICAL AND EXPERIMENTAL STUDY OF A NEW METHOD FOR PREDICTION OF PROFILE DRAG OF AIRFOIL SECTIONS

S. H. Goradia and D. E. Lilley

Prepared by
LOCKHEED-GEORGIA COMPANY
Marietta, Ga. 30060
for Langley Research Center

NATIONAL AERONAUTICS AND SPACE ADMINISTRATION • WASHINGTON, D. C. • JUNE 1975

1. Report No.	2. Government Accession No.	3. Recipient's Catalog No.
NASA CR-2539		

4. Title and Subtitle	5. Report Date
THEORETICAL AND EXPERIMENTAL STUDY OF A NEW METHOD FOR PREDICTION OF PROFILE DRAG OF AIRFOIL SECTIONS	JUNE 1975
	6. Performing Organization Code
7. Author(s)	8. Performing Organization Report No.
S. H. Goradia and D. E. Lilley	
9. Performing Organization Name and Address	10. Work Unit No.
Lockheed Aircraft Corporation Lockheed-Georgia Company Marietta, GA 30060	760-64-01-02
	11. Contract or Grant No.
	NAS1-12170
12. Sponsoring Agency Name and Address	13. Type of Report and Period Covered
National Aeronautics & Space Administration Washington, DC 20546	Contractor Report
	14. Sponsoring Agency Code

15. Supplementary Notes

FINAL REPORT

16. Abstract

This report describes theoretical and experimental studies which were conducted for the purpose of developing a new generalized method for the prediction of profile drag of single component airfoil sections with sharp trailing edges. This method aims at solution for the flow in the wake from the airfoil trailing edge to the large distance in the downstream direction; the profile drag of the given airfoil section can then easily be obtained from the momentum balance once the shape of velocity profile at a large distance from the airfoil trailing edge has been computed. Computer program subroutines have been developed for the computation of the profile drag and flow in the airfoil wake on CDC6600 computer. The required inputs to the computer program consist of free stream conditions and the characteristics of the boundary layers at the airfoil trailing edge or at the point of incipient separation in the neighborhood of airfoil trailing edge. The method described in this report is quite generalized and hence can be extended to the solution of the profile drag for multi-component airfoil sections.

Subject Category 01

17. Key Words (Suggested by Author(s))	18. Distribution Statement
Two-dimensional airfoil theory Profile drag Wake velocity profile	Unclassified - Unlimited

19. Security Classif. (of this report)	20. Security Classif. (of this page)	21. No. of Pages	22. Price*
Unclassified	Unclassified	166	$6.25

*For sale by the National Technical Information Service, Springfield, Virginia 22151

TABLE OF CONTENTS

FIGURE INDEX

FIGURE INDEX (Continued)

FIGURE INDEX (Continued)

FIGURE INDEX (Continued)

FIGURE INDEX (Continued)

FIGURE INDEX (Continued)

LIST OF TABLES

LIST OF SYMBOLS

c or C	Airfoil chord
C_D	Drag coefficient $\text{Drag}/\frac{1}{2}\rho U_\infty^2 \cdot c \cdot \text{span}$
C_P	Constant pressure specific heat or pressure coefficient $\{P-P_\infty\}/\frac{1}{2}\rho U_\infty^2$
C_L	Lift coefficient, $\text{Lift}/\frac{1}{2}\rho U_\infty^2$
$f_{(\eta)}$ or $g_{(\xi)}$	Function for defining the velocity profile similarity
H	Form factor for airfoil surface or wake boundary layer δ^*/θ
I	Hot wire current
k	Curvature 1/R or thermal conductivity
K_1 or K_2	Value of similarity parameter at the upper or lower edge of the wake boundary layer
l	Length of hot wire
M	Mach number
P or P_s	Value of static pressure at the airfoil surface or in the boundary layer
P_T	Value of total pressure in the boundary layer
P_∞	Free stream static pressure
P_{T_∞} or P_{T_e}	Value of total pressure at the edge of the boundary layer or in the free stream
q_∞	Free stream dynamic head $\frac{1}{2}\rho U_\infty^2$
Q	Convective heat flux defined by equation (III-3)
R	Universal gas constant, or Radius of curvature of the stream lines in the wake flow, or Electrical resistance of hot wire
RN	Reynolds number
t	Value of the maximum thickness of airfoil, or Thickness of the blunt trailing edge
T	Absolute temperature

u, U	X component of velocity
U_e	Velocity at the edge of the boundary layer over the airfoil surface or at the edges of airfoil wake boundary layer
U_w	Value of u on the locus of minimum velocity in the airfoil wake
U_∞	Free stream velocity
u'	Turbulent fluctuations in X-component velocity
v, V	Y-component of velocity
v'	Turbulent fluctuations in Y-component velocity
x, y	Rectangular coordinate system
x'	X Distance measured in the airfoil wake from the trailing edge of the airfoil
X	Transformed x-coordinates for pressure distribution at wake edges by equation (IV-6)
$Yi_{i=1,2,3 \text{ etc.}}$	Distances of the various characteristic loci in the wake measured from the reference line
α	Angle of attack in degrees
β	Transformed x-coordinate for the pressure distribution along the locus of minimum velocity defined by equation (IV-8)
η and ξ	Parameters for the similarity of velocity profiles
θ	Momentum thickness for the boundary layer on the airfoil surface or for the wake boundary layer
δ	Boundary layer thickness for the boundary layer on the airfoil surface or the boundary layer in airfoil wake
δ^*	Displacement thickness for the boundary layer on the airfoil surface or for the wake boundary layer
γ	Parameter for the non-dimensional pressure at wake edge defined by equation (IV-5)
τ or T	Algebraic sum of shear stresses due to molecular viscosity and turbulent fluctuations
ρ	Density
u	Dynamic viscosity

Kinematic viscosity = u/ρ

Subscripts

∞	Free stream values
e	Edge of boundary layer
u	Upper surface of airfoil or upper wake
L	Lower surface of the airfoil or lower wake
T.E.	Value at the trailing edge
A,B	Value at station A or B, respectively
o or w	Value at the wall

THEORETICAL AND EXPERIMENTAL STUDY OF A NEW METHOD FOR PREDICTION OF PROFILE DRAG OF AIRFOIL SECTIONS

By S. H. Goradia and D. E. Lilley
Lockheed-Georgia Company

SUMMARY

This report describes theoretical and experimental studies which were conducted for the purpose of developing a new generalized method for the prediction of profile drag of single component airfoil sections. This method aims at solution for the flow in the wake from the airfoil trailing edge to the large distance in the downstream direction; the profile drag of the given airfoil section can then easily be obtained from the momentum balance once the shape of velocity profile at a large distance from the airfoil trailing edge has been computed. Computer program subroutines have been developed for the computation of the profile drag and flow in the airfoil wake on UNIVAC 1108 computer. The required inputs to the computer program consist of free stream conditions and the characteristics of the boundary layers at the airfoil trailing edge or at the point of incipient separation in the neighborhood of airfoil trailing edge. The method described in this report is quite generalized and hence can be extended to the solution of the profile drag for multi-component airfoil sections.

Experimental measurements of velocity profiles and static pressure distribution in the wake of sharp trailing edge test airfoil were obtained by use of a pitot static tube. Shear stress profiles in the airfoil wake were computed by the indirect method. A hot-wire anemometer was used for the measurements of velocity profiles in the wake of the blunt trailing edge test airfoil. The above measurements were obtained for a 15 percent thick modified NACA four digit airfoil section which was modified near the leading edge for the purpose of increasing the maximum lift coefficient.

A physical flow model for the wake flow was developed from the experimental data. This flow model is divided into regions and layers depending upon the characteristics of velocity profiles. Parameters for velocity profile similarity functions were developed from experimental measurements in different regions. Integral equations were derived for the solution of wake flow and these equations are coupled, ordinary nonlinear and nonhomogeneous differential equations. Parameters, such as shear and static pressures at the edges of various layers appear in the above equations as coupling terms. Functional representation of these parameters in terms of dependent variables, arranged in dimensionaless groups, was accomplished with the help of the principle of local dynamic similarity.

The numerical solution of the above equations was accomplished by the modified Euler method with repeated iterations. Results of computations of the

computer program subroutines for the flow in the wake and profile drag were compared with experimental data for three airfoil sections. Reasonable agreement was obtained between measured and calculated flow quantities in the wake and profile drag corresponding to the occurrence of incipient separation on the upper surface of airfoil.

I. INTRODUCTION

With the recent energy crisis and shortage of fuel, it has become imperative to search for ways of reducing the drag of aircraft operating in the low and high subsonic speed regime, for their economical operation during cruise. The reduction in the drag of an aircraft, and hence saving in the fuel consumption, can be accomplished by proper design of the wing section. The effective design of wing sections, however, requires an accurate and reliable method for predicting profile drag. The trade-offs between aerodynamic and structural characteristics of airfoils must consider profile drag as a merit factor. A prediction method, which is based on theoretically sound principles consistent with real flow phenomena, can be used to evaluate candidate wing sections without resorting to the elaborate, expensive and time consuming wind tunnel tests. Moreover, the development of airfoils for special applications, such as minimum drag at specified lift conditions, requires a method with general applicability. The development of such a method was aimed during this study contract with NASA, Langley.

In order to estimate the drag of a body or to design a body for minimum drag, it is necessary to understand the origin and mechanism of the aerodynamic drag produced by a body. D'Alembert's paradox states that in an inviscid fluid a body can experience no drag. This can be proved relatively easily by use of the momentum theorem. Why then does a body experience drag in a real fluid? In the case of two-dimensional bodies, e.g. airfoil section at a positive angle of attack, the induced drag associated with lift is nonexistent, but profile drag or parasite drag of such bodies have a finite value depending upon free stream conditions and geometrical shape of two-dimensional bodies. The above mentioned profile drag of a two-dimensional body is composed of two parts, namely, the skin friction drag and the form or pressure drag. These parts may be of equal magnitude or the one may completely overshadow the other, depending upon the shape of the body. The skin friction drag is the result of the shearing stresses in the fluid as it passes over the surface of the body. The form drag results from the unbalance in normal pressure forces around the body due to the presence of attached or separated boundary layer around the surface of a body. These statements are exemplified by the use of Figure I-1; this figure shows the cases of flat plate at 0° and 90° angles of attack and an airfoil at an angle of attack corresponding to the desired lift condition.

In Figure I-1(a) the drag is entirely the result of skin friction, whereas in Figure I-1(b) it is entirely form or pressure drag. If some means could be used to prevent the separation of the flow at the edges of the plate shown in Figure I-1(b), the drag could be reduced to zero. The total or profile drag for the airfoil section of Figure I-1(c) depends upon geometrical contour of the

(a) Flat Plate at 0°
Angle of Attack

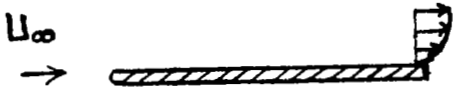

(b) Flat Plate at 90°
Angle of Attack

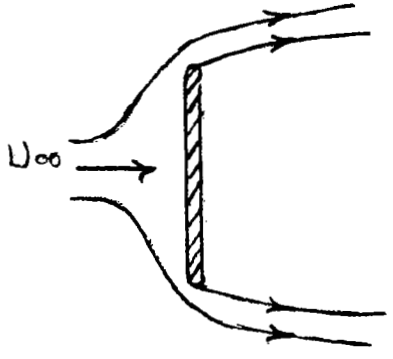

(c) Airfoil at an Angle
of Attack

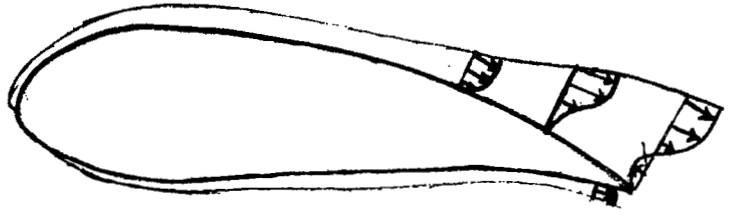

Case (a) — Presence of Skin Friction Drag only ✓

Case (b) — Presence of Pressure Drag only ✓

Case (c) — Both Skin Friction and Pressure Drag Constitute Total Drag ✓

FIGURE I-1 - EXAMPLE SHOWING PRESENCE OF VARYING PROPORTION OF SKIN FRICTION AND PRESSURE DRAG CONSTITUENTS OF TOTAL PROFILE DRAG

body and free stream conditions such as Reynolds number, angle of attack, and Mach number. Combination of the above factors affect physical parameters, such as location and value of pressure peak on the upper surface of airfoil, existence of laminar boundary layer separation or transition, and conditions and growth of turbulent or laminar boundary layer on the upper and lower surfaces of the airfoil near its trailing edge. These physical parameters then determine the total profile drag of a given airfoil section and also the ratio of its constituents, namely, skin friction and pressure drag. The relation between pressure and friction drag of an axially-symmetric afterbody behind a long circular cylinder is of interest both from the point of view of practical application in design and the theoretical studies. Available experimental data for the drag coefficient, C_D, for blunt and sharp afterbodies, which are shown in Figures I-2(a) and I-2(b), reveal an interesting phenomenon. Figure I-2(a) shows the plots of measured drag coefficients, C_D, versus L_R/R_o for blunt and sharp afterbodies; in this Figure L_R denotes the length of the afterbody and R_o denotes the base radius of the afterbody. The experimental data shown in this figure reveal that blunt or thicker afterbody has a lower drag coefficient than the sharp afterbody. This result is quite surprising because it is known from available experimental data on airfoil sections (for example NACA four digit series) that thicker sections have higher values of profile drag than lower thickness ratio airfoil sections. The above-mentioned discrepancy of experimental results of Figure I-2(a) can be explained with the aid of detailed analysis of experimental results shown in Figure I-2(b). This figure shows the breakdown of the local total drag into local integrated values of skin friction drag and pressure drag. Values of integrals I_1 and I_2, which are shown plotted as a function of X/L_R in Figure I-2(b) for both thicker and sharp afterbodies, represent local integrated values of skin friction and pressure drag, respectively. The algebraic sum of I_1 and I_2 at particular X location on the afterbody is equal to the total drag of afterbody up to that X location. The local integrated value of the pressure drag I_2 for blunt afterbody increases up to $X/L_R \approx 0.75$ and then starts decreasing up to the tail end because of better pressure recovery; this better pressure recovery is due to the absence of flow separation. For the sharp afterbody, however, the value of I_2 increases continuously up to the tail end because of flow separation at $X/L_R \approx 0.8$. Thus, the sum of I_1 and I_2 at the tail end, which represents the total drag coefficient, is higher for the sharp afterbody than for the blunt afterbody.

The total drag of an arbitrary airfoil section, at least in theory, can be computed from the knowledge of pressure distribution and airfoil geometry. From the knowledge of either experimental or calculated pressure distribution on the surface of the airfoil and the airfoil geometry, the pressure drag can be calculated from the C_p versus Z/C relationship of that airfoil, where Z/C is the nondimensional ordinate of the given airfoil section, the determination of the algebraic sum of the familiar thrust and drag loops gives the resultant pressure drag. The boundary layer characteristics and hence the skin friction drag can be calculated for the given pressure distribution by the use of pertinent boundary layer theories. In actual practice, however, it is extremely difficult to obtain accurate drag level by the above mentioned which is defined as the Direct Method. Slight errors in pressure distribution, while not significantly affecting the boundary layer characteristics, lift and pitching moment, can create errors in the thrust and drag loops that are seriously magnified when calculating pressure drag by taking the difference of these two loops. Hence,

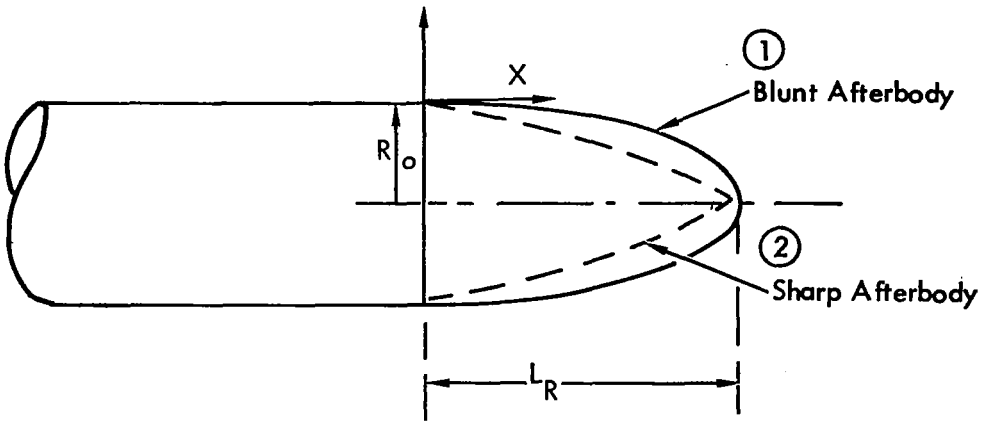

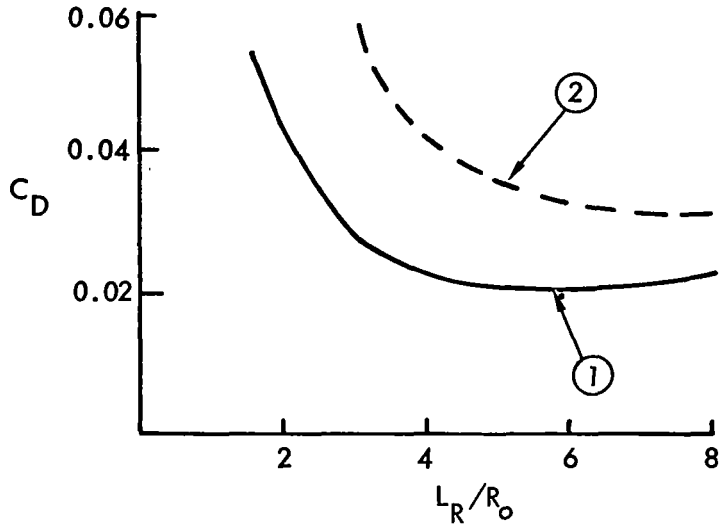

FIGURE I-2(a) - COMPARISON OF MEASURED DRAG COEFFICIENTS FOR BLUNT AND SHARP AFTERBODIES

I_1 = Local Integrated Value for Skin Friction Drag

$$= \int_0^{x/L_R} 2 \frac{L_R}{R_o} \frac{R}{R_o} \frac{\tau_w}{q} \frac{d(x)}{L_R}$$

I_2 = Local Integrated Value for Pressure Drag

$$= \int_0^{x/L_R} 2 \frac{x}{L_R} \quad Cp \quad \frac{d(x)}{L_R}$$

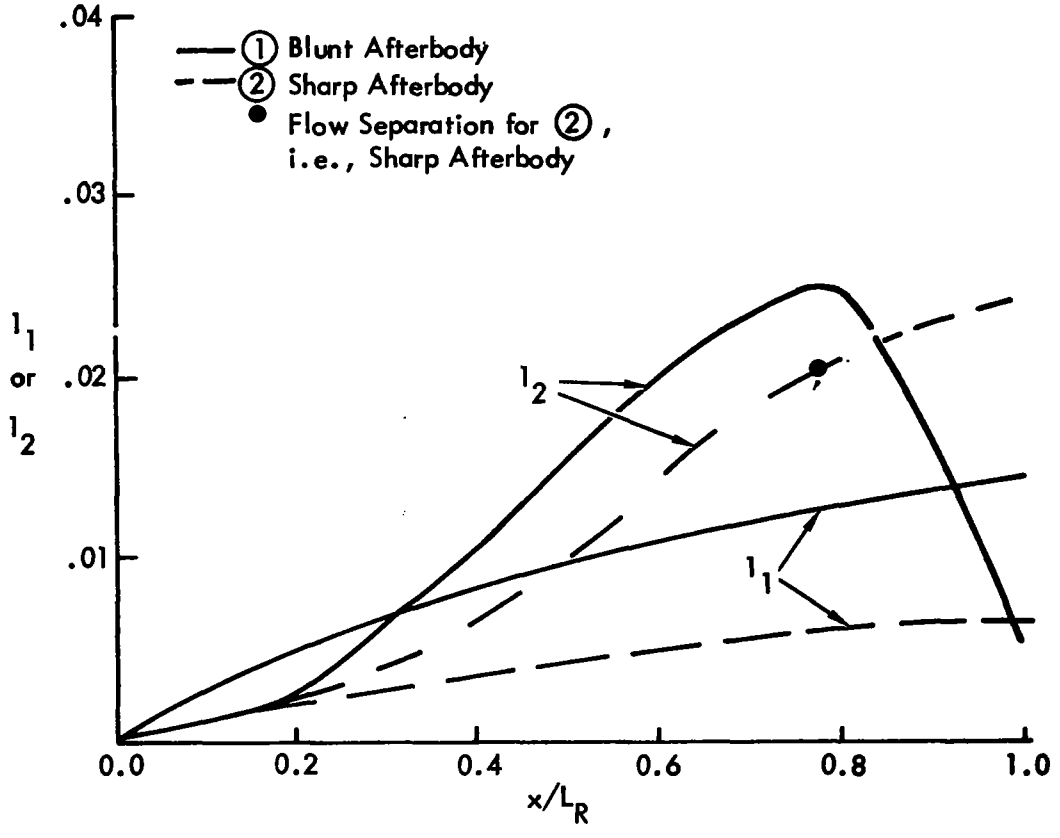

FIGURE I-2(b) - BREAKDOWN OF THE TOTAL DRAG OF BLUNT AND SHARP AFTERBODIES INTO INTEGRATED VALUES OF SKIN FRICTION AND PRESSURE DRAG

the use of the Direct Method is not recommended either for the purpose of data analysis or for the optimization study for the development of an airfoil configuration.

The profile or total drag of the airfoil section is usually calculated by some form of the Indirect Method. The calculation of the profile drag of a given airfoil section by use of the Indirect Method is dependent upon the ability of this method to reliably calculate the shape of the velocity profile at a very large distance downstream of the airfoil trailing edge. This very large downstream distance corresponds to the distance behind the trailing edge at which location static pressure is essentially constant and its value is equal to free stream static pressure. The drag of the given airfoil can then be calculated by substracting the flow momentum corresponding to the above velocity profile at the large downstream distance from the corresponding momentum of the free stream air.

Use of the Indirect Method for the calculation of the profile drag, however, requires knowledge of the characteristics of the boundary layer on both upper and lower surfaces of the given airfoil in the vicinity of its trailing edge. These boundary layer characteristics, known as initial conditions, can be calculated, for example, for attached flow conditions by the use of methods in Reference 1.

The Indirect Method for calculations of profile drag, which is available up to the present time, is the Squire & Young's method of Reference 2. The simplified solution for the profile drag by the above method is obtained, however, at the sacrifice of making some assumptions which are inconsistent with physical reality. For example, logarithmic relation of velocity profile in wake, namely, the assumption of constancy of the ratio $\text{Log}_e(U_\infty/U_e)/H-1$ along the wake, is contradicted by several experimental measurements in airfoil wakes. Moreover, while the Squire & Young approach can be used to advantage in some instances, its limitations prevent reliable application to many problems of practical interest.

It is thus desirable to develop a generalized theoretical prediction method for the calculation of profile drag of an arbitrary airfoil, which is free from restrictions and limitations, such as discussed in the above paragraphs. Specifically, the method should be valid at high and low angles of attack and applicable to either single or multi-component airfoil. Specific objectives to be accomplished under the present studies are:

(1) To obtain measurements of velocity profile and pressure distributions in the wake of a single component airfoil for the purpose of developing a physical wake flow model.

(2) To derive the equations to provide a generalized mathematical model of airfoil wake and to develop a numerical method and a computer program for the solution of these equations.

(3) To determine the validity of the method by correlation with measurements of the viscous flow in the airfoil wake and profile drag measurements.

II. THEORETICAL STUDY

II.1 General Discussion

The profile drag or total drag of the airfoil section is made up of two parts, namely, skin friction drag and pressure drag. Thus

$$C_{D_{profile}} = C_{D_{pressure}} + C_{D_{skin\ friction}} \qquad (II\text{-}1)$$

In the Direct Method, the total drag of the airfoil section is computed by evaluating the two components of the right-hand side of equation (II-1) separately, namely, (a) calculation of pressure drag and (b) skin friction drag. A brief description of this method was given in Section I. In the Indirect Method, the total drag is computed without evaluating the two components of the right-hand side of equation (II-1). This is accomplished from the knowledge of boundary layer parameters on the upper and lower surface in the vicinity of the trailing edge.

Figure II-1 illustrates the basic principle behind the Indirect Method for the purpose of calculating the profile drag of single or multi-component airfoil section. From the knowledge of the characteristics of the boundary layer on the upper and lower surfaces in the vicinity of the trailing edge, the Indirect Method is used for the purpose of calculating the velocity profile in the wake, at a large downstream distance behind the airfoil trailing edge, where static pressure distribution has stabilized to the freestream value. The expression for the profile drag of the two-dimensional airfoil section can then be written as

$$\text{Total Drag} = s\rho \int_{-\infty}^{+\infty} U(U_\infty - u)\, dy \qquad (II\text{-}2)$$

where s = span of airfoil
u = local velocity in the wake boundary layer
U_∞ = freestream velocity
ρ = density.

The drag of the airfoil can then be determined if it is possible to use known velocity profile characteristics at the trailing edge of the airfoil to calculate the far downstream wake velocity distribution, $U_{(x \to \infty,\, y)}$, point 4, Figure II-1.

$$U_{(x \to \infty,\, y)} = Fi(U_{(x = T.E.,\, y)},\ P_1,\ P_2,\ P_3 \ldots P_n) \qquad (II\text{-}3)$$

where P_i, $i = 1 \ldots n$ are n different parameters required for the functional representation of equation (II-3). For example, in the case of a single component airfoil with a blunt trailing edge and with boundary layer separation ahead of the trailing edge in its vicinity, P_1 may be free stream velocity, P_2 may be local outer flow velocity at separation, P_3 the trailing edge thickness and P_4

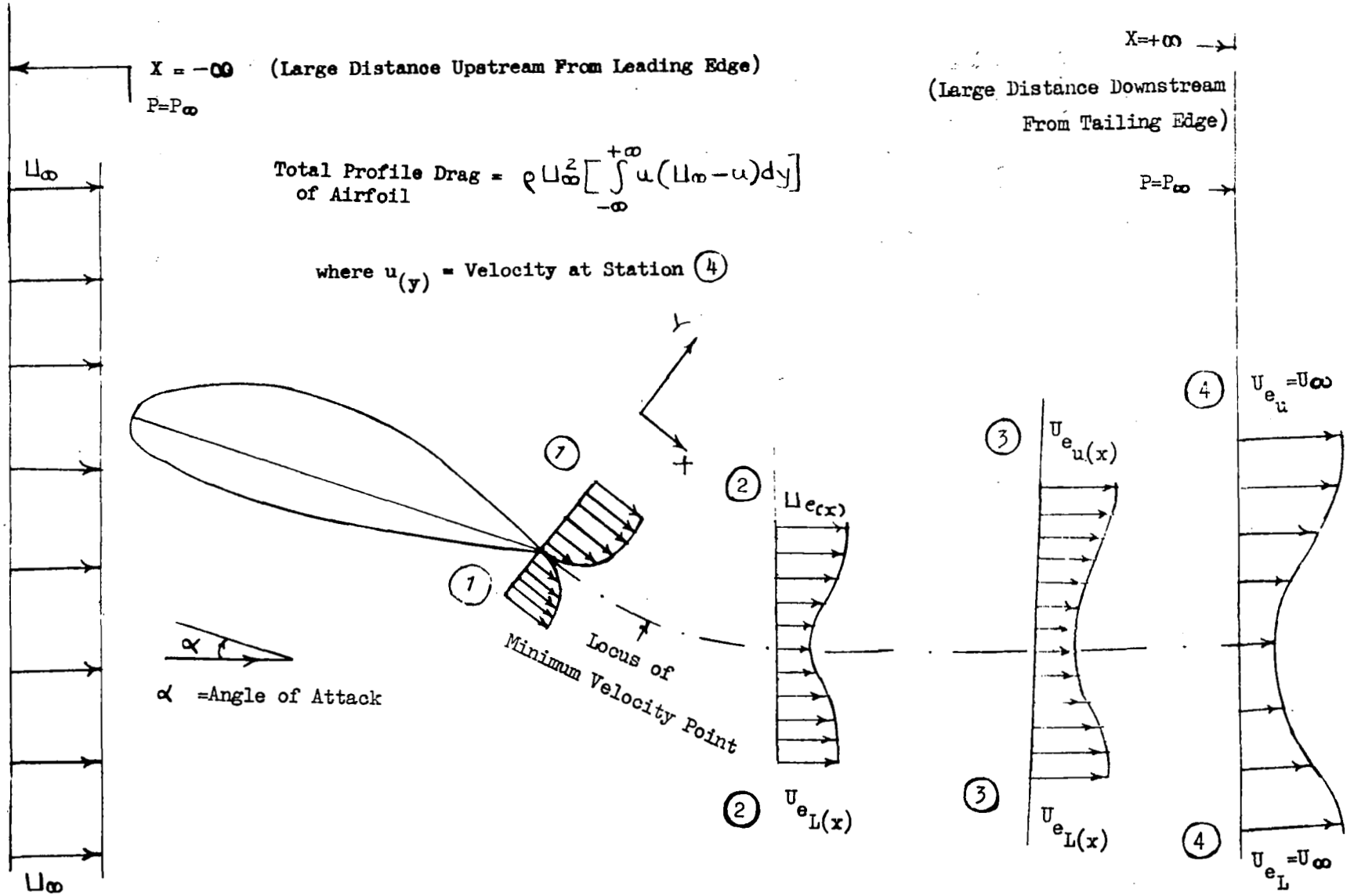

FIGURE II-1 - SCHEMATIC REPRESENTATION OF AIRFOIL WAKE FOR COMPUTATION OF PROFILE DRAG

may be the distance between separation point and the trailing edge. Each pair of parameters are also related to each other through the general velocity distribution $U_{(x,y)}$ at any point in the wake. For example, if $U_{e(x)}$ is the velocity at the edge of the boundary layer in the wake, and U_∞ is the free stream velocity, then it is found from experimental data that it is possible to express the functional relationship as follows

$$U_{e(x)} = F \quad (U_\infty, \bar{u}) \qquad (11\text{-}4)$$

where $\bar{u} = \frac{1}{\delta} \int_0^\delta u \, dy$ = average velocity in the wake boundary layer.

Thus, (n-1) auxiliary equations, such as equation (11-4), are required for the complete solution of equation (11-3).

In the case of a single component airfoil with a sharp trailing edge, which does not exhibit any separation ahead of the trailing edge, only two parameters in equation (11-3) need to be considered. These parameters are U_∞ and the pressure distribution or $U_{e(x)}$ along the wake. Squire and Young proposed the following empirical relation for the purpose of obtaining an analytic expression for the drag of a single component airfoil, i.e.

$$\frac{\text{Log}_e \left(\frac{U_\infty}{U_{e(x)}}\right)}{H_{(x)} - 1} = \frac{\text{Log}_e \left(\frac{U_\infty}{U_{e(T.E.)}}\right)}{H_{T.E.} - 1} = \text{Constant} \qquad (11\text{-}5)$$

where

$H_{(x)}$ = wake boundary layer form factor

$U_{e(x)}$ = velocity distribution at the outer edge of the wake.

By making use of equation (11-5) in the von Karman momentum integral equation, Squire and Young were able to derive an analytic expression for the total drag coefficient of a single component airfoil with a sharp trailing edge. This expression, which is theoretically valid only in the absence of boundary layer separation ahead of the airfoil trailing edge, is given by

$$Cd = 2(\theta_u + \theta_L) \left(\frac{U_{e_{T.E.}}}{U_\infty}\right)^{(H_{T.E.} + 5)/2} \qquad (11\text{-}6)$$

It may be pointed out here that the above simple analytic expression for drag coefficient is obtained at the sacrifice of making some simplifying assumptions which are inconsistent with physical reality. For example, experimental data in the wake behind airfoils indicate that the empirical relation of equation (11-5) used by Squire and Young does not hold. Figure 11-2 shows the plot of experimental data for the ratio $(\text{Log}_e(U_\infty/U_e))/(H-1)$ at various distances aft of the trailing edge for a Joukowski airfoil. These results show that

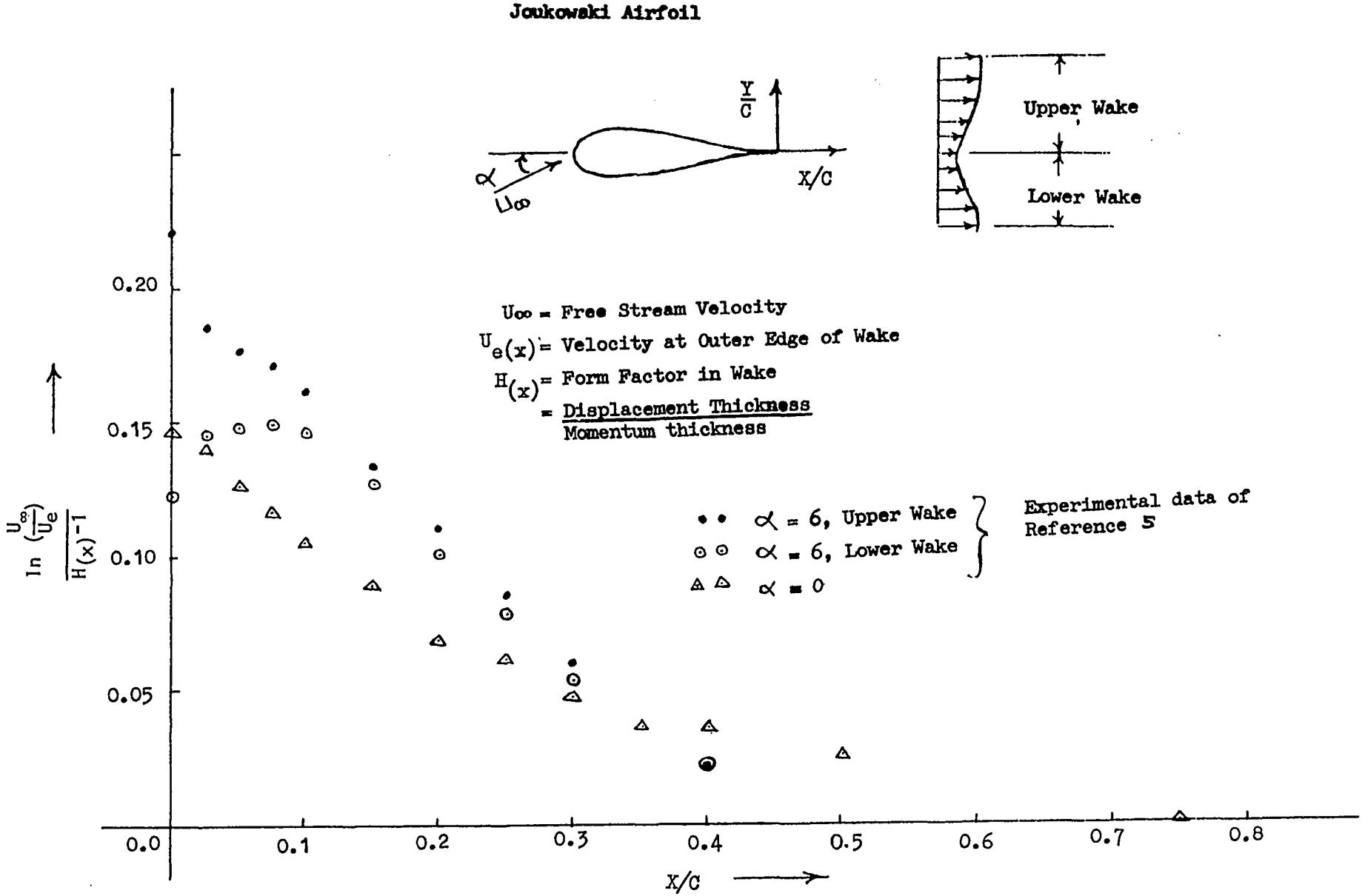

FIGURE II-2 - PLOT OF H. B. SQUIRE'S PARAMETER IN THE WAKE OF JOUKOWSKI AIRFOIL

assumption implied by equation (11-5) in the Squire and Young method is unrealistic. Specifically, Squire and Young's approach is unable to deal directly with the following situations:

(1) Blunt trailing edge airfoils.

(2) Airfoils composed of two or more components.

(3) High or low angles of attack when boundary layer thickness on the upper and lower surfaces of the trailing edges are very difficult.

(4) Incipient boundary layer separation in the neighborhood of the trailing edge on either the upper or lower surface or both.

11.2 Description of the Present Theoretical Method

Figure 11-3 shows the curvilinear system of coordinates in which x denotes the distance along the locus of minimum velocity and y the distance normal to it. The radius of curvature of the lower edge of the wake will be denoted by R_1 and of an equidistance line by R. It is assumed in this theoretical development that R_1 is large in comparison with the width of wake, but not very large in comparison with typical wake layer width. Defining curvature K as

$$K = \frac{1}{R_1} \tag{11-7}$$

then one has

$$\frac{R_0}{R} = \frac{1}{1 \pm Ky} \tag{11-8}$$

The complete Navier-Stokes equations for the orthogonal directions, when local curvature in flow is taken into account, can be written as follows:

$$\frac{R_1}{R} u \frac{\partial u}{\partial x} + v \frac{\partial u}{\partial y} + \frac{uv}{R} + \frac{1}{\rho} \frac{R_1}{R} \frac{\partial P}{\partial x} = \nu \left[\frac{R_1}{R^2} \frac{\partial^2 u}{\partial x^2} + \frac{\partial^2 u}{\partial y^2} - \right.$$

$$\left. - \frac{R_1^3}{R^3} y \frac{\partial \left(\frac{1}{R_1}\right)}{\partial x} \cdot \frac{\partial u}{\partial x} + \frac{1}{R} \frac{\partial u}{\partial y} - \frac{1}{R^2} u + 2 \frac{R_1}{R^2} \frac{\partial v}{\partial x} + \frac{R_1^3}{R^3} v \frac{\partial}{\partial x} \left(\frac{1}{R_1}\right) \right] \tag{11-9}$$

X - Momentum Equation

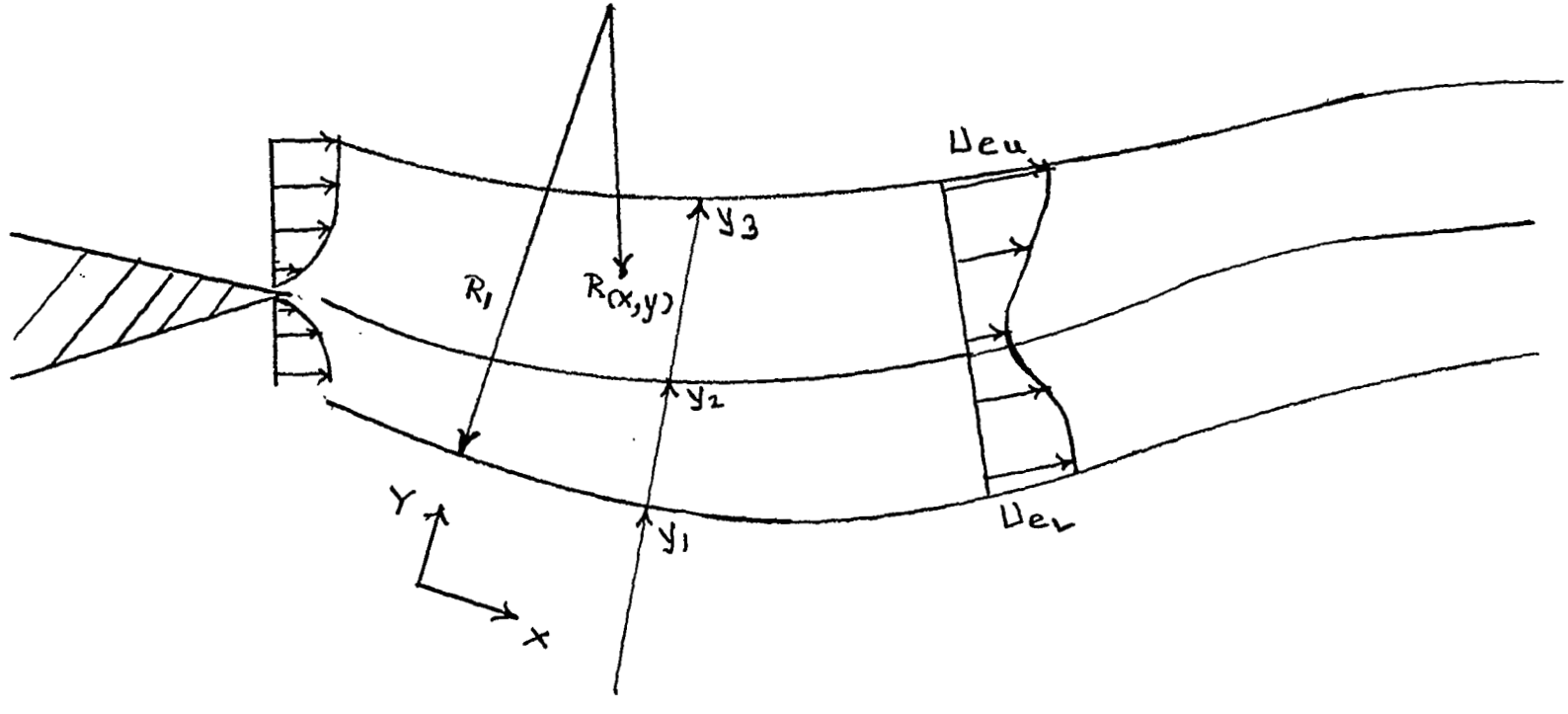

FIGURE II-3 - SYSTEM OF CURVILINEAR COORDINATES

$$\frac{R_1}{R} u \frac{\partial v}{\partial x} + V \frac{\partial v}{\partial y} - \frac{u^2}{R} + \frac{1}{\rho} \frac{\partial P}{\partial y} = \nu \left[\frac{R_1^2}{R^2} \frac{\partial^2 v}{\partial x^2} + \frac{\partial^2 v}{\partial y^2} - \right.$$

$$\left. - \frac{R_1^3}{R^3} y \frac{\partial}{\partial x} \left(\frac{1}{R_1}\right) \frac{\partial v}{\partial x} + \frac{1}{R} \frac{\partial v}{\partial y} - \frac{v}{R^3} - \frac{R_1^3}{R^3} u \frac{\partial}{\partial x} \left(\frac{1}{R_1}\right) - 2 \frac{R_1}{R^2} \frac{\partial u}{\partial x} \right] \qquad (II\text{-}10)$$

Y Momentum Equation

The equation of continuity, considering effects of curvature, can be written as

$$\frac{\partial u}{\partial y} + \frac{\partial}{\partial y} \left(\frac{R}{R_1} v\right) = 0 \qquad (II\text{-}11)$$

By performing time averaging operation on the terms of equation (II-9) and (II-10), the equations for the mean turbulent flow in the wake behind the trailing edge of the airfoil can be derived. These equations can be further simplified from the consideration of the order of magnitude analysis. The following time averaged equations can be written after appropriate simplification for the presently considered wake flow.

$$\bar{u} \frac{\partial \bar{u}}{\partial x} + \frac{R}{R_1} \bar{v} \frac{\partial \bar{u}}{\partial y} + \frac{1}{R_1} \overline{uv} = - \frac{1}{\rho} \frac{\partial P}{\partial x} + \frac{R}{R_1} \frac{1}{\rho} \frac{\partial Txy}{\partial y} + \frac{1}{R_1} \frac{1}{\rho} Txy \qquad (II\text{-}12)$$

$$+ \frac{1}{\rho} \frac{\partial \bar{P}}{\partial y} = \frac{\overline{u^2}}{R} \left(\frac{1}{1 + y/R}\right) - \frac{R}{R} \frac{\partial Txy}{\partial x} \qquad (II\text{-}13)$$

$$\frac{\partial u}{\partial x} + \frac{\partial}{\partial y} \left(\frac{R}{R_1} \bar{v}\right) = 0 . \qquad (II\text{-}14)$$

In the above equations, terms of the order δ/R and of higher magnitude are retained and the terms of the order smaller than δ/R_1 are eliminated; here δ is the characteristic width of the wake boundary layer. The shear stress $T(x,y)$ which appear in above equations is the algebraic sum of laminar and turbulent shear stress contributions, i.e.

$$T(x,y) = \mu \frac{\partial \bar{u}}{\partial y} - \rho \overline{u'v'} . \qquad (II\text{-}15)$$

In the further derivation of equations for the wake flow the bar above qualities, such as u, v, p, etc., will be omitted; however, it will be implied that they represent the time averaged value at any point in the flow behind airfoil wake.

Physical Flow Model: Figure II-4 shows the physical flow model of the wake aft of blunt base multi-component airfoil. This flow model was derived from available experimental data. The success of predicting the complex viscous flow,

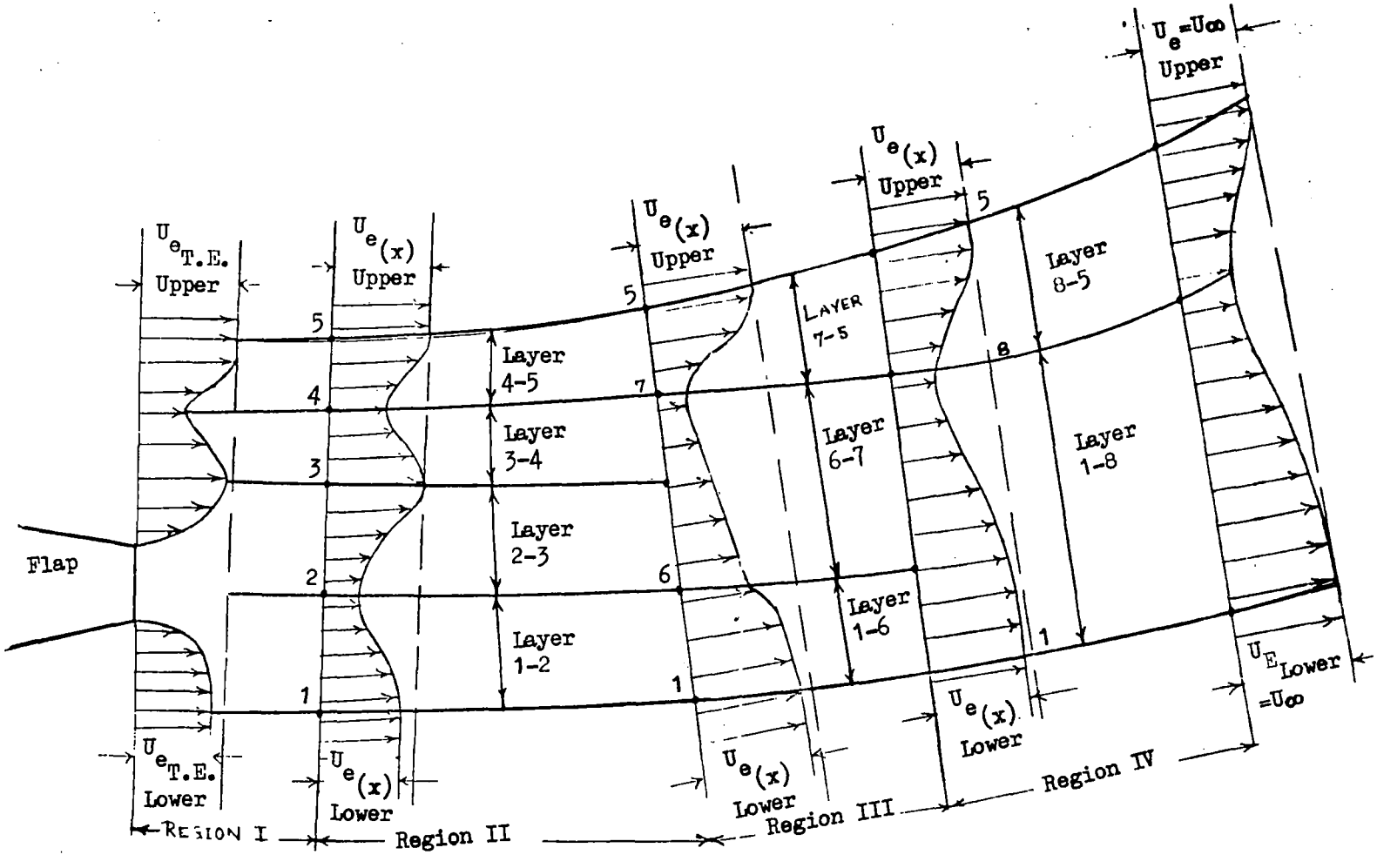

FIGURE II-4 - PHYSICAL MODEL FOR THE VISCOUS FLOW IN THE WAKE OF SINGLE COMPONENT OR TWO-COMPONENT AIRFOILS (cont'd)

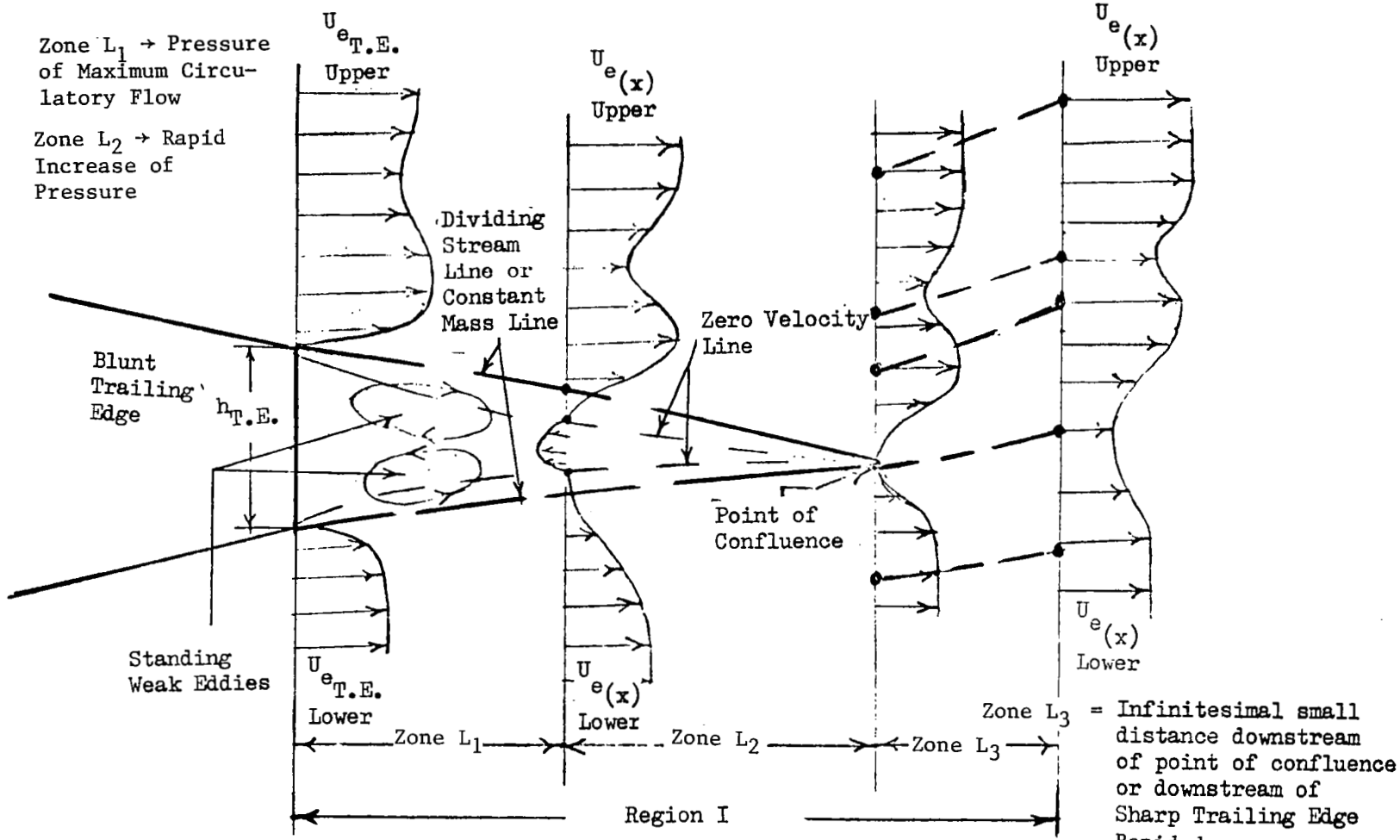

FIGURE II-4

(Continued)

such as shown in Figure II-4, for an arbitrary airfoil case by direct solution of simplified Navier-Stokes equation (II-12), (II-13) and (II-14) would be highly improbable, if not impossible. For this reason, the flow model of Figure II-4 is divided into various regions and layers in which the flow behavior has certain physical characteristics. For example, experimental measurements in the channel flow suggest that Region I can be divided into three Zones L1, L2, and L3. In Zone L1, the maximum circulatory flow is present as the pressure is almost constant, whereas in Zone L2, pressure increases rapidly to near stagnation value at the point of confluence. In Zone L3, which is infinitesimally small, pressure decreases at a rapid rate and the changes in velocity profile shape are quite abrupt.

From the present experimental measurement in the wake of a sharp trailing edge airfoil, it is observed that velocity profiles in the individual layers of Region IV of Figure II-4 become "similar" or "one parameter family" if appropriate parameters are chosen. If the characteristics of the flow are such that it is possible to derive similarity parameters for all layers in different regions of Figure II-4, then sets of ordinary differential equations for this wake flow can be derived from the governing partial differential equation such as (II-12), (II-13), and (II-14). These sets of ordinary differential equations, however complex, can then be solved by presently available numerical methods for the solution of the flow in the wake of an arbitrary airfoil. The discussion of similarity parameters for velocity profiles and generalized physical parameters for shear stress and pressure distributions in the wake behind single component airfoil will be given in Section IV. However, in the following derivations of theoretical equations for wake flow behind thin trailing edge single component airfoil section, it will be assumed that such similarity or generalized physical parameters do exist for the considered viscous flow.

II.3 Theoretical Derivations

Equations for Zone L3 of Region 1: As the presently considered case is for single component airfoil with the sharp trailing edge, Zones L1 and L2 are absent; solution for the flow is thus required for Zone L3 only of Region 1 for this case. Schematic representation for Zone L3 for single component airfoil is shown in Figure II-5. Initial conditions for the boundary layer quantities on upper and lower surfaces of airfoil are specified at Section AA, shown in this figure; this Section AA corresponds to either trailing edge location or is situated at the point of incipient separation on the airfoil which is in the neighborhood of airfoil trailing edge. The Section BB, shown in Figure II-5, corresponds to the end of Zone L3 of Region I. This Section BB is located at an infinitesimal distance from Section AA; however, due to rapid mixing of boundary layers of upper and lower surfaces of an airfoil in Zone L3, characteristic viscous flow quantities such as static pressure, displacement and momentum thickness and magnitude of minimum velocity U_w change at much faster rates in Zone L3 than in downstream regions of flow. A starting value of U_w is obtained by making a momentum balance at the trailing edge. The use of momentum integral equation in the following form is made:

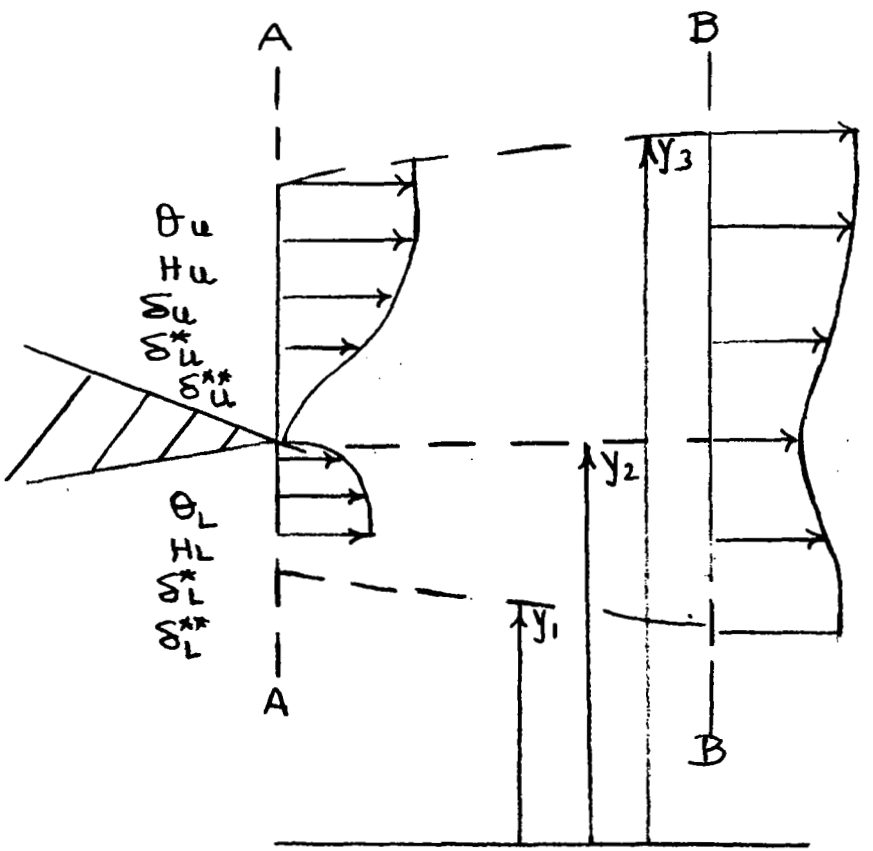

Station A-A -- Beginning of Zone L-3

Station B-B -- End of Zone L-3

Subscript u corresponds to Upper surface of airfoil

Subscript L corresponds to lower surface of airfoil

Momentum Thickness θ, Form Factor H, Boundary Layer Thickness δ and U_e are specified at Station A-A.

FIGURE II-5 - SCHEMATIC REPRESENTATION FOR ZONE L-3 FOR SINGLE COMPONENT AIRFOIL

$$\frac{d\theta}{dx} + (H+2) \quad \frac{\theta}{U_e} \frac{d\ Ue}{dx} = 0. \tag{II-16}$$

The parameter and function for the similarity of velocity profiles in Zone L3 are assumed to have the following form, namely,

For Upper Half Wake:

$$\eta_1 = \frac{y - y_2}{y_3 - y_2};\ f(\eta_1) = \frac{U_{e_u} - U}{U_{e_u} - U_{W_1}} \tag{II-17}$$

For Lower Half Wake:

$$\eta_2 = \frac{y_2 - y}{y_2 - y_1};\ f(\eta_2) = \frac{U_{e_L} - U}{U_{e_L} - U_{W_1}} \tag{II-18}$$

By making use of equations (II-17) and (II-18) in the usual definitions for momentum and displacement thickness, the expressions for these quantities for upper and lower wakes in Zone L3 can be derived in terms of parameters of equations (II-17) and (II-18). Thus,

$$\theta_{\substack{\text{Upper}\\\text{Wake}}} = -(y_3 - y_2)\left[\left(\frac{U_{W_1}}{U_{e_u}} - 1\right)\int_0^1 f(\eta_1)d\eta_1 + \left(\frac{U_{W_1}}{U_{e_u}} - 1\right)^2 \int_0^1 f(\eta_1)^2 d\eta_1\right] \tag{II-19}$$

$$\theta_{\substack{\text{Lower}\\\text{Wake}}} = -(y_2 - y_1)\left[\left(\frac{U_{W_1}}{U_{e_L}} - 1\right)\int_0^1 f(\eta_2)d\eta_2 + \left(\frac{U_{W_1}}{U_{e_L}} - 1\right)^2 \int_0^1 f(\eta_2)^2 d\eta_2\right] \tag{II-20}$$

$$\delta^*_{\substack{\text{Upper}\\\text{Wake}}} = (y_3 - y_2)\left(1 - \frac{U_{W_1}}{U_{e_u}}\right)\int_0^1 f(\eta_1)d\eta_1 \tag{II-21}$$

$$\delta^*_{\substack{\text{Lower}\\\text{Wake}}} = (y_2 - y_1)\left(1 - \frac{U_{W_1}}{U_{e_L}}\right)\int_0^1 f(\eta_2)d\eta_2 \tag{II-22}$$

By making use of equations (II-17) through (II-22) in equation (II-16) and performing needed mathematical manipulations, the following quadratic equation can be derived for computing the ratio (U_{W_1}/U_{ea}) at the end of Zone L3.

$$A_1 \left(\frac{U_{W_1}}{U_{ea}}\right)^2 + A_2 \left(\frac{U_{W_1}}{U_{ea}}\right) + A_3 = 0. \tag{II-23}$$

Where the values of coefficients are determined from following equations,

$$A_1 = -(y_3 - y_2)\left\{\int_0^1 f^2(\eta_1)d\eta_1\right\} - (y_2 - y_1)\left\{\int_0^1 f^2(\eta_2)d\eta_2\right\}\left(\frac{U_{eu}}{U_{e_L}}\right)^2_B$$

$$- \left[(U_{e_B} - U_{e_A})\frac{1}{U_{e_B}}\right]_{\substack{\text{UPPER}\\ \text{WAKE}}} \cdot (y_3 - y_2) \cdot \int_0^1 f^2(\eta_1)d\eta_1$$

$$- (U_{e_B} - U_{e_A})\frac{1}{U_{e_B}}_{\substack{\text{LOWER}\\ \text{WAKE}}} \cdot (y_2 - y_1)\left\{\int_0^1 f^2(\eta_2)d\eta_2\right\} \cdot \left(\frac{U_{eu}}{U_{e_L}}\right)^2_B$$

$$A_2 = (y_3 - y_2)\left[2\left\{\int_0^1 f^2(\eta_1)d\eta_1\right\} - \left\{\int_0^1 f(\eta_1)d\eta_1\right\}\right]$$

$$+ (y_2 - y_1)\left[2\left\{\int_0^1 f^2(\eta_2)\, d\eta_2\right\} - \left\{\int_0^1 f(\eta_2)d\eta_2\right\}\right]\left(\frac{U_{eu}}{U_{e_L}}\right)_B$$

$$- \frac{1}{2}\left[(U_{e_B} - U_{e_A}) \cdot \frac{1}{U_{e_B}}\right]_{\substack{\text{UPPER}\\ \text{WAKE}}} \cdot (y_3 - y_2)\left\{\int_0^1 f(\eta_1)d\eta_1\right\}$$

$$- \frac{1}{2}\left[(U_{e_B} - U_{e_A}) \cdot \frac{1}{U_{e_B}}\right]_{\substack{\text{LOWER}\\ \text{WAKE}}} \cdot (y_2 - y_1)\left(\frac{U_{eu}}{U_{e_L}}\right)\left\{\int_0^1 f(\eta_2)d\eta_2\right\}_B$$

$$+ \left[(U_{e_B} - U_{e_A}) \cdot \frac{1}{U_{e_B}}\right]_{\substack{\text{UPPER}\\ \text{WAKE}}} \cdot (y_3 - y_2) \cdot \left\{2\int_0^1 f^2(\eta_1)d\eta_1 - \int_0^1 f(\eta_1)d\eta_1\right\}$$

$$+ \left[(U_{e_B} - U_{e_A}) \cdot \frac{1}{U_{e_B}}\right]_{\substack{\text{LOWER}\\ \text{WAKE}}} \cdot (y_2 - y_1) \cdot \left\{2\int_0^1 f(\eta_1)d\eta_2 - \int_0^1 f(\eta_2)d\eta_2\right\} \cdot \left(\frac{U_{eu}}{U_{e_L}}\right)_B$$

and

$$A_3 = (y_3 - y_2) \cdot \left[\int_0^1 f(\eta_1) d\eta_1 - \int_0^1 f^2(\eta_1) d\eta_1 \right]$$

$$+ (y_2 - y_1) \cdot \left[\int_0^1 f(\eta_2) d\eta_2 - \int_0^1 f^2(\eta_2) d\eta_2 \right]$$

$$- \theta \Big|_{\substack{\text{T.E.} \\ \text{UPPER} \\ \text{SURFACE}}} - \theta \Big|_{\substack{\text{T.E.} \\ \text{LOWER} \\ \text{SURFACE}}}$$

$$+ \frac{1}{2} \left(H_{\substack{\text{T.E.} \\ \text{UPPER} \\ \text{SURFACE}}} + 2 \right) \cdot \frac{\theta}{U_e} \Big|_{\substack{\text{T.E.} \\ \text{UPPER} \\ \text{SURFACE}}} \cdot (U_{e_B} - U_{e_A})_{\substack{\text{UPPER} \\ \text{WAKE}}}$$

$$+ \frac{1}{2} \left(H_{\substack{\text{T.E.} \\ \text{LOWER} \\ \text{SURFACE}}} + 2 \right) \cdot \frac{\theta}{U_e} \Big|_{\substack{\text{T.E.} \\ \text{LOWER} \\ \text{SURFACE}}} \cdot (U_{e_B} - U_{e_A})_{\substack{\text{LOWER} \\ \text{WAKE}}}$$

$$+ \frac{1}{2} \left[(U_{e_B} - U_{e_A}) \cdot \frac{1}{U_{e_B}} \right]_{\substack{\text{UPPER} \\ \text{WAKE}}} \cdot (y_3 - y_2) \cdot \left\{ \int_0^1 f(\eta_1) d\eta_1 \right\}$$

$$+ \frac{1}{2} \left[(U_{e_B} - U_{e_A}) \cdot \frac{1}{U_{e_B}} \right]_{\substack{\text{LOWER} \\ \text{WAKE}}} \cdot (y_2 - y_1) \cdot \left\{ \int_0^1 f(\eta_2) d\eta_2 \right\}$$

$$+ \left[(U_{e_B} - U_{e_A}) \cdot \frac{1}{U_{e_B}} \right]_{\substack{\text{UPPER} \\ \text{WAKE}}} \cdot (y_3 - y_2) \cdot \left[\int_0^1 f(\eta_1) d\eta_1 - \int_0^1 f^2(\eta_1) d\eta_1 \right]$$

$$+ \left[(U_{e_B} - U_{e_A}) \cdot \frac{1}{U_{e_B}} \right]_{\substack{\text{LOWER} \\ \text{WAKE}}} \cdot (y_2 - y_1) \cdot \left\{ \int_0^1 f(\eta_2) d\eta_2 - \int_0^1 f^2(\eta_2) d\eta_2 \right\} .$$

The variation of the width of the upper and lower wakes in Zone L3 is expressed by the following growth rate equations,

$$\frac{d}{dx}(y_3 - y_2) = Cl_u \cdot \left(\frac{1 - \frac{U_{W_1}}{U_{e_u}}}{1 + \frac{U_{W_1}}{U_{e_u}}} \right) \qquad (11\text{-}24)$$

and,

$$\frac{d}{dx}(y_2 - y_1) = Cl_L \cdot \left(\frac{1 - \frac{U_{e_u}}{U_{e_L}} \frac{U_{W_1}}{U_{e_u}}}{1 + \frac{U_{e_u}}{U_{e_L}} \frac{U_{W_1}}{U_{e_u}}} \right)$$

where Cl_u and Cl_L are constants and initial values of $(y_3 - y_2)$ and $(y_2 - y_1)$ for equations (11-24) and (11-25) correspond to values of boundary layer thickness at Section AA on upper and lower surface of the airfoil, respectively. The implied assumptions for the validity of equations (11-24) and (11-25) are that growth rate of these layers is controlled by the transverse perturbation velocity and that the transverse perturbation velocity is proportional to the average gradients of velocity for upper and lower wakes in Zone L3. Simultaneous solutions of equations (11-23), (11-24), and (11-25) give the starter values for (U_{W_1}/U_{e_u}), $(y_3 - y_2)$ and $(y_2 - y_1)$ at the end of Zone L3 of Region 1. In the case of single component airfoil, the Regions II and III of Figure 11-4 are not present; and, thus, these starter values form the initial conditions for Region IV in the wake behind single component airfoil.

Equations for Region IV: For single component airfoil, the Region IV extends from the end of Zone L3 of Region I for a distance very far downstream of the airfoil trailing edge where the pressure has stabilized to the free stream value. Experimental data of the velocity profiles for layers 8-5 and 1-8 in Region IV indicate that velocity profiles in these layers become "similar" if the similarity parameters and similarity functions are defined in the following manner:

For layer 1-8:

$$\eta_3 = \frac{y_8 - y}{y_8 - y_C}; \quad f(\eta_3) = \frac{U_{e_L} - u}{U_{e_L} - U_{W8}} \qquad (11\text{-}26)$$

where u = velocity at any point y in layer 1-8
U_{e_L} = velocity at lower edge of wake boundary layer
U_{W8} = minimum velocity on the locus of $y_8(x)$
y_{1C} = distance y in the layer 1-8 where $u = 1/2\ (U_{W8} + U_{e_L})$

and for layer 8-5 define:

$$\eta_4 = \frac{y - y_8}{y_{8C} - y_8}; \quad f(\eta_4) = \frac{U_{e_u} - u}{U_{e_u} - U_{W8}} \tag{II-27}$$

where u = velocity at any point y in layer 8-5
U_{e_u} = velocity at upper edge of wake boundary layer
y_{8C} = distance y in the layer 8-5 where $u = 1/2\ (U_{e_u} + U_{W8})$.

In the definition of similarity parameters η_3 and η_4, as given by equations (II-26) and (II-27), the distances y_{1C} and y_{8C} are used because it is difficult to determine the exact values of boundary layer thickness from measurements at large distances downstream of the airfoil trailing edge. The Euler equation at the upper edge of the wake can be written as:

$$\frac{dP}{dx} = - \rho\ U_{e_u} \frac{d\ U_{e_u}}{dx} \tag{II-28}$$

whereas for the lower edge of wake, the Euler equation is written as:

$$\frac{dP}{dx} = - \quad U_{e_L} \frac{d\ U_{e_L}}{dx} \tag{II-29}$$

The expression for the transverse velocity V(y) at any point in the layer 1-8 or layer 8-5 can be derived from the continuity equation (II-11) as follows,

$$V(y) \quad \frac{R(y)}{R1} = V(y8)\ \frac{R2}{R1} - \int_{y8}^{y} \frac{\partial u}{\partial x}\, dy \tag{II-30}$$

where $R(y)$ = radius of curvature of stream line in wake boundary layer at any point y
$R2$ = radius of curvature for the locus of minimum velocity $y = y_{8(x)}$
$R1$ = radius of curvature for lower edge of wake boundary layer
$V(y8)$ = transverse velocity on the locus $y = y_{8(x)}$ of minimum velocity $U_{8(x)}$.

Applicable boundary layer conditions for the layer 8-5 and layer 1-8 are:

at $y = y_5$: $u = U_{e_u}$, $f(\eta_4) = 0$, $\eta_4 = K_{1u}$, $Cp = Cp(y_5)$, $\tau = \tau(y_5) = 0$,

and $\frac{1}{\rho} \frac{d\ Pe_u}{dx} = - U_{e_u} \frac{d\ Ue_u}{dx}$

at $y = y_8$: $u = Ue_8$, $f(\eta_4) = f(\eta_3) = 1$, $\eta_3 = \eta_4 = 0$, $Cp = Cp(y_8)$,

and $V(y) = V(y_8)$

and at $y = y_1$: $u = U_{eL}$, $f(\eta_3) = 0$, $\eta_3 = K_{1L}$

$$Cp = Cp(y_1),\ \tau = \tau(y_1) = 0, \text{ and } \frac{1}{\rho}\frac{d\ P_{eL}}{dx} = -\ U_{eL}\frac{d\ U_{eL}}{dx}. \quad (11\text{-}31)$$

In order to obtain momentum integral equation for layer 8-5, individual terms of equation can be integrated from $y = y_8$ to $y = y_5$. During the mathematical manipulations, use is made of equations (11-30), (11-29), (11-26), boundary conditions (11-31) and Leibnitz's rule. Radius of curvature R for the wake flow boundary is assumed large compared to the thickness of boundary layer for the purpose of analytical simplification. Integration of the term

$$\int_{y_8}^{y_5} \frac{1}{R1}\ uv\ dy$$

needs some mention at this time. In order to perform this integration, the information regarding variation of integrand in the layer 8-5 is necessary. Experimental data indicate similarity in velocity profile for longitudinal velocity u; however, such generalized information regarding transverse component v is not available at the present time. Under this circumstance, the results of analytical solution for Tollmien's (Reference 3) plane turbulent source are used for the purpose of evaluating this integral. Figure 11-6(a) shows the schematic representation of Tollmien's plane turbulent source. Tollmien investigated the velocity distribution in the free jet flow which is formed when the flow of fluid emanates through the narrow rectangular slit. The x-axis coincides with the axis of symmetry and the y-axis is perpendicular to x-axis at the exit of the slit. The results of analytical solution, obtained by Tollmien for the flow conditions of Figure 11-6(a) are used for the present purpose as follows:

$$I_1 = \int_{y_8}^{y_5} \frac{1}{R_1}\ uv\ dy \quad (11\text{-}32)$$

Let

$$g_1(\xi) = \frac{U_{e_u} - U}{U_{e_u} - U_{W8}};\ g_2(\xi) = \frac{V}{U_{e_u} - U_{W8}} \text{ and } \xi = \frac{y - y_8}{y_{8C} - y_8} \quad (11\text{-}33)$$

when $y = y_8$, $\xi = 0$, $y = y_5$, $\xi = K_{2u}$.

Substitution of (11-33) in (11-32) and simplifying,

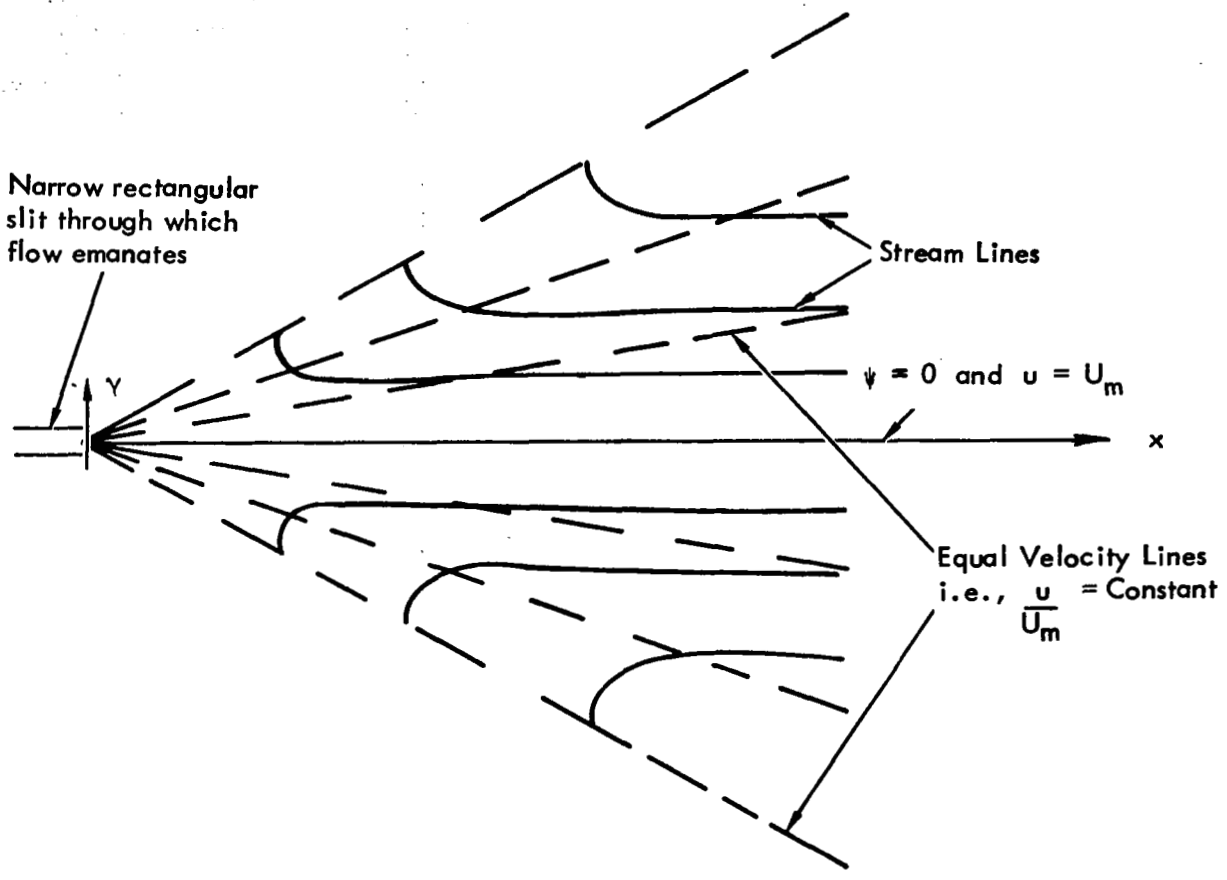

FIGURE II-6(a) - SCHEMATIC REPRESENTATION OF TOLLMIEN'S PLANE TURBULENT SOURCE

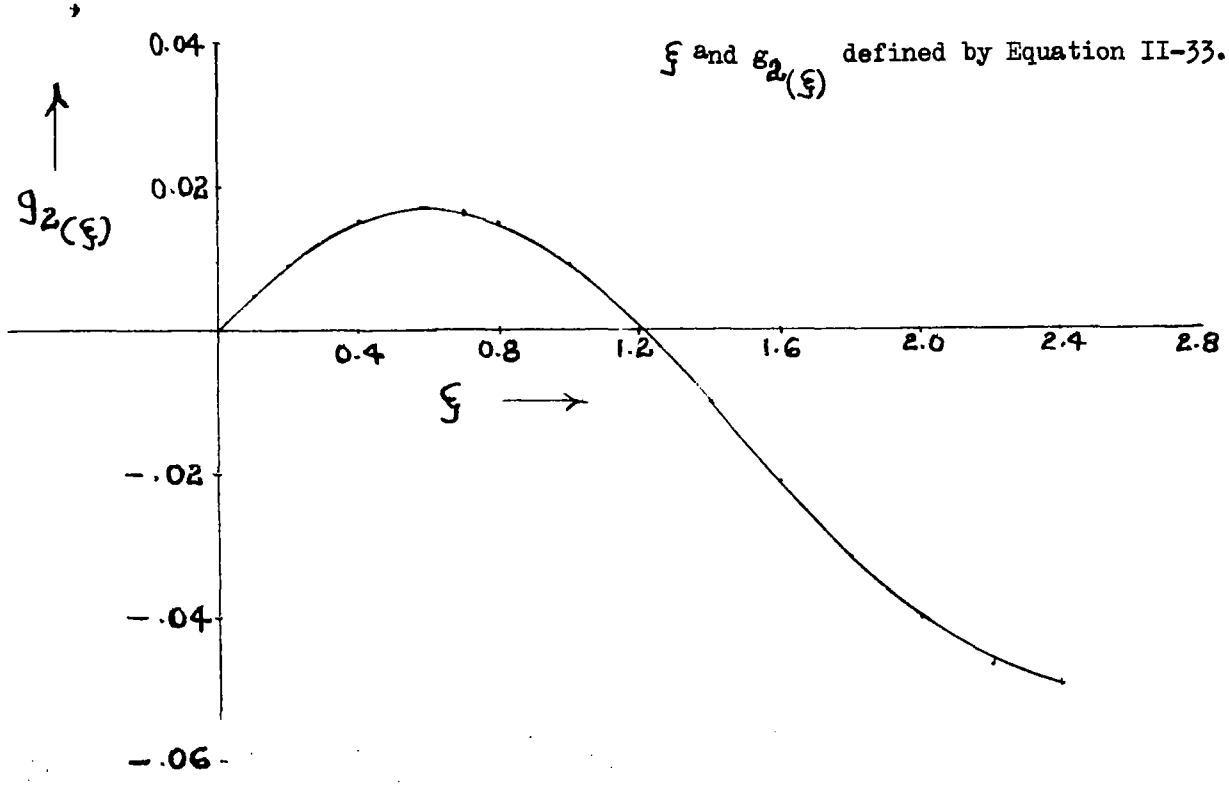

FIGURE II-6(b) - PLOT OF $g_{2(\xi)}$ FROM TOLLMIEN'S SOLUTION

$$I_1 = \frac{1}{R1}\,(U_{e_u})\,(U_{e_u} - U_{W8})\,(y_{8C} - y_8)\int_0^{K_{2u}} g_2(\xi)\,d\xi$$

$$- \frac{1}{R1}\,(U_{e_u} - U_{W8})^2\,(y_{8C} - y_8)\int_0^{K_{2u}} g_1(\xi)\,g_2(\xi)\,d\xi \qquad (11\text{-}34)$$

Figures II-6(b) and II-7 show the plots $g_2(\xi)$ and $g_1(\xi)$. $g_2(\xi)$ versus (ξ); these curves are obtained from theoretical results for Tollmien's plane turbulent source solution. From the above figures, the values of integrals can be written as:

$$\int_0^{K_{2u}} g_2(\xi)\,d\xi \approx -.0214 \quad \text{and} \quad \int_0^{K_{2u}} g_1(\xi)\,g_2(\xi)\,d\xi = .0065 \qquad (11\text{-}35)$$

Thus, the momentum integral equation for the layer 8-5 can be derived as

$$-\frac{d}{dx}\left[(y_{8C} - y_8)\,(U_{e_u})\,(U_{e_u} - U_{W8})\right]\cdot\left\{\int_0^{K_{1u}} f(\eta_4)d\eta_4\right\}$$

$$+\frac{d}{dx}\left[(y_{8C} - y_8)\cdot(U_{e_u} - U_{W8})^2\right]\left\{\int_0^{K_{1u}} f^2(\eta_4)d\eta_4\right\}$$

$$-\left(\frac{dy_8}{dx}\right)(U_{W8})\,(U_{e_u} - U_{W8}) + U_{e_u}\frac{d\,U_{e_u}}{dx}\,(y_5 - y_8)$$

$$-\frac{d\,U_{e_u}}{dx}\,(y_{8C} - y_8)\cdot(U_{e_u} - U_{W8})\left\{\int_0^{K_{1u}} f(\eta_4)d\eta_4\right\} + V(y_8)\,\frac{R5}{R1}\,(U_{e_u} - U_{W8})$$

$$+\frac{1}{R1}\,(U_{e_u})\,(U_{e_u} - U_{W8})\,(y_{8C} - y_8)\left\{\int_0^{K_{2u}} g_2(\xi)\,d\xi\right\}$$

$$-\frac{1}{R1}\,(U_{e_u} - U_{W8})\,(y_{8C} - y_8)\int_0^{K_{2u}} g_1(\xi)\,g_2(\xi)\,d\xi$$

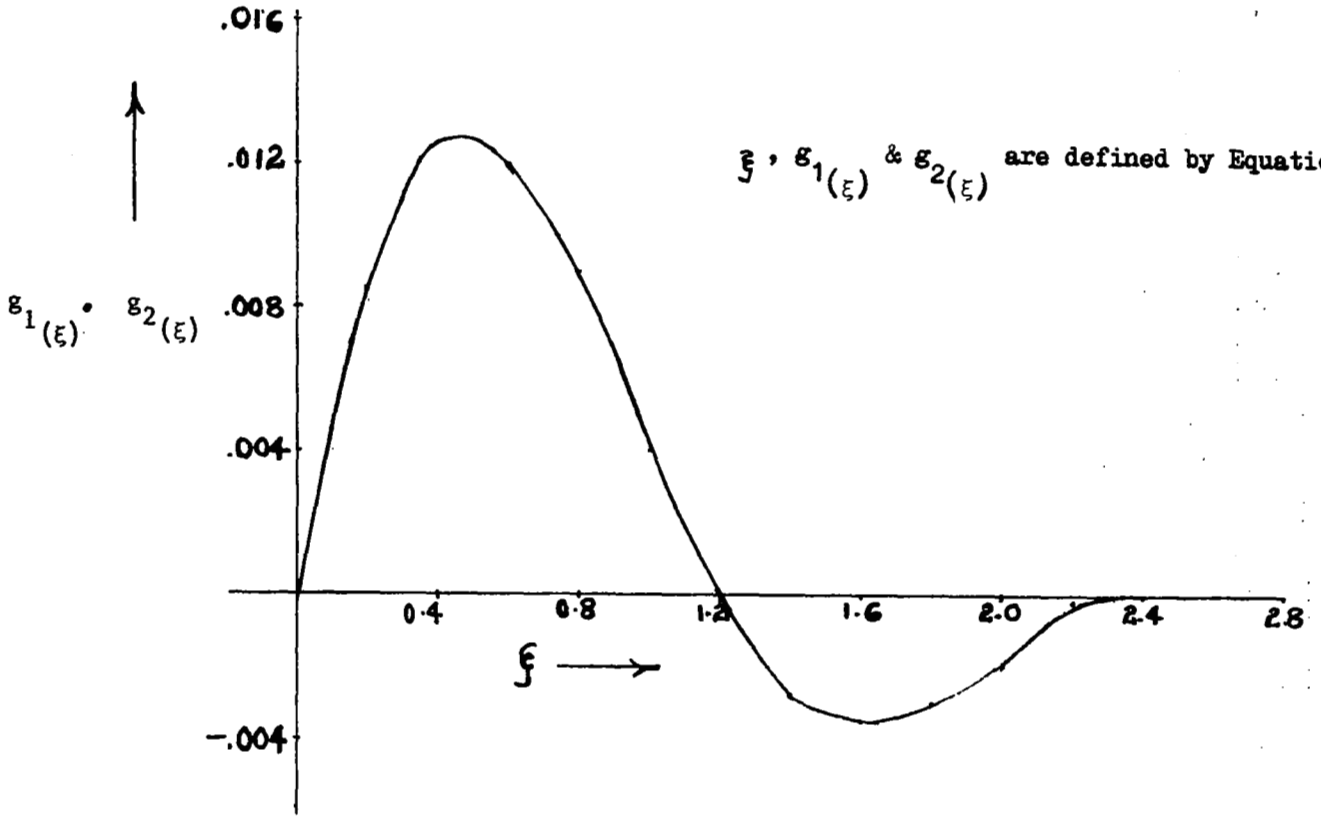

ξ , $g_{1(\xi)}$ & $g_{2(\xi)}$ are defined by Equation II-33.

FIGURE II-7 - PLOT OF $g_{1(\xi)} \cdot g_{2(\xi)}$ FROM TOLLMIEN'S SOLUTION

$$+ \frac{U_\infty^2}{2} \frac{d}{dx} \left[\int_{y_8}^{y_5} Cp \, dy \right] - \frac{U_\infty^2}{2} Cp\,(y_8) \frac{dy_8}{dx} + \frac{U_\infty^2}{2} Cp(y_8) \frac{dy_8}{dx}$$

$$= \frac{\bar{R}_{8-5}}{R1} \left(\frac{\tau(y_5)}{\rho} - \frac{\tau(y_8)}{\rho} \right) + \frac{1}{R1} \int_{y_5}^{y_8} \frac{\tau}{\rho} \, dy. \qquad (11\text{-}36)$$

If we assume that the rate of growth of the layer 8-5 is controlled by the transverse perturbation velocity, and — as experimental evidence indicates — similarity of velocity profile for this layer, then this growth rate can be expressed by the following equation:

$$\frac{d}{dx} \quad (y_{8C} - y_8) = C_{2u} \frac{1 - \frac{U_{W8}}{U_{e_u}}}{1 + 3 \frac{U_{W8}}{U_{e_u}}} \qquad (11\text{-}37)$$

where C_{2u} is an empirical constant.

In the manner similar to the derivation of equation (11-36), the momentum integral equation for the layer 1-8 can be derived as:

$$- \frac{d}{dx} \left[(y_8 - y_{1C}) \cdot (U_{e_L}) \quad (U_{e_L} - U_{W8}) \right] \int_0^{K_{1L}} f(\eta_3) d\eta_3 \}$$

$$+ \frac{d}{dx} \left[(y_8 - y_{1C}) \quad (U_{e_L} - U_{W8})^2 \right] \int_0^{K_{1L}} f^2(\eta_3) d\eta_3$$

$$+ (\frac{dy_2}{dx}) (U_{W8}) \quad (U_{e_L} - U_{W8}) + U_{e_L} \frac{d \, U_{e_L}}{dx} (y_8 - y_1)$$

$$- (\frac{d \, U_{e_L}}{dx}) \quad (y_8 - y_{1C}) (U_{e_L} - U_{W8}) \{ \int_0^{K_{1L}} f(\eta^3) d\eta_3 \} + V(y_8) \frac{R8}{R1} (U_{e_u} - U_{W8})$$

$$+ \frac{1}{R1} (U_{e_L}) (U_{e_L} - U_{W8}) \quad (Y_8 - y_{1C}) \{ \int_0^{K_{2L}} g_2(\xi) \, d\xi \}$$

$$- \frac{1}{R1} (U_{e_L} - U_{W8})^2 (y_8 - y_{1C}) \int_0^{K_{2L}} g_1(\xi) g_2(\xi) d\xi$$

$$+ \frac{U_\infty^2}{2} \frac{d}{dx} \left[\int_{y_1}^{y_8} Cp dy \right] - \frac{U_\infty^2}{2} Cp(y_8) \frac{dy_8}{dx} + \frac{U_\infty^2}{2} Cp(y_1) \frac{dy_1}{dx}$$

$$= \frac{\bar{R}_{1-8}}{R1} \left(\frac{\tau(y_8)}{\rho} - \frac{\tau(y_1)}{\rho} \right) + \frac{1}{R1} \int_{y_1}^{y_8} \frac{\tau}{\rho} dy \qquad (11\text{-}38)$$

$\bar{R}_{8-5}$ and $\bar{R}_{1-8}$, appearing in equations (11-36) and (11-38) can be approximated as the arithmetic mean values of radii of curvature for the layers 8-5 and 1-8 respectively. The growth rate equation for the layer 1-8 can be written in a manner similar to that for layer 8-5, as follows:

$$\frac{d}{dx} (y_5 - y_{1C}) = C_{2L} \frac{1 - \frac{U_{W8}}{U_{e_L}}}{1 + 3 \frac{U_{W8}}{U_{e_L}}} \qquad (11\text{-}39)$$

where C_{2L} is an empirical constant.

Thus, equations (11-36), (11-37), (11-38) and (11-39) are four equations for the simultaneous solution of four variables y_1, y_2, y_3 and U_{W8} in the Region IV, which is shown in Figure 11-4. These equations can be arranged in a manner to form the Initial Value Problem. Various single-step or multi-step methods can be used for the solution of this initial value problem. The most commonly used methods are the single step Euler method, the single-step modified Euler method, the multi-step predictor corrector method, the Runge-Kutta method, and a few others. The choice of a method depends upon the particular problem and is governed by the desired accuracy, time of computation, core size available in a particular computer, and other factors.

Equations (11-23), (11-36), and (11-38) contain terms such as

$$\int_0^{K_1} f(\eta) d\eta, \quad \int_0^{K_1} f^2(\eta) d\eta, \quad \int_0^{K_2} g_1(\xi) g_2(\xi) d\xi,$$

shear stress terms, terms containing shear and pressure integrals and CP distributions at the edges of various layers. In order to be able to solve these equations, however, the values of the above quantities either have to be known priori and/or more auxiliary equations are required which express the above

quantities as the functional relationships in terms of dependent variables. As the viscous flow under consideration is turbulent wake flow, theoretical expressions for the above quantities are not available as in the case of laminar boundary layers. Recourse is then made to experimental measurements to obtain empirical expressions for the above parameters by the use of experimental data for the particular flow which is being investigated. This matter is further discussed in Sections III and IV.

III. EXPERIMENTAL WORK

In order to facilitate understanding of turbulent wake flow, which exists behind the trailing edge of airfoil model, for the purpose of developing an analytical model and also to check the validity of theoretical predictions, an experimental program was conducted in the research wind tunnel facility at Lockheed-Georgia Company. In this section, a brief description is given for airfoil model, the experimental facility, probes for measurements of velocity and static pressure profiles, and types of tests. Detailed description of instrumentation, side wall blowing requirements in tunnel working section, and data acquisition and reduction is given in the appendices.

III.1 Description of Airfoil Model

Airfoil model is 15 percent thick and is symmetrical airfoil section. It is basically the NASA four digit airfoil section with slight modification near the leading edge. Figure III-1 shows the geometry of the test airfoil configuration; the difference in geometry near the leading edge of the test airfoil from NACA 0015 is also indicated in this figure. Computer program of Reference 1 indicated the existence of laminar stall on the original NACA 0015 airfoil at a Reynolds number of approximately 1 million. The leading edge geometry for the test airfoil was arrived at by the use of the computer program of Reference 1 such that turbulent separation near the trailing edge was predicted before the occurrence of laminar stall prediction on this test airfoil. The above phenomena then makes it possible to conduct systematic studies for the flow in the wake behind the airfoil trailing edge.

Figure III-2 shows the comparison between predicted $C_{L-\alpha}$ curve of the test airfoil with experimental measurements. It can be seen from this figure that viscous prediction agrees quite well with experimental measurements up to an angle of attack of $\alpha \approx 9°$ to $10°$. Experimental measurements of boundary layer velocity profiles indicate that turbulent boundary layer separation on the upper surface of the test airfoil near the trailing edge appears for angles of attack α greater than $9°$ to $10°$. Theoretical methods which are used in Reference 1 for computations of aerodynamic characteristics of airfoils are not valid in the presence of separated flow on the airfoil surfaces. For this reason, theoretical predictions of lift coefficients differ from experimental measurements for angles of attack α greater than approximately $9°$ to $10°$.

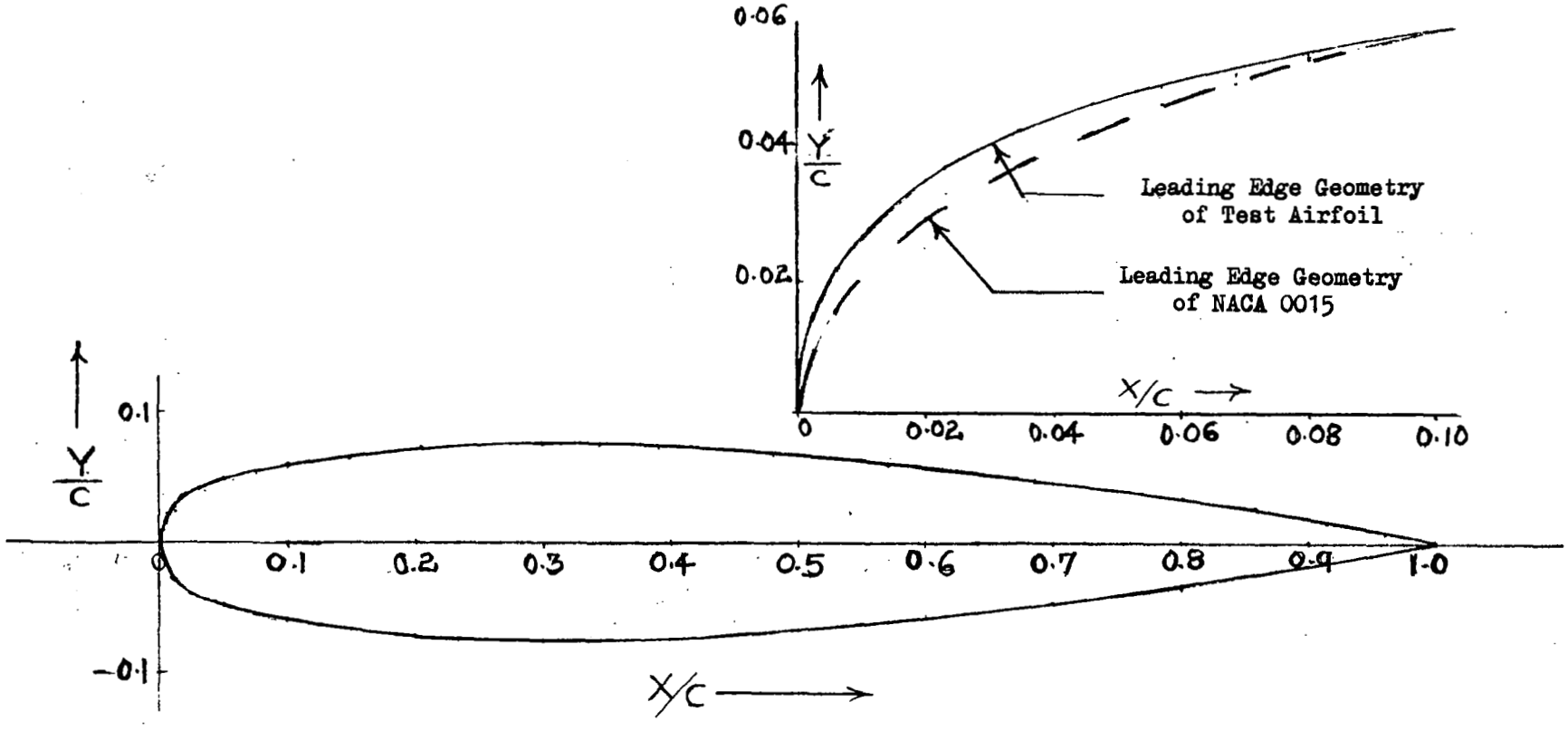

FIGURE III-1 - GEOMETRY OF THE TEST AIRFOIL

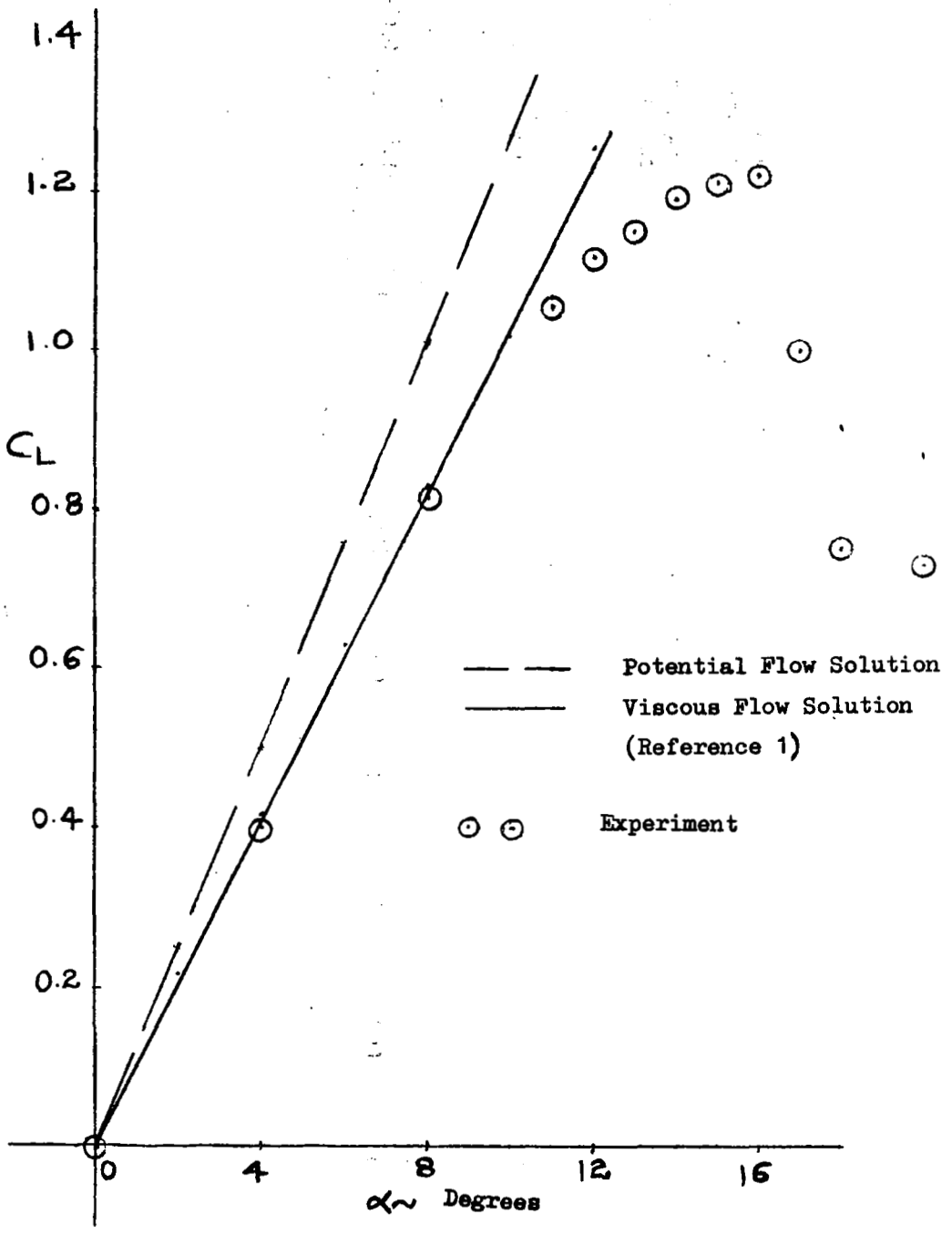

FIGURE III-2 - PREDICTED C_L-α CURVE FOR TEST AIRFOIL AND COMPARISON WITH EXPERIMENTS

Pressure distribution for the test airfoil at various angles of attack are shown in Figures III-3(a), III-3(b), III-3(c) and III-3(d). Computed results for potential and viscous pressure distributions are shown in the above figures and experimentally measured pressures at various chordwise locations on test airfoils at various angles of attack are shown plotted for comparison purposes. Comparison shown in Figures III-3(a) and III-3(b) indicate that theoretical predictions agree quite well with experimental measurements for angles of attack α equal to 0° and 8°; however, for angles of attack α of 12° and 14°, agreement between computed and experimental pressure distributions is not so good because of the existence of turbulent boundary layer separation on the upper surface of the airfoil.

Figures III-4(a) and III-4(b) show the plots of computed boundary layer development on the upper surface of the test airfoil for angles of attack of 8° and 12°, respectively; experimental measurements of boundary layer quantities on the airfoil surface aft of X/C of 0.8 are also shown in these figures. For the case of angle of attack of 8°, shown in Figure III-4(a), incipient separation may be present aft of X/C of 0.96 near the trailing edge of the airfoil (as indicated in this figure by the computed value of the turbulent boundary layer form factor H which becomes greater than 2.0 near the trailing edge). In this case the computed values of boundary layer displacement and momentum thicknesses and form factor agree reasonably well with experimental data. However, when the angle of attack is 12°, the results of computations of boundary layer quantities do not agree very well with experimental measurements on the upper surface of the airfoil because of the presence of appreciable region of flow separation on it. The boundary layer separation takes place at $X/C \geq 0.8$ at an angle of attack of 12° approximately, and for this reason measured boundary layer thicknesses are much larger than computed values aft of $X/C \approx 0.8$.

The model was mounted vertically in the working section of the tunnel spanning the 76.2 centimeters test section. The chord of the airfoil model is 29.2 centimeters. Total of 16 static pressure orifices are provided on the upper surface and 10 orifices are provided on the lower surface of the model along Butt Line 0.00, i.e. along the center span of the model. In addition, a total of 15 additional static pressure orifices are provided on the upper and lower surfaces at Butt Lines ±3.00 for checking the two dimensionality of the flow on the airfoil model. Table 3-1 gives coordinates and Table 3-2 shows the chordwise locations of the static pressure orifices on the model.

Forward of chordwise location X/C of 0.7, the model is comprised of a central load-carrying beam covered by a contoured maple shell. The shell consists of a solid maple leading edge and upper and lower surface "skins". The leading edge is bolted to the front of the beam. Aft of X/C of 0.7 the model is made of solid aluminum. A tolerance of ±.0127 centimeters is maintained on the airfoil contour across the span.

III.2 Wind Tunnel Facility

Experiments for the studies of the wake flow behind the single component test airfoil were conducted in the Lockheed Research Wind Tunnel facility which

$M_\infty = 0.201; \alpha = 0^\circ; R_N \approx 1.4 \times 10^6$

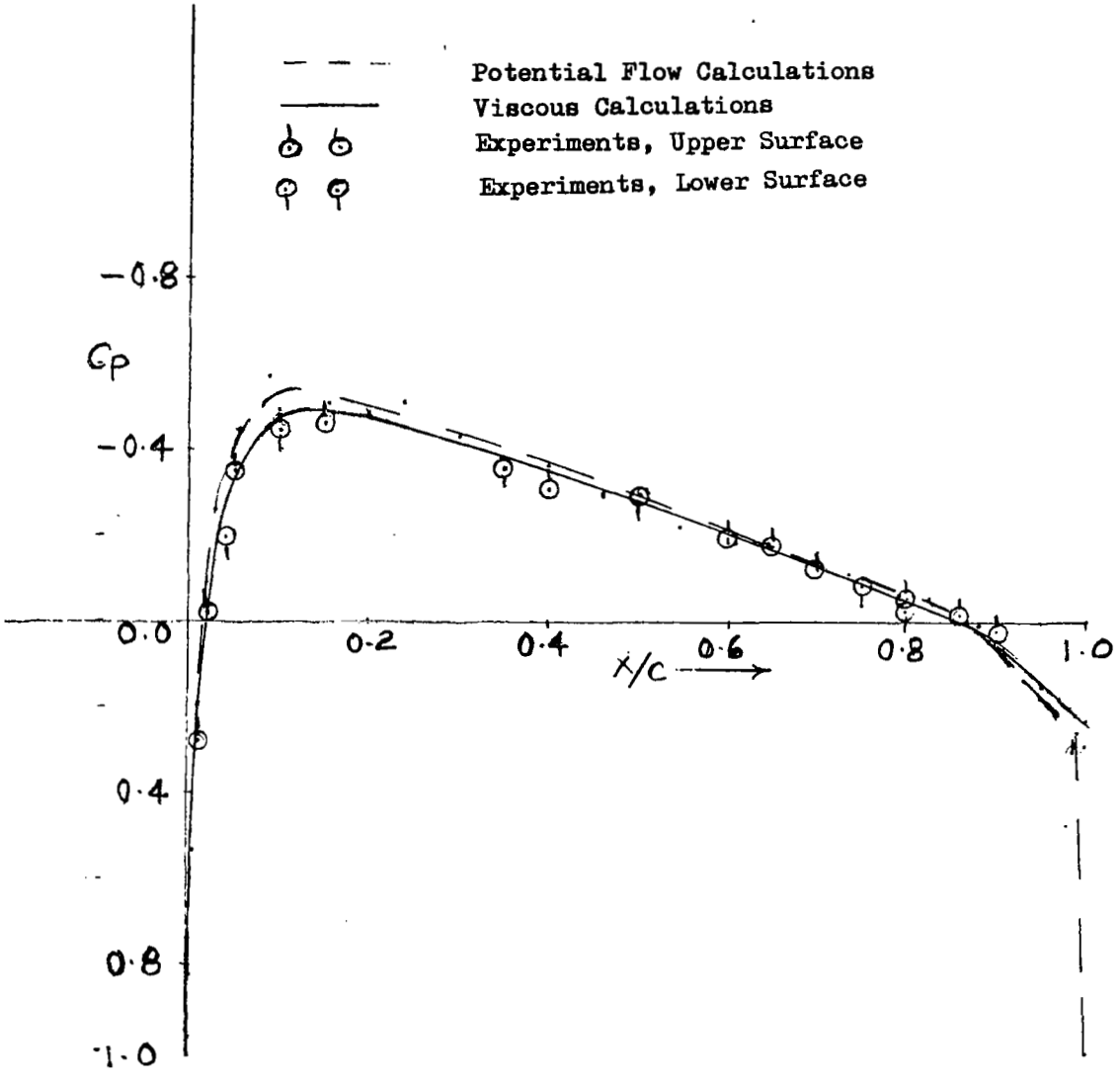

FIGURE III-3(a) - COMPARISON OF PRESSURE DISTRIBUTIONS FOR THE TEST AIRFOIL (SHARP T.E.) AT AN ANGLE OF ATTACK OF 0°

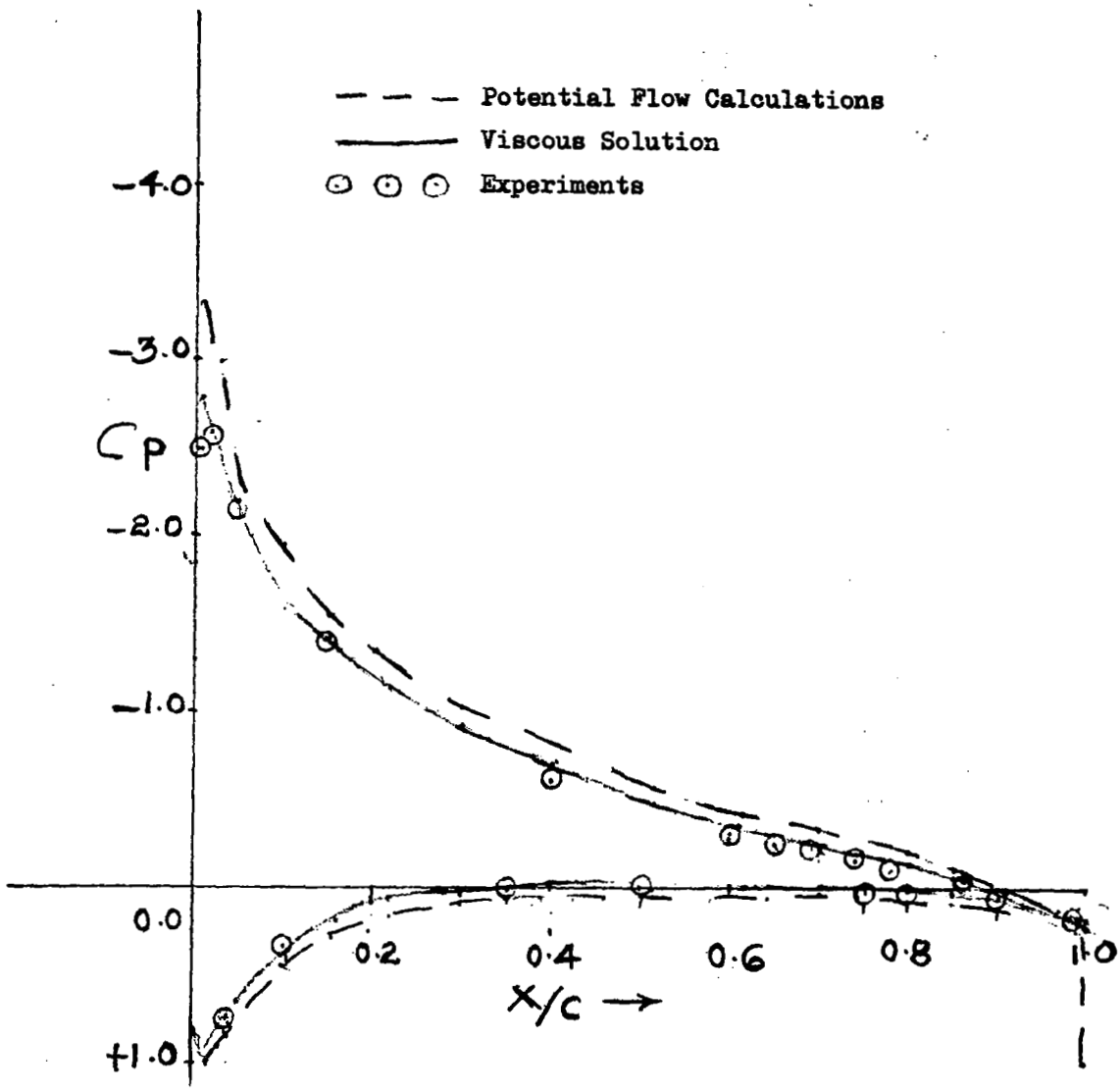

FIGURE III-3(b) - COMPARISON OF PRESSURE DISTRIBUTIONS ON TEST AIRFOIL (SHARP T.E.) AT AN ANGLE OF ATTACK OF 8°

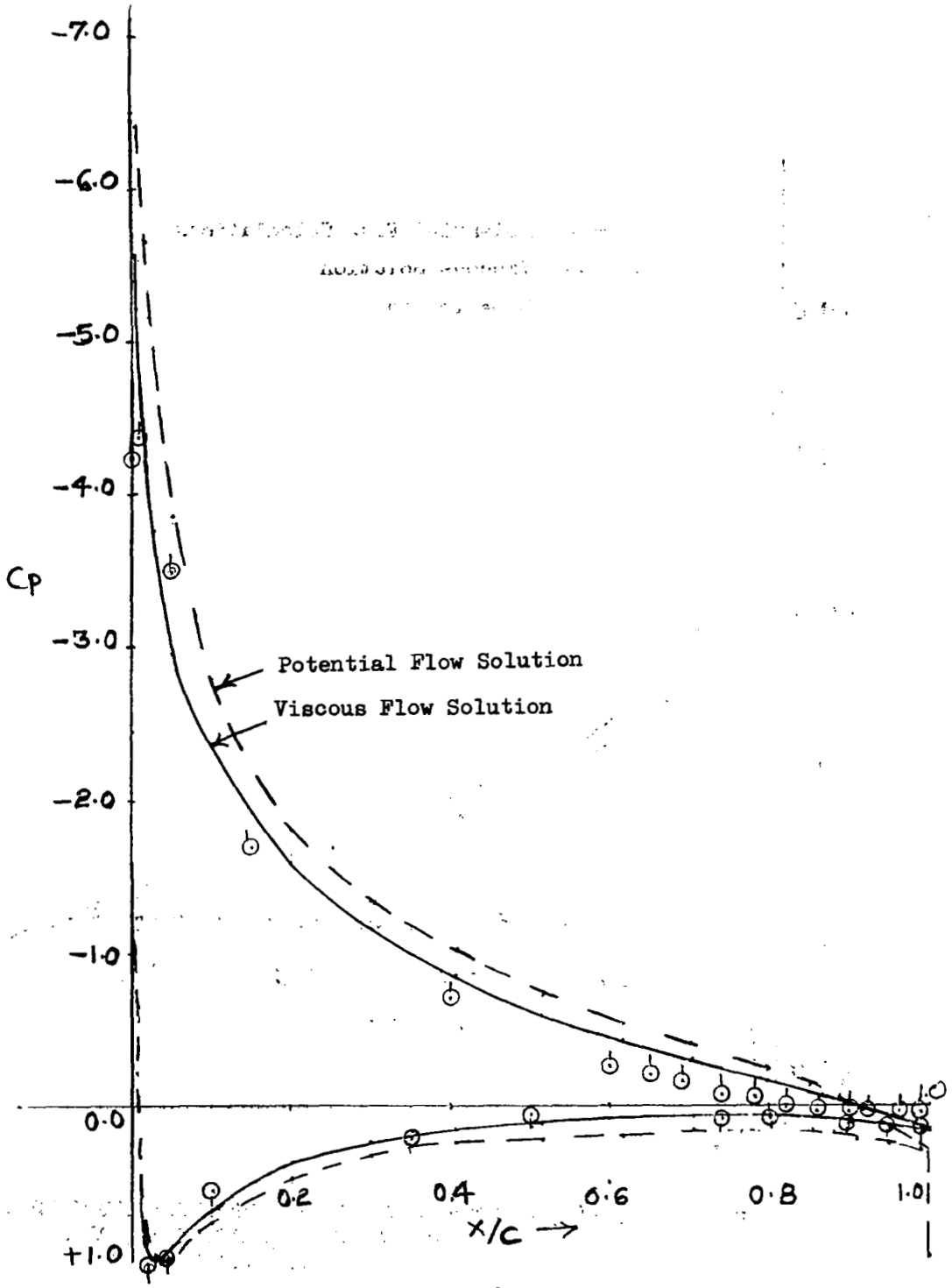

FIGURE III-3(c) - COMPARISON OF PRESSURE DISTRIBUTIONS ON TEST AIRFOIL (SHARP T.E.) AT AN ANGLE OF ATTACK OF 12°

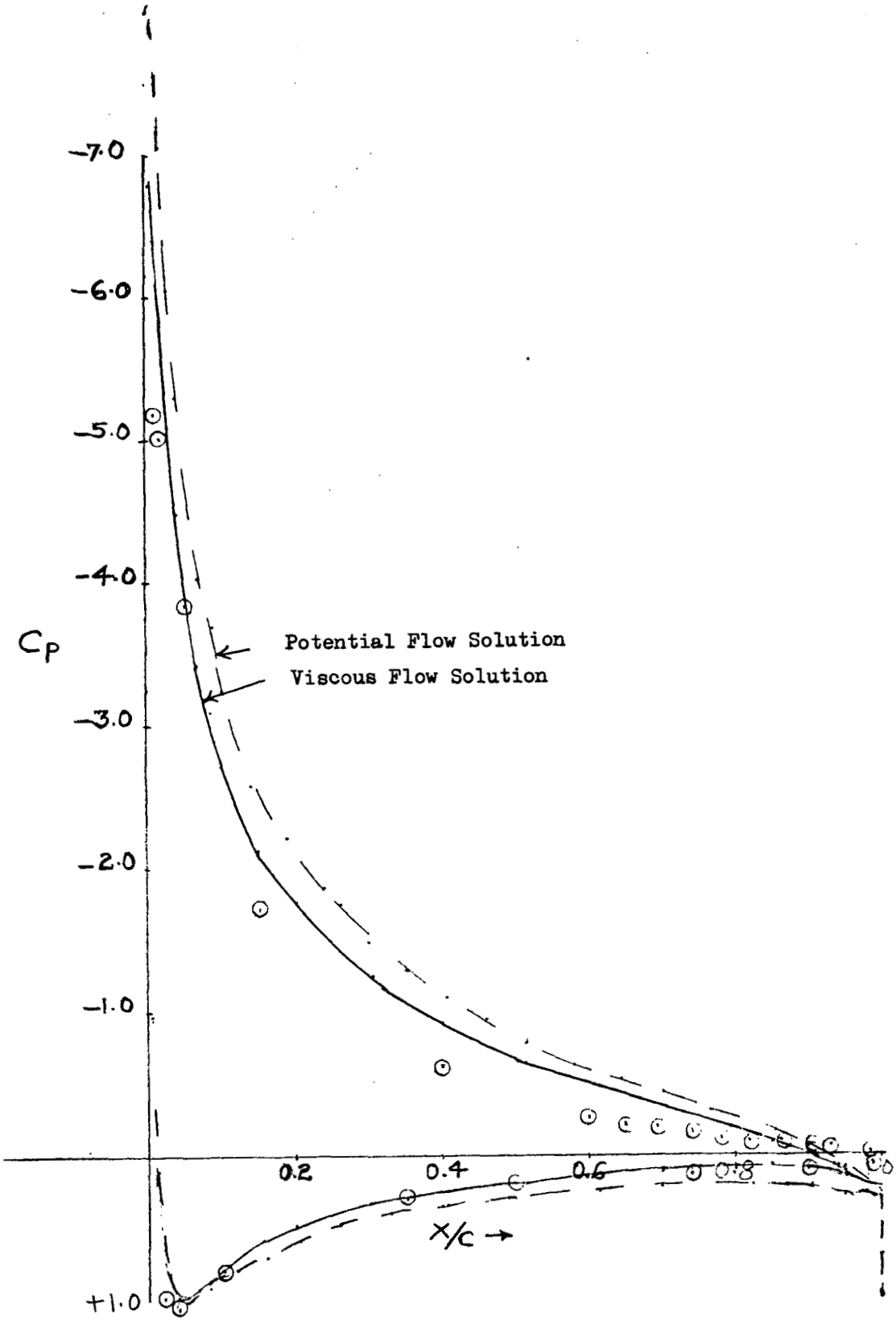

FIGURE III-3(d) - COMPARISON OF PRESSURE DISTRIBUTIONS ON TEST AIRFOIL (SHARP T.E.) AT AN ANGLE OF ATTACK OF 14°

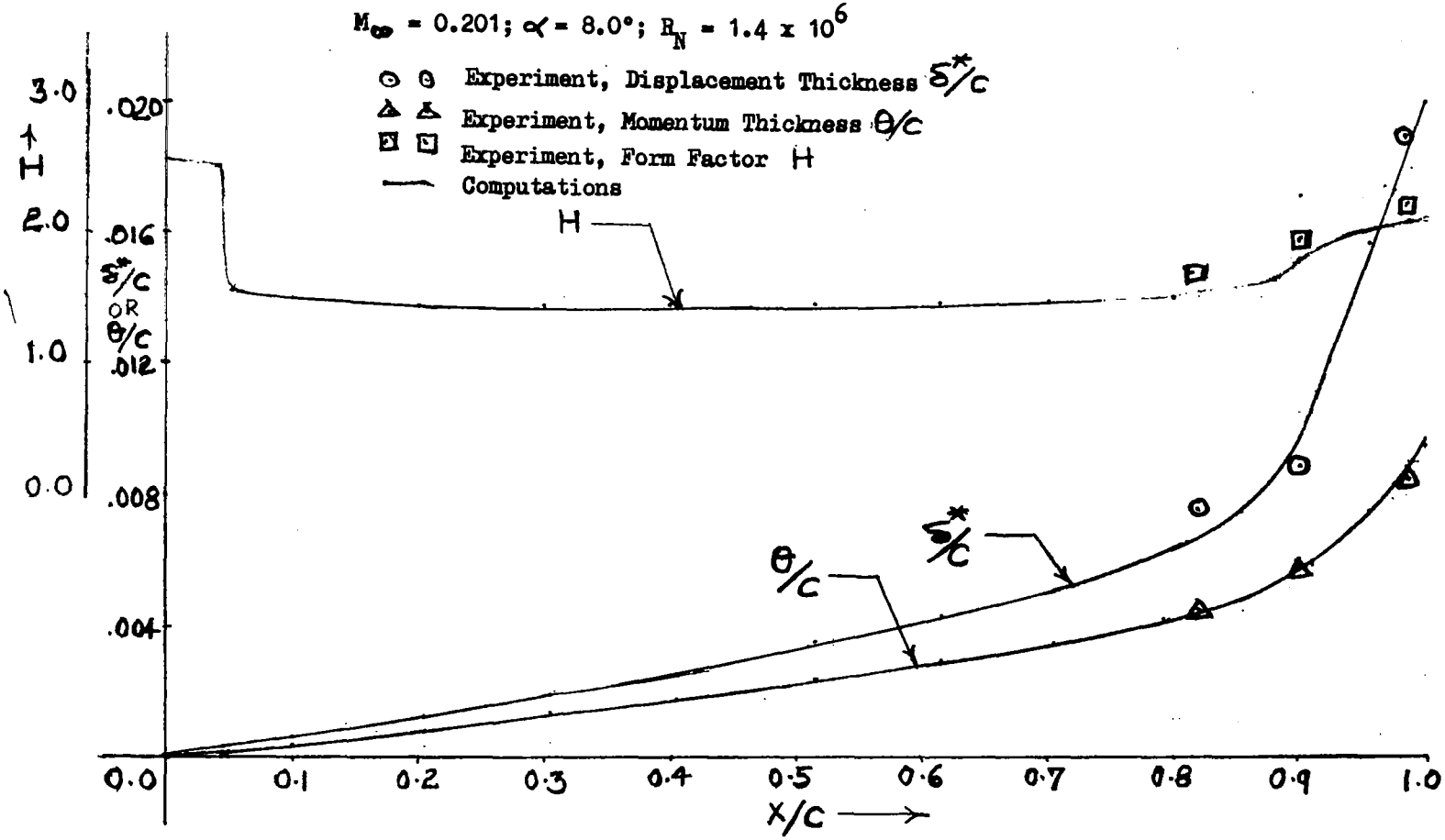

FIGURE III-4(a) - BOUNDARY LAYER DEVELOPMENT ON THE UPPER SURFACE OF THE TEST AIRFOIL (SHARP T.E.) AT AN ANGLE OF ATTACK OF 8° AND COMPARISON WITH EXPERIMENTS

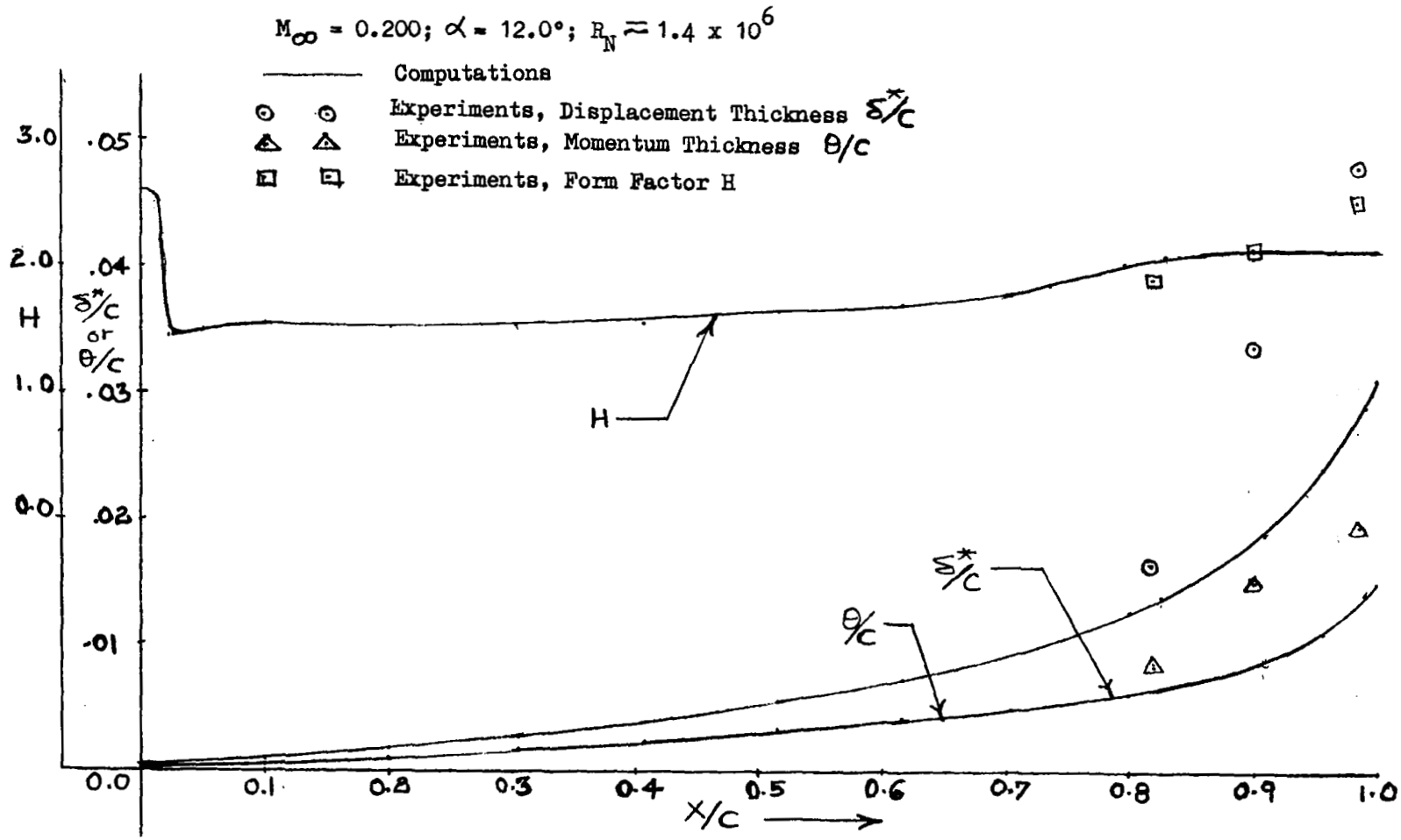

FIGURE III-4(b) - BOUNDARY LAYER DEVELOPMENT ON THE UPPER SURFACE OF THE TEST AIRFOIL (SHARP T.E.) AT AN ANGLE OF ATTACK OF 12° AND COMPARISON WITH EXPERIMENTS

Table 3-1 - COORDINATES OF THE TEST AIRFOIL SECTION (SYMMETRICAL AIRFOIL)

Airfoil Chord, C = 29.2 inches

Station, Percent Chord X/C x 100	Airfoil Section Ordinate Percent Chord Z/C x 100
0.00	0.00
0.23	1.45
0.57	2.20
1.14	2.87
1.72	3.36
2.29	3.76
3.43	4.33
4.58	4.73
5.72	5.00
6.87	5.32
8.01	5.45
10.30	5.90
12.59	6.32
14.88	6.64
17.17	6.93
20.60	7.21
25.18	7.46
30.00	7.50
34.33	7.44
38.91	7.29
43.49	7.04
48.07	6.72
52.65	6.33
57.22	5.90
62.95	5.38
68.67	4.78
74.39	4.08
80.11	3.35
85.84	2.52
91.56	1.60
96.14	0.77
100.00	0.00

Table 3-2 - LOCATION OF PRESSURE ORIFICES ON THE AIRFOIL MODEL SURFACES

Tube Number	Surface	Butt Line	X/C	Number	Surface	Butt Line	X/C
1	Upper	0.0	0.00	22	Upper	-3.0	0.05
2	Upper	0.0	0.01	23	Upper	-3.0	0.40
3	Upper	0.0	0.05	24	Upper	-3.0	0.69
4	Upper	0.0	0.15	25	Upper	-3.0	0.90
5	Upper	0.0	0.40	26	Upper	-3.0	0.96
6	Upper	0.0	0.60	27	Lower	0.0	0.02
7	Upper	0.0	0.65	28	Lower	0.0	0.04
8	Upper	0.0	0.69	29	Lower	0.0	0.10
9	Upper	0.0	0.74	30	Lower	0.0	0.35
10	Upper	0.0	0.78	31	Lower	0.0	0.50
11	Upper	0.0	0.82	32	Lower	0.0	0.74
12	Upper	0.0	0.86	33	Lower	0.0	0.80
13	Upper	0.0	0.90	34	Lower	0.0	0.90
14	Upper	0.0	0.93	35	Lower	0.0	0.95
15	Upper	0.0	0.96	36	Lower	0.0	0.985
16	Upper	0.0	0.985	37	Lower	+3.0	0.35
17	Upper	+3.0	0.05	38	Lower	+3.0	0.985
18	Upper	+3.0	0.40	39	Lower	-3.0	0.35
19	Upper	+3.0	0.69	40	Lower	-3.0	0.90
20	Upper	+3.0	0.93	41	Lower	-3.0	0.985
21	Upper	+3.0	0.985				

is located in the Aerospace Sciences Laboratory of the Lockheed-Georgia Company. The cross-section of the test section is rectangular having an area of 0.836 square meters with a height to width ratio of 0.7; this results in a test section of approximately 76.2 x 109.2 centimeters with a length of 122 centimeters. This wind tunnel is a closed circuit, single return, low speed wind tunnel and is powered by a 400 horsepower synchronous speed induction motor driving a 183 centimeters, 10-bladed, single stage axial flow fan. The fan speed can be varied over the range from 0 to 1150 revolutions per minute by means of an eddy current clutch. A standard friction brake rated at 103.7 meters kilogram torque will bring the fan to rest from full speed in less than 15 seconds.

The velocity range of the tunnel with an empty test section is 0 to 91.5 meters per second resulting in a maximum dynamic pressure of 508.3 kilograms per square meter. The dynamic pressure variations in the test section can be maintained within approximately 0.1 percent during a boundary layer survey which typically takes about ten minutes in this test facility. With the present screens, the turbulence factor is less than 1.3 based on turbulence sphere measurements. At a dynamic pressure of 293 kilograms per square meter, the nominal Reynolds number is $.439 \times 10^6$ per meter of chord length. A general layout of the test facility is shown in Figure III-5.

Figure III-6 shows the variation of static pressure along the test section centerline at various free stream dynamic pressures. This figure shows that the static pressure at the location of the quarter chord of the model is within about 3 percent of the static pressure at any other location on the model centerline. The calibration done at the location of the model quarter chord was used in reducing data from these tests. This calibration is shown in Figure III-7.

The test section is equipped with blowing boundary layer control slits on the ceiling floor. The auxiliary air, for boundary layer control on the test section side walls, is provided from the storage tanks which are capable of delivering air at a maximum pressure of 22.73 kilograms per square centimeter. A regulator reduces this pressure to 11.23 kilograms per square centimeter, a few meters from the test section. This air is further throttled to a desired pressure in the plenums for boundary layer control slits.

The boundary layer control slits, which are located on the ceiling and the floor of the test section, are 77.2 centimeters wide and .0635 centimeters high. These slits are located approximately one chord length upstream of the model leading edge. The heights of the blowing slits can be varied from .0254 to .254 centimeters. Relatively high velocity air is introduced through the slits into the tunnel floor and ceiling boundary layers such that boundary layer separation is prevented on these side walls when the given model is in the tunnel at a given angle of attack with respect to the free stream. When the angles of attack for a given two-dimensional model in the tunnel is increased from low values to high values corresponding to $C_{L_{MAX}}$ condition, the boundary layer separation on the tunnel side walls occur upstream of the model leading edge due to the presence of adverse pressure gradient in the flow direction. If the above flow separation is present, then the reliable two-dimensional data cannot be obtained, especially near the $C_{L_{MAX}}$ conditions. The method used to determine the proper amount of blowing and the desired pressure ratio required to eliminate this boundary layer separation on wind tunnel side walls is discussed in

RESEARCH LOW SPEED WIND TUNNEL

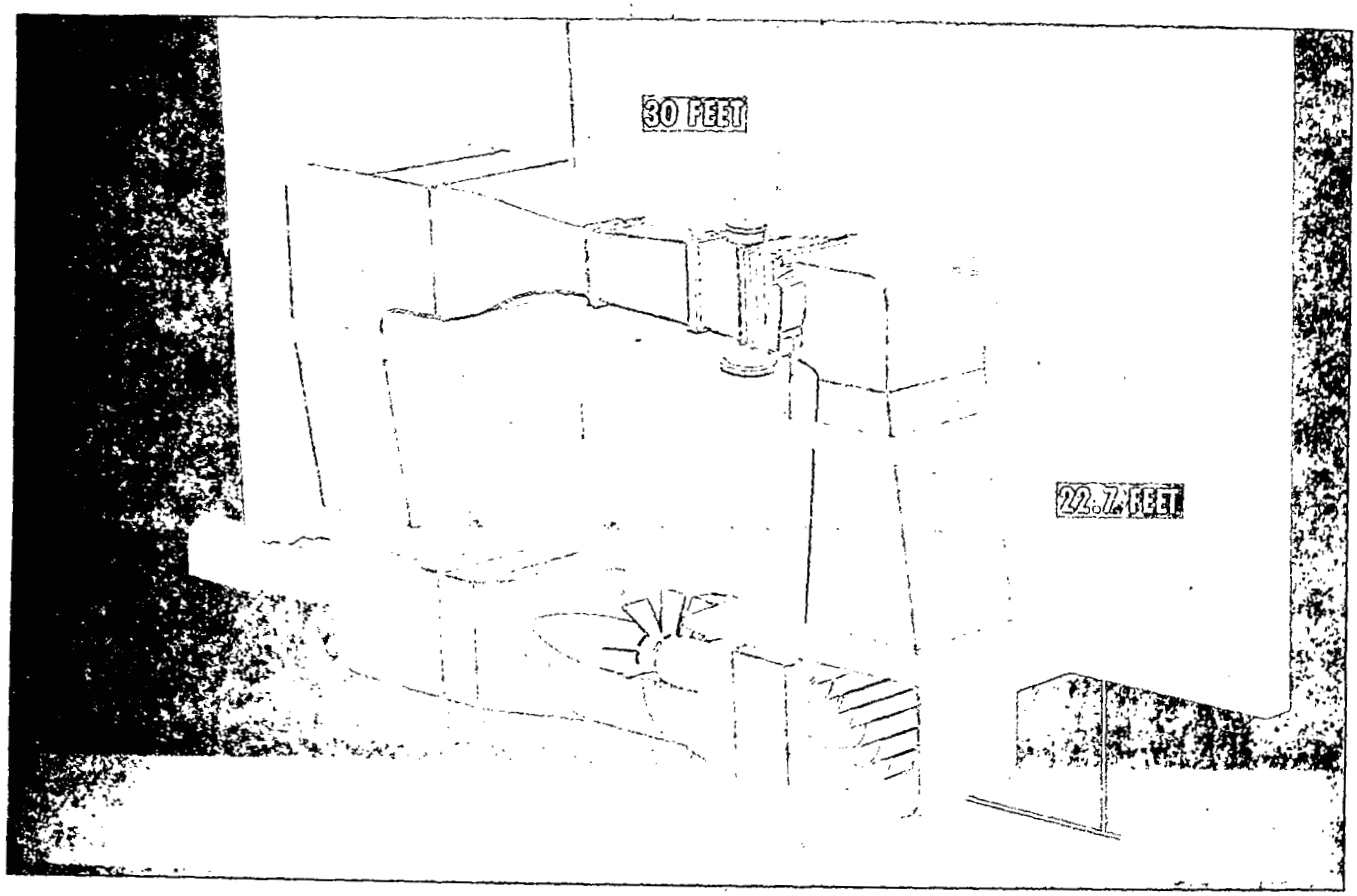

FIGURE III-5 - TEST FACILITY GENERAL LAYOUT

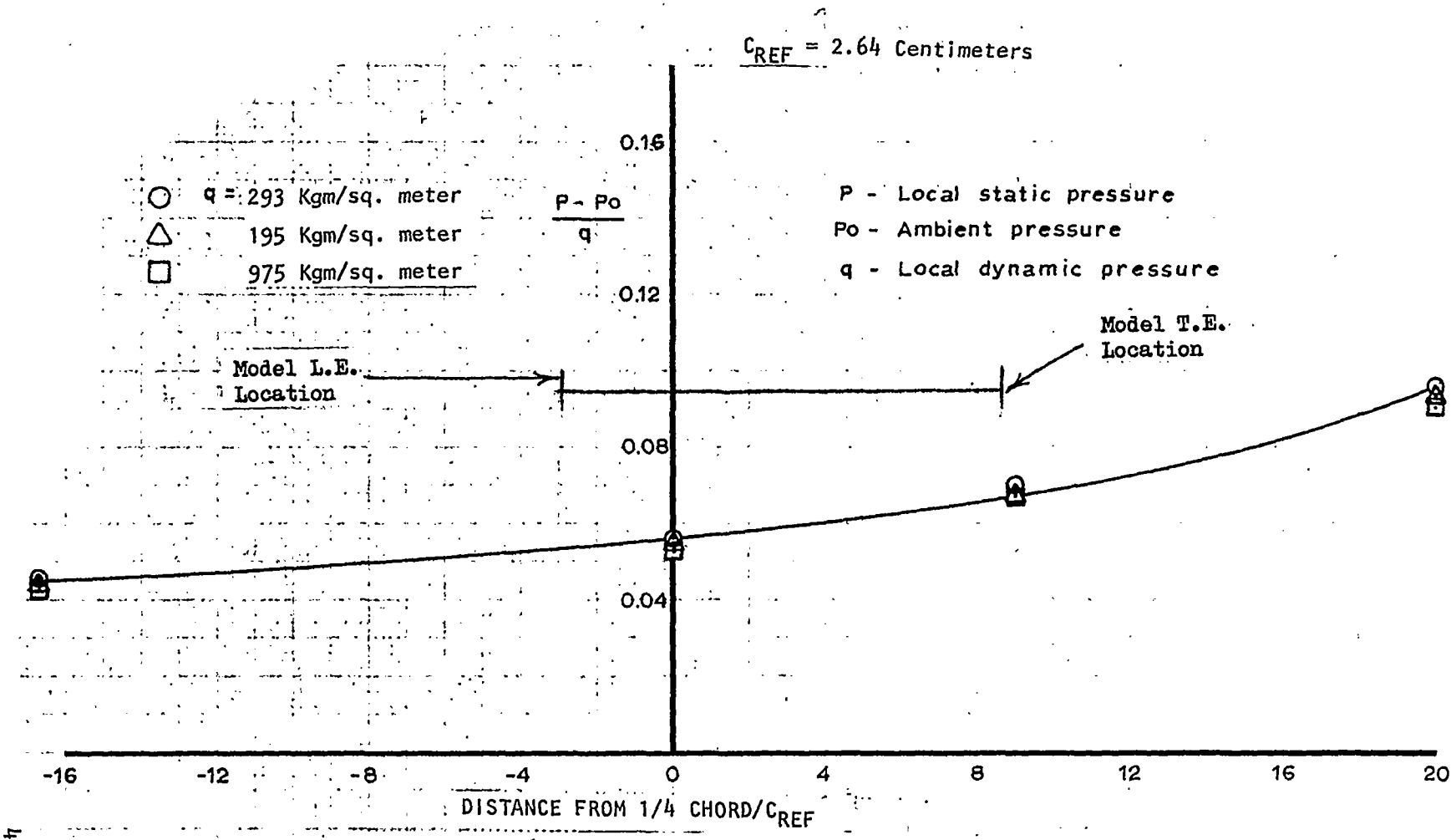

FIGURE III-6 - TEST SECTION STATIC PRESSURE VARIATION

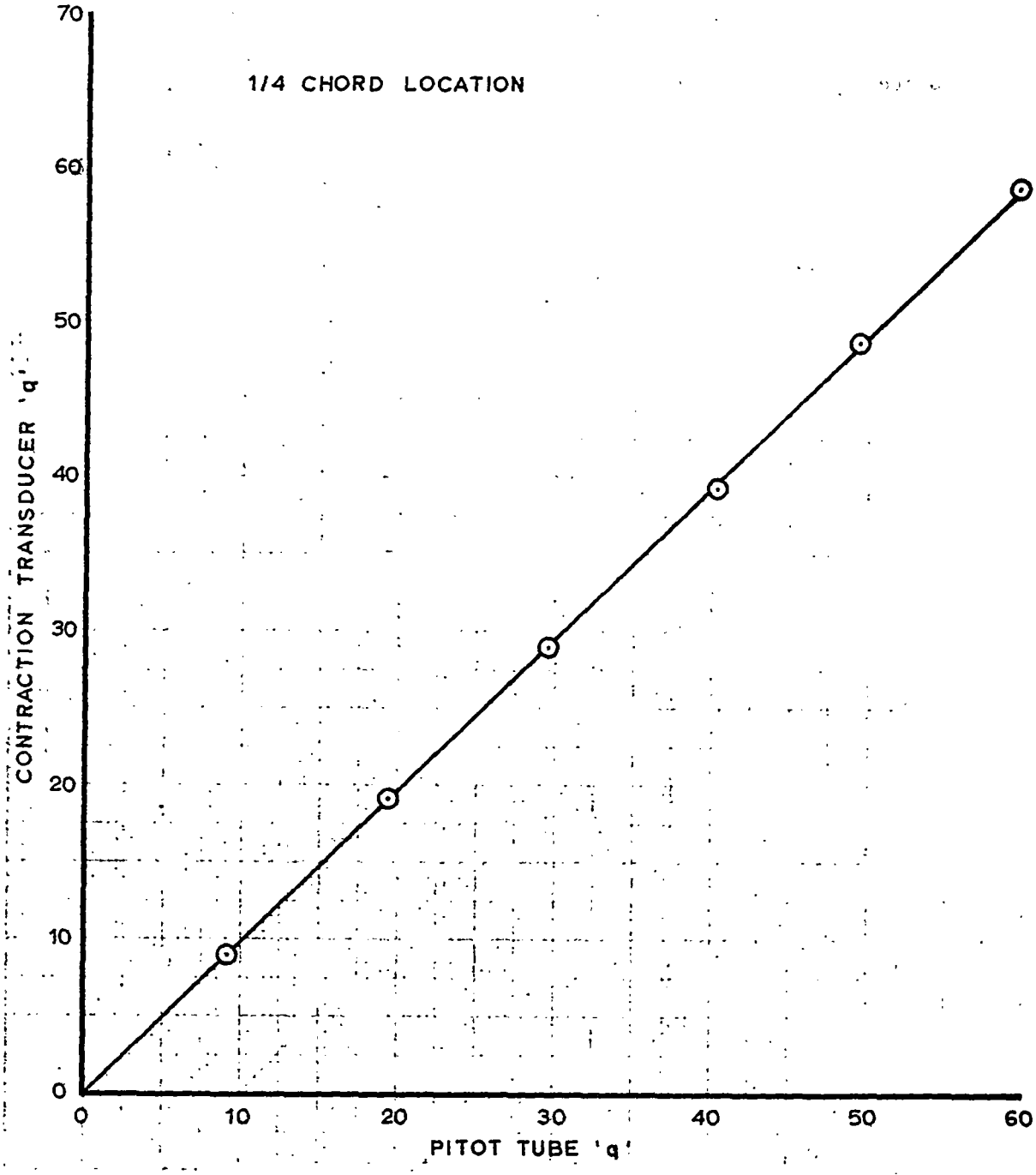

FIGURE III-7 - TEST SECTION SPEED CALIBRATION

Appendix A. Figure III-8 shows the details of the boundary layer control system used for the present study contract.

III-3 Special Instrumentation - Pressure Probe, Hot Wire Anemometer and Probe Drive Mechanism

Measurements of flow in the wake as well as on the upper surface of the test airfoil in the vicinity of the trailing edge were performed by the use of pressure probe and hot wire anemometer probe. In the case of sharp trailing edge airfoil, flow measurements in the airfoil wake were performed by use of a special type of pressure probe, whereas in the case of test airfoil with 1 percent thick trailing edge, hot wire anemometer probe was used for wake flow measurements. In the case of blunt trailing edge, the velocity profiles have reverse flow or negative velocity associated with them up to some distance downstream of the trailing edge. Hence, in this case, pressure probe alone cannot be used for determination of flow quantities in this region and hence additional instrumentation, such as hot wire probe is necessary for the determination of flow associated with reverse flow velocity profiles. The following paragraphs give the brief description of these two types of probes used during the experimental program of the present studies. The details of the additional instrumentation, used for acquisition and reduction of experimental measurements is given in Appendix B.

III.3.1 Pressure Probe: Measurements of static and total pressures in the boundary layer, for the purpose of determining boundary layer velocity profiles in the wake of test airfoil as well as on its upper surface, were made using the specially designed three element probe shown in Figure III-9. For the purpose of developing accurate mathematical model for the calculation of wake flow and profile drag of airfoils, it was desired to know the true variations of static pressure distribution across the boundary layer of the airfoil wake at various chordwise locations. Hence the selection of the probe tip design for the measurements of total and static pressures in the viscous flow in the wake was based on the following considerations.

It is known that it is relatively easy to measure an accurate value of total pressure in the flow with little effect arising from incidental variation in flow conditions. On the other hand, the selection of hole positions on the probe for the measurements of static pressure in the flow is much more difficult. This is so because it is observed that the measured value of the static pressure in the flow is very sensitive to any parameters, e.g. pitch angle of the probe, local flow direction in the flow, conditions of the boundary layer on the probe, proximity of static pressure holes on the probe to solid boundaries and several other factors. The above difficulty can, however, be overcome if it is possible to derive the value of velocity in the boundary layer from measured pressure differences arising between holes which sense pressures greater than the local static pressure but which show negligible sensitivity to the above-mentioned parameters. A simple relationship for dynamic pressure then still holds good and can be expressed as,

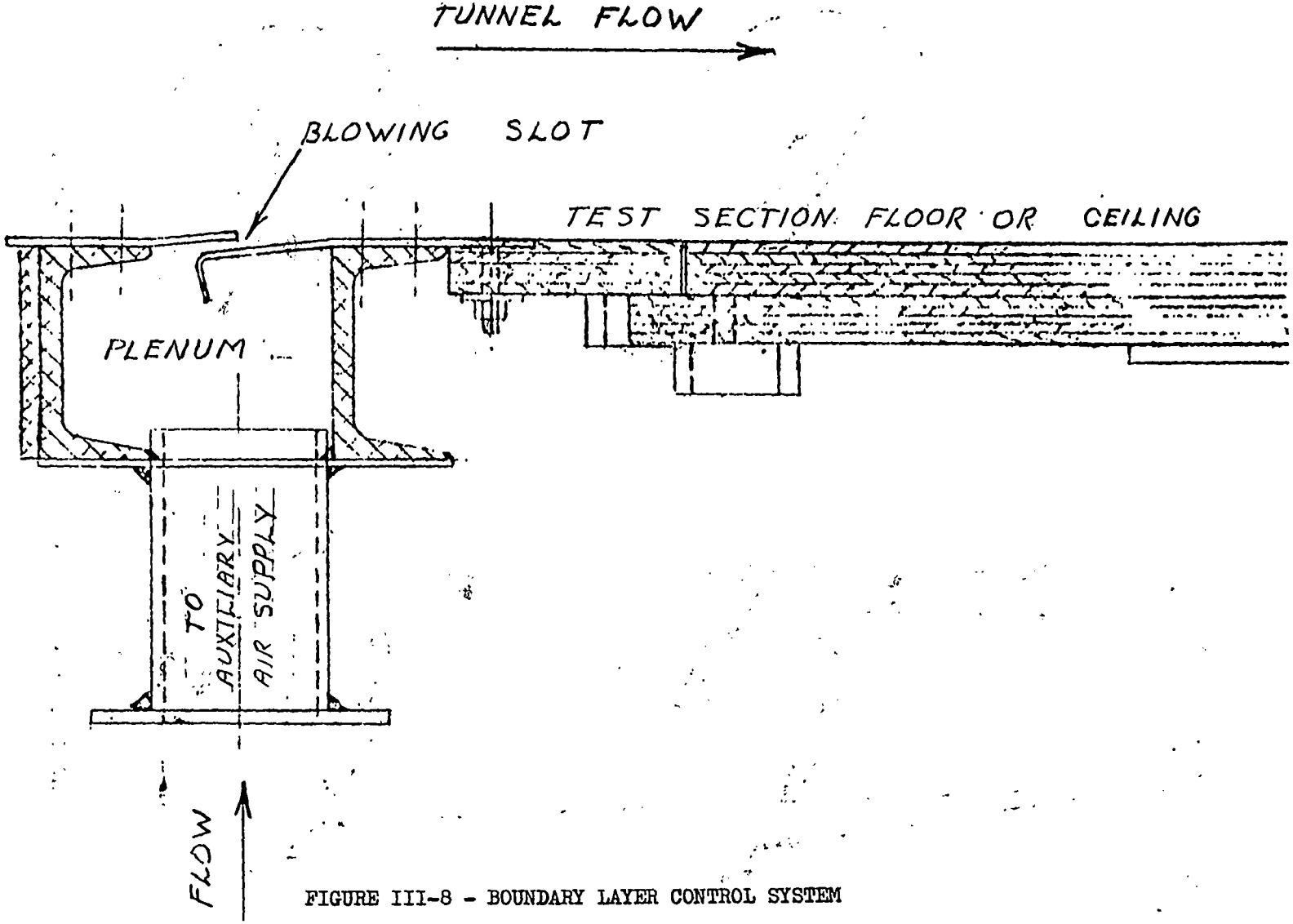

FIGURE III-8 - BOUNDARY LAYER CONTROL SYSTEM

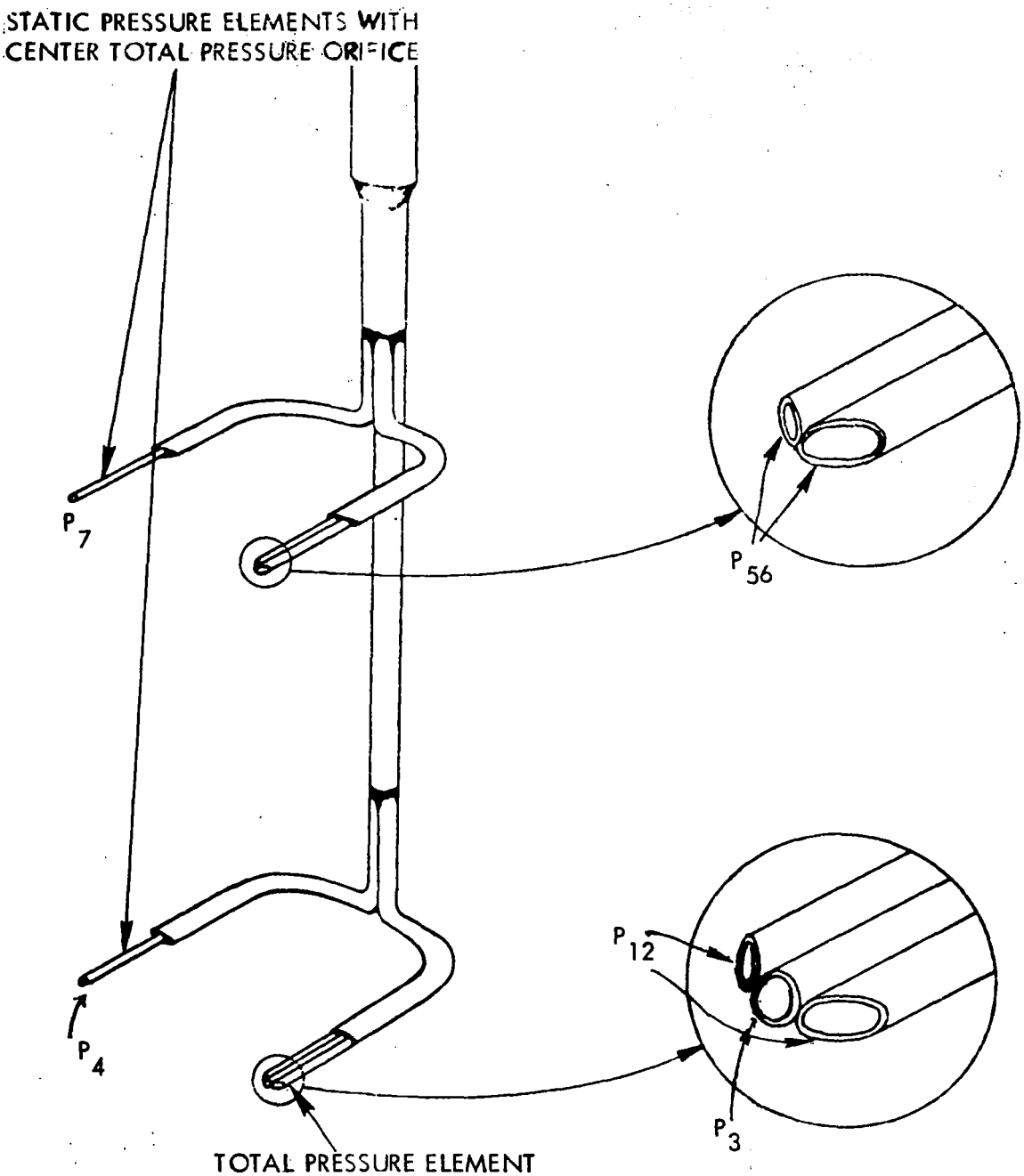

FIGURE III-9 - TOTAL-STATIC PRESSURE PROBE COMBINATION

$$\frac{1}{2}\rho u^2 = K\,(P_1 - P_2) \qquad \text{(III-1)}$$

where ρ = density
u = local velocity
P_1 and P_2 = pressure sensed at different hole positions, and
K = calibration factor and may depend on wind speed.

Probe tip design which has been fabricated in order to remove the above-mentioned sensitivities, and hence to be able to measure local velocity and static pressure to desired accuracy are shown in Figures III-9 and III-10. The upper and lower right-hand elements are designed to measure both static and total pressures. The lower left-hand element is designed to measure total pressure only. The total pressure tubes on the lower element thus provide a check or comparison. The upper element is used when the thickness of boundary layer exceed 7.62 centimeters.

The left-hand, or total pressure, element is constructed of 0.0508 centimeter diameter stainless steel tubing which has been flattenee at the end as shown in Figure III-10. Measurement of total pressure within .01015 centimeters of the model surface are possible with this arrangement. The two side orifices were tied together and used to measure static pressure in the boundary layer. They were formed by beveling the side tubes 30 degrees as shown in Figure III-10.

The beveled tubes on the upper and lower elements measure the pressure which is proportional to the difference between total and static pressure and this measured pressure is related to local dynamic pressure by a calibration factor. Thus, a calibration of the probe reading versus true static and total pressure is necessary. Calibration of the probe was accomplished in the wind tunnel using the pitot tube shown in Figure III-11 as a reference. The calibration curves for this probe are shown in Figure III-12. The above calibration was performed in the absence of the solid boundary and therefore the correction due to the presence of wall proximity has to be used when velocity profile measurements near the solid surface are desired. It has been found by MacMillan (Reference 4) that, for a pitot tube of ratio $d/D = 0.6$, the measured value of total pressure is less than the true value when the probe is nearer than 2D to a solid boundary; here d is equal to internal diameter of the tubing and D is equal to outside diameter of the tubing for the total pressure tube. This wall proximity correction curve, which is obtained from Reference 4, is shown in Figure III-13. Thus, total pressure, static pressure, and dynamic pressure at a desired point in the boundary layer is determined from measurements by probe, which is shown in Figure III-9, as given by the following expressions:

$$P_{T_c} = P_T + P_{T_{wc}}$$

$$q = \frac{1}{2}\rho u^2 = K_{C_L}\,(P_{T_c} - P_{12})$$

$$P_{S_c} = P_{T_c} - K_{C_L}\,(P_{T_c} - P_{12})$$

$$u = \sqrt{\frac{2q}{(P_{S_c}/RT)}}$$

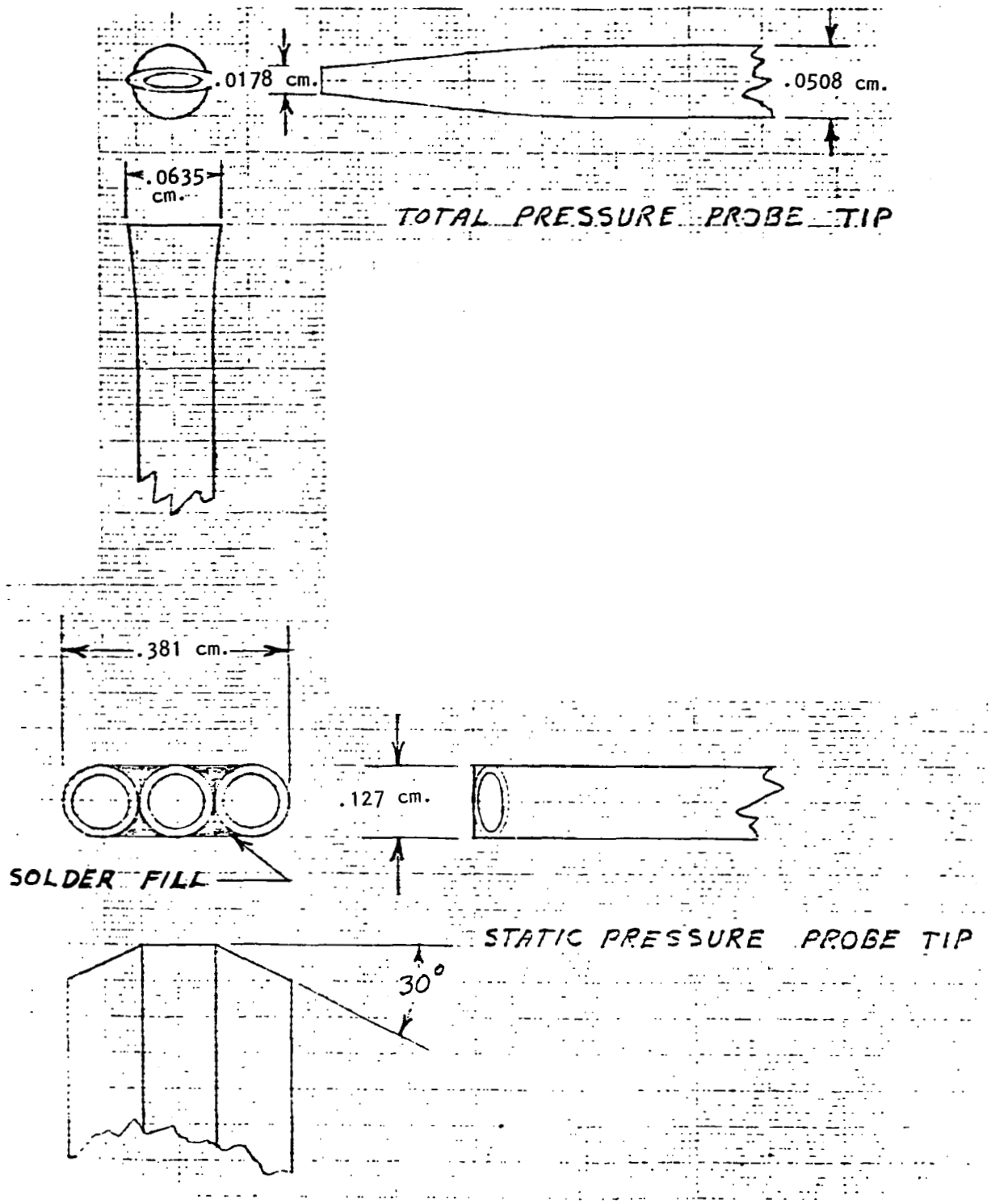

FIGURE III-10 - DETAILS OF BOUNDARY LAYER PROBES

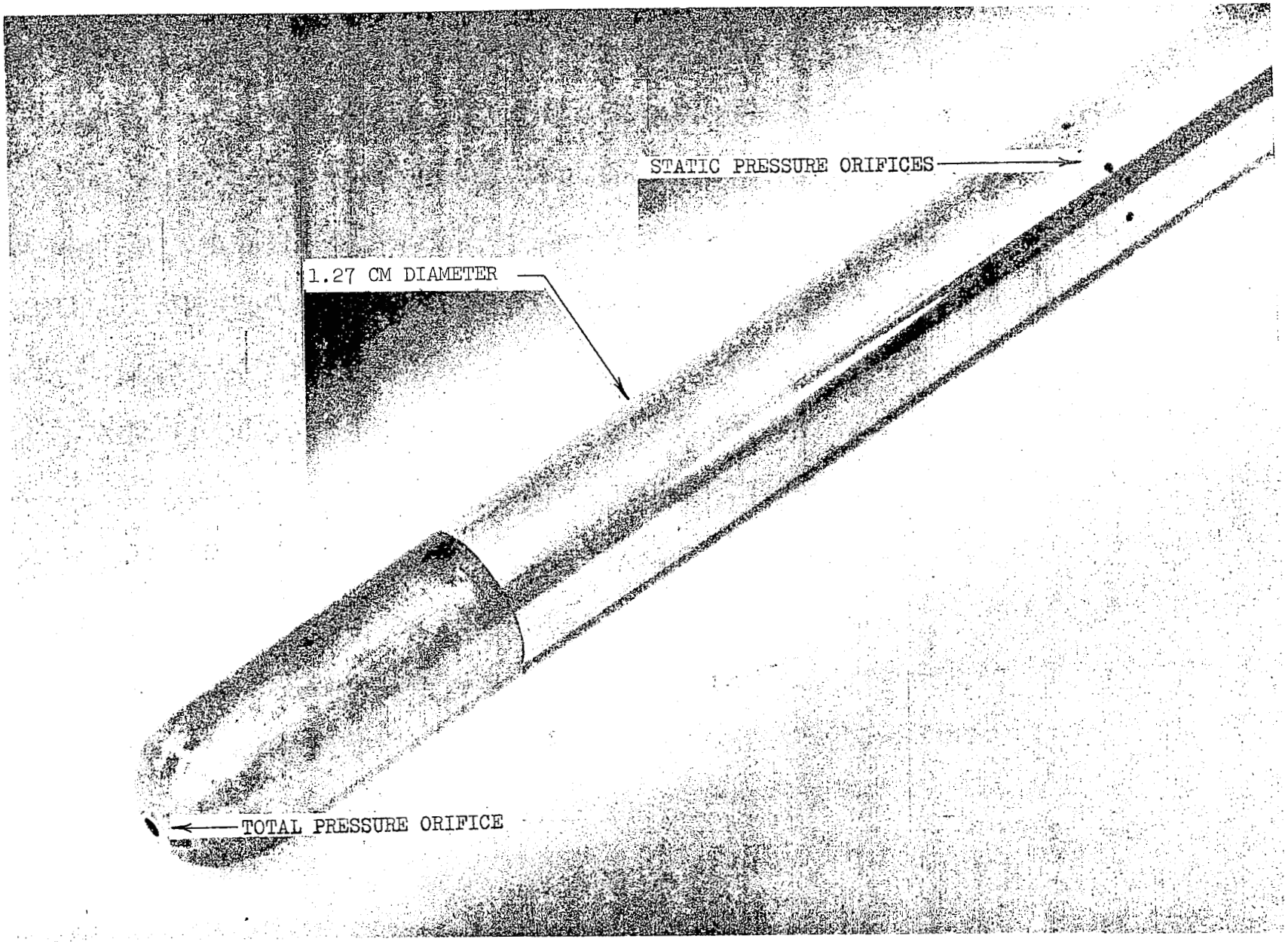

Figure III-11 - CALIBRATION PITOT TUBE

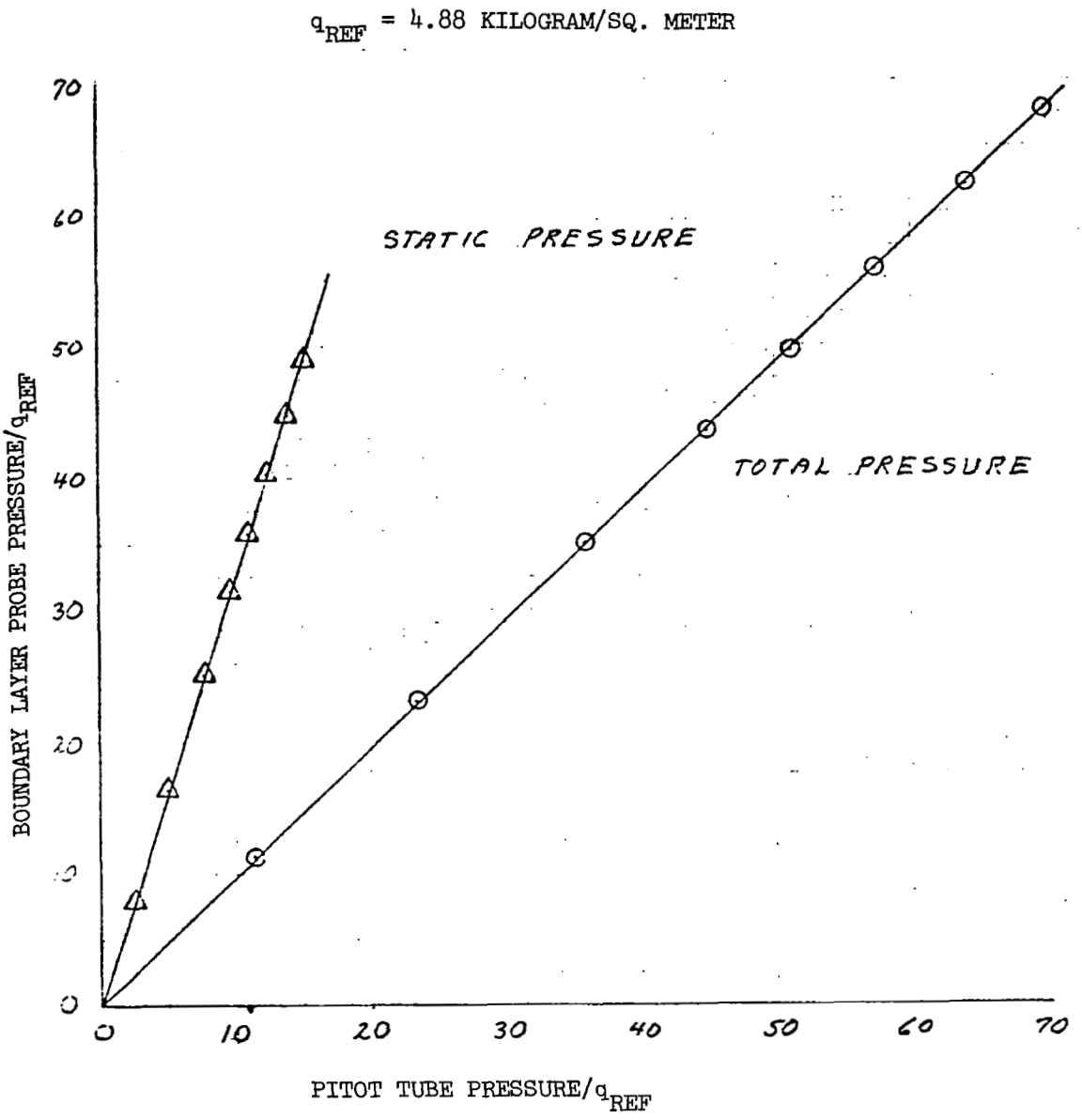

FIGURE III-12 - BOUNDARY LAYER PROBE CALIBRATION

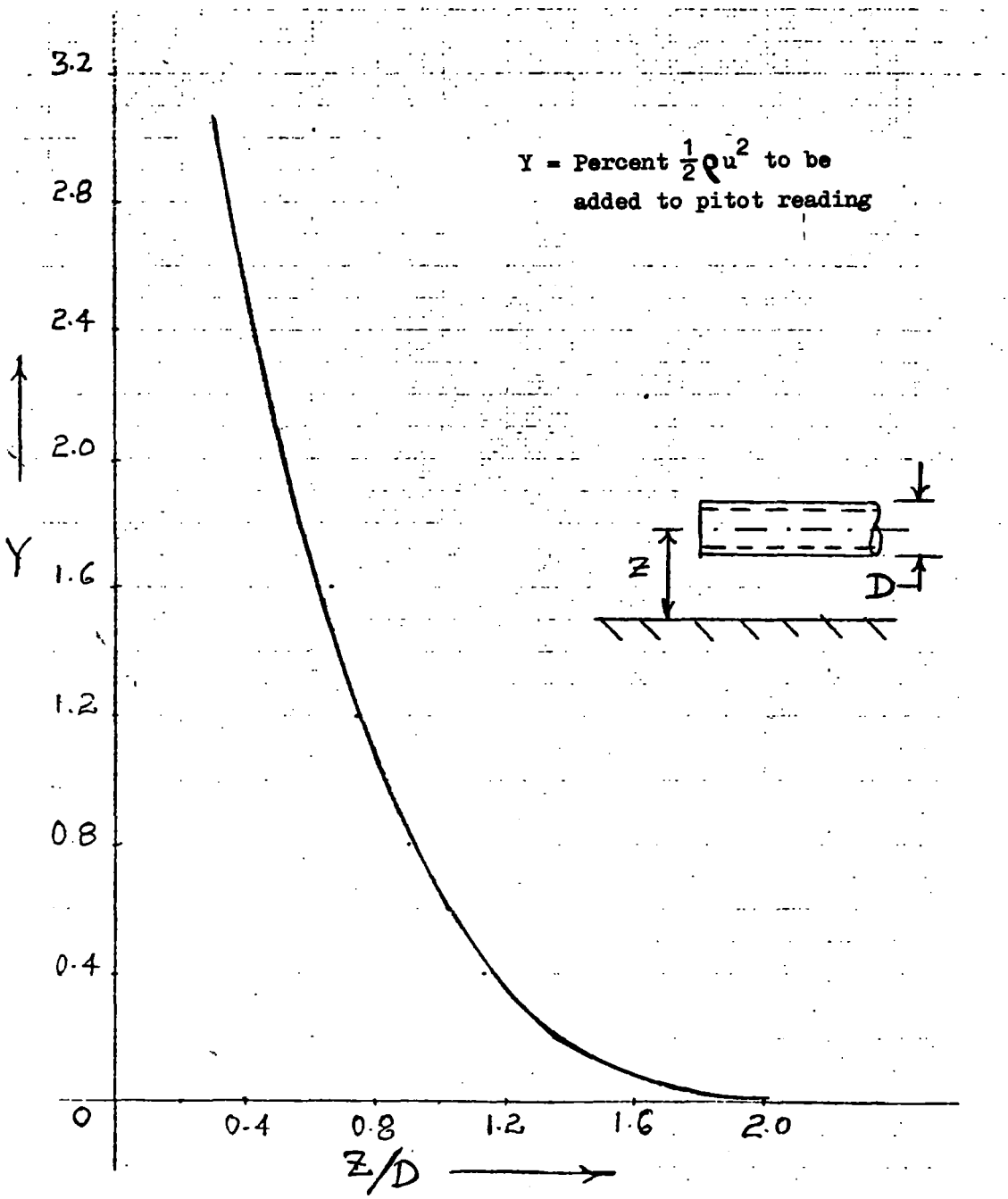

FIGURE III-13 - WALL PROXIMITY CORRECTION FOR TOTAL PRESSURE TUBE MEASUREMENTS

where P_{T_c} = corrected value of total pressure

P_T = total pressure measured by total pressure tube P and corrected by the use of Figure III-12

$P_{T_{wc}}$ = wall proximity correction from Figure III-13

P_{S_c} = corrected value of static pressure

K_{C_L} = calibration factor for obtaining static pressure from measured pressure by beveled tube P_{12} by the use of curves in Figure III-12

u = local velocity in boundary layer

R = universal gas constant

and T = absolute temperature in boundary layer.

III.3.2 Hot Wire Anemometer Probe: The hot wire anemometer is a very desirable instrument for the analysis of the micro structure of the velocity of a streaming gas or liquid. Measurements of the micro structure of a stream require a very small sensitive element having a short response time, sufficient sensitivity and little disturbing effect on the original stream. The sensitive element is a thin electrically heated wire suspended between two needle points or a thin electrically heated metal film fused to a glass support. Figure III-14 shows the sketch of hot wire anemometer probe; also shown in this figure is the enlarged view of the single sensor and sensor support used during the present investigation.

The use of a hot sensing element for measurements of particle velocity in fluid flows relies on laws governing convective heat transfer. These laws are generally too complicated to permit a theoretical calculation of the relation between the particle velocity and the heat flux from a probe, and the relation must therefore be found experimentally using laws of similarity. The expression for the heat flux for the two-dimensional heat transfer in an incompressible potential flow is given by

$$Q = K_\ell \{1 + \sqrt{(2\pi\rho C_p dU/K)}\} (T - T_o) \qquad (III-3)$$

where Q = heat flux
K = thermal conductivity
ℓ = length of wire
ρ = density of fluid
C_p = constant pressure specific heat of fluid
d = diameter of wire
U = flow velocity
T = film temperature
T_o = fluid temperature.

For thermal-equilibrium conditions, the rate of heat loss from the hot wire must be equal to the heating power generated in the wire by the electric current. i.e. it must equal to I^2R/J. Thus, from the point of view of hot wire anemometry,

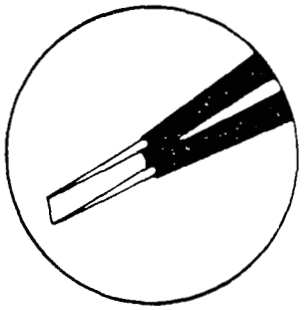

3 TIMES ACTUAL SIZE

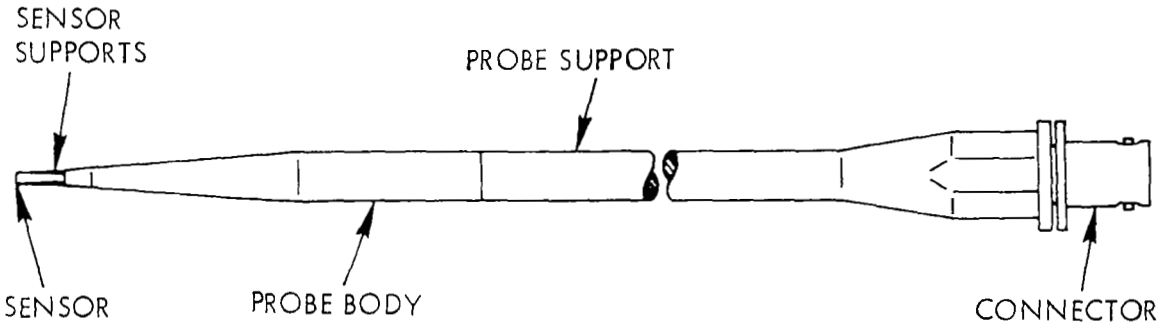

FIGURE III-14 - HOT WIRE ANEMOMETER PROBE WITH SINGLE SENSOR

the relation between fluid particle velocity and electrically generated heating power takes the following form:

$$\frac{R}{R - R_o} I^2 = A + B\sqrt{U} \qquad \text{(III-4)}$$

where A and B are constant for a specific probe wire operating in a specific fluid,

u = local velocity
I = heating current
R = operating resistance of hot wire
R_o = resistance of hot wire at fluid temperature.

However, empirical formula for the heat loss from a hot wire is generally written as,

$$\frac{R}{R - R_o} I^2 = A + B\,(u)^n \qquad \text{(III-5)}$$

and the values of A, B and n are determined from calibration. The output of the anemometer is a bridge voltage V, and the squared voltages V^2 and V_o^2 (V_o = bridge voltage when the flow velocity is zero) are linearly related to the heat loss of the wire at the velocity in question and at zero velocity respectively. At very low velocities, the heat loss due to forced convection is a minor part of the total heat loss, resulting in a typical calibration curve shown in Figure III-15(a). In cases where measurements of high degrees of turbulence are concerned, such as in wake flow behind airfoil, or where large series of measurements are to be performed over a wide velocity range at a great number of points, such as in the case of boundary layer measurements over the surface of an airfoil, it is necessary to linearize the anemometer output voltage in order to avoid nonlinear distortion and ensure rational operation. Figure III-15(b) shows the plot of anemometer output voltage versus flow velocity made in conjunction with hot wire anemometer.

There are two modes of operation for the hot-wire anemometer, namely, (i) constant-current operation and (ii) constant-temperature operations. The constant current operation has the advantage of simpler electronic circuitry, however, constant temperature operation is more suited for measurements of fluctuations of high frequencies such as turbulent flows and measurements of a boundary layer where velocity varies from essentially zero near the wall to large value at the edge of the boundary layer in a small boundary layer thickness. Another advantage of constant temperature operation is the possibility of obtaining greater flow sensitivity using high overheating with no risk of probe burn out owing to sudden velocity decrease. For these reasons the constant temperature operation for hot wire anemometer was used during the present experimental measurements in the case of blunt trailing edge airfoil test. The constant temperature operation is briefly described in the following paragraph.

Figure III-16 shows the schematic diagram of the principle of constant temperature operation. The idea behind the constant temperature system is to minimize the effect of thermal inertia of the probe by keeping the sensitive

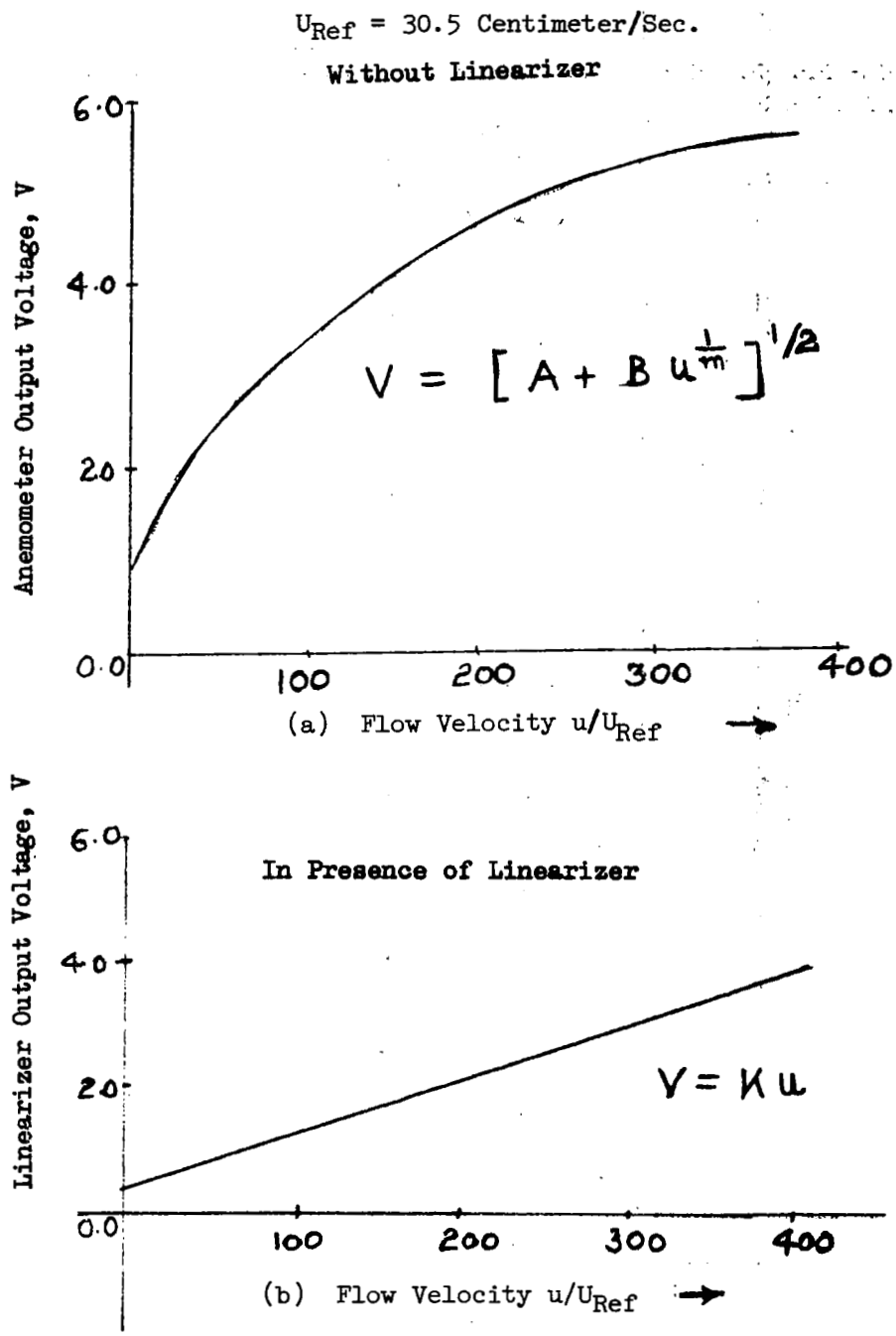

FIGURE III-15 - RELATION BETWEEN ANEMOMETER VOLTAGE AND FLOW VELOCITY WITH AND WITHOUT THE USE OF LINEARIZER

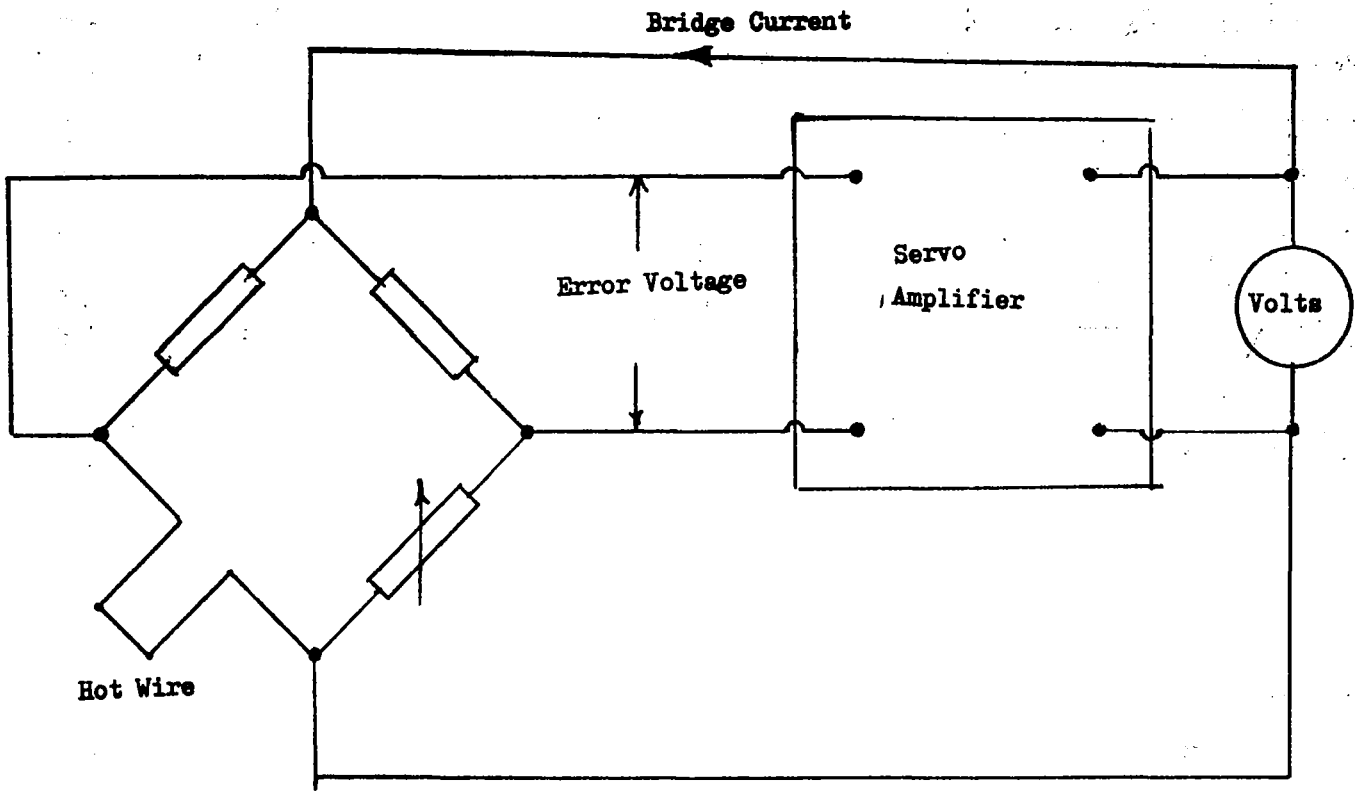

FIGURE III-16 - PRINCIPLE OF CONSTANT TEMPERATURE ANEMOMETER

element at a constant temperature and using the heating current as the measure of heat transfer and hence velocity. The principle requires a sophisticated and well-designed electronic system, and it can be explained with the aid of Figure III-16. Under conditions of bridge balance a voltage is present across the vertical bridge diagonal. This voltage is supplied by the servo amplifier. A slight change in the convective cooling of the sensor will cause a small voltage to appear across the horizontal diagonal. The latter voltage, after having undergone considerable amplification, is fed back to the vertical bridge diagonal, its polarity being selected so that it will automatically balance the bridge. In this way the temperature variations of the hot wire are kept extremely small.

III.3.3 Probe Drive Mechanism: Boundary layer surveys, both on the upper surface of the airfoil as well as in the wake behind airfoil trailing edge, were obtained by using an automatic probe drive unit to position the probe at pre-selected heights above the model surface. This unit, which is shown in Figure III-17, was mounted on the outside wall of the test section with the probe extending through the wall into the test section. Figure III-18 shows the typical model installation in the wind tunnel facility and the boundary layer probe arrangement. This boundary layer probe can be located at any chordwise location on the airfoil as well as in the wake aft of the airfoil trailing edge. This probe is driven in the direction perpendicular to the local airfoil contour or normal to the airfoil chord line extended in the airfoil wake. The probe drive units consist of a 28-volt gear motor, lead screw, drive nut, and position potentiometer. A maximum of 50 pre-selected probe positions may be input to the data acquisition program. During the run the program will signal the gear motor to drive the probe assembly to each position in sequence and pause while the data are read by a scanivalve and transducer located outside the test section. Minimum increment of probe travel is .0318 centimeters. Maximum travel is 8.9 centimeters. Limit switches are provided to protect the mechanism and prevent the probe from crashing into the model.

A multi-post scanivalve and pressure transducer were used to read the probe pressures. The transducer is rated at 0.175 kilogram per square centimeter differential.

III.4 Data Acquisition, Reduction and Analysis Technique

Figure III-19 shows the schematic diagram of the system used for the acquisition and reduction of the raw test data. The heart of the system is a Lockheed Electronics MAC 16 computer. The raw data was made available, in an abbreviated form, on teletype for outline monitoring of the test, and in its entirety on paper tape using a high speed punch. Final data reduction was accomplished on a Univac 1106 Central Computing System with remote access terminals. General description of Data Acquisition Unit and MAC 16 computer is given in Appendix C. In this section, however, main equations used in the reduction of data are given and the technique and the computer program for the analysis of data in the airfoil wake is described in brief.

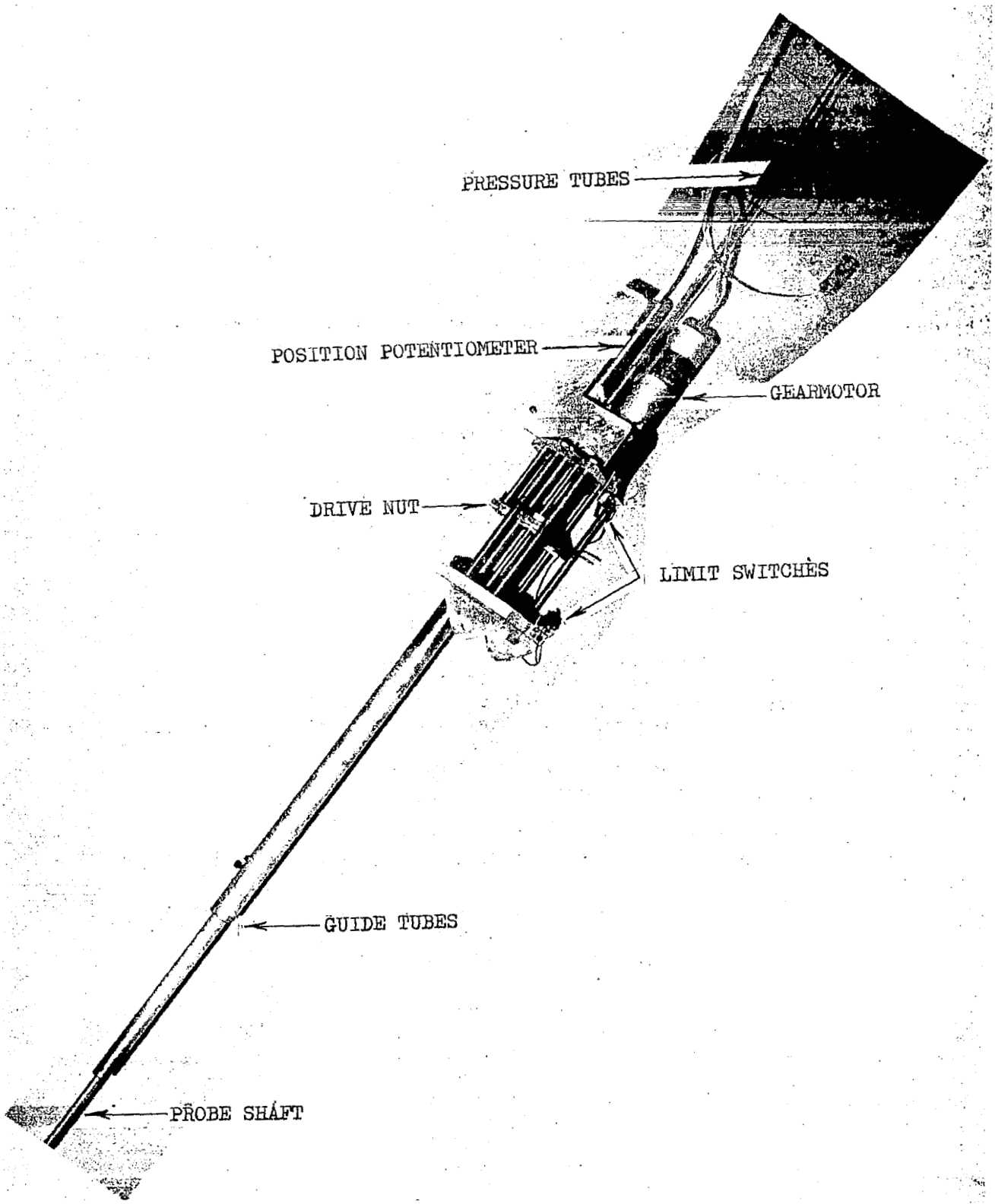

Figure III-17 - PROBE DRIVE UNIT

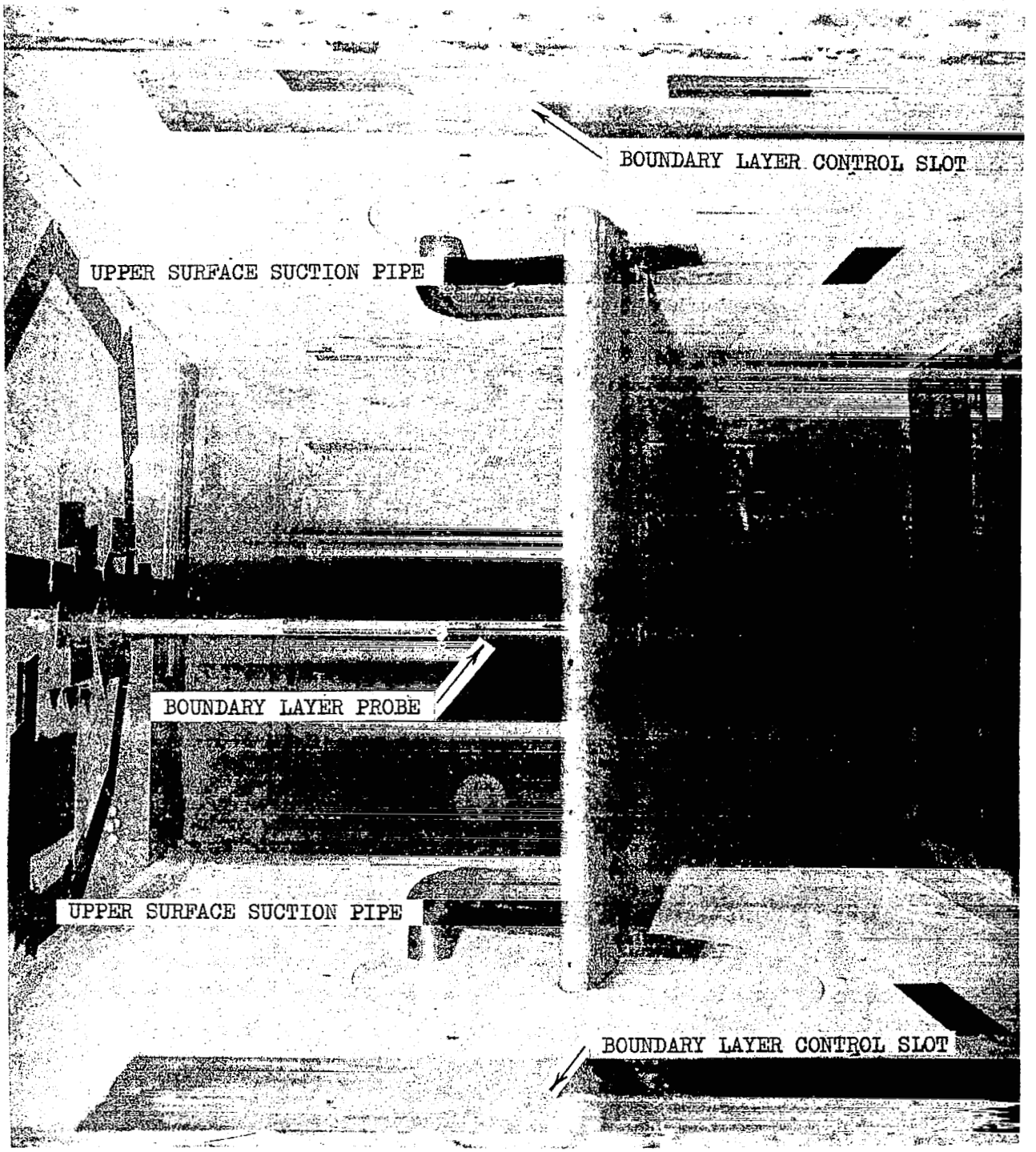

FIGURE III-18 - MODEL INSTALLATION - FRONT VIEW

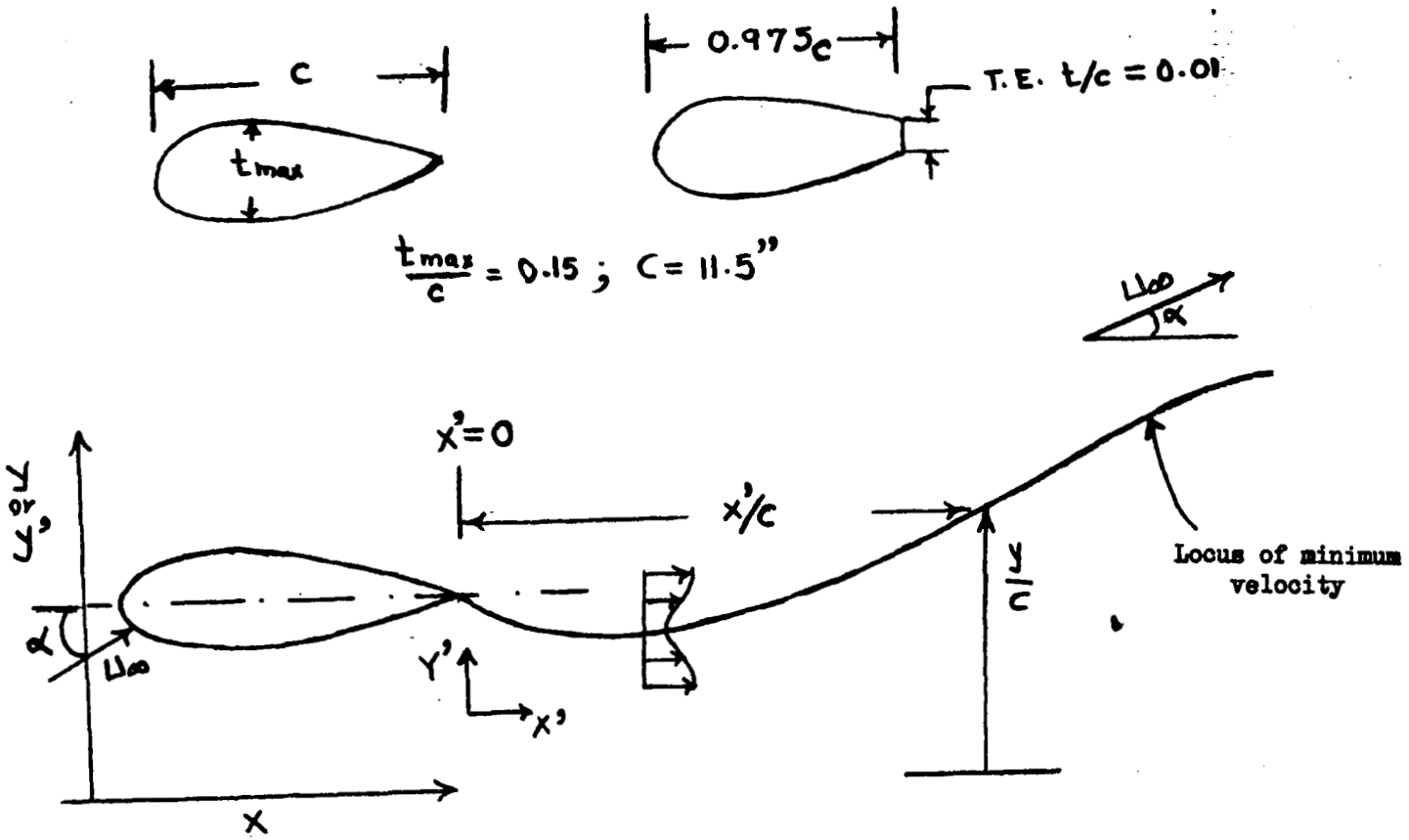

FIGURE III-19 - SCHEMATIC REPRESENTATION OF TYPES OF MODELS FOR TEST AND COORDINATE SYSTEM FOR MEASUREMENTS

III.4.1 Data Reduction Equations: Tunnel conditions acquired at each data point consisted of the dynamic pressure q_m, the total pressure H_m, and the total temperature T_m. In addition the barometric pressure P_a is obtained from a thumb-wheel switch input. These conditions are corrected to free stream condition using standard procedure.

An initial estimate of the free stream Mach number,

$$M^2_{est} = \frac{q_m}{0.7\ P_a\ (1 + .000171\ q_m)} \qquad \text{(III-6)}$$

from which the compressible dynamic pressure is,

$$q = q_m\ (1 + K\ (2 - M^2_{est})) \qquad \text{(III-7)}$$

where K is the solid blockage factor calculated as,

$$K = \frac{K_1 \tau\ V_w}{(C\ (1 - M^2_{est})^{3/2}} + \left(\frac{1 + 0.4\ M^2_{est}}{1 - M^2_{est}}\right)\left(\frac{0.5\ C_{D_m}\bar{c}}{W_t}\right) \qquad \text{(III-8)}$$

where K_1 = wing blockage shape factor

τ = blockage correction factor relating model span to tunnel width

V_w = model volume (cubic feet)

C_1 = tunnel cross-sectional area (square feet)

C_{D_m} = model drag coefficient

$\bar{c}$ = model chord

and W_t = tunnel width (ft)

The free stream total pressure is

$$P_{T_c} = H_m + K_{H_1}\ q_m + K_{H_2}\ q_m^2 + P_a \qquad \text{(III-9)}$$

where K_{H_1} and K_{H_2} are airstream calibration constants for the test section.

The free stream static pressure, mach number, static temperature and density can now be calculated as,

$$P_{S_\infty} = P_{T_\infty} - q_\infty$$

$$M_\infty = \left\{5\left(\frac{P_{T_\infty}}{P_S}\right)^{.286} - 5\right\}^{1/2}$$

$$T_\infty = \frac{T_m + 459.6}{1 + .2\ M_\infty^2}$$

$$\rho_\infty = .0005826\left(\frac{P_{T_\infty}}{T_\infty}\right) \qquad \text{(III-10)}$$

The finally reduced data assumes incompressible flow conditions and are therefore based on

$$q_o = \frac{q_\infty}{1 + \frac{M_\infty^2}{4} + \frac{M_\infty^4}{40} + \frac{M_\infty^6}{1000}} \qquad \text{(III-11)}$$

and

$$\rho_o = \rho_\infty\ (1 - .2\ M_\infty^2)^{2.5}.$$

Denoting the static pressure measured during the surveys as P_s then,

$$C_P = \frac{P_s - P_\infty}{q_o} \qquad \text{(III-12)}$$

from which the local Mach number and density are obtained...

$$M_e = \left[5\left\{\frac{1 + 0.2\ M_\infty^2}{(1 + .7\ M_\infty^2\ C_p)^{.286}} - 1\right\}\right]^{1/2} \qquad \text{(III-13)}$$

and

$$\rho_e = \rho_o\left(\frac{1 + .2\ M_\infty^2}{1 + .2\ M_e^2}\right)^{2.5}$$

III.4.2 Data Analysis Technique: A computer program was formulated for the data analysis of the experimental measurements obtained in the viscous flow in the wake. Experimentally measured variations across the airfoil wake, values of total pressure, static pressure, ambient temperature, free stream dynamic head and barometric pressures at two closely spaced X locations constitute the input to the computer program for the data analysis. This program then calculates and prints out the following information:

(1) nondimensional velocity profiles at two stations,

(2) shear stress distribution across the viscous layer between two stations,

(3) mixing length distribution, eddy viscosity ratio distribution, and slope of the velocity profiles at various y locations for the station between input stations X_1 and X_2,

(4) turbulent dissipation or shear work integral, displacement thickness, momentum thickness and energy thickness at both stations,

(5) similarity parameters for velocity profile and values of similarity functions at both stations, and

(6) various integrals at each station, such as

$$\int_0^{y_1} \frac{u}{U_e}\, dy, \quad \int_0^{y_1} \left(\frac{u}{U_e}\right)^2 dy, \quad u(y_1)\cdot \int_0^{y_1} \frac{u}{U_e}\, dy ,$$

and

$$u(y_1)\cdot \int_0^{y_1} \left(\frac{u}{U_e}\right)^2 dy ,$$

where y_1 is any distance above the lower edge of wake in the viscous region and $u_{(y_1)}$ is the velocity at distance y above the lower edge of wake.

In order to calculate the shear distribution, eddy viscosity ratio and variation of mixing length across the airfoil wake the use of the following basic equations was made:

$$\rho V = -\int_0^{y} \frac{\partial}{\partial x}(\rho_u)\, dy + \rho_o V_o \qquad \text{(III-14)}$$

$$\rho_u \frac{\partial u}{\partial x} + \rho_v \frac{\partial u}{\partial y} = -\frac{\partial p}{\partial x} + \frac{\partial \tau}{\partial y}. \qquad \text{(III-15)}$$

The Euler equation at the upper and lower edges of the wake is given by

$$\frac{dP_{e_L}}{dx} = -\rho_{e_L} U_{e_L} \frac{dU_{e_L}}{dx}; \quad \frac{dP_{e_u}}{dx} = -\rho_{e_u} U_{e_u} \frac{dU_{e_u}}{dx} . \qquad \text{(III-16)}$$

By integrating equation (III-15) from $y = 0$ (lower edge of wake) to $y = y_1$, making use of equations (III-14) and (III-16), and using Leibnitz's rule and integration by parts, the following equation can be derived after some algebraic simplification:

$$\frac{\tau(y_1)}{\rho_{e_m} U_{e_m}^2} - \frac{\tau_o}{\rho_{e_m} U_{e_m}^2} + \left(\frac{\rho_o}{\rho_{e_m}}\right)\left(\frac{V_o}{U_{e_m}}\right)\left\{\frac{U_{e_L}}{U_{e_m}} - \frac{U(y_1)}{U_{e_m}}\right\}$$

$$= + \frac{d}{dx}\left[\int_o^{y_1}\left(\frac{\rho}{\rho_{e_m}}\right)\left(\frac{u}{U_{e_m}}\right) dy\right] - \left(\frac{u(y_1)}{U_{e_m}}\right)\frac{\partial}{\partial x}\left[\int_o^{y_1} \frac{\rho}{\rho_{e_m}} \frac{u}{U_{e_m}} dy\right]$$

$$+ \left(\frac{0.5}{U_{e_m}}\right)\left(\frac{dU_{e_m}}{dx}\right)\left[\int_o^{y_1}\left\{\left(\frac{\rho}{\rho_{e_m}}\right)\left(\frac{u}{U_{e_m}}\right)^2 - \left(\frac{U(y_1)}{U_{e_m}}\right)\left(\frac{\rho}{\rho_{e_m}}\right)\left(\frac{u}{U_{e_m}}\right)\right\} dy\right]$$

$$+ \left(\frac{0.5}{U_{e_m}}\right)\left(\frac{dU_{e_m}}{dx}\right)\left[\int_o^{y_1}\left\{\left(\frac{\rho}{\rho_{e_m}}\right)\left(\frac{u}{U_{e_m}}\right)^2 - \left(\frac{U_{e_u}}{U_{e_m}}\right)\frac{\rho_{e_u}}{\rho_{e_m}}\right\} dy\right]$$

$$+ \left(\frac{0.5}{U_{e_m}}\right)\left(\frac{dU_{e_L}}{dx}\right)\left[\int_o^{y_1}\left\{\left(\frac{\rho}{\rho_{e_m}}\right)\left(\frac{u}{U_{e_m}}\right)^2 - \left(\frac{U(y_1)}{U_{e_m}}\right)\left(\frac{\rho}{\rho_{e_m}}\right)\left(\frac{u}{U_{e_m}}\right) dy\right]\right.$$

$$+ \left(\frac{0.5}{U_{e_m}}\right)\left(\frac{dU_{e_L}}{dx}\right)\left[\int_o^{y_1}\left\{\left(\frac{\rho}{\rho_{e_m}}\right)\left(\frac{u}{U_{e_m}}\right)^2 - \left(\frac{U_{e_L}}{U_{e_m}}\frac{\rho_{e_L}}{\rho_{e_m}}\right)\right\} dy\right]$$

$$+ \left(\frac{0.5}{U_{e_m}^2}\frac{1}{\rho_{e_m}}\right)\left[\int_o^{y}\left(\frac{\partial P}{\partial x} - \frac{dP_{e_u}}{dx}\right) dy\right]$$

$$+ \left(\frac{0.5}{U_{e_m}^2}\frac{1}{\rho_{e_m}}\right)\left[\int_o^{y_1}\left(\frac{\partial P}{\partial x} - \frac{dP_{e_L}}{dx}\right) dy\right] \qquad \text{(III-17)}$$

In the above equation the symbols have the following meaning:

y_1 = distance above the lower edge of wake

U_{e_L} = average velocity at the lower edge of wake for stations X_1 and X_2

U_{e_u} = average velocity at the upper edge of wake for stations X and X

U_{e_m} = $\frac{1}{2}$ $(U_{e_L} + U_{e_u})$

y_o = lower edge of wake

V_o = y component velocity at lower edge of wake

P_{e_u} = average value of pressure at the upper edge of wake

P_{e_L} = average value of pressure at the lower edge of wake

ρ_{e_u} = average value of density on the upper edge of wake between stations X_1 and X_2

ρ_{e_L} = average value of density on the lower edge of wake between stations X_1 and X_2

$\rho_{e_m} = \frac{1}{2}(\rho_{e_u} + \rho_{e_L})$

$\tau(y_1)$ = value of shear stress at $y = y_1$

$\tau(y_o)$ = value of shear stress at lower edge of wake

= 0

The right-hand side of equation (III-17) was programmed to compute shear stress $\tau(y_1)$ at various distances, y_1, above the lower edge of the wake. Values of shear stresses at the lower and upper edges of the wake were assumed to be zero. The same equation and the same numerical procedure was used to compute shear distribution, eddy viscosity ratio and turbulent dissipation in the various regions of the wake flow behind the airfoil trailing edge.

III.4.3 Determination of Profile Drag from Experimental Measurements in the Wake: The expression due to Betz, Reference 11, for the computation of profile drag of airfoil from the measurements of total pressures and static pressures across the wake behind the airfoil is given by:

$$C_D = \int \left\{ \frac{P_{T_\infty} - P_{T(y)}}{q} \right\} d\,(y/c) + \int \left[\left\{ \left(\frac{P_{T_\infty} - P_{T(y)}}{q_\infty} \right)^{\frac{1}{2}} - \left(\frac{P_{T(y)} - P_{S(y)}}{q} \right)^{\frac{1}{2}} \right\} \cdot \left\{ \left(\frac{P_T - P_{S(y)}}{q_\infty} \right)^{\frac{1}{2}} + \left(\frac{P_{T(y)} - P_{S(y)}}{q_\infty} \right)^{\frac{1}{2}} - 2 \right\} \right] d\,(y/c) \qquad \text{(III-18)}$$

where C_D = profile drag coefficient of an airfoil

$P_{T_\infty} = P_{T_e}$ = total pressure of free stream

$P_{S(y)}$ = static pressure across the wake

q_∞ = free stream dynamic head = $\frac{1}{2}\rho U_\infty^2$

P_∞ = free stream static pressure

C = airfoil chord

If static pressure $P_{s(y)}$ in the above equation (III-18) is assumed to be constant and equal to the free stream static pressure, the equation (III-18) can be simplified to,

$$C_D = \int \left\{ -2\left(\frac{P_{T(y)} - P_\infty}{q_\infty}\right) + 2\left(\frac{P_{T(y)} - P_\infty}{q_\infty}\right)^{\frac{1}{2}} \right\} d\ (y/c)$$

or

$$C_D = 2\int -\left(\frac{u}{U_\infty}\right)^2 + \left(\frac{u}{U_\infty}\right) d\ y/c = 2\int \frac{u}{U_\infty}\left(1 - \frac{u}{U_\infty}\right) d\ y/c$$

or

$$C_D = 2\,\frac{\theta_\infty}{c} \qquad \text{(III-19)}$$

where θ_∞ = momentum thickness in the wake far downstream of airfoil trailing edge where static pressure has stabilized to the free stream value.

III.5 Types of Tests

Experimental data were obtained for model under two conditions, namely (i) sharp trailing edge airfoil, and (ii) blunt trailing edge airfoil. In the case of blunt trailing edge airfoil, the trailing edge thickness was kept at 1 percent of the airfoil chord. Airfoil chord c is equal to 29.2 centimeters and the value of the maximum thickness of the airfoil tested is 15 percent. The chord of the blunt trailing edge airfoil is approximately equal to 0.975c where c is the chord of the airfoil with the sharp trailing edge. This is shown schematically in Figure III-19 which also shows the coordinate system under which measurements are obtained during the tests.

All the measurements taken during the tests were obtained at free stream Mach number of approximately 0.2 and free stream dynamic head of 60 psf. These conditions would correspond to the free stream Reynolds number during the tests of approximately 1.3 to 1.4 million based on the chord of the airfoil. Measurements were obtained at angles of attack between 0° and angle of attack corresponding to the occurrence of incipient separation on the upper surface of the airfoil in the neighborhood of the trailing edge; the latter condition corresponds to $\alpha \simeq 10.8^\circ$ for the test airfoil. Measurements taken during the tests can be classified by two categories namely (i) measurements of pressure distribution on the surface of the airfoil and (ii) viscous flow measurements. Measurements of the viscous flow were obtained both on the upper surface of the

airfoil in the neighborhood of the trailing edge as well as in the airfoil wake at several chordwise locations.

In the case of test airfoil with the sharp trailing edge the viscous flow measurements were obtained by the use of total-static pressure probe which is shown in Figure III-9. For the test airfoil with the blunt trailing edge, the viscous flow measurements were obtained by use of hot wire anemometer probe which is shown in Figure III-14. Figures III-20, III-21 and III-22 show the plots of measured pressure distributions and loci of minimum velocity for the airfoil with the sharp trailing edge. Boundary layer surveys in the airfoil wake have been obtained at x'/c locations shown in Figures III-20, III-21 and III-22 by triangular symbols. These measurements are tabulated in Table 3-3 for sharp trailing edge airfoil. As seen in this table these measurements at a particular chordwise location x'/c in the wake consist of values of (i) total pressure P_t, (ii) static pressure P_s, (iii) free stream dynamic head q_∞, and (iv) ratio of u/U_∞ at several y locations in the wake flow boundary layer.

Figure III-23, III-24 and III-25 show the plot of measured pressure distributions on the airfoil surface and the loci of minimum velocity in the wake of blunt trailing edge test airfoil. Boundary layer surveys are obtained, by the use of hot wire anemometer probe, at the chordwise locations s'/c indicated by the triangular symbols on measured loci in the above figures. The boundary layer surveys consist of measurements of u/U_∞ or u/U_e and q_∞ for several y values and for a given chordwise location x'/c. These measurements are tabulated in Table 3-4.

IV. RESULTS AND DISCUSSION

In the previous section the description of experimental facility, type and number of experimental measurements and the computer program for the analysis of the fundamental wake flow parameters was given. From the output of this computer program various physical parameters for the flow in the wake of single component airfoils are studied. The relationships among various physical parameters, which appeared in theoretical equations of Section II, are derived and described in this section. Establishment of these relationships between various physical parameters is of vital importance for the prediction of drag of arbitrary configuration single or multi-component airfoils by the generalized theoretical method such as described in this report.

IV.1 Presentation of Typical Measured Experimental Data

Figures IV-1 through IV-5 show the measurements of velocity profile on the upper surface of the test airfoil with sharp trailing edge. These measurements were performed by use of total-static pressure probe combination shown schematically in Figure III-9. This type of boundary layer measurements on the surface of the airfoil were obtained for the purpose of determining (i) the approximate location of the point of incipient separation on the airfoil

Table 3-3 - MEASUREMENTS IN THE WAKE OF SHARP T.E. TEST AIRFOIL BY THE USE OF TOTAL STATIC PRESSURE PROBE COMBINATION

Station 1; q_{ref} = 4.88 kilogram/square meter
x'/C = 0.017; α = 0.0°
Free Stream Total Pressure/q_{ref} = 2103.3
Free Stream Static Pressure/q_{ref} = 2038.3
Free Stream Total Temperature = 308° K

y/c	$\frac{q_\infty}{q_{ref}}$	$\frac{P_t}{q_{ref}}$	$\frac{P_s}{q_{ref}}$	$\frac{u}{U_\infty}$
-.0911	61.36	2105.0	2052.2	.9067
-.0548	61.15	2105.0	2052.8	.9012
-.0304	61.36	2102.3	2053.4	.8893
-.0861	61.23	2098.8	2054.5	.8662
-.0839	61.31	2096.3	2055.0	.8170
-.0817	61.34	2095.0	2055.3	.7805
-.01955	61.30	2088.8	2055.7	.7313
-.0174	61.19	2086.0	2056.2	.6701
-.0152	61.36	2080.0	2056.5	.6161
-.01305	61.45	2076.5	2057.0	.5611
-.01086	61.28	2072.5	2057.2	.4670
-.0087	61.35	2069.2	2057.4	.4364
-.00652	61.32	2066.8	2057.5	.3875
-.00435	61.34	2065.5	2057.5	.3594
-.00217	61.34	2065.0	2057.5	.3479
0.0	61.43	2066.5	2057.5	.3812
.00218	61.41	2070.0	2057.4	.4510
.00432	61.36	2074.0	2057.3	.5192
.00652	61.41	2077.0	2057.0	.5683
.00872	61.37	2081.2	2056.6	.6305
.01087	61.34	2085.5	2056.2	.6879
.01305	61.41	2089.3	2055.5	.7390
.0152	61.45	2092.3	2052.9	.7775
.0174	61.38	2096.0	2054.5	.8191
.0196	61.39	2098.7	2053.9	.8511
.0217	61.30	2100.5	2053.2	.8729
.0239	61.33	2101.4	2052.5	.8895
.0261	61.35	2102.3	2051.8	.9041
.0304	61.31	2102.8	2051.0	.9154
.0348	61.23	2105.0	2050.5	.9221
.0392	61.31	2105.0	2050.5	.9221

Station 2; q_{ref} = 4.88 kilogram/square meter
x'/c = .044; α = 0.0°
Free Stream Total Pressure/q_{ref} = 2103
Free Stream Static Pressure/q_{ref} = 2038.3
Free Stream Total Temperature = 308° K

y/c	$\frac{q_\infty}{q_{ref}}$	$\frac{P_t}{q_{ref}}$	$\frac{P_s}{q_{ref}}$	$\frac{u}{U_\infty}$
-.0435	61.19	2103.0	2051.5	.9131
-.0991	61.31	2103.0	2051.5	.9131
-.0348	61.31	2102.9	2051.7	.9104
-.0304	61.22	2101.7	2052.1	.8960
-.0861	61.25	2097.8	2053.1	.8505
-.0839	61.20	2095.0	2053.7	.8172
-.0817	61.40	2090.8	2054.2	.7692
-.01955	61.43	2086.7	2054.5	.7215
-.0174	61.20	2082.8	2054.8	.6727
-.0152	61.26	2078.5	2055.0	.6163
-.01305	61.28	2074.5	2055.0	.5614
-.01086	61.33	2071.3	2055.0	.5133
-.0087	61.44	2069.5	2055.1	.4884
-.00652	61.39	2068.7	2055.2	.4671
-.00435	61.76	2068.5	2055.2	.4636
-.00217	61.45	2068.9	2055.2	.4705
0.0	61.58	2070.7	2055.2	.5005
.00218	61.48	2074.5	2055.0	.5614
.00432	61.62	2078.7	2054.9	.6208
.00652	61.30	2082.7	2054.7	.6727
.00872	61.34	2086.0	2054.3	.7159
.01087	61.25	2089.2	2054.0	.7544
.01305	61.41	2093.2	2053.5	.8015
.01580	61.36	2096.2	2053.0	.8360
.0174	61.40	2098.8	2052.5	.8656
.0196	61.20	2100.5	2052.0	.8860
.0217	61.18	2101.9	2051.5	.9055
.0239	61.07	2102.5	2051.0	.9132
.0261	61.21	2102.7	2050.7	.9177
.0304	61.29	2102.8	2050.0	.9244
.0348	61.47	2102.9	2049.9	.9267
.0392	61.30	2103.0	2049.9	.9275
.0435	61.53	2103.0	2049.9	.9275

Station 3; q_{ref} = 4.88 kilogram/square meter
x'/c = .172; α = 0.0°
Free Stream Total Pressure/q_{ref} = 2103.0
Free Stream Static Pressure/q_{ref} = 2038.15
Free Stream Total Temperature = 309° K

y/c	$\frac{q_\infty}{q_{ref}}$	$\frac{P_t}{q_{ref}}$	$\frac{P_s}{q_{ref}}$	$\frac{u}{U_\infty}$
-.0478	61.41	2105.0	2046.5	.9589
-.0435	61.38	2105.0	2046.3	.9589
-.0991	61.42	2102.9	2046.5	.9589
-.0348	61.35	2102.0	2046.6	.9478
-.0304	61.28	2100.2	2047.2	.9869
-.0861	61.40	2095.6	2048.0	.8783
-.0839	61.50	2093.0	2048.2	.8510
-.0817	61.47	2089.5	2048.5	.8150
-.01955	61.41	2086.5	2048.8	.7815
-.0174	61.39	2083.5	2049.1	.7464
-.0152	61.58	2080.7	2049.3	.7151
-.01305	61.38	2077.6	2049.4	.6758
-.01086	61.36	2076.2	2049.5	.6575
-.0087	61.35	2075.5	2049.4	.6501
-.00652	61.35	2075.3	2049.3	.6489
-.00435	61.39	2075.7	2049.2	.6551
-.00217	61.32	2076.5	2049.0	.6674
0.0	61.31	2078.2	2048.4	.6889
.00218	61.35	2080.7	2048.9	.7177
.00438	61.53	2085.7	2048.7	.7530
.00652	61.50	2087.0	2048.5	.7898
.00872	61.36	2090.0	2048.2	.8230
.01087	61.35	2093.5	2047.8	.8606
.01305	61.31	2095.9	2047.6	.8848
.0152	61.31	2097.8	2047.7	.9048
.0174	61.30	2099.6	2047.1	.9226
.0196	61.34	2100.5	2046.8	.9331
.0217	61.37	2101.2	2046.5	.9418
.0239	61.40	2101.7	2046.3	.9479
.0261	61.32	2102.1	2046.2	.9522
.0304	61.46	2102.4	2046.1	.9556
.0348	61.42	2102.6	2046.0	.9582
.0392	61.40	2102.8	2046.0	.9598
.0435	61.53	2103.0	2046.0	.9615
.0478	61.35	2103.0	2046.0	.9615

Station 4; q_{ref} = 4.88 kilogram/square meter
x'/c = .258; α = 0.0°
Free Stream Total Pressure/q_{ref} = 2108.5
Free Stream Static Pressure/q_{ref} = 2044.3
Free Stream Total Temperature = 306° K

y/c	$\frac{q_\infty}{q_{ref}}$	$\frac{P_t}{q_{ref}}$	$\frac{P_s}{q_{ref}}$	$\frac{u}{U_\infty}$
-.052	61.35	2108.5	2051.0	.9638
-.0478	61.23	2108.5	2051.0	.9637
-.0435	61.27	2108.4	2051.0	.9630
-.0991	61.38	2108.2	2051.1	.9604
-.0348	61.37	2107.9	2051.4	.9553
-.0304	61.30	2106.3	2052.0	.9364
-.0261	61.24	2102.8	2052.7	.8993
-.0239	61.22	2101.0	2053.0	.8808
-.0217	61.28	2098.5	2053.2	.8550
-.01955	61.28	2095.8	2053.5	.8261
-.0174	61.28	2093.5	2053.6	.8024
-.0152	61.30	2091.1	2053.8	.7757
-.01305	61.20	2089.0	2054.0	.7514
-.01086	61.30	2087.0	2054.0	.7246
-.0087	61.42	2085.6	2054.0	.7140
-.00652	61.42	2084.6	2054.0	.7026
-.00435	71.40	2084.2	2054.0	.6980
-.00217	61.36	2084.3	2054.0	.6991
0.0	61.47	2085.3	2054.0	.7106
.00218	61.28	2086.9	2053.8	.7308
.00432	61.31	2088.9	2053.5	.7558
.00652	61.30	2090.8	2053.2	.7790
.00872	61.20	2092.8	2053.0	.8015
.01087	61.21	2095.3	2052.7	.8292
.01305	61.16	2098.0	2052.5	.8570
.0152	61.33	2100.2	2052.4	.8785
.0174	61.00	2102.5	2052.5	.9005
.0196	61.03	2104.6	2052.0	.9286
.0217	61.51	2106.1	2051.8	.9364
.0239	61.28	2107.3	2051.4	.9502
.0261	61.40	2107.7	2051.2	.9553
.0304	61.26	2108.2	2051.1	.9604
.0348	61.27	2108.3	2051.0	.9621
.0392	61.31	2108.4	2050.8	.9647
.0435	61.30	2108.5	2050.8	.9655
.0498	61.32	2108.5	2050.8	.9655

Table 3-3 (Continued)

Station 5; q_{ref} = 4.88 kilogram/square meter
x'/c = 0.517; α = 0.0°
Free Stream Total Pressure/q_{ref} = 2112.5
Free Stream Static Pressure/q_{ref} = 2047.9
Free Stream Total Temperature = 305° K

y/c	$\frac{q_\infty}{q_{ref}}$	$\frac{P_t}{q_{ref}}$	$\frac{P_s}{q_{ref}}$	$\frac{u}{U_\infty}$
-.0695	61.46	2112.5	2052.9	.9886
-.0588	61.34	2112.5	7052.9	.9826
-.0469	61.46	2111.8	2052.9	.9768
-.0417	61.18	2111.0	2053.5	.9647
-.0365	61.30	2104.4	2053.8	.9488
-.0304	61.10	2107.2	2053.85	.9294
-.0260	61.27	2104.2	2054.4	.9079
-.0217	61.21	2101.2	2054.6	.8685
-.0174	61.13	2048.4	2054.7	.8410
-.0139	61.42	2-96.4	2055.0	.8185
-.0087	61.44	2094.7	2054.9	.8026
-.00304	61.38	2094.7	2054.7	.8046
.00861	61.25	2096.4	2054.35	.8251
.00782	61.27	2098.7	2054.1	.8498
.0121	61.29	2108.5	2053.7	.8890
.0174	61.38	2105.7	2053.4	.9205
.0217	61.50	2107.8	2053.2	.9404
.0261	61.55	2104.4	2052.9	.9567
.0304	61.49	2110.4	2052.8	.9660
.0348	61.49	2111.6	2052.6	.9777
.0392	61.48	2112.1	2052.5	.9827
.0435	61.52	2112.2	2052.5	.9895
.0521	61.35	2112.3	2052.5	.9843
.0609	61.28	2112.5	2052.4	.9868
.0695	61.38	2112.5	2052.4	.9868
.0695	61.38	2112.5	2052.4	.9868

Station 6; q_{ref} = 4.88 kilogram/square meter
x'/c = .8851; α = 0.0°
Free Stream Total Pressure/q_{ref} = 2112.5
Free Stream Static Pressure/q_{ref} = 2047.9
Free Stream Total Temperature = 305° K

y/c	$\frac{q_\infty}{q_{ref}}$	$\frac{P_t}{q_{ref}}$	$\frac{P_s}{q_{ref}}$	$\frac{u}{U_\infty}$
-.0905	61.29	2112.5	2052.1	.9894
-.0800	61.30	2112.5	2052.1	.9894
-.0695	61.38	2112.35	2052.1	.9881
-.0582	61.24	2111.5	2052.1	.9811
-.0469	61.47	2110.0	2052.3	.9670
-.0417	61.42	2108.75	2052.5	.9547
-.0365	61.25	2107.5	2052.8	.9414
-.0304	61.35	2105.85	2053.25	.9177
-.0260	61.12	2103.8	2053.5	.9086
-.0217	61.29	2102.25	2053.75	.8862
-.0174	61.20	2101.2	2054.0	.8742
-.0139	61.40	2100.5	2053.95	.8688
-.0087	61.34	2099.65	2053.9	.8607
-.0304	61.49	2099.4	2053.8	.8595
.00861	61.55	2100.2	2053.6	.8687
.00782	61.42	2101.25	2053.5	.8794
.0121	61.51	2102.25	2053.25	.8909
.0174	61.47	2104.0	2053.0	.9089
.0217	61.42	2105.6	2052.5	.9276
.0261	61.58	2107.15	2052.25	.9441
.0304	61.56	2108.6	2052.1	.9569
.0348	61.51	2109.5	2052.0	.9653
.0392	61.48	2110.2	2052.0	.9712
.0435	61.55	2110.85	2051.9	.9775
.0521	61.47	2111.4	2051.8	.9889
.0609	61.41	2111.9	2051.7	.9878
.0695	61.50	2112.5	2051.6	.9936
.0782	61.40	2112.5	2051.6	.9936

Station 7; q_{ref} = 4.88 kilogram/square meter
x'/c = 1.187; α = 0.0°
Free Stream Total Pressure/q_{ref} = 2112.5
Free Stream Static Pressure/q_{ref} = 2047.9
Free Stream Total Temperature = 305° K

y/c	$\frac{q_\infty}{q_{ref}}$	$\frac{P_t}{q_{ref}}$	$\frac{P_s}{q_{ref}}$	$\frac{u}{U_\infty}$
-.0905	61.45	2112.5	2052.7	.9884
-.0800	61.33	2112.5	2052.7	.9884
-.0695	61.37	2112.3	2052.9	.9851
-.0582	61.46	2111.4	2052.95	.9772
-.0464	61.31	2110.2	2053.1	.9658
-.0417	61.37	2109.1	2053.5	.9529
-.0365	61.35	2107.8	2053.7	.9399
-.0304	61.38	2106.5	2053.8	.9277
-.0260	61.38	2105.3	2053.9	.9161
-.0217	61.34	2104.05	2054.0	.9040
-.0174	61.29	2103.2	2054.115	.8949
-.0139	61.45	2102.7	2054.2	.8898
-.0087	61.28	2102.3	2054.2	.8862
-.00304	61.21	2101.7	2054.1	.8816
.00261	61.41	2101.6	2053.9	.8825
.00782	61.40	2102.5	2053.7	.8927
.0121	61.44	2053.6	2053.6	.8982
.0174	61.35	2103.9	2053.55	.9068
.0217	61.41	2104.5	2053.4	.9136
.0261	61.52	2105.5	2053.2	.9243
.0304	61.49	2106.7	2053.1	.9357
.0348	61.42	2107.7	2052.9	.9462
.0392	61.55	2108.9	2052.7	.9582
.0435	61.32	2109.45	2052.6	.9638
.0521	61.32	2110.7	2052.5	.9752
.0609	61.38	2111.78	2052.3	.9859
.0695	61.19	2112.5	2052.3	.9918
.0782	61.26	2112.5	2052.3	.9918

Table 3-3 (Continued)

Station 1; q_{ref} = 4.88 Kilogram/square meter
x'/c = .0865; α = 8.0°
Free Stream Total Pressure/q_{ref} = 2120.0
Free Stream Static Pressure/q_{ref} = 2058.1
Free Stream Total Temperature = 303.5° K
Free Transition

y/c	$\frac{q_\infty}{q_{ref}}$	$\frac{P_t}{q_{ref}}$	$\frac{P_s}{q_{ref}}$	$\frac{u}{U_\infty}$
.3060	61.32	2120.0	2067.7	.9340
.3175	61.30	2118.1	2068.1	.9890
.3278	61.07	2112.0	2069.2	.8990
.3340	61.22	2098.6	2070.1	.6490
.3392	61.11	2086.9	2070.1	.5850
.3442	61.15	2082.1	2069.9	.6600
.3500	60.96	2083.2	2068.8	.4880
.3560	61.11	2087.9	2067.5	.5790
.3610	61.10	2094.3	2066.2	.6800
.3660	61.14	2100.9	2065.7	.7680
.3720	61.09	2108.0	2065.7	.8560
.3773	61.15	2115.8	2066.9	.8800
.3826	61.21	2117.2	2067.5	.9060
.3880	61.05	2119.1	2067.8	.9210
.3940	61.00	2119.8	2068.6	.9300
.4075	61.15	2120.0	2068.6	.9280

Station 2; q_{ref} = 4.88 Kilogram/square meter
x'/c = 0.2231; α = 8.0°
Free Stream Total Pressure/q_{ref} = 2120.0
Free Stream Static Pressure/q_{ref} = 2058.1
Free Stream Total Temperature = 306.1° K
Free Transition

y/c	$\frac{q_\infty}{q_{ref}}$	$\frac{P_t}{q_{ref}}$	$\frac{P_s}{q_{ref}}$	$\frac{u}{U_\infty}$
.2345	61.36	2117.0	2061.5	.9484
.2580	61.34	2117.0	2061.5	.9484
.2695	61.28	2117.0	2061.5	.9484
.2870	61.79	2117.0	2061.5	.9484
.3042	61.23	2116.9	2061.5	.9484
.3130	61.34	2116.7	2061.25	.9480
.3220	61.17	2116.2	2061.0	.9459
.3307	61.27	2114.85	2061.0	.9543
.3390	6030	2109.5	2060.5	.8913
.3440	61.34	2103.75	2060.4	.8984
.3480	61.35	2097.5	2060.25	.7778
.3580	61.83	7098.2	2060.0	.7886
.3567	61.13	2089.2	2060.0	.6881
.3600	61.33	2088.0	2060.2	.6714
.3650	61.45	2089.5	2060.3	.6889
.3695	61.41	2092.8	2060.5	.7857
.3740	61.45	2096.5	2060.6	.7689
.3880	61.35	2103.5	2060.8	.8580
.3900	61.43	2110.0	2061.0	.8912
.3995	61.29	2115.8	2061.3	.9398
.4080	61.30	2116.4	2061.3	.9501
.4165	61.19	2117.0	2061.2	.9510
.4260	61.31	2117.0	2061.0	.9587
.4340	61.30	2117.0	2061.0	.9587
.4430	61.21	2117.0	2061.0	.9587

Station 3; q_{ref} = 4.88 Kilogram/square meter
x'/c = 0.3441; α = 8.0°
Free Stream Total Pressure/q_{ref} = 2117.0
Free Stream Static Pressure/q_{ref} = 2050.8
Free Stream Total Temperature = 308.2° K
Free Transition

y/c	$\frac{q_\infty}{q_{ref}}$	$\frac{P_t}{q_{ref}}$	$\frac{P_s}{q_{ref}}$	$\frac{u}{U_\infty}$
.2680	61.48	2117.0	2060.5	.9588
.2698	61.28	2117.0	2060.5	.9588
.2870	61.41	2117.0	2060.5	.9588
.3040	61.31	2117.0	2060.3	.9588
.3230	61.18	2116.6	2060.2	.9585
.3302	61.19	2115.8	2060.15	.9588
.3390	61.21	2113.3	2060.1	.9588
.3480	61.31	2109.0	2060.0	.9814
.3570	61.31	2101.2	2060.0	.8936
.3610	61.43	2098.5	2059.9	.7912
.3650	61.26	2095.7	2059.85	.7685
.3695	61.29	2094.2	2059.85	.7664
.3730	61.18	2093.5	2059.8	.7583
.3788	61.30	2093.6	2059.8	.7686
.3850	61.19	2095.8	2059.8	.7785
.3870	61.38	2097.8	2059.75	.7773
.3910	61.73	2100.5	2060.7	.8938
.4000	61.89	2106.5	2059.6	.8986
.4085	61.35	2112.6	2059.5	.9089
.4170	61.18	2114.6	2059.4	.9089
.4260	61.29	2115.8	2059.4	.9088
.4350	61.25	2116.5	2059.3	.9090
.4438	60.88	2117.0	2059.25	.9099
.4518	61.12	2117.0	2059.25	.9099
.4610	61.28	2117.0	2059.15	.9099

Station 4; q_{ref} = 4.88 Kilogram/square meter
x'/c = 0.5171; α = 8.0°
Free Stream Total Pressure/q_{ref} = 2117.0
Free Stream Static Pressure/q_{ref} = 2050.8
Free Stream Total Temperature = 306° K
Free Transition

y/c	$\frac{q_\infty}{q_{ref}}$	$\frac{P_t}{q_{ref}}$	$\frac{P_s}{q_{ref}}$	$\frac{u}{U_\infty}$
.2755	61.40	2117.0	2060.3	.9589
.2925	61.34	2117.0	2060.3	.9584
.3100	61.35	2117.0	2060.3	.9589
.3275	61.27	2116.7	2059.9	.9578
.3450	61.35	2114.4	2059.6	.9412
.3540	61.35	2112.3	2059.5	.9238
.3625	61.40	2108.5	2059.5	.8900
.3710	61.25	2102.2	2059.45	.8313
.3800	61.31	2099.4	2059.4	.8041
.3840	61.35	2098.8	2059.35	.7986
.3895	61.30	2099.0	2059.3	.8011
.3930	61.04	2099.5	2059.25	.8047
.3975	61.70	2100.0	2059.2	.8122
.4015	61.25	2101.0	2059.2	.8221
.4063	61.26	2102.2	2059.15	.8343
.4100	61.22	2104.0	2059.15	.8515
.4150	61.28	2106.7	2059.15	.8768
.4242	61.26	2111.0	2059.1	.9160
.4380	61.17	2113.85	2059.0	.9417
.4415	61.33	2115.5	2059.0	.9558
.4500	61.23	2116.5	2059.0	.9651
.4590	61.14	2116.9	2059.0	.9693
.4670	61.17	2117.0	2058.8	.9705
.4750	61.31	2117.0	2058.75	.9705
.4850	61.21	2117.0	2058.75	.9705

Station 5; q_{ref} = 4.88 Kilogram/square meter
x'/c = 0.8051; α = 8.0°
Free Stream Total Pressure/q_{ref} = 2117.0
Free Stream Static Pressure/q_{ref} = 2054.2
Free Stream Total Temperature = 312.8° K
Free Transition

y/c	$\frac{q_\infty}{q_{ref}}$	$\frac{P_t}{q_{ref}}$	$\frac{P_s}{q_{ref}}$	$\frac{u}{U_\infty}$
.5480	61.10	2117.0	2058.05	.9890
.5570	61.84	2117.0	2058.05	.9890
.5650	61.89	2117.0	2058.05	.9890
.5740	61.85	2117.0	2058.1	.9888
.5830	61.27	2115.5	2058.1	.9685
.5915	61.23	2115.5	2058.15	.9588
.6000	61.28	2110.9	2058.15	.9898
.6085	61.35	2108.5	2058.15	.9089
.6175	61.24	2106.5	2058.2	.8884
.6260	61.30	2105.0	2058.5	.8700
.6350	61.32	2104.3	2059.3	.8575
.6430	61.19	2104.3	2059.7	.8540
.6515	61.14	2104.9	2059.7	.8580
.6610	61.10	2106.1	2059.5	.8721
.6700	61.19	2107.9	2059.5	.8891
.6785	61.10	2109.8	2059.5	.9061
.6870	61.21	2111.8	2059.0	.9258
.6950	61.07	2113.4	2058.5	.9463
.7052	61.03	2114.8	2058.3	.9605
.7150	61.03	2115.6	2058.1	.9688
.7220	61.20	2117.0	2057.9	.9850
.7300	61.22	2117.0	2057.9	.9850
.7390	61.22	2117.0	2057.8	.9850

Table 3-3 (Continued)

Station 1; q_{ref} = 4.88 Kilogram/square meter
x'/c = .044; α = 10.8°
Free Stream Total Pressure/q_{ref} = 2121.5
Free Stream Static Pressure/q_{ref} = 2060.1
Free Stream Total Temperature = 311.1° K
Free Transition

y/c	$\frac{q_{\infty}}{q_{ref}}$	$\frac{P_t}{q_{ref}}$	$\frac{P_s}{q_{ref}}$	$\frac{u}{u_{\infty}}$
-.0861	61.43	2121.5	2060.3	.9304
-.0817	61.19	2121.5	2060.3	.9304
-.0174	61.29	2121.5	2060.3	.9304
-.0152	61.37	2121.0	2060.4	.9051
-.0131	61.49	2119.7	2060.5	.9127
-.0109	61.42	2117.4	2060.6	.8910
-.0087	61.36	2112.5	2060.6	.8451
-.0065	61.32	2104.5	2060.7	.7631
-.0043	61.42	2096.0	2060.4	.6639
-.0022	61.49	2087.5	2064.2	.5455
0.0	61.39	2080.6	2069.5	.4287
.0022	61.40	2076.0	2069.9	.3149
.0044	61.44	2074.1	2070.2	.2518
.0065	61.41	2073.2	2070.5	.2095
.0087	61.53	2073.0	2070.4	.2056
.0131	61.36	2074.3	2070.1	.2613
.0174	61.47	2076.5	2069.9	.3276
.0817	61.41	2079.4	2069.5	.4012
.0861	61.39	2085.0	2069.4	.4705
.0304	61.54	2087.2	2064.3	.5395
.0347	61.40	2091.7	2069.2	.6049
.0391	61.31	2047.2	2064.1	.6760
.0434	61.43	2108.8	2069.1	.7403
.0477	61.50	2108.0	2064.0	.7964
.0522	61.34	2112.5	2064.0	.8411
.0565	61.34	2115.5	2068.8	.8716
.0608	61.60	2117.5	2068.5	.8928
.0651	61.50	2119.0	2068.0	.9110
.0694	61.45	2120.2	2067.5	.9262
.0738	61.51	2121.1	2067.2	.9367
.0782	61.42	2121.5	2067.0	.9430
.0825	61.50	2121.5	2067.0	.9430
.0870	61.35	2121.5	2067.0	.9430

Station 2; q_{ref} = 4.88 Kilogram/square meter
x'/c = .0861; α = 10.8°
Free Stream Total Pressure/q_{ref} = 2121.5
Free Stream Static Pressure/q_{ref} = 2060.15
Free Stream Total Temperature = 311.1° K
Free Transition

y/c	$\frac{q_{\infty}}{q_{ref}}$	$\frac{P_t}{q_{ref}}$	$\frac{P_s}{q_{ref}}$	$\frac{u}{u_{\infty}}$
-.0861	61.43	2121.5	2060.5	.9086
-.0817	61.49	2121.5	2060.5	.9086
-.0174	61.48	2119.0	2060.6	.9059
-.0152	61.46	2117.0	2060.6	.8873
-.0131	61.38	2112.5	2060.6	.8451
-.0109	61.47	2106.2	2060.7	.7840
-.0087	61.51	2100.2	2060.7	.7150
-.0065	61.45	2094.2	2060.8	.6488
-.0043	61.22	2088.7	2869.2	.5691
-.0022	61.40	2084.6	2869.4	.4972
0.0	61.57	2081.3	2869.5	.4388
.0022	61.41	2079.0	2869.5	.3939
.0044	61.37	2077.8	2869.7	.3689
.0065	61.44	2077.5	2869.8	.3588
.0087	61.35	2078.0	2870.0	.3586
.0131	61.39	2079.7	2870.0	.3871
.0174	61.31	2082.5	2869.8	.4544
.0817	61.31	2085.7	2869.8	.5084
.0861	61.38	2089.5	2869.7	.5676
.0304	61.37	2094.0	2869.5	.6318
.0347	61.38	2099.2	2869.5	.6948
.0393	61.47	2104.7	2869.4	.7576
.0434	61.52	2109.2	2869.2	.8086
.0477	61.44	2105.3	2868.7	.7588
.0522	61.43	2105.9	2868.3	.7881
.0565	61.48	2107.6	2868.1	.8047
.0608	61.49	2108.9	2867.9	.8168
.0651	61.49	2180.0	2867.7	.9886
.0691	61.38	2180.7	2867.5	.9389
.0738	61.25	2121.2	2867.3	.9367
.0782	61.43	2121.4	2867.1	.9402
.0825	61.43	2121.5	2867.0	.9389
.0870	61.37	2121.5	2867.0	.9389

Station 3; q_{ref} = 4.88 Kilogram/square meter
x'/c = .172; α = 10.8°
Free Stream Total Pressure/q_{ref} = 2121.5
Free Stream Static Pressure/q_{ref} = 2060.15
Free Stream Total Temperature = 310.5° K
Free Transition

y/c	$\frac{q_{\infty}}{q_{ref}}$	$\frac{P_t}{q_{ref}}$	$\frac{P_s}{q_{ref}}$	$\frac{u}{u_{\infty}}$
-.0879	61.38	2121.5	2067.5	.9363
-.0235	61.31	2121.5	2067.5	.9363
-.0191	61.42	2118.3	2067.5	.9081
-.0148	61.33	2113.5	2067.5	.8641
-.0104	61.33	2108.0	2067.5	.8108
-.0083	61.35	2105.0	2067.5	.7802
-.0061	61.41	2102.0	2067.5	.7484
-.0039	61.46	2099.2	2067.5	.7173
-.0017	61.29	2096.0	2067.5	.6808
.0004	61.27	2093.5	2067.5	.6497
.0026	61.30	2091.2	2067.5	.6203
.0048	61.46	2084.5	2867.8	.5948
.0070	61.35	2088.3	2068.0	.5740
.0091	61.45	2087.5	2068.2	.5596
.0113	61.36	2087.0	2068.4	.5494
.0135	61.57	2087.5	2068.5	.5552
.0156	61.43	2088.0	2068.5	.5625
.0200	61.49	2090.2	2068.5	.5934
.0244	61.29	2093.5	2068.5	.6343
.0287	61.28	2097.0	2068.5	.6800
.0330	61.39	2101.0	2068.5	.7262
.0374	61.41	2104.6	2068.4	.7664
.0417	61.39	2108.2	2068.0	.8077
.0461	61.41	2111.7	2067.7	.8451
.0504	61.49	2114.1	2067.5	.8697
.0548	61.48	2116.3	2067.4	.8910
.0592	61.41	2118.0	2067.2	.9082
.0635	61.44	2119.5	2067.0	.9233
.0679	61.51	2120.4	2066.7	.9338
.0722	61.32	2120.9	2066.5	.9399
.0765	61.47	2121.4	2066.0	.9487
.0809	61.29	2121.4	2066.0	.9487
.0853	61.27	2121.5	2066.0	.9495
.0895	61.43	2121.5	2066.0	.9495
.0939	61.41	2121.5	2066.0	.9495

Station 4; q_{ref} = 4.88 Kilogram/square meter
x'/c = .258; α = 10.8°
Free Stream Total Pressure/q_{ref} = 2121.5
Free Stream Static Pressure/q_{ref} = 2060.2
Free Stream Total Temperature = 306.0° K
Free Transition

y/c	$\frac{q_{\infty}}{q_{ref}}$	$\frac{P_t}{q_{ref}}$	$\frac{P_s}{q_{ref}}$	$\frac{u}{u_{\infty}}$
-.2260	61.12	2121.50	2065.5	.9550
-.0966	61.18	2121.5	2065.5	.9550
.0095	61.30	2116.0	2065.5	.9869
.0078	61.23	2113.0	2065.5	.8896
.0122	61.24	2109.8	2065.8	.8665
.0165	61.31	2105.0	2066.0	.7969
.0209	61.26	2101.0	2066.3	.7516
.0231	61.21	2099.2	2066.4	.7307
.0252	61.20	2097.8	2066.5	.7139
.0274	61.23	2096.5	2066.6	.6977
.0296	61.30	2095.5	2066.8	.6895
.0318	61.30	2094.8	2067.0	.6736
.0340	61.29	2094.5	2067.0	.6690
.0361	61.39	2094.4	2067.0	.6678
.0383	61.28	2094.7	2067.0	.6714
.0405	61.38	2095.2	2067.2	.6750
.0427	61.22	2095.8	2067.3	.6810
.0449	61.31	2096.8	2067.3	.6989
.0470	61.16	2097.5	2067.3	.7010
.0514	61.15	2099.3	2067.3	.7216
.0557	61.27	2102.5	2067.3	.7568
.0601	61.31	2106.2	2067.3	.7956
.0645	61.34	2109.0	2067.3	.8238
.0688	61.27	2111.7	2067.2	.8510
.0732	61.30	2113.7	2067.0	.8718
.0775	61.13	2115.7	2066.7	.8831
.0819	61.31	2117.8	2066.5	.9139
.0862	61.22	2119.0	2066.3	.9263
.0906	61.29	2120.2	2066.0	.9394
.0949	61.17	2121.0	2066.0	.9464
.0991	61.32	2121.2	2065.7	.9507
.1035	61.31	2121.3	2065.7	.9516
.1078	61.15	2121.4	2065.7	.9534
.1123	61.34	2121.5	2065.5	.9550
.1166	61.13	2121.5	2065.5	.9550

Table 3-3 (Continued)

Station 5; q_{ref} = 4.88 Kilogram/square meter
x'/c = 0.3961; α = 10.8°
Free Stream Total Pressure/q_{ref} = 2121.5
Free Stream Static Pressure/q_{ref} = 2060.3
Free Stream Total Temperature = 303° K
Free Transition

y/c	$\frac{q_{loc}}{q_{ref}}$	$\frac{P_s}{q_{ref}}$	$\frac{P_{tl}}{q_{ref}}$	$\frac{u}{U_\infty}$
-.0870	61.19	2121.5	2065.0	.9586
-.0791	61.31	2121.5	2065.0	.9586
-.0701	61.35	2119.5	2065.0	.9615
-.0651	61.36	2118.1	2065.0	.9694
-.0617	61.35	2116.8	2065.0	.9186
.0086	61.36	2115.5	2065.0	.8888
.0070	61.39	2110.5	2065.0	.8605
.0113	61.36	2107.8	2065.0	.8885
.0136	61.19	2104.3	2065.0	.7995
.0188	61.29	2101.8	2065.0	.7737
.0243	61.25	2100.2	2065.0	.7567
.0287	61.24	2099.0	2065.1	.7485
.0330	61.12	2098.5	2065.5	.7385
.0376	71.26	2098.4	2065.5	.7314
.0417	61.18	2099.5	2065.7	.7391
.0460	61.15	2100.5	2065.8	.7511
.0504	61.19	2102.2	2065.7	.7704
.0540	61.14	2104.5	2065.7	.7943
.0591	61.19	2107.0	2065.7	.8195
.0634	61.20	2109.5	2065.5	.8459
.0680	61.19	2111.7	2065.5	.8668
.0722	61.25	2113.3	2065.2	.8845
.0765	61.39	2115.4	2065.0	.9054
.0809	61.25	2117.0	2064.7	.9234
.0852	61.19	2118.3	2064.5	.9356
.0895	61.21	2119.2	2064.5	.9434
.0950	61.37	2120.0	2064.5	.9502
.0988	61.29	2120.5	2064.4	.9554
.1025	61.29	2120.8	2064.3	.9588
.1068	61.29	2121.0	2064.3	.9605
.1115	61.26	2121.1	2064.2	.9622
.1158	61.20	2121.2	2064.2	.9631
.1200	61.19	2121.3	2064.2	.9639
.1243	61.23	2121.5	2064.2	.9656
.1285	61.20	2121.5	2064.2	.9656

Station 6; q_{ref} = 4.88 Kilogram/square meter
x'/c = 0.5171; α = 10.8°
Free Stream Total Pressure/q_{ref} = 2119.5
Free Stream Static Pressure/q_{ref} = 2058.25
Free Stream Total Temperature = 308.5° K
Free Transition

y/c	$\frac{q_{loc}}{q_{ref}}$	$\frac{P_s}{q_{ref}}$	$\frac{P_{tl}}{q_{ref}}$	$\frac{u}{U_\infty}$
-.0504	61.86	2119.5	2061.5	.9727
-.0530	60.95	2119.5	2061.5	.9727
-.0156	61.11	2119.5	2061.5	.9727
.0017	61.05	2119.3	2061.5	.9711
.0191	61.80	2117.5	2061.5	.9958
.0878	61.25	2115.0	2061.6	.9335
.0365	61.25	2111.3	2061.7	.8991
.0458	61.34	2108.0	2061.9	.8671
.0495	61.29	2106.2	2062.0	.8491
.0539	61.17	2104.2	2062.1	.8286
.0588	61.22	2102.7	2062.2	.8137
.0636	61.21	2101.8	2062.3	.8051
.0715	61.18	2101.0	2062.3	.7944
.0800	61.20	2100.2	2062.4	.8061
.0887	61.22	2104.3	2062.6	.8066
.0974	61.27	2106.8	2062.5	.8499
.1060	61.19	2110.2	2062.5	.8819
.1147	61.19	2112.8	2062.0	.9098
.1235	61.19	2115.0	2061.8	.9316
.1320	61.20	2116.9	2061.5	.9505
.1409	61.15	2117.9	2061.4	.9601
.1496	61.20	2118.5	2061.2	.9669
.1585	61.15	2119.0	2061.0	.9729
.1670	61.06	2119.2	2060.8	.9765
.1757	61.21	2119.3	2060.6	.9788
.1845	61.05	2119.4	2060.5	.9801
.2080	61.33	2119.5	2060.5	.9813
.2190	61.20	2119.5	2060.5	.9815

Station 7; q_{ref} = 4.88 Kilogram/square meter
x'/c = .6841; α = 10.8°
Free Stream Total Pressure/q_{ref} = 2119.5
Free Stream Static Pressure/q_{ref} = 2058.25
Free Stream Total Temperature = 308.5° K
Free Transition

y/c	$\frac{q_{loc}}{q_{ref}}$	$\frac{P_s}{q_{ref}}$	$\frac{P_{tl}}{q_{ref}}$	$\frac{u}{U_\infty}$
.0217	61.17	2119.5	2060.6	.9805
.0304	61.29	2119.5	2060.6	.9805
.0392	61.35	2119.5	2060.5	.9784
.0565	61.31	2118.0	2060.5	.9688
.0739	61.24	2115.0	2060.5	.9432
.0913	61.15	2110.8	2060.5	.9061
.1000	61.28	2109.1	2060.5	.8907
.1086	61.24	2107.2	2060.8	.8707
.1173	61.12	2106.0	2061.0	.8569
.1217	61.19	2105.7	2061.0	.8536
.1260	61.21	2105.6	2060.8	.8546
.1304	61.22	2105.7	2060.8	.8562
.1348	61.26	2105.8	2060.8	.8570
.1434	61.11	2106.5	2060.7	.8651
.1522	61.26	2107.9	2060.5	.8746
.1608	61.26	2109.4	2060.4	.8943
.1696	61.24	2110.8	2060.5	.9079
.1782	61.16	2112.6	2060.2	.9253
.1870	61.26	2114.4	2060.1	.9415
.1957	61.07	2115.5	2060.0	.9519
.2045	61.22	2116.5	2060.0	.9613
.2128	61.11	2117.3	2059.8	.9689
.2220	61.13	2118.0	2059.7	.9757
.2305	61.08	2118.4	2059.7	.9795
.2390	61.25	2118.65	2059.5	.9828
.2475	61.11	2118.8	2059.5	.9841
.2565	61.25	2119.0	2059.5	.9857
.2740	61.27	2119.4	2059.5	.9886
.2823	61.27	2119.5	2059.5	.9899
.2915	61.26	2119.5	2059.5	.9899

Table 3-4 - MEASUREMENTS IN THE WAKE OF BLUNT T.E. TEST AIRFOIL BY THE USE OF HOT-WIRE ANEMOMETER PROBE

Station 1 - Free Transition
x'/c = .0261; α = 0.0°
q_{ref} = 4.88 Kilogram/square meter

y/c	$\frac{u}{U_\infty}$	$\frac{q_\infty}{q_{ref}}$
-.1296	.9130	61.54
-.1078	.9040	61.48
-.0852	.8920	61.46
-.0635	.8800	61.46
-.0530	.8715	61.30
-.0417	.8655	61.45
-.0313	.8540	61.51
-.0270	.8470	61.52
-.0226	.8405	61.43
-.0185	.8150	61.36
-.0165	.7945	61.37
-.0131	.7580	61.40
-.0113	.7220	61.29
-.0096	.6700	61.19
-.0069	.5920	61.20
-.0052	.5550	61.15
-.0086	.4985	61.27
-.0009	.3980	61.18
.0017	.3155	61.35
.0035	.2790	61.40
.0061	.2760	61.05
.0078	.3040	61.14
.0104	.3695	61.22
.0122	.4405	61.17
.0139	.5045	61.08
.0165	.5520	61.12
.0183	.6165	60.97
.0217	.6730	61.32
.0252	.7680	61.14
.0304	.8225	61.01
.0339	.8415	61.12
.0452	.8565	61.26
.0565	.8645	61.17
.0670	.8690	61.13
.0887	.8850	61.11
.1104	.8930	61.15
.1320	.8975	61.31

Station 2 - Free Transition
x'/c = .174; α = 0.0°
q_{ref} = 4.88 Kilogram/square meter

y/c	$\frac{u}{U_\infty}$	$\frac{q_\infty}{q_{ref}}$
-.1183	.8710	61.19
-.0965	.8617	61.21
-.0739	.8565	61.28
-.0530	.8530	61.18
-.0417	.8495	61.16
-.0305	.8485	61.17
-.0200	.8280	61.04
-.0148	.7775	61.12
-.0113	.7576	60.99
-.0061	.6928	61.14
-.0044	.6900	61.14
-.0026	.6720	61.17
0.0	.6530	61.19
.0017	.6515	61.05
.0044	.6390	61.17
.0061	.6430	61.12
.0087	.6450	61.08
.0104	.6451	61.03
.0131	.6650	61.13
.0148	.6850	61.16
.0174	.7081	61.08
.0192	.7300	61.14
.0217	.7485	61.14
.0235	.7715	61.26
.0261	.7900	60.92
.0278	.7935	61.01
.0304	.8115	61.17
.0322	.8235	61.08
.0374	.8325	61.15
.0417	.8370	61.07
.0461	.8350	61.07
.0574	.8370	61.10
.0678	.8405	61.07
.0783	.8410	61.08
.1008	.8407	60.88
.1217	.8450	61.19
.1443	.8480	61.02

Station 3 - Free Transition
x'/c = .521; α = 0.0°
q_{ref} = 4.88 Kilogram/square meter

y/c	$\frac{u}{U_\infty}$	$\frac{q_\infty}{q_{ref}}$
-.1165	.8710	61.16
-.0913	.8690	61.21
-.0635	.8650	61.22
-.0417	.8605	61.22
-.0313	.8360	61.24
-.0217	.8040	61.16
-.0096	.7815	61.21
-.0052	.7750	61.19
-.0009	.7690	61.11
.0035	.7680	61.20
.0061	.7650	61.32
.0078	.7790	61.11
.0104	.7710	61.17
.0122	.7700	61.23
.0148	.7775	61.13
.0165	.7850	61.11
.0191	.7850	61.31
.0208	.7810	61.18
.0234	.7900	61.35
.0252	.7985	61.07
.0278	.8025	61.16
.0296	.8120	61.23
.0321	.8170	61.17
.0339	.8165	61.20
.0365	.8212	61.04
.0382	.8220	61.20
.0408	.8280	61.17
.0426	.8300	61.10
.0469	.8400	61.14
.0521	.8430	61.02
.0556	.8430	61.12
.0678	.8440	61.12
.0774	.8480	61.01
.0886	.8490	61.10
.1112	.8500	61.18
.1320	.8520	60.95
.1548	.8500	61.11

Station 4 - Free Transition
x'/c = 0.74; α = 0.0°
q_{ref} = 4.88 Kilogram/square meter

y/c	$\frac{u}{U_\infty}$	$\frac{q_\infty}{q_{ref}}$
-.1070	.8730	61.28
-.0848	.8730	61.25
-.0635	.8715	61.30
-.0508	.8520	61.30
-.0296	.8580	61.32
-.0191	.8115	61.39
-.0078	.7985	61.27
-.0095	.7900	61.30
0.0	.7915	61.32
.00521	.7850	61.34
.00695	.7930	61.47
.0087	.7870	61.33
.0113	.7985	61.39
.0139	.7885	61.38
.0156	.7980	61.43
.0174	.8065	61.35
.0200	.8015	61.35
.0217	.8075	61.30
.0243	.8060	61.26
.0261	.8150	61.46
.0287	.8195	61.34
.0304	.8190	61.38
.0330	.8280	61.31
.0348	.8270	61.37
.0374	.8370	61.35
.0391	.8380	61.42
.0417	.8385	61.36
.0443	.8425	61.36
.0477	.8450	61.41
.0530	.8480	61.35
.0573	.8550	61.21
.0677	.8545	61.36
.0790	.8600	61.29
.0895	.8600	61.37
.1050	.8612	61.20
.1330	.8620	61.40
.1555	.8610	61.30

Station 5 - Free Transition
x'/c = .985; α = 0.0°
q_{ref} = 4.88 Kilogram/square meter

y/c	$\frac{u}{U_\infty}$	$\frac{q_\infty}{q_{ref}}$
-.1034	.8780	61.27
-.0809	.8778	61.23
-.0591	.8700	61.38
-.0374	.8530	61.25
-.0269	.8425	61.30
-.0156	.8170	61.25
-.0052	.8025	61.25
-.0009	.8100	61.45
.0035	.7975	61.27
.0078	.8020	61.41
.0104	.7950	61.24
.0122	.8020	61.24
.0148	.8100	61.44
.0165	.8030	61.27
.0191	.8100	61.30
.0208	.8150	61.45
.0234	.8090	61.32
.0252	.8200	61.19
.0278	.8160	61.20
.0295	.8275	61.37
.0322	.8325	61.31
.0339	.8230	61.43
.0356	.8270	61.39
.0383	.8370	61.36
.0407	.8325	61.38
.0426	.8355	61.39
.0452	.8385	61.18
.0478	.8420	61.31
.0513	.8450	61.26
.0556	.8480	61.34
.0608	.8570	61.25
.0713	.8630	61.36
.0843	.8655	61.23
.0930	.8620	61.23
.1148	.8625	61.28
.1365	.8590	61.27
.1590	.8620	61.28

Table 3-4 (Continued)

Station 1 - Free Transition
$x'/c = .044$; $\alpha = 4.0°$
$q_{ref} = 4.88$ Kilogram/square meter

y/c	$\frac{u}{U_\infty}$	$\frac{q_{local}}{q_{ref}}$
-.1480	.9990	61.16
-.1295	.9980	61.22
-.1017	.9890	61.23
-.0800	.9730	61.18
-.0695	.9700	61.20
-.0588	.9610	61.22
-.0478	.9530	61.35
-.0435	.9490	61.35
-.0391	.9430	61.23
-.0348	.9380	61.26
-.0322	.9360	61.26
-.0304	.9890	61.26
-.0278	.9880	61.26
-.0261	.9820	61.33
-.0235	.9100	61.23
-.0219	.9080	61.26
-.0191	.8600	61.20
-.0174	.8540	61.19
-.0148	.7885	61.26
-.0131	.6980	61.26
-.0104	.6150	61.26
-.0087	.5850	61.11
-.0061	.4330	61.35
-.0043	.3690	61.27
-.0017	.3295	61.33
0.0	.3256	61.33
.0086	.3560	61.11
.0043	.4000	61.21
.0087	.5210	61.23
.0139	.6275	61.26
.0183	.7815	61.33
.0287	.9050	61.26
.0400	.9470	61.26
.0504	.9605	61.14
.0721	.9775	61.21
.0948	.9930	61.23
.1165	1.0010	61.26

Station 2 - Free Transition
$x'/c = 0.174$; $\alpha = 4.0°$
$q_{ref} = 4.88$ Kilogram/square meter

y/c	$\frac{u}{U_\infty}$	$\frac{q_{local}}{q_{ref}}$
-.1314	1.0080	61.27
-.1097	1.0040	61.41
-.0870	1.0000	61.21
-.0625	.9975	61.38
-.0539	.9922	61.37
-.0434	.9875	61.40
-.0331	.9830	61.31
-.0287	.9750	61.35
-.0844	.9560	61.37
-.0191	.9250	61.23
-.0174	.9125	61.33
-.0157	.8750	61.21
-.0131	.8525	61.19
-.0113	.8185	61.33
-.0087	.7770	61.29
0.0070	.7580	61.41
-.0052	.7270	61.29
-.0086	.7040	61.24
-.0009	.6920	61.27
.0017	.6800	61.27
.0043	.6810	61.20
.0061	.6985	61.27
.0087	.6950	61.30
.0104	.7350	61.51
.0131	.7590	61.23
.0148	.7872	61.42
.0174	.8215	61.34
.0191	.8485	61.28
.0844	.8850	61.24
.0287	.9270	61.20
.0530	.9550	61.20
.0435	.9700	61.30
.0548	.9735	61.11
.0652	.9750	61.32
.0878	.9800	61.32
.1087	.9830	61.33
.1305	.9900	61.21

Station 3 - Free Transition
$x'/c = .521$; $\alpha = 4.0°$
$q_{ref} = 4.88$ Kilogram/square meter

y/c	$\frac{u}{U_\infty}$	$\frac{q_{local}}{q_{ref}}$
-.0982	1.0060	61.21
-.0757	1.0040	61.21
-.0540	1.0080	61.13
-.0322	.9970	61.20
-.0218	.9750	61.53
-.0104	.9370	61.27
0.0	.8895	61.18
.0043	.8705	61.10
.0087	.8470	61.31
.0139	.8480	61.21
.0157	.8535	61.22
.0174	.8600	61.20
.0200	.8500	61.28
.0217	.8680	61.28
.0244	.8385	61.11
.0261	.8650	61.27
.0278	.8760	61.16
.0305	.8730	61.37
.0331	.8990	61.88
.0348	.9070	61.17
.0374	.9085	61.21
.0392	.9250	61.34
.0417	.9230	61.15
.0435	.9310	61.06
.0461	.9430	61.15
.0478	.9500	61.15
.0505	.9510	61.06
.0522	.9670	61.16
.0565	.9735	61.15
.0618	.9790	61.25
.0661	.9810	61.16
.0765	.9850	61.19
.0878	.9860	61.11
.0983	.9850	61.23
.1200	.9861	61.10
.1417	.9885	61.12
.1635	.9900	61.21

Station 4 - Free Transition
$x'/c = 0.74$; $\alpha = 4.0°$
$q_{ref} = 4.88$ Kilogram/square meter

y/c	$\frac{u}{U_\infty}$	$\frac{q_{local}}{q_{ref}}$
-.0739	1.0150	61.22
-.0478	1.0120	61.20
-.0861	1.0060	61.25
-.0044	.9750	61.72
.0061	.9425	61.17
.0174	.8950	61.07
.0287	.8695	61.29
.0330	.8725	61.30
.0374	.8850	61.21
.0417	.8850	61.30
.0435	.8852	61.16
.0461	.8900	61.21
.0478	.8890	61.38
.0505	.8880	61.22
.0522	.8990	61.14
.0548	.9075	61.05
.0565	.9180	61.13
.0583	.9300	61.06
.0609	.9330	61.06
.0626	.9290	61.03
.0652	.9358	61.14
.0679	.9450	61.07
.0695	.9500	61.12
.0722	.9565	61.11
.0739	.9730	61.14
.0765	.9678	61.00
.0782	.9700	61.12
.0808	.9625	61.11
.0852	.9730	61.13
.0895	.9830	61.09
.0938	.9815	61.04
.1043	.9820	60.99
.1155	.9840	61.09
.1260	.9820	61.04
.1477	.9885	60.87
.1695	.9840	60.90
.1922	.9851	60.98

Station 5 - Free Transition
$x'/c = .973$; $\alpha = 4.0°$
$q_{ref} = 4.88$ Kilogram/square meter

y/c	$\frac{u}{U_\infty}$	$\frac{q_{local}}{q_{ref}}$
-.0365	1.0100	61.31
-.0339	1.0080	61.32
-.0122	.9650	61.34
.0096	.9360	61.21
.0200	.9140	61.30
.0313	.8900	61.31
.0417	.9003	61.15
.0462	.8945	61.35
.0505	.9275	61.27
.0548	.9230	61.19
.0574	.9300	61.36
.0591	.9225	61.27
.0618	.9300	61.31
.0635	.9330	61.16
.0662	.9215	61.33
.0678	.9170	61.19
.0705	.9282	61.36
.0722	.9510	61.30
.0748	.9541	61.30
.0765	.9570	61.24
.0792	.9650	61.24
.0808	.9585	61.14
.0835	.9640	61.28
.0853	.9690	61.29
.0878	.9689	61.31
.0895	.9770	61.32
.0923	.9780	61.24
.0940	.9775	61.09
.0983	.9760	61.18
.1035	.9868	61.20
.1079	.9850	61.14
.1184	.9860	61.27
.1296	.9855	61.29
.1400	.9890	61.23
.1617	.9875	61.16
.1845	.9900	61.26
.2050	.9905	61.33

Table 3-4 (Continued)

Station 1 - Free Transition
x'/c = .0475; α = 10.7°
q_{ref} = 4.88 Kilogram/square meter

y/c	$\frac{u}{U_\infty}$	$\frac{q_\infty}{q_{ref}}$
-.1270	.8880	61.11
-.1052	.8850	61.25
-.0893	.8760	61.15
-.0617	.8110	61.29
-.0504	.8050	61.24
-.0400	.8015	61.25
-.0896	.8030	61.17
-.0843	.8040	61.04
-.0809	.7990	61.52
-.0157	.7940	61.23
-.0139	.7910	61.30
-.-122	.7800	61.05
-.0096	.7780	61.26
-.0070	.7475	61.28
-.0052	.7349	61.21
-.0095	.6705	61.17
-.0009	.6070	61.12
.0017	.4750	61.72
.00348	.3585	61.08
.0061	.2360	61.12
.0078	.1889	61.31
.0096	.1405	61.33
.0122	.1307	61.05
.0139	.1643	61.13
.0165	.1568	61.19
.0191	.2410	61.17
.0809	.2430	61.08
.0835	.2773	61.17
.0878	.3190	61.06
.0522	.4215	61.04
.0365	.4815	61.06
.0470	.6400	61.06
.0582	.7880	61.09
.0687	.8120	61.02
.0905	.8300	61.17
.1130	.8415	61.09
.1348	.8487	61.18

Station 2 - Free Transition
x'/c = .087; α = 10.7°
q_{ref} = 4.88 Kilogram/square meter

y/c	$\frac{u}{U_\infty}$	$\frac{q_\infty}{q_{ref}}$
-.1260	.7970	61.28
-.1043	.7900	61.18
-.0887	.7825	61.18
-.0609	.7760	61.27
-.0496	.7725	61.12
-.0391	.7710	61.10
-.0878	.7685	61.13
-.0844	.7670	61.02
-.0191	.7615	61.01
-.0148	.7500	61.21
-.0131	.7420	61.26
-.0104	.7280	61.22
-.0087	.7160	61.30
-.0061	.6785	61.41
-.0043	.6570	61.35
-.0026	.5815	61.28
0.0	.4768	61.13
.0026	.4015	61.40
.0044	.3420	61.25
.0069	.2910	61.37
.0087	.2665	61.23
.0113	.2760	61.24
.0130	.2770	61.21
.0156	.2870	61.28
.0174	.2740	61.25
.0800	.2850	61.17
.0817	.3120	61.18
.0843	.3910	61.11
.0287	.4185	61.40
.0331	.5230	61.23
.0374	.5720	61.35
.0478	.7050	.6126
.0591	.7650	61.22
.0695	.7800	61.24
.0913	.7875	61.36
.1130	.8080	61.31
.1357	.8120	61.33

Station 3 - Free Transition
x'/c = .174; α = 10.7°
q_{ref} = 4.88 Kilogram/square meter

y/c	$\frac{u}{U_\infty}$	$\frac{q_\infty}{q_{ref}}$
-.0975	.8122	61.16
-.0757	.8050	61.33
-.0539	.8020	61.30
-.0322	.7960	61.36
-.0208	.7880	61.34
-.0104	.7860	61.23
.0009	.7660	61.28
.0044	.7385	61.25
.0096	.7000	61.15
.0139	.6440	61.30
.0157	.6090	61.27
.0183	.5850	61.16
.0200	.5500	61.10
.0226	.5312	61.20
.0244	.5015	61.15
.0270	.4900	61.22
.0287	.4700	61.24
.0313	.4565	61.29
.0331	.4420	61.29
.0357	.4770	61.20
.0374	.4482	61.38
.0400	.4715	61.35
.0417	.4850	61.27
.0443	.5165	61.33
.0461	.4840	61.29
.0487	.5640	61.26
.0505	.5650	61.29
.0530	.5820	61.37
.0574	.6000	61.23
.0617	.6385	61.20
.0661	.7070	61.42
.0765	.7560	61.24
.0878	.7775	61.28
.0983	.7850	61.32
.1200	.7900	61.36
.1417	.7985	61.16
.1645	.8030	61.21

Station 4 - Free Transition
x'/c = .521; α = 10.7°
q_{ref} = 4.88 Kilogram/square meter

y/c	$\frac{u}{U_\infty}$	$\frac{q_\infty}{q_{ref}}$
-.0287	1.0580	61.39
-.0061	1.0560	61.40
.0243	1.0435	61.11
.0374	.9950	61.19
.0478	.9500	61.29
.0626	.8990	61.24
.0695	.8795	61.17
.0788	.8560	61.05
.0782	.8550	61.28
.0825	.8610	61.14
.0852	.8680	61.18
.0870	.8760	61.23
.0895	.8750	61.19
.0912	.8825	61.16
.0938	.8850	61.22
.0956	.8930	61.15
.0983	.9100	61.23
.1000	.9130	61.29
.1025	.9225	61.17
.1043	.9180	61.25
.1069	.8950	61.24
.1086	.9270	61.24
.1112	.9420	61.18
.1130	.9540	61.09
.1155	.9210	61.03
.1173	.9680	61.08
.1200	.9715	61.11
.1216	.9640	61.10
.1269	.9750	61.18
.1303	.9925	61.04
.1348	1.9780	61.12
.1460	1.0040	61.11
.1574	1.0115	61.05
.1677	1.0235	61.00
.1895	1.0285	61.14
.2112	1.0260	61.07
.2340	1.0270	61.13

Station 5 - Free Transition
x'/c = 0.78; α = 10.7°
q_{ref} = 4.88 Kilogram/square meter

y/c	$\frac{u}{U_\infty}$	$\frac{q_\infty}{q_{ref}}$
.0078	1.0100	61.18
.0304	1.0000	61.17
.0522	.9700	61.21
.0739	.9120	61.35
.0843	.8850	61.24
.0957	.8675	61.33
.1060	.8625	61.23
.1114	.8485	61.14
.1147	.8410	61.24
.1200	.8540	61.34
.1217	.8810	61.16
.1234	.8628	61.24
.1260	.8880	61.24
.1278	.8790	61.16
.1305	.8850	61.16
.1322	.8900	61.27
.1338	.8980	61.26
.1375	.9090	61.17
.1390	.9030	61.31
.1408	.9050	61.29
.1435	.8915	61.11
.1453	.9080	61.24
.1478	.9135	61.19
.1497	.9300	61.03
.1522	.9225	61.03
.1540	.9300	61.29
.1566	.9375	61.27
.1585	.9185	61.23
.1635	.9450	61.11
.1680	.9475	61.24
.1772	.9625	61.27
.1827	.9740	61.23
.1940	.9750	61.20
.2045	.9760	61.01
.2260	.9815	61.32
.2480	.9850	61.21
.2707	.9850	61.19

Station 6 - Free Transition
x'/c = .975; α = 10.7°
q_{ref} = 4.88 Kilogram/square meter

y/c	$\frac{u}{U_\infty}$	$\frac{q_\infty}{q_{ref}}$
.0461	.9570	61.32
.0678	.9380	61.38
.0895	.8980	61.22
.1112	.8600	61.31
.1226	.8550	61.21
.1330	.8350	61.25
.1442	.8460	61.27
.1486	.8475	61.39
.530	.8650	61.23
.1573	.8690	61.29
.1590	.8560	61.35
.1617	.8815	61.24
.1634	.8675	61.30
.1660	.8900	61.26
.1677	.8730	61.14
.1703	.8830	61.32
.1720	.8640	61.26
.1738	.8760	61.26
.1765	.8835	61.15
.1790	.9050	61.26
.1807	.9120	61.17
.1835	.8700	61.14
.1851	.8960	61.05
.1878	.8975	61.03
.1895	.8412	61.08
.1920	.9060	61.29
.1938	.9050	61.19
.1965	.9055	61.16
.2007	.9130	61.15
.2050	.9100	61.03
.2095	.9175	61.11
.2210	.9250	61.13
.2310	.9335	61.10
.2417	.9300	61.00
.2640	.9320	61.09
.2850	.9360	61.00
.3080	.9340	61.03

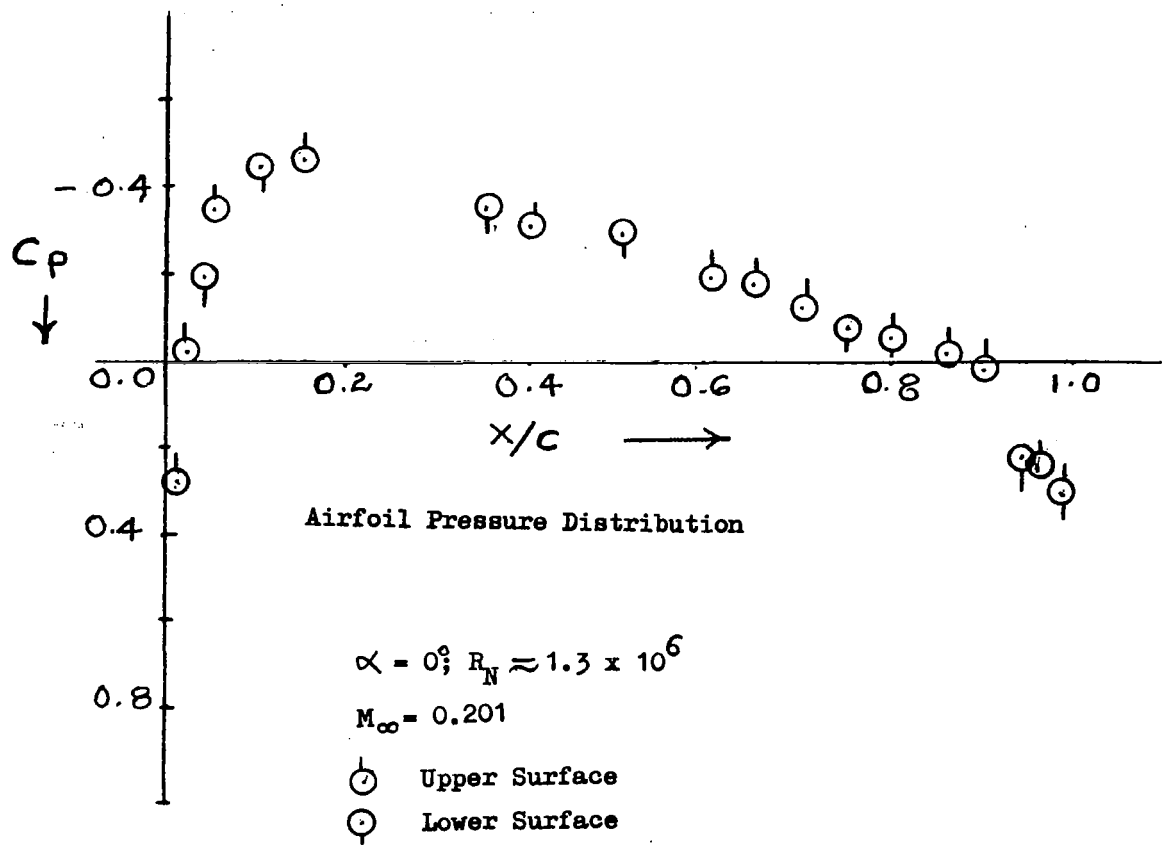

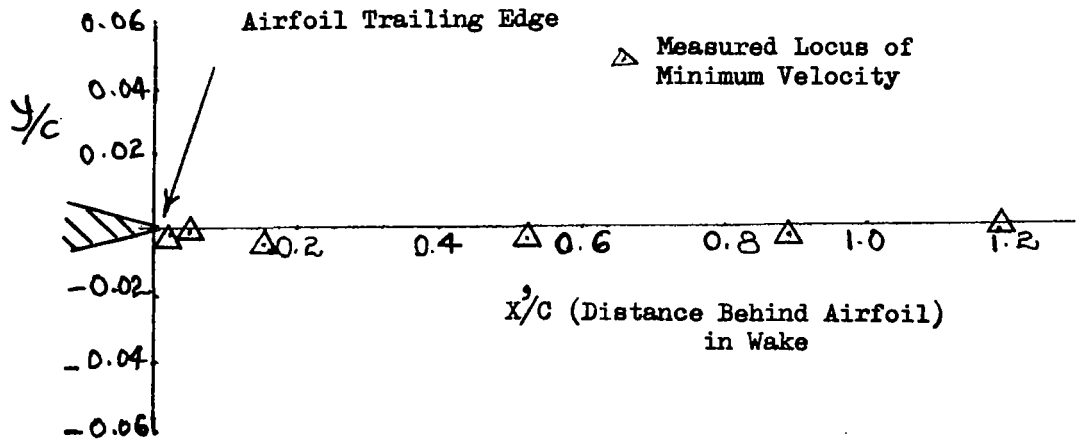

FIGURE III-20 - MEASURED PRESSURE DISTRIBUTION ON AIRFOIL SURFACE AND LOCUS OF MINIMUM VELOCITY AT $\alpha = 0°$ (FREE TRANSITION)

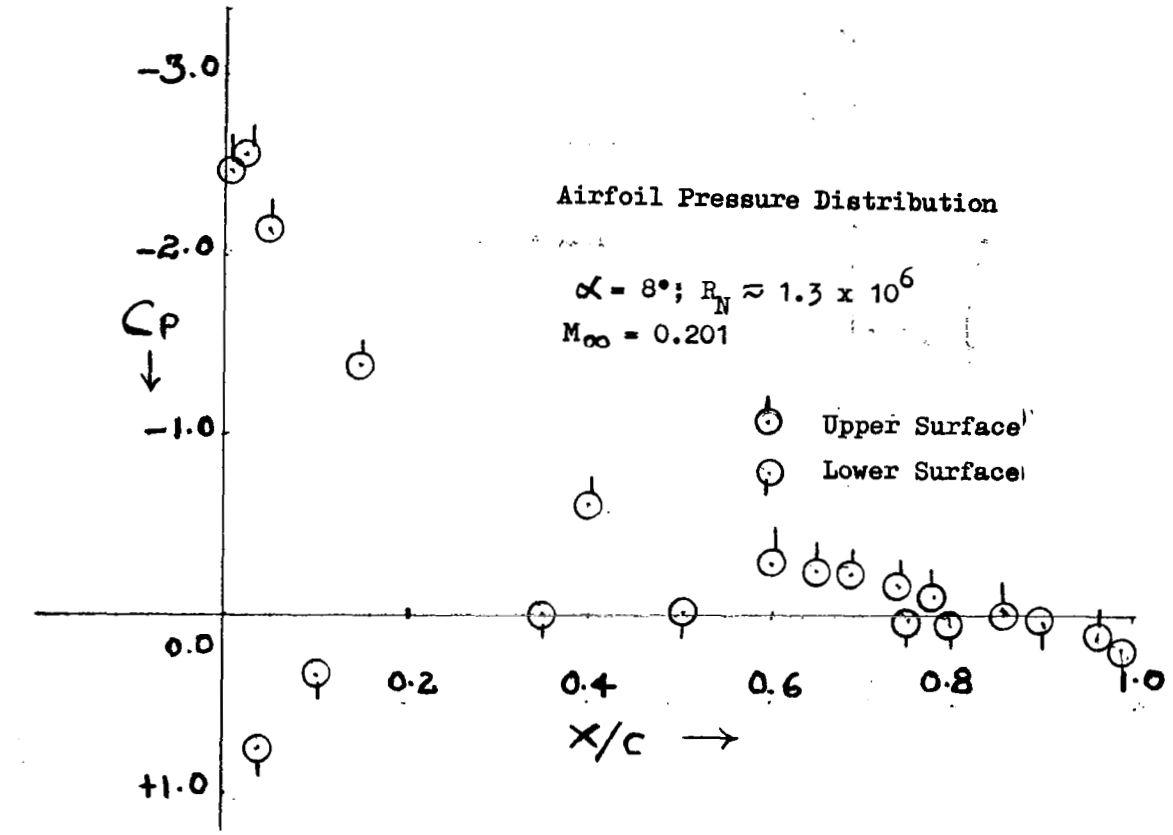

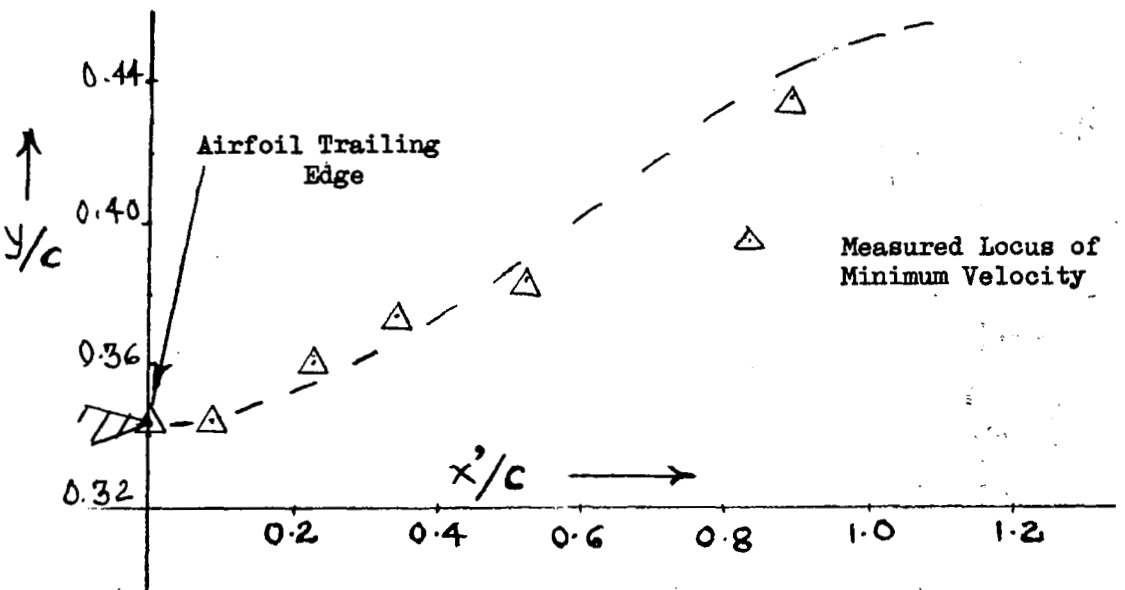

FIGURE III-21 - MEASURED PRESSURE DISTRIBUTION ON AIRFOIL SURFACE AND LOCUS OF MINIMUM VELOCITY AT α = 8.0° (FREE TRANSITION)

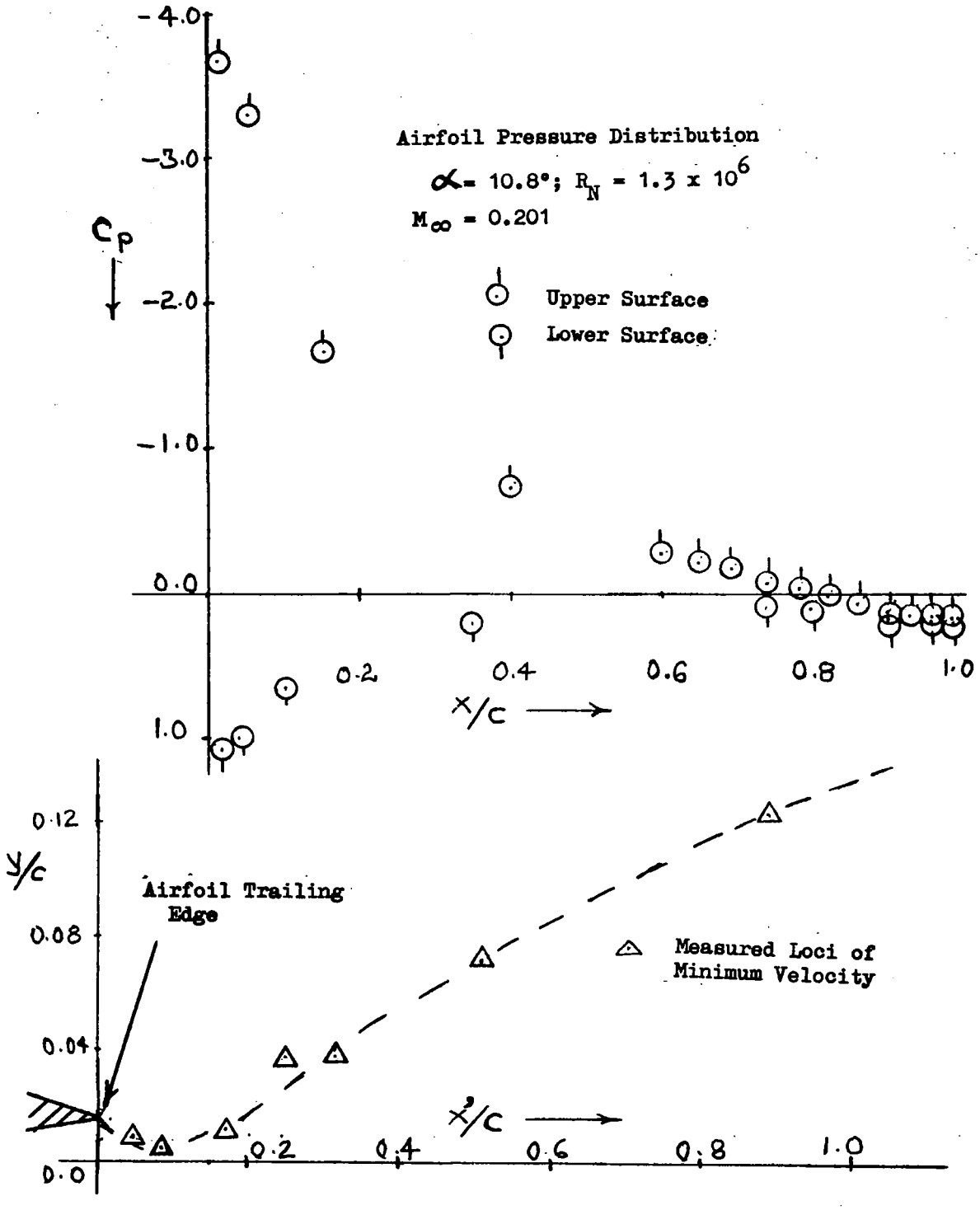

FIGURE III-22 - MEASURED PRESSURE DISTRIBUTION ON AIRFOIL SURFACE AND LOCUS OF MINIMUM VELOCITY AT α = 10.8° (FREE TRANSITION)

Blunt Trailing Edge (T.E. t/c = .01)

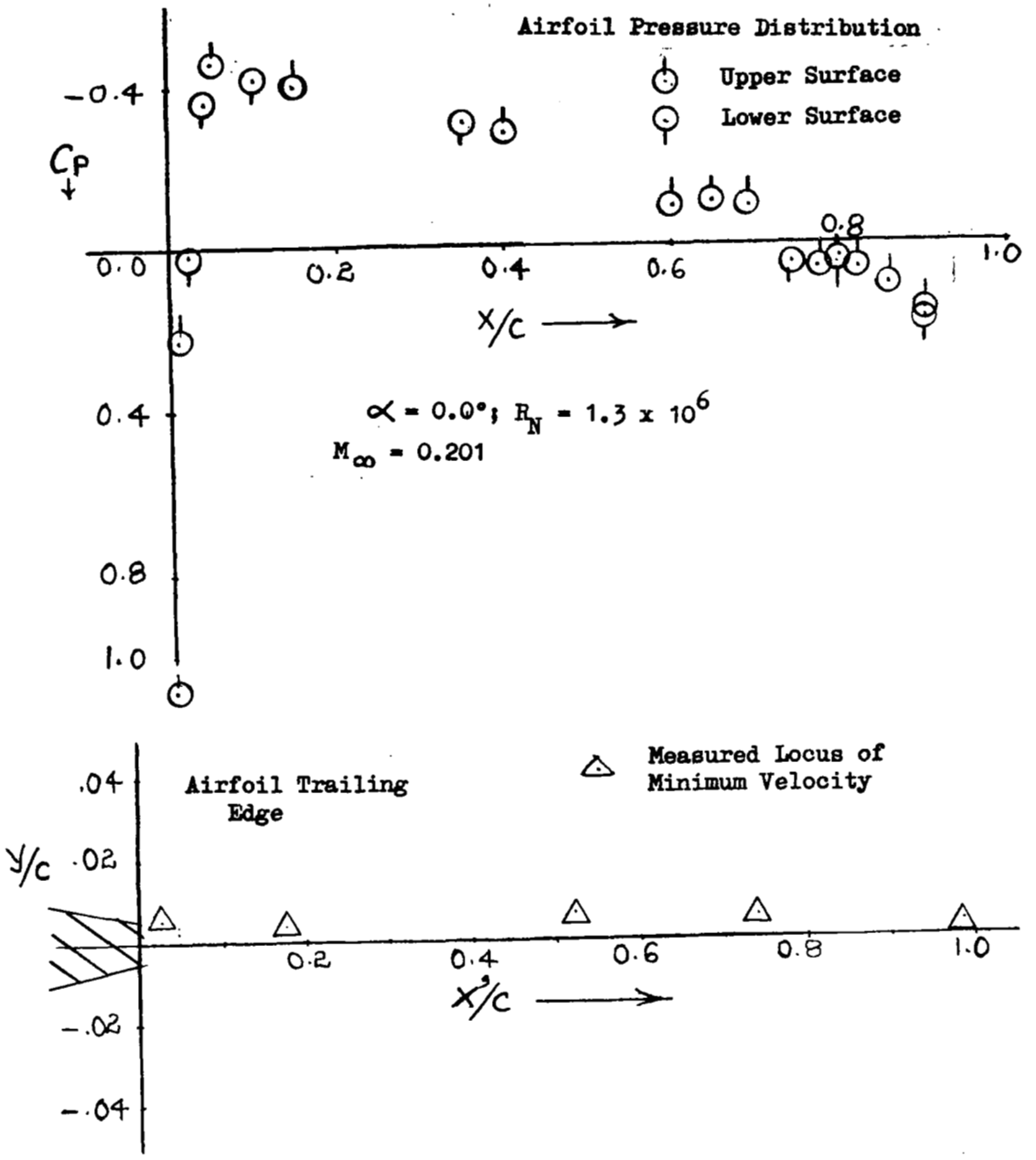

FIGURE III-23 - MEASURED PRESSURE DISTRIBUTION ON AIRFOIL SURFACE AND LOCI OF MINIMUM VELOCITY AT $\alpha = 0°$ FOR BLUNT TRAILING EDGE AIRFOIL (FREE TRANSITION)

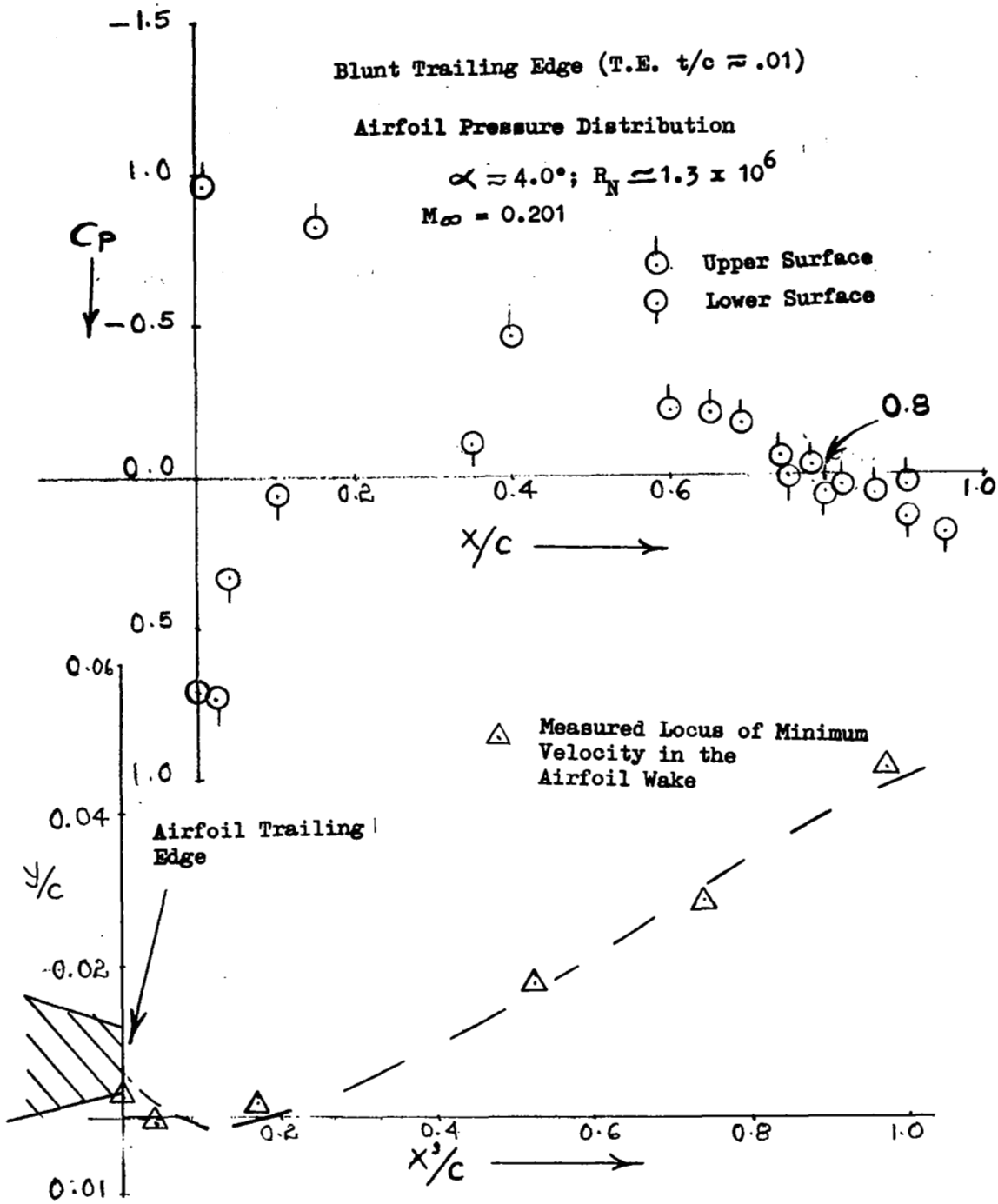

FIGURE III-24 - MEASURED PRESSURE DISTRIBUTION ON AIRFOIL SURFACE AND LOCUS OF MINIMUM VELOCITY IN THE WAKE FOR BLUNT TRAILING EDGE AIRFOIL AT α = 4.0° (FREE TRANSITION)

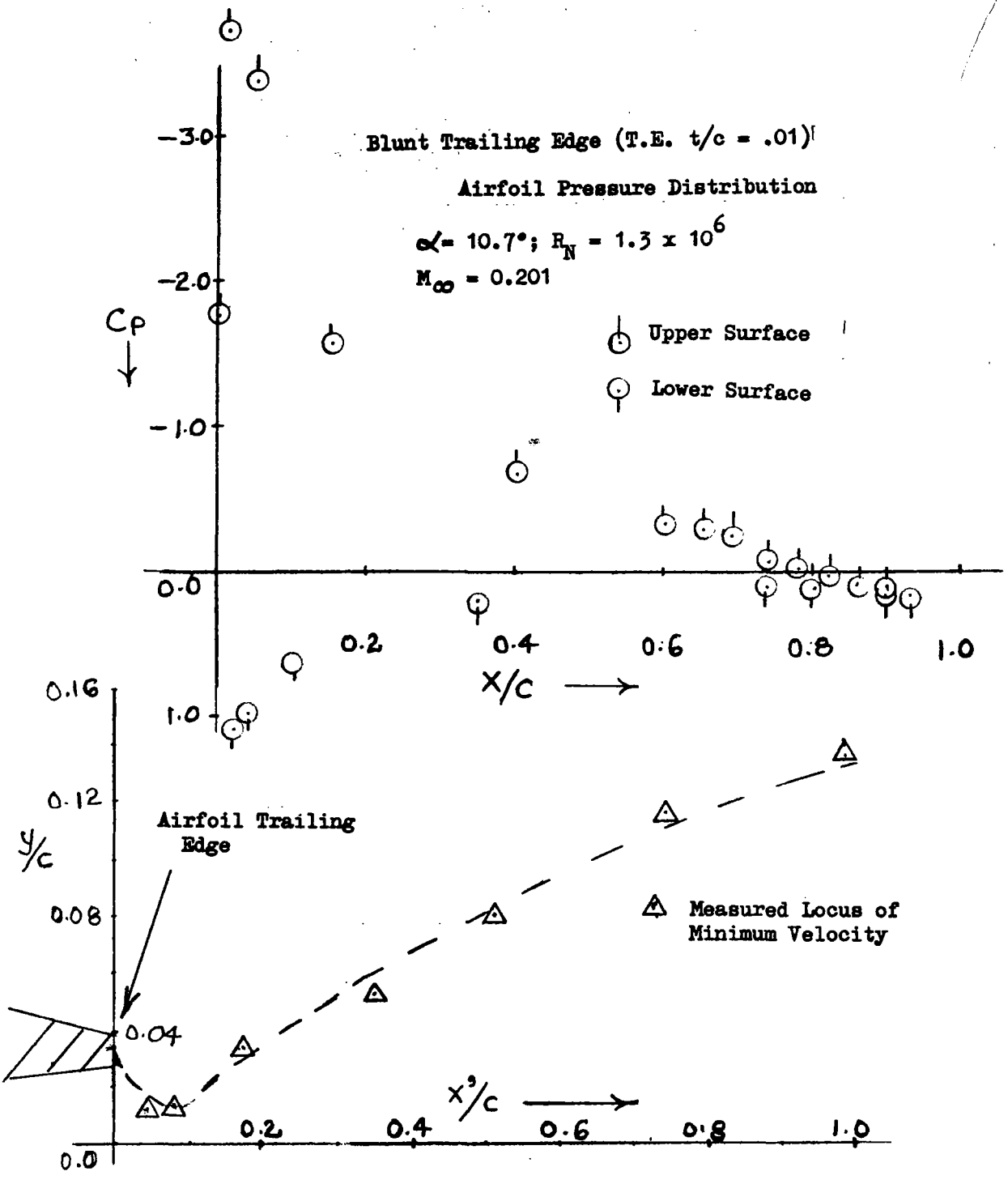

FIGURE III-25 - MEASURED PRESSURE DISTRIBUTION ON AIRFOIL SURFACE AND LOCUS OF MINIMUM VELOCITY AT α = 10.7° for BLUNT TRAILING EDGE AIRFOIL (FREE TRANSITION)

surface and, (ii) to obtain the initial conditions for the purpose of wake flow calculations by the theoretical profile drag method developed under the present studies. Figures IV-1 through IV-4 show the results of measurements of velocity profiles on the upper surface of the airfoil for angles of attack α of 0°, 8°, 11° and 13°, respectively; chordwise locations of measurements are also indicated in these figures. It can be seen from these figures that, for angles of attack of 0° and 8° and for X/C locations forward of or equal to 0.9 in case of α of 8°, the shape of velocity profile is smooth and there is an absence of scatter in the measured values. However, for angles of attack α of 11° and 13°, and in particular for chordwise location close to the trailing edge, the shape of the velocity profile is not smooth near the surface as evidenced by the appreciable scatter in the measured data. The cause of the above phenomena is found in the ability of total-static pressure probe combination to measure reliable velocity profiles under various flow conditions. The pressure probe of Figure III-9 is reliable when the viscous flow measurements are made for attached flow conditions. However, the measurements of velocity profile by this probe, for the boundary layer which is approaching separation or in separated flow region, are not reliable and are subject to interpretations. Hence, the measurements by this probe design under the above-mentioned conditions can be used for the purpose of qualitative analysis only. However, in order to determine the position of initial separation and the extent of separated flow region, measurements performed by the present design of the pressure probe can be effectively used for this purpose by the procedure such as shown in Figure IV-5. Various investigators have observed from experimental measurements of velocity profiles that the value of the form factor H at initial separation point for ordinary turbulent boundary layer is greater than approximately 2.0 and that exact value of H at separation depends upon surface roughness. Thus, in order to determine the initial separation as well as the extent of the separation region from pressure probe measurements, growth rate of integral thickness, such as the displacement or momentum thickness, needs to be examined in addition to Form Factor H. This is done in Figure IV-5 and the following conclusion can be drawn from this figure:

(1) Separation at T.E. starts at $\alpha = 8.0°$

(2) Separation at X/C = 0.9 starts at $\alpha = 11.5$ to 12°

(3) Separation at X/C = 0.8 starts at $\alpha = 13.0°$

Figures IV-6, IV-7 and IV-8 show the plots of velocity profile measured by the hot wire anemometer technique. These velocity profiles were measured on the upper surface of the airfoil with the blunt trailing edge of 1 percent thicknesses. Angles of attack corresponding to Figures IV-6, IV-7 and IV-8 are 4°, 10.8° and 13° respectively. It can be seen from these figures that measurements of velocity profiles by hot wire anemometer are smooth and reliable for attached boundary layer flow as well as for viscous flow approaching separation. Hot wire anemometer technique is unable to give any indication about the direction of the flow in the boundary layer; i.e., it gives indication only of the absolute magnitude of velocity. In addition, as the magnitude of the flow velocity approaches zero at a point in the flow, the relative magnitude of the velocity of fluctuation is large compared to the mean flow velocity at that point. Under this circumstance the accuracy of measurements by the hot wire anemometer techniques suffer as low

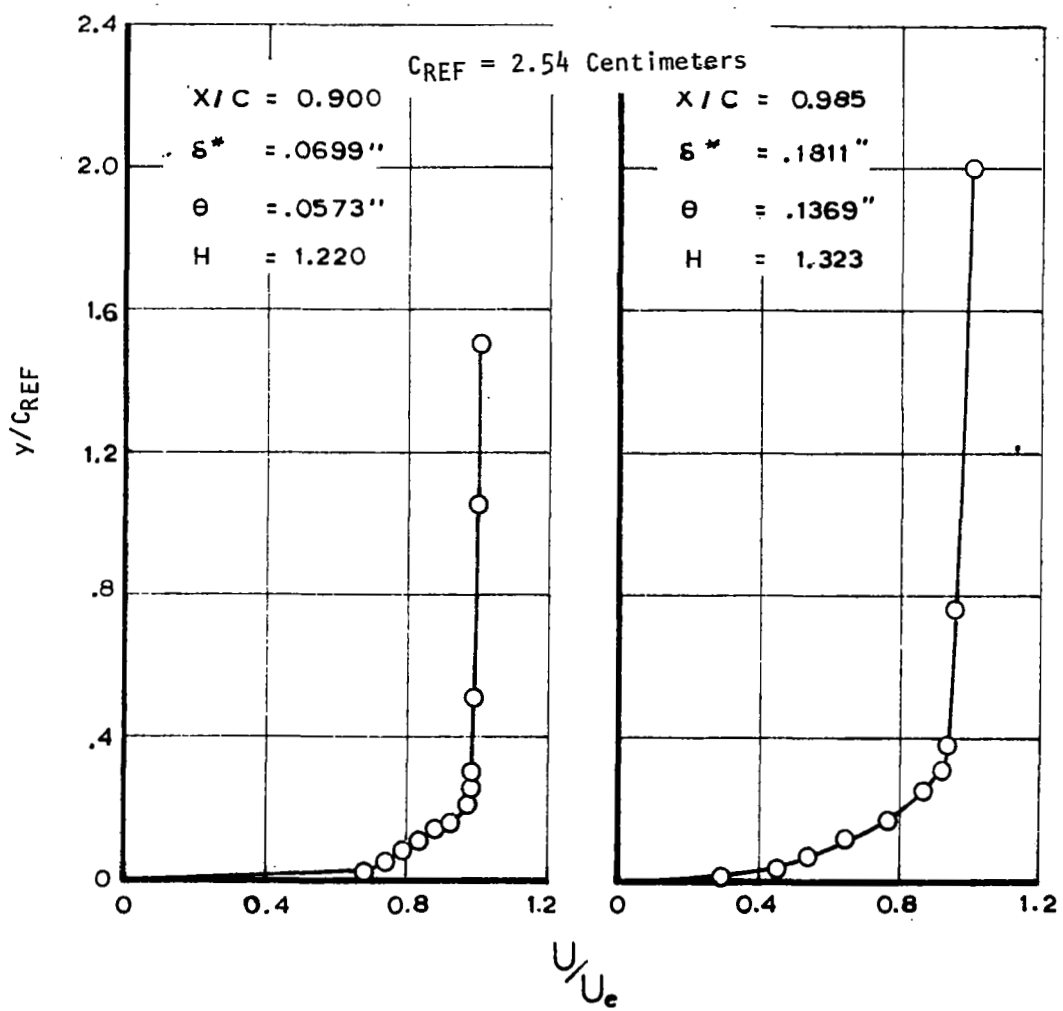

FIGURE IV-1 - VELOCITY PROFILE MEASUREMENTS ON UPPER SURFACE OF AIRFOIL AT α = 0° AND FOR SHARP TRAILING EDGE

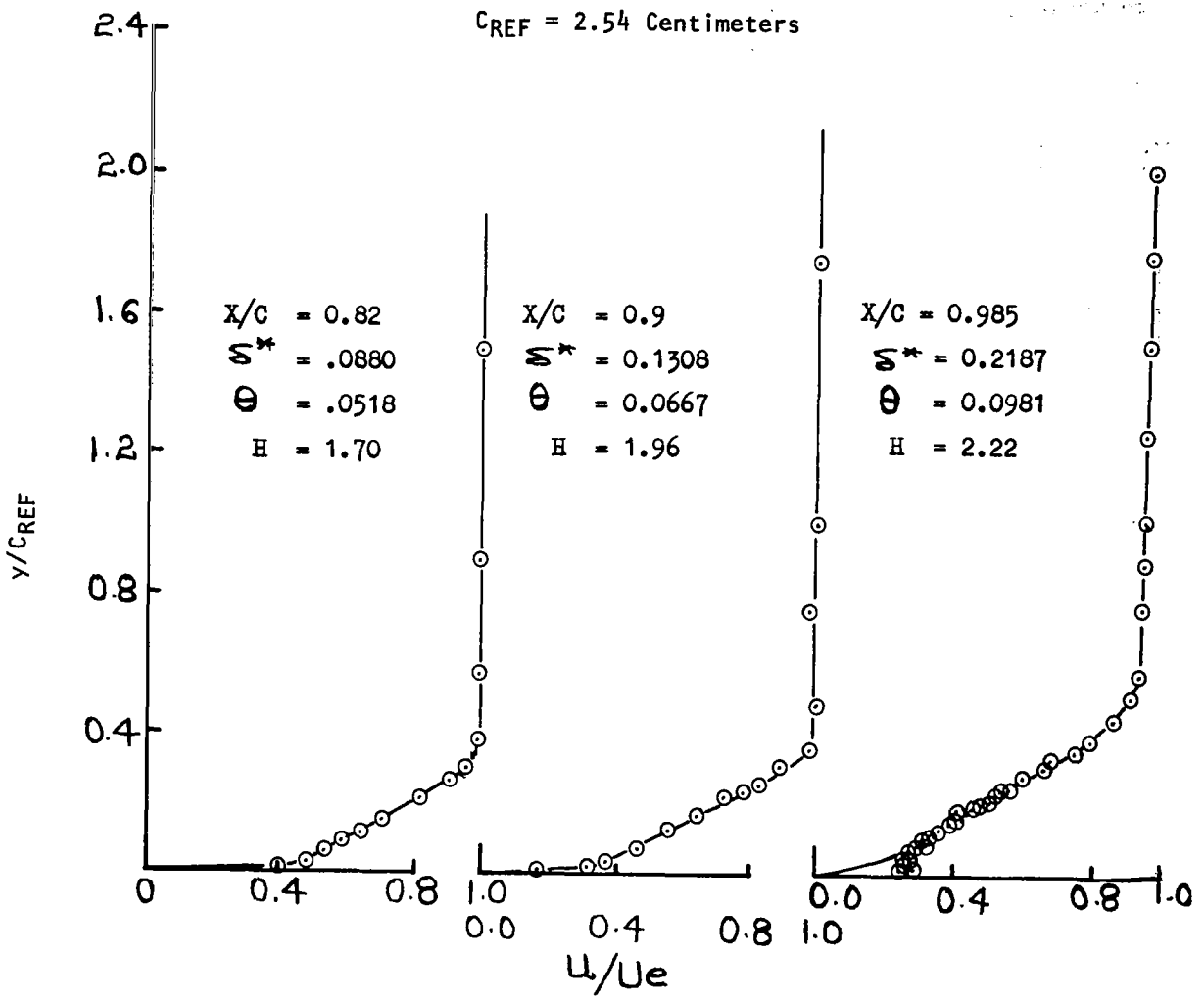

FIGURE IV-2 - UPPER SURFACE PROFILE MEASUREMENTS ON TEST AIRFOIL WITH SHARP TRAILING EDGE AT α = 8° (FREE TRANSITION)

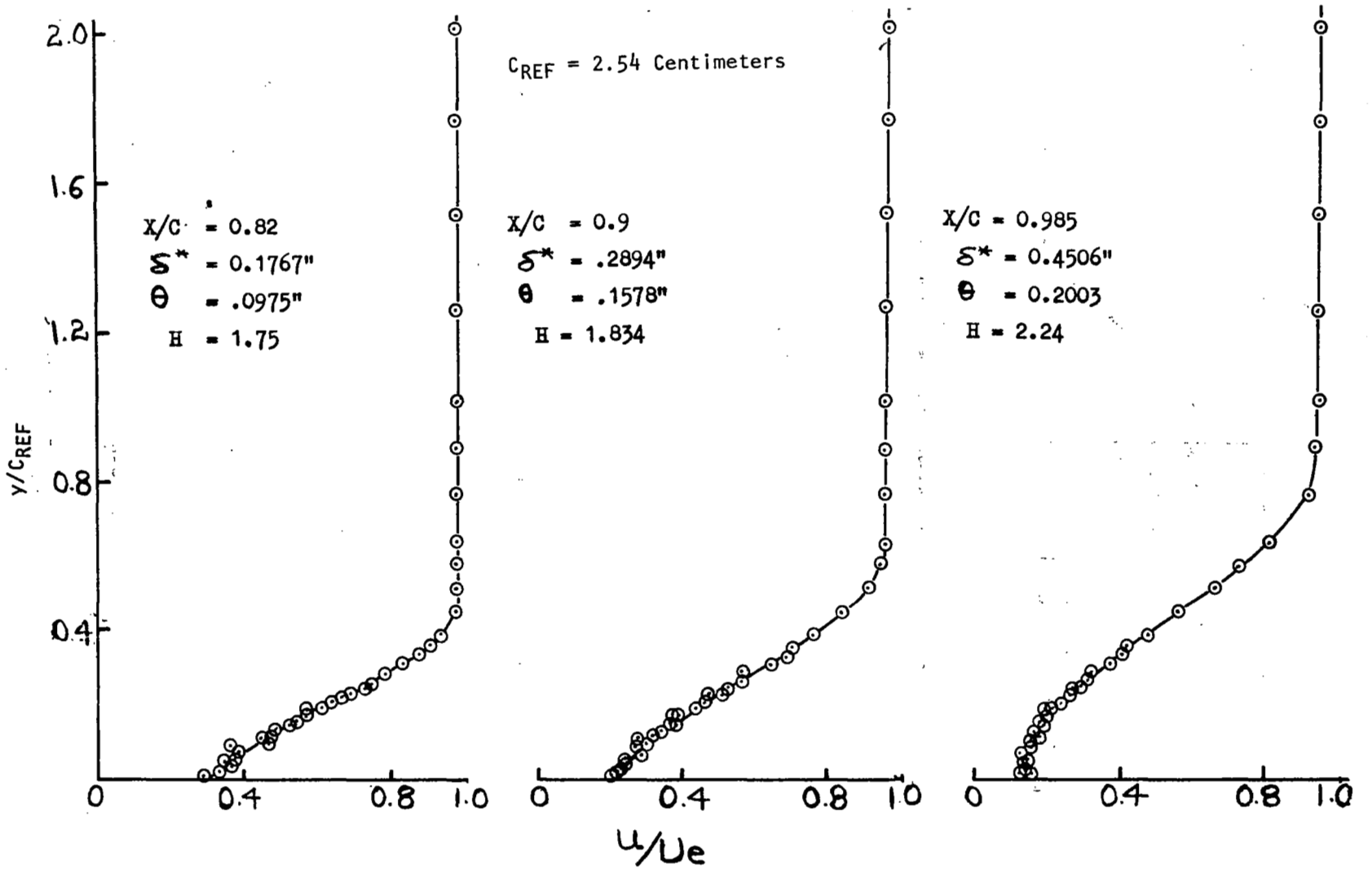

FIGURE IV-3 - VELOCITY PROFILE MEASUREMENTS ON UPPER SURFACE OF SHARP T.E. TEST AIRFOIL AT α = 11° (FREE TRANSITION)

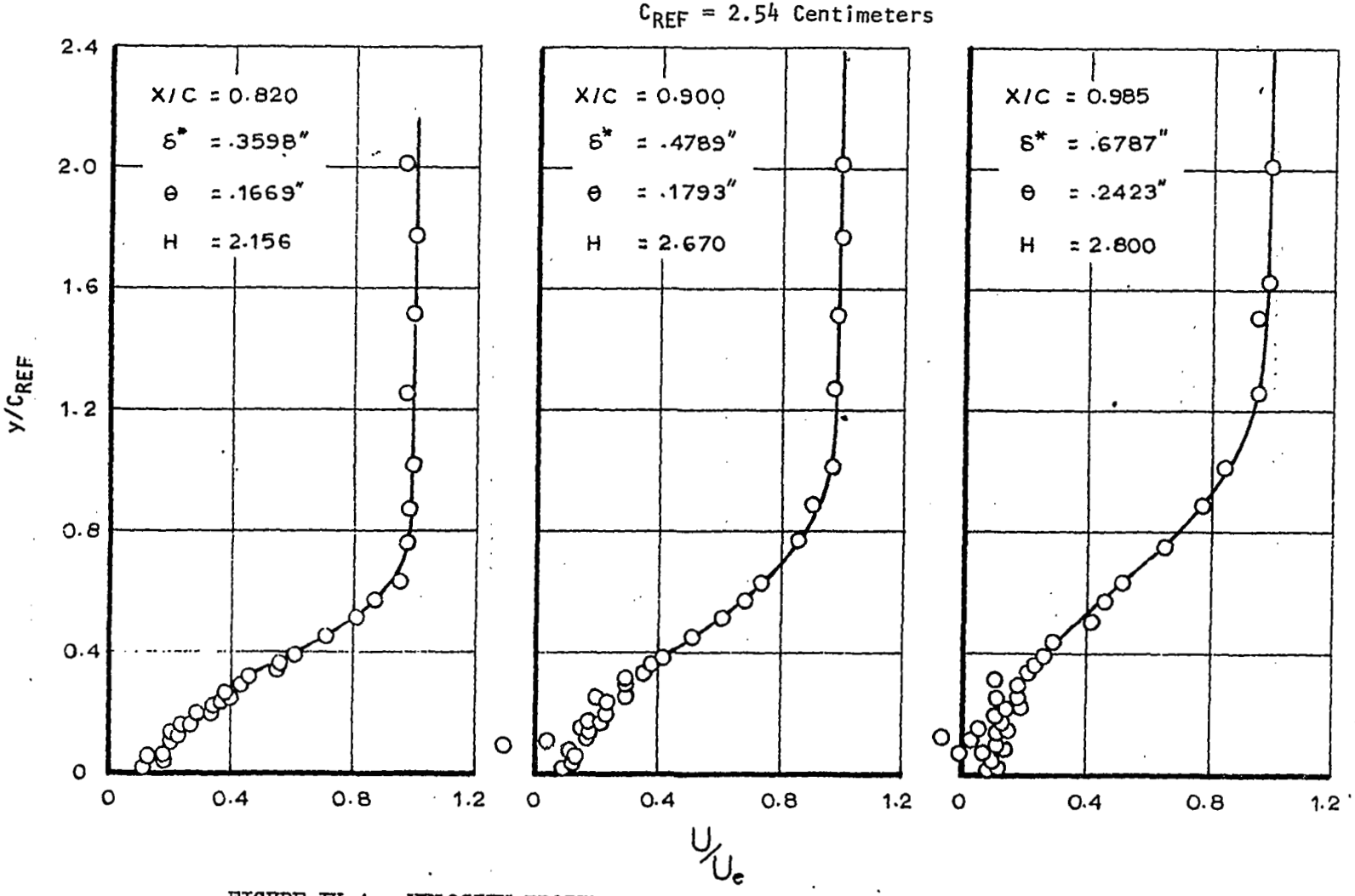

FIGURE IV-4 - VELOCITY PROFILE MEASUREMENTS ON UPPER SURFACE OF SHARP T.E. TEST AIRFOIL AT α = 13° (FREE TRANSITION)

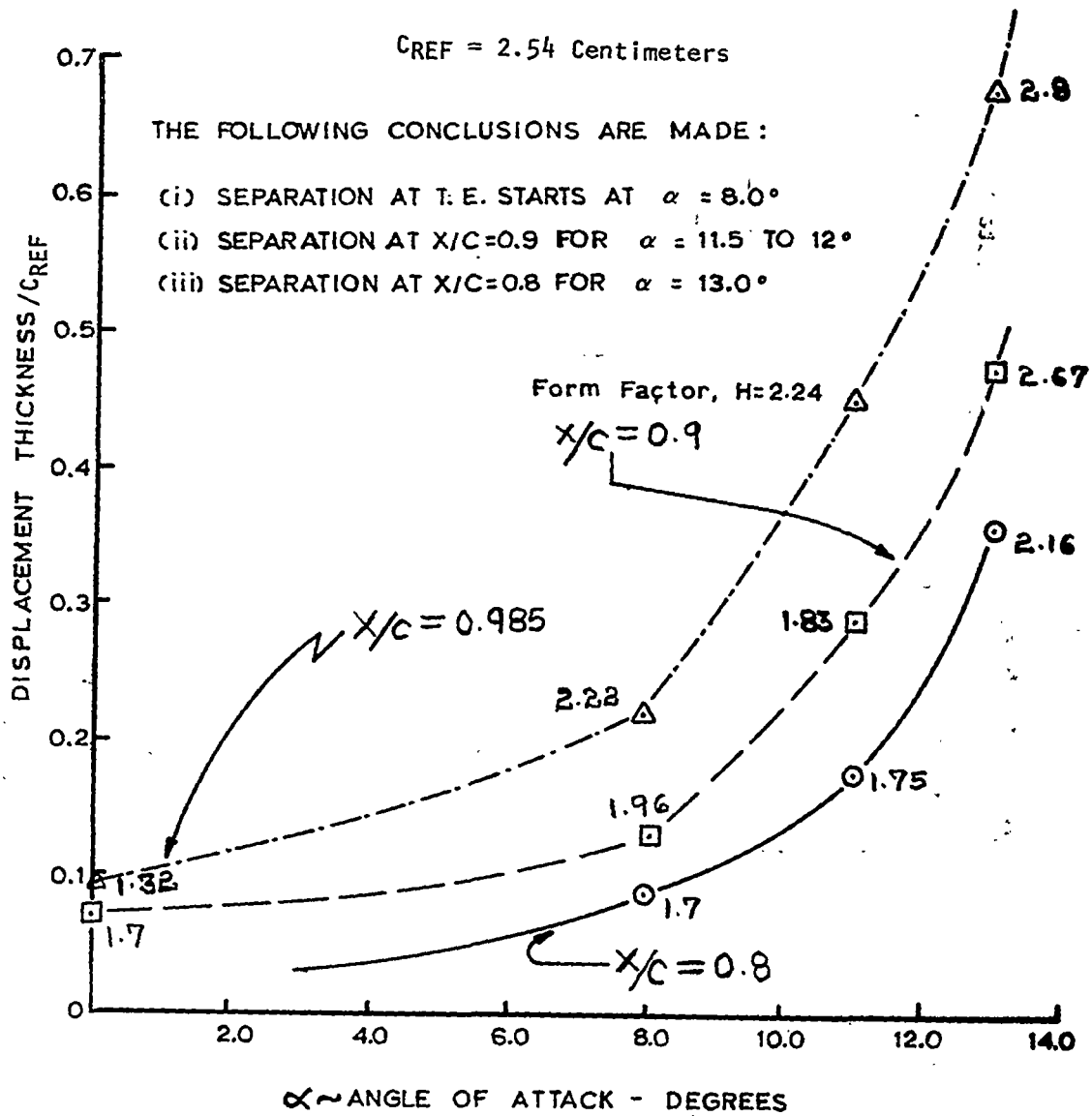

FIGURE IV-5 - PLOT OF DISPLACEMENT THICKNESS VS. ANGLE OF ATTACK AT THREE CHORDWISE LOCATIONS FOR TEST AIRFOIL (UPPER SURFACE)

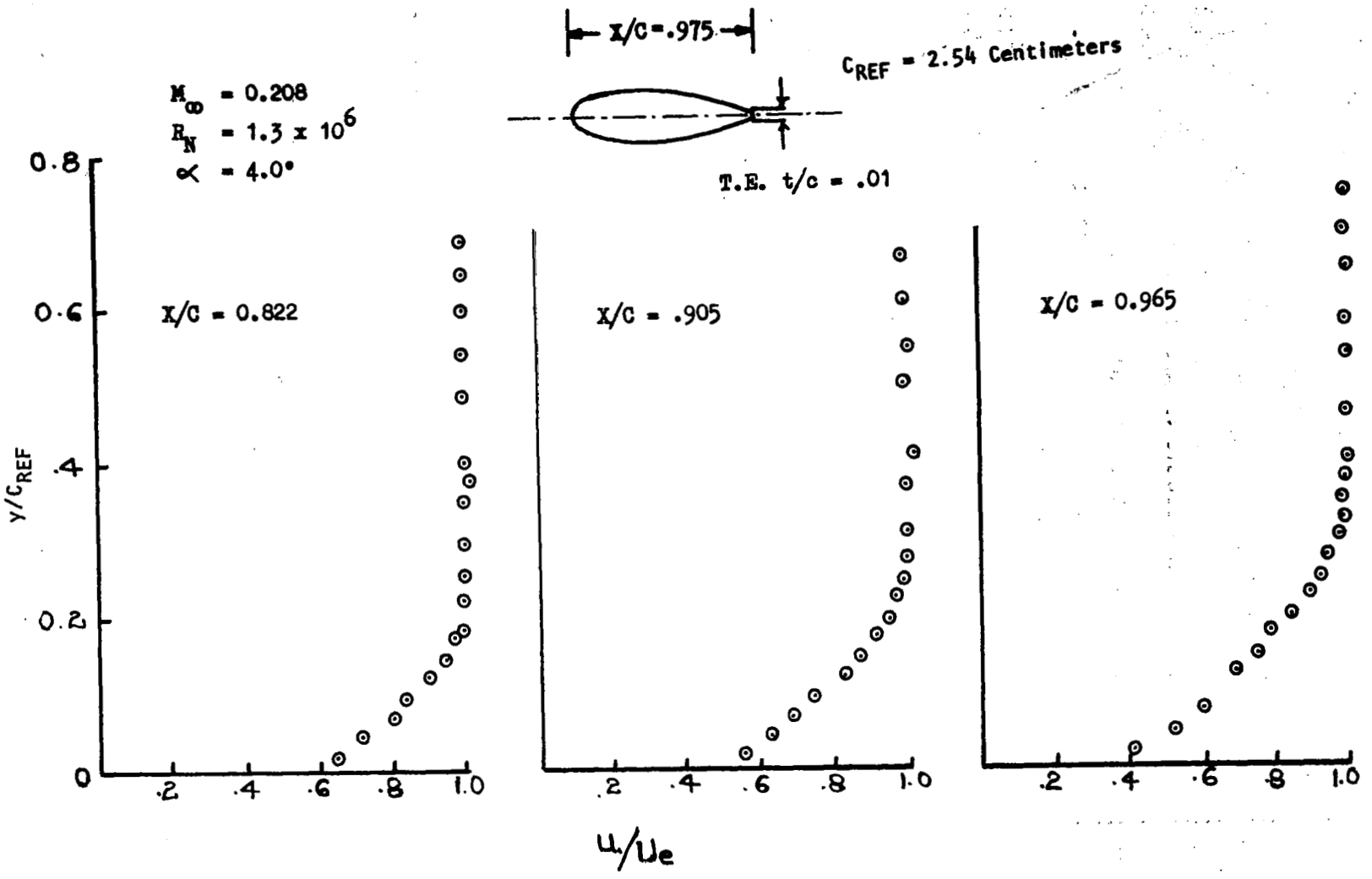

FIGURE IV-6 - EXPERIMENTAL VELOCITY PROFILES BY HOT WIRE ANEMOMETER AT α = 4.0° ON THE UPPER SURFACE OF AIRFOIL WITH BLUNT TRAILING EDGE

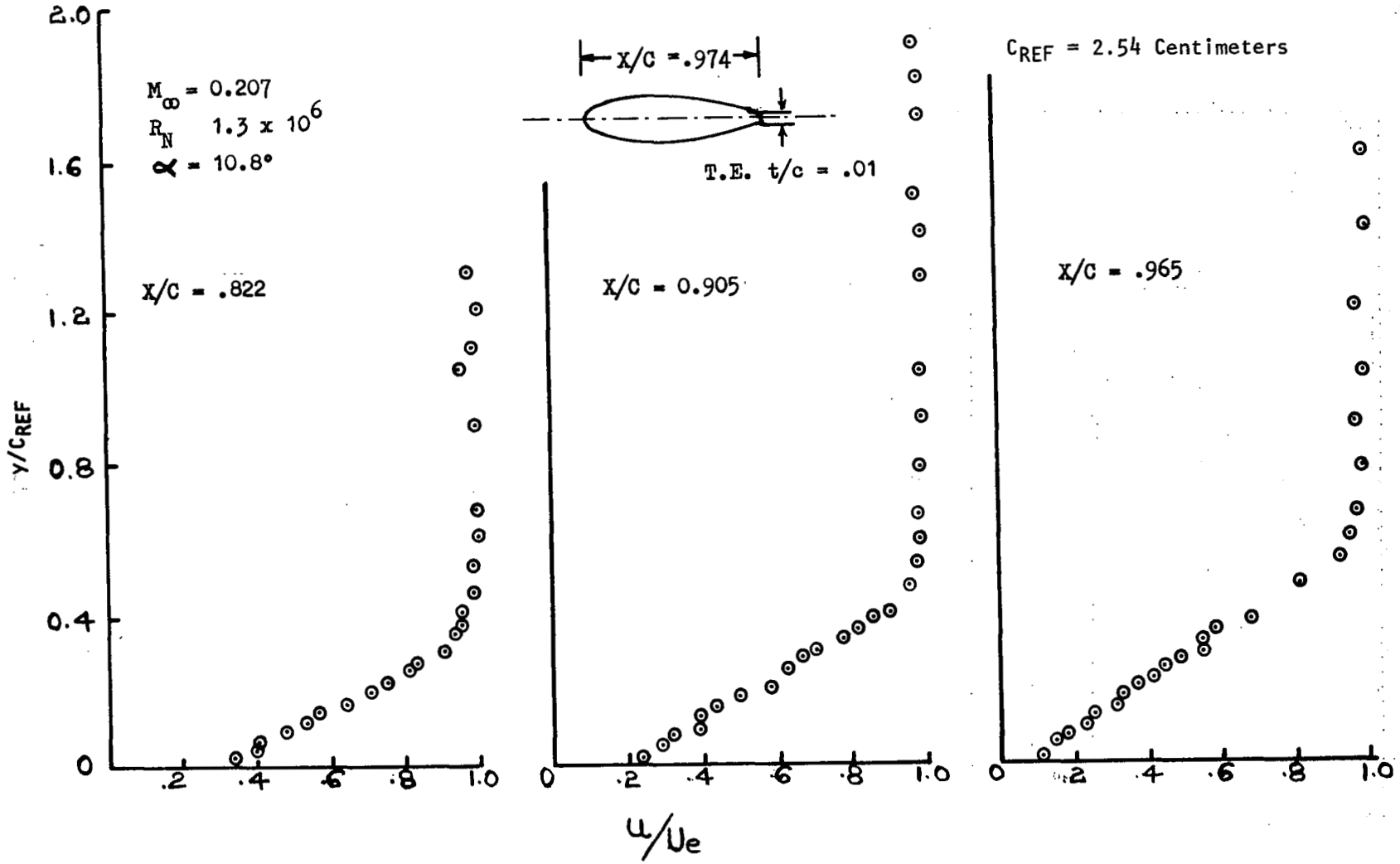

FIGURE IV-7 - EXPERIMENTAL VELOCITY PROFILES BY HOT WIRE ANEMOMETER AT $\alpha = 10.8°$ ON THE UPPER SURFACE OF AIRFOIL WITH BLUNT TRAILING EDGE

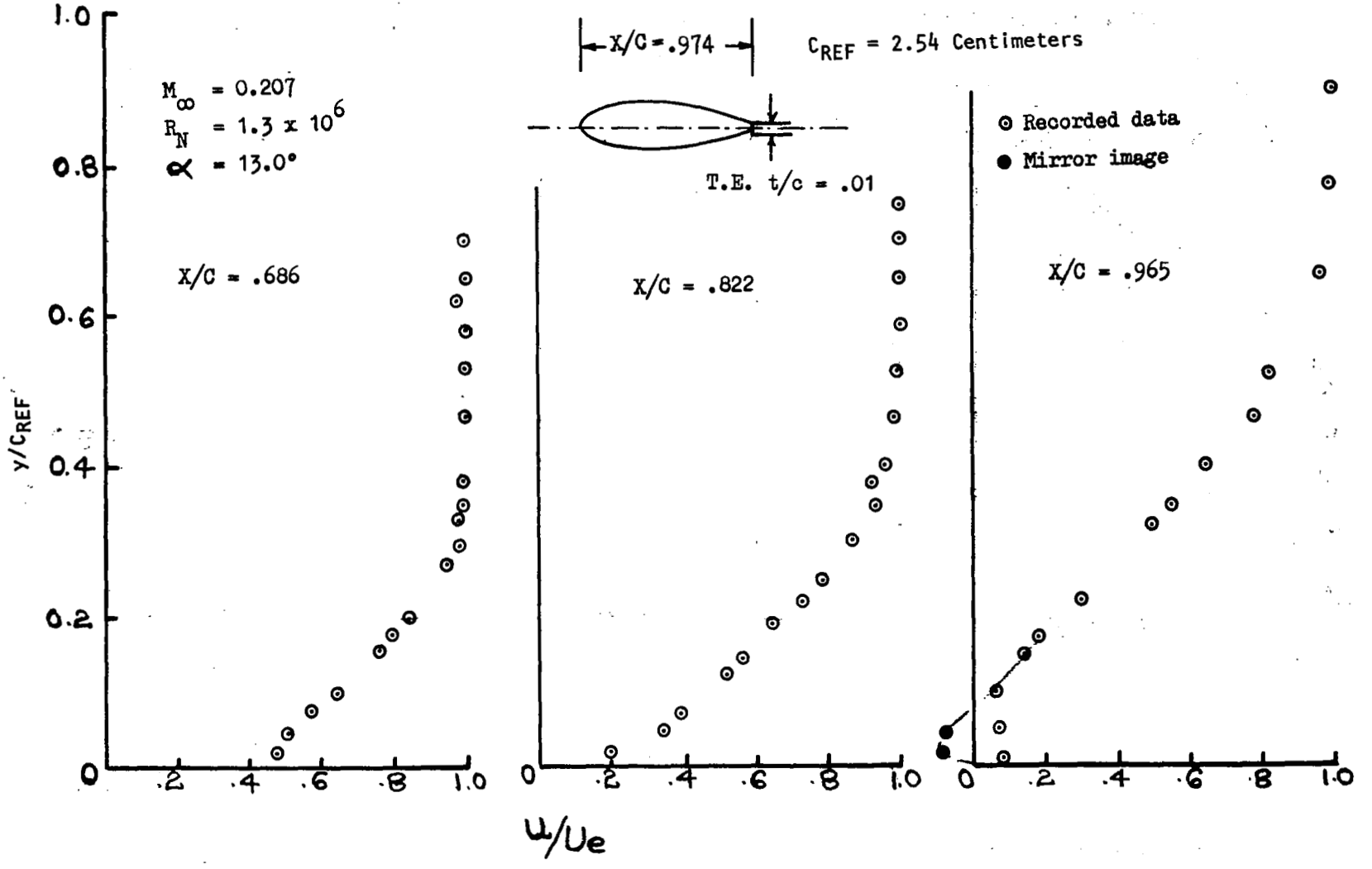

FIGURE IV-8 - EXPERIMENTAL VELOCITY PROFILES BY HOT WIRE ANEMOMETER AT α = 13.0° ON THE UPPER SURFACE OF AIRFOIL WITH BLUNT TRAILING EDGE

values of velocities are approached in a turbulent flow with reverse flow velocity profiles. Because of the above two reasons, it is necessary to exercise some judgment in fairing the velocity profile shape when measurements are made with the hot wire anemometer techniques in a boundary layer flow having reverse flow velocity profiles. Moreover, large numbers of data points, in the vicinity of values of y locations where the zero velocity is approached, would make it possible to exercise sounder judgment in fairing reverse flow velocity profiles near the y locations when the values of velocity are near zero and near the wall where negative velocities are encountered. An example of this type of fairing is shown in Figure IV-8 for value of X/C = 0.965.

An example of the type variations of velocity profile in the wake of the test airfoil with sharp trailing edge is shown in Figure IV-9. These wake surveys correspond to an angle of attack α of 8° and when transition on the lower and upper surfaces of the airfoil were fixed at 10 percent chord by the use of grit strips. The wake surveys shown in this figure were performed by the use of total-static pressure probe combination shown in Figure III-9. Near the trailing edge the rate of increase in minimum velocity U_w with respect to the distance X'/C is quite large compared to the large distance downstream from the trailing edge. This figure also points out that the rate of variations in the width of the wake is small at a far distance downstream compared to near the trailing edge. It should be mentioned that this figure is not plotted to give true relative y locations for velocity profiles at different X'/C locations but to indicate relative shape of the velocity profiles at different X'/C locations in the wake behind the airfoil.

Figure IV-10 shows the example of experimentally measured variations of momentum thickness and form factor in the wake behind the sharp trailing edge test airfoil. The data shown in this figure are for an angle of attack of 8°, for conditions of free transition on the airfoil surfaces and for free stream Reynolds number of approximately 1.3 million. It can be seen from this figure that values of momentum thickness and form factor decrease in the downstream direction in the airfoil wake and at far distance downstream in the wake their values become approximately constant.

Examples of typical measurements of static pressure distributions across the airfoil wake behind the sharp trailing edge test airfoil are shown in Figures IV-11, IV-12 and IV-13; corresponding measurements of velocity profiles are also shown in these figures. Figure IV-11 is for angle of attack α = 0.0°, IV-12 is for α = 8.0° and fixed transition on upper and lower surfaces of the airfoil; and Figure IV-13 is for α = 10.8°. Measurements shown in these figures indicate that static pressure is not constant across the wake but has an approximate parabolic variation. These figures indicate that static pressure has a higher value at lower edge of wake and lower value at the upper edge of wake for angles of attack greater than zero degree. In addition, it is seen from these figures that the maximum value of the static pressure in the wake occurs in the vicinity of y location corresponding to minimum velocity point in the wake velocity profile.

Figures IV-14, IV-15 and IV-16 show indirect measurements of shear stress profiles at angles of attack of 0° and 10.8° and at few chordwise locations in the wake behind the airfoil trailing edge. These shear stress profiles are

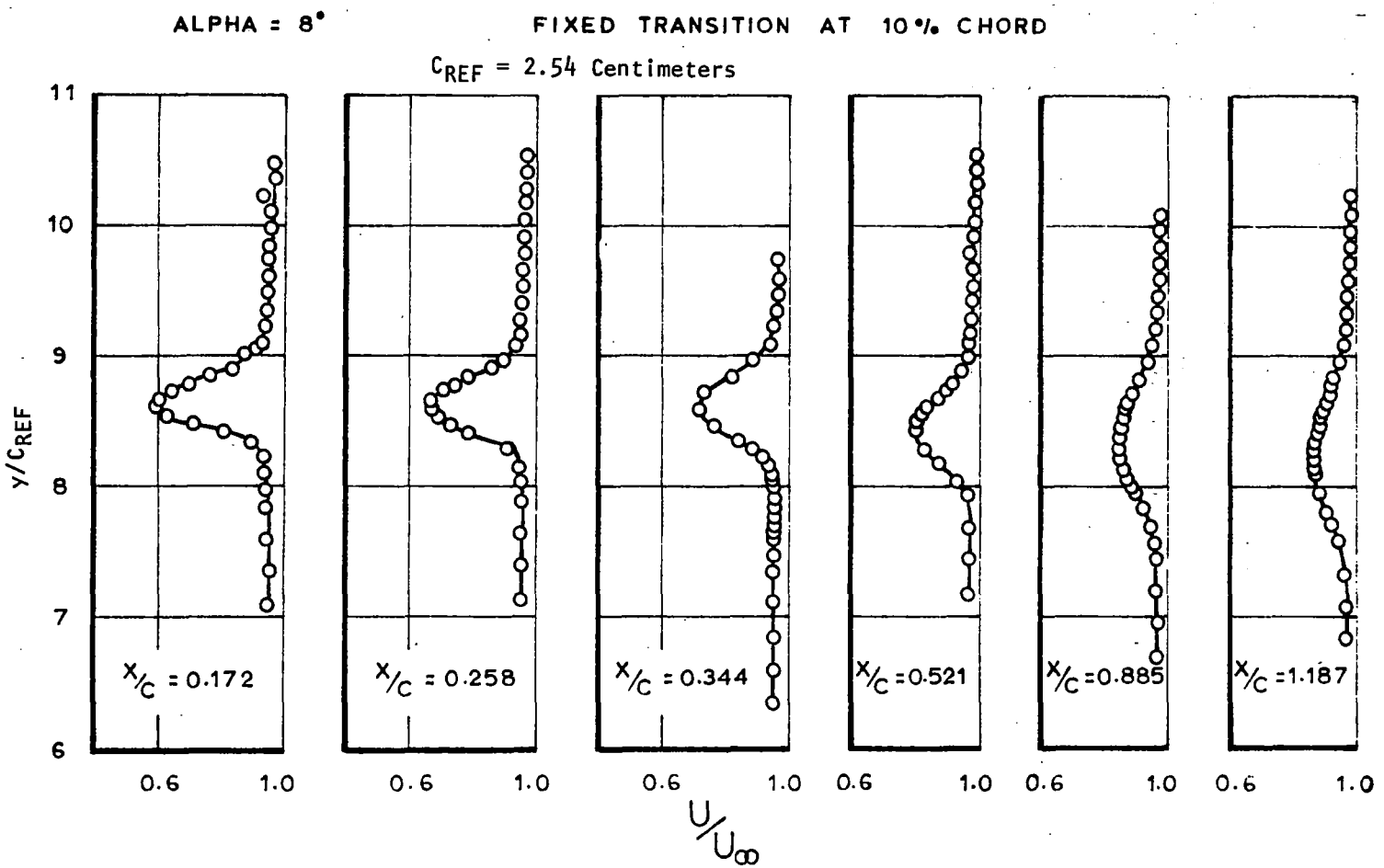

FIGURE IV-9 - WAKE SURVEY FOR SHARP TRAILING EDGE TEST AIRFOIL WITH FIXED TRANSITION AND ANGLE OF ATTACK OF 8°

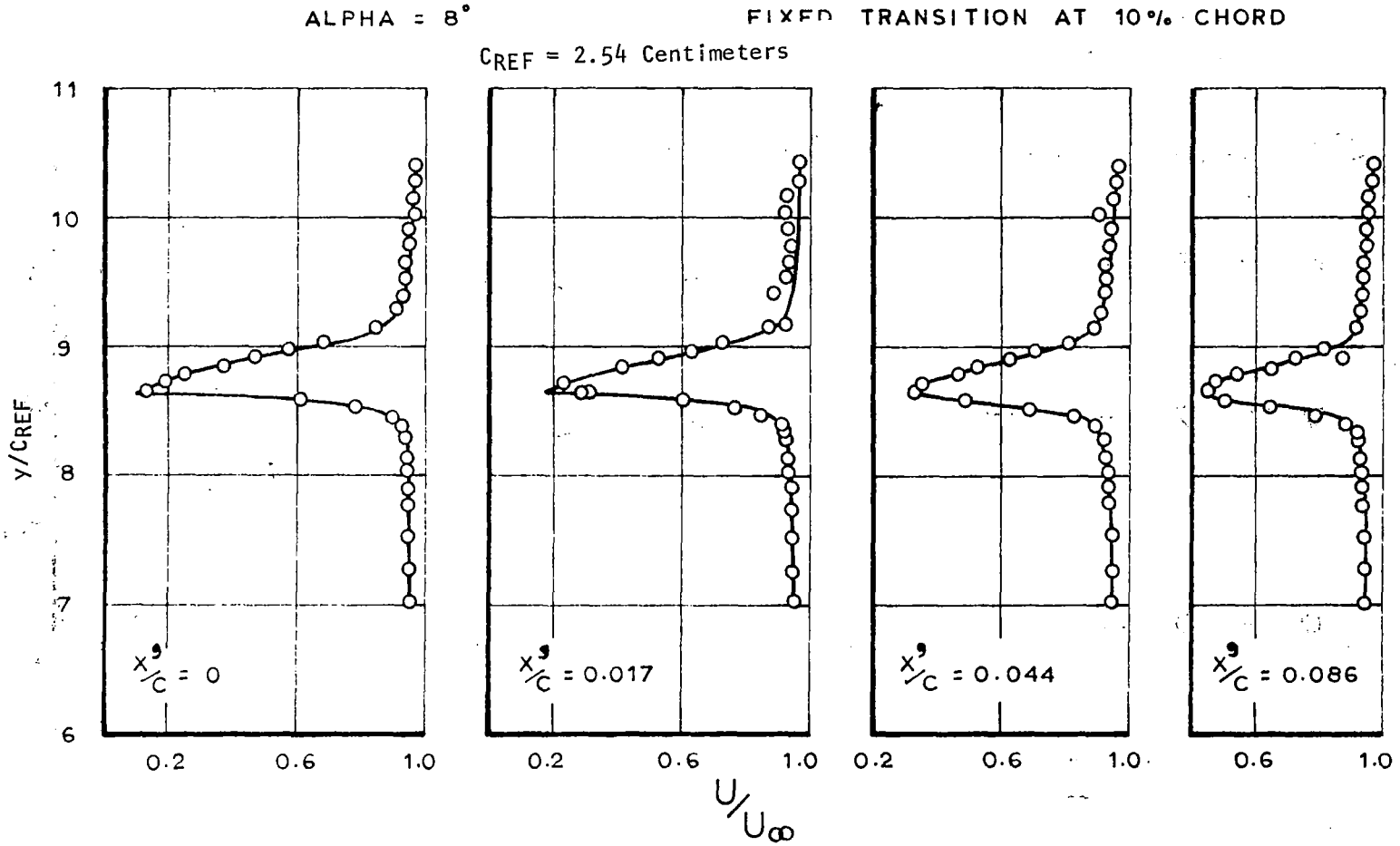

FIGURE IV-9 - WAKE SURVEY FOR SHARP TRAILING EDGE TEST AIRFOIL WITH FIXED TRANSITION AND ANGLE OF ATTACK OF 8°

(Continued)

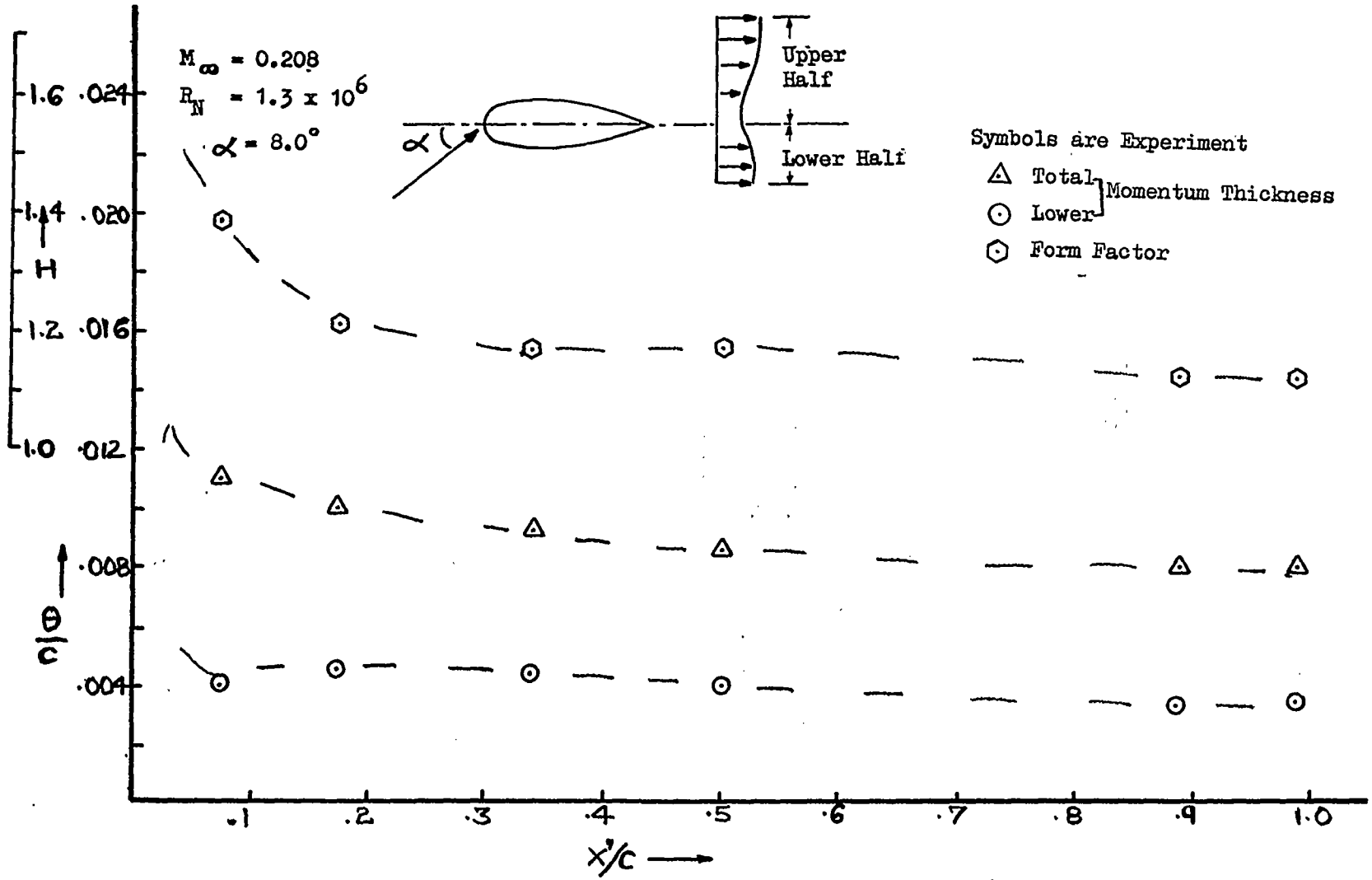

FIGURE IV-10 - MOMENTUM THICKNESS AND FORM FACTOR DISTRIBUTION IN THE WAKE OF SHARP T.E. TEST AIRFOIL AT ANGLE OF ATTACK OF 8° (FREE TRANSITION)

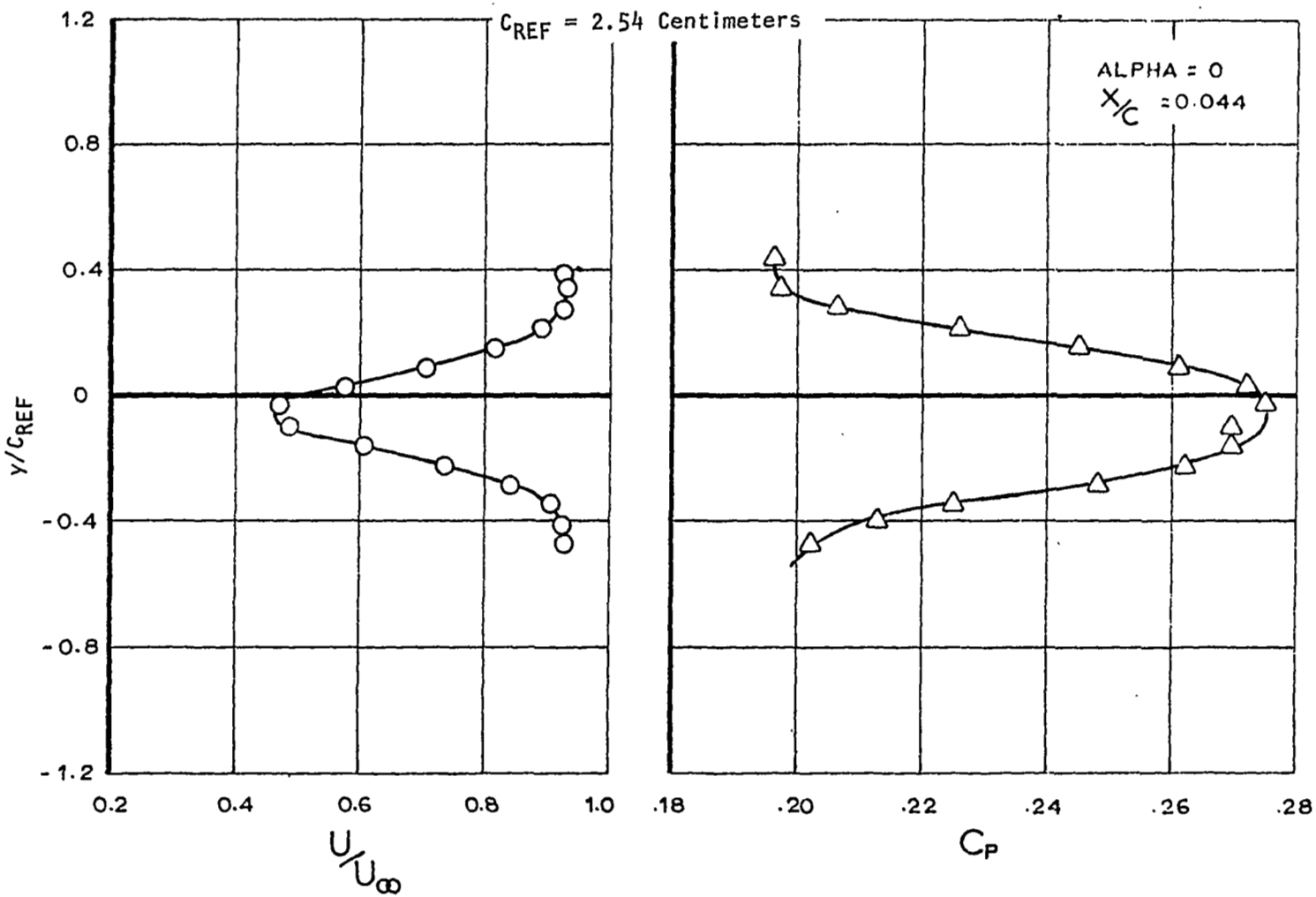

FIGURE IV-11 - VARIATION OF MEASURED STATIC PRESSURE DISTRIBUTION AND VELOCITY PROFILE ACROSS THE WAKE OF SHARP T.E. TEST AIRFOIL AT $\alpha = 0.0°$

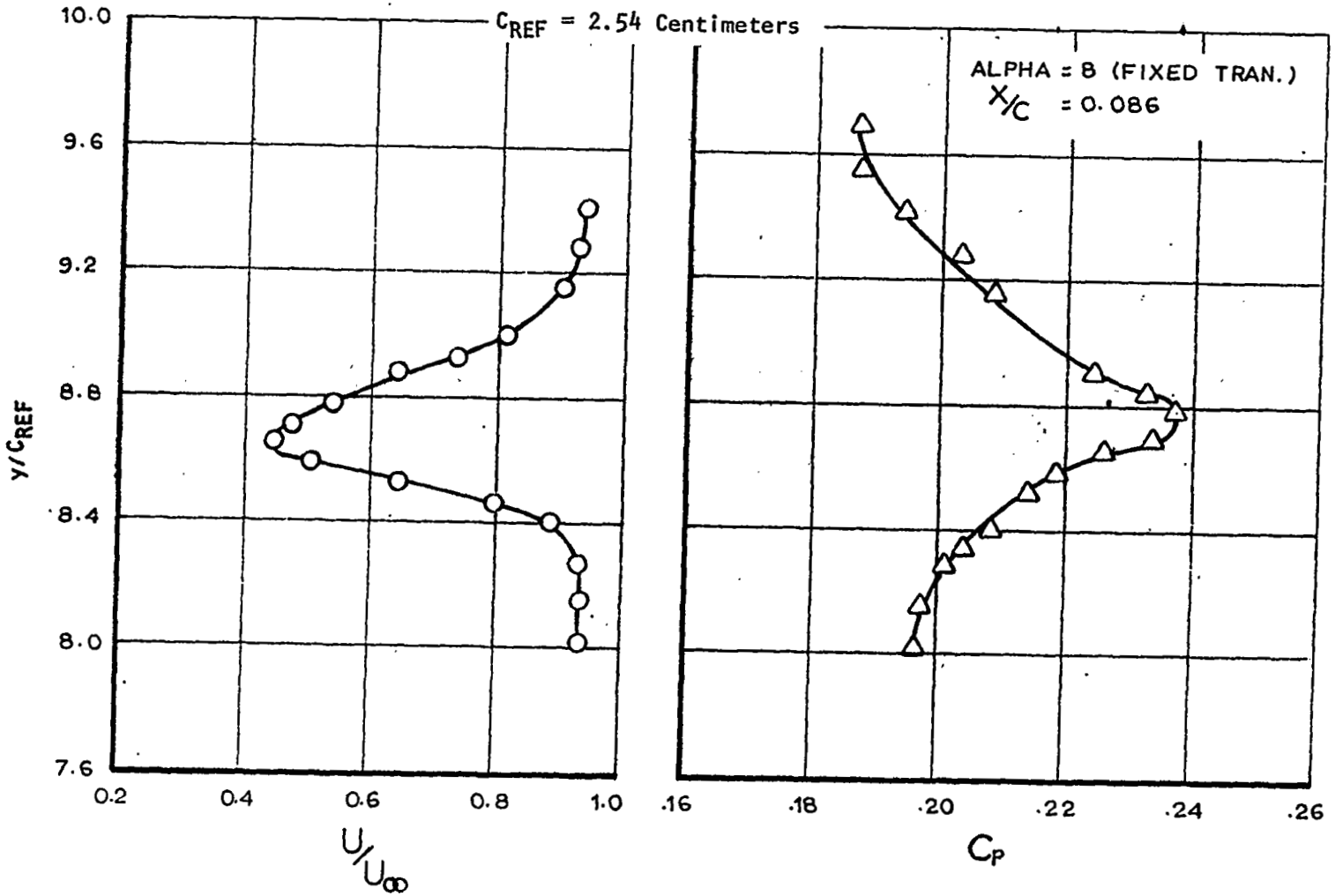

FIGURE IV-12 - VARIATION OF MEASURED STATIC PRESSURE DISTRIBUTION AND VELOCITY PROFILES ACROSS THE WAKE OF SHARP T.E. TEST AIRFOIL AT α = 8°

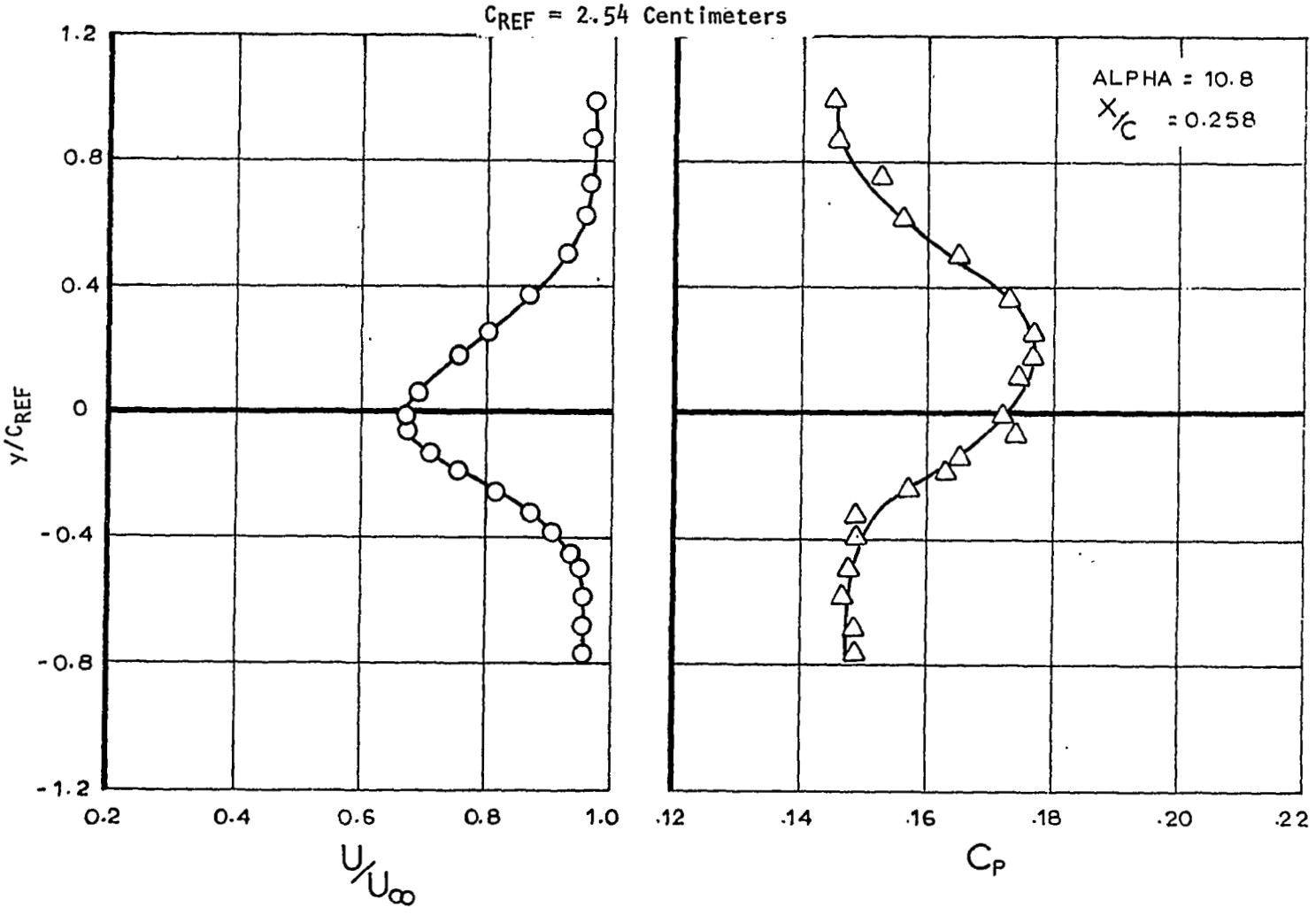

FIGURE IV-13 - VARIATION OF MEASURED STATIC PRESSURE DISTRIBUTION AND VELOCITY PROFILE ACROSS THE WAKE OF SHARP T.E. TEST AIRFOIL AT α = 10.79°

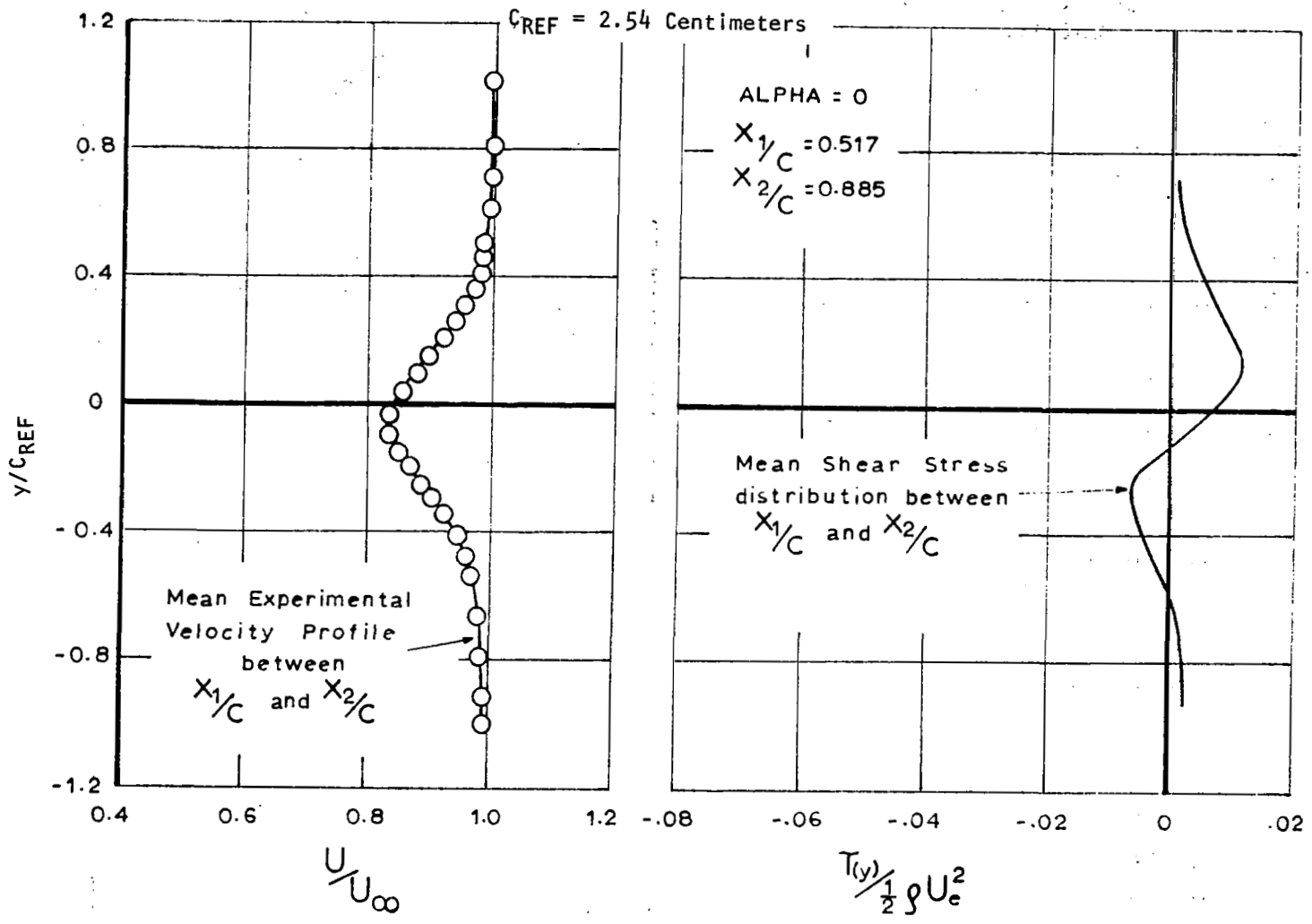

FIGURE IV-14 - COMPUTED SHEAR STRESS DISTRIBUTION AND EXPERIMENTAL VELOCITY PROFILE IN THE WAKE OF SHARP T.E. TEST AIRFOIL AT $\alpha = 0.0°$

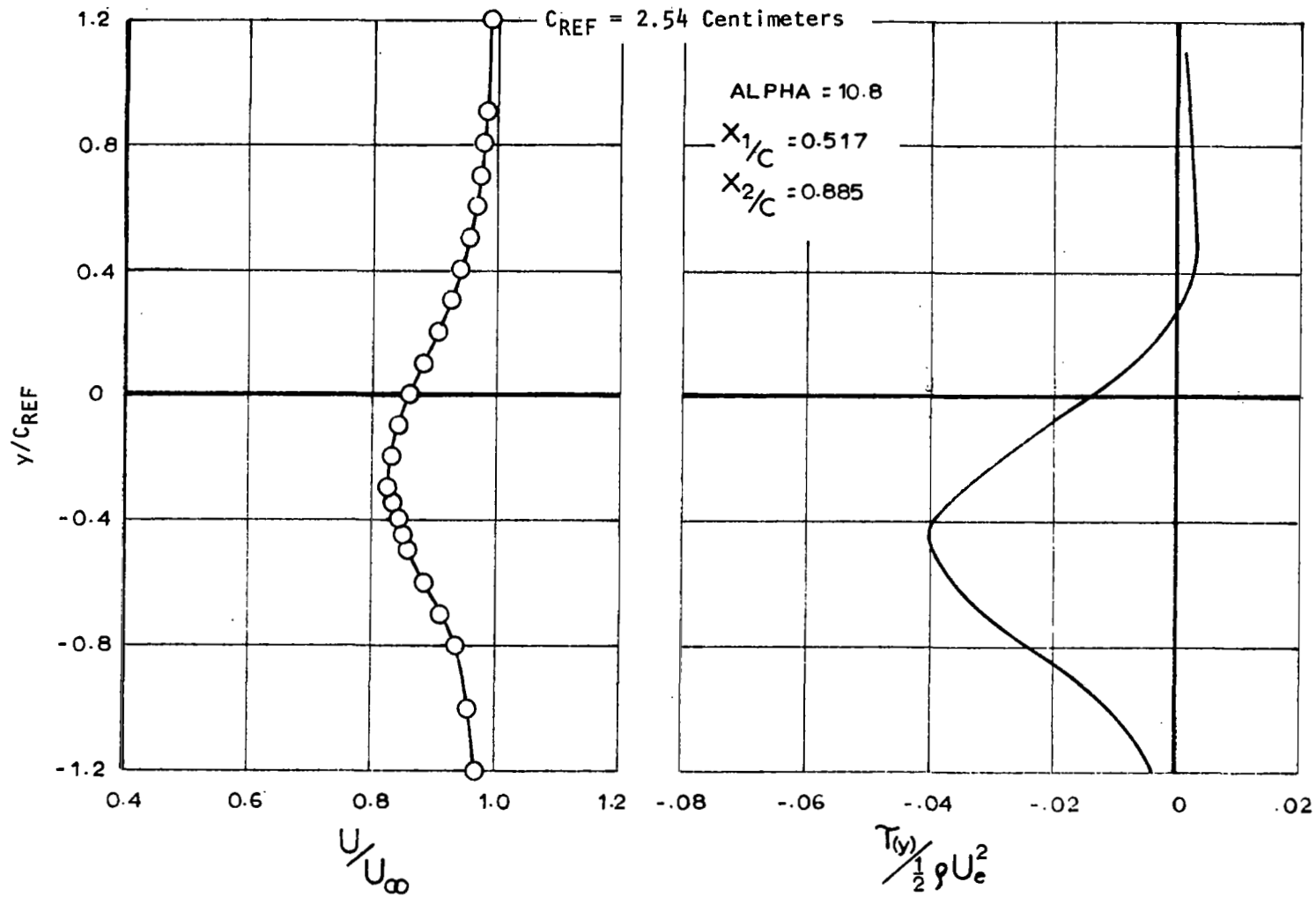

FIGURE IV-15 - COMPUTED SHEAR STRESS DISTRIBUTION AND EXPERIMENTAL VELOCITY PROFILE IN THE WAKE OF SHARP T.E. TEST AIRFOIL AT α = 10.79°

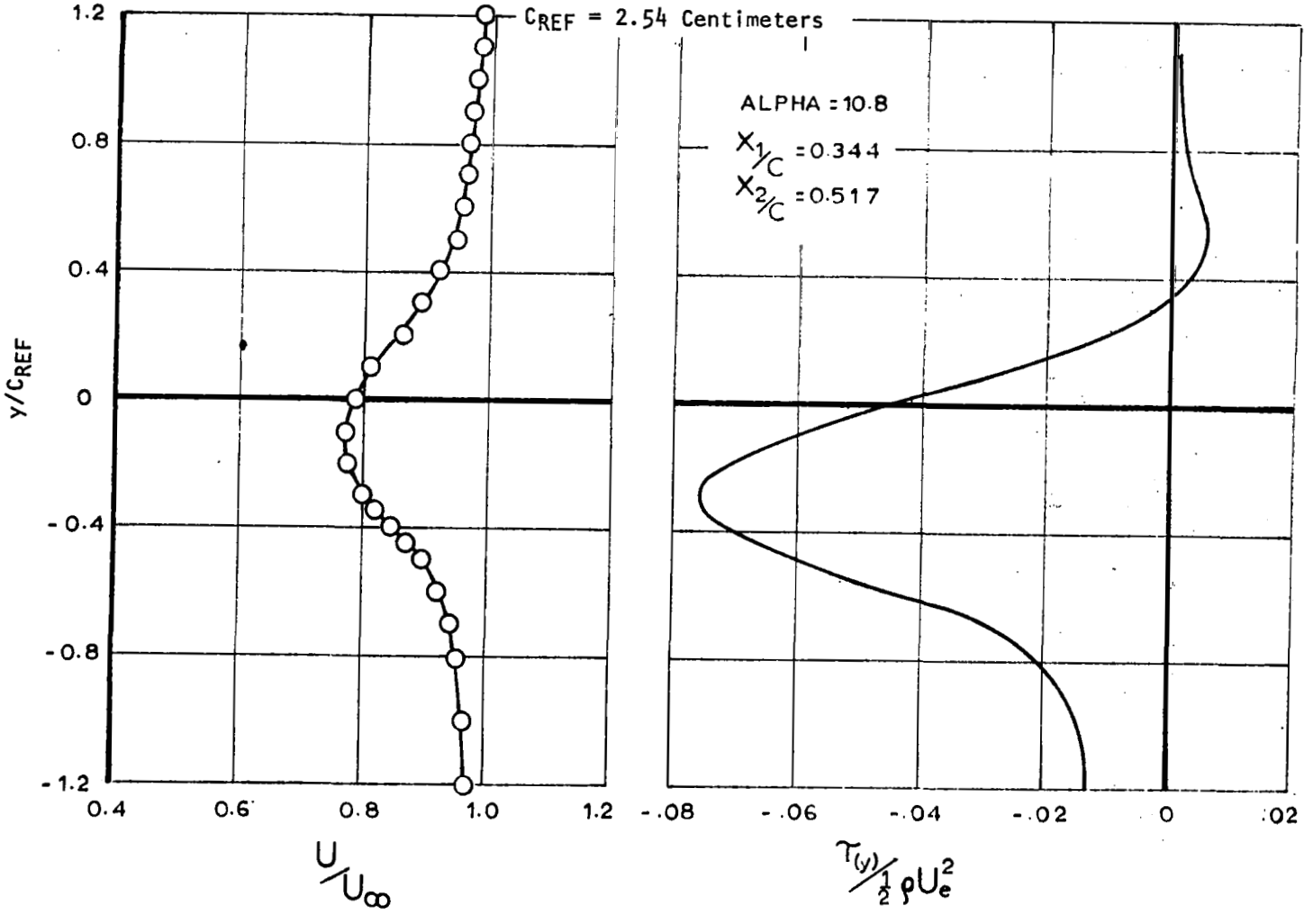

FIGURE IV-16 - COMPUTED SHEAR STRESS DISTRIBUTION AND EXPERIMENTAL VELOCITY PROFILE IN AIRFOIL WAKE AT α = 10.8° (X_1/C = 0.344; X_2/C = 0.517)

computed by the numerical solution of integro-differential equation (III-17) in which the boundary conditions of experimentally measured velocity profiles and static pressure distribution is used. These figures show some interesting results such as the value of the shear stress $T_{(y)}$ is maximum (or minimum) at the y location in the wake velocity profile where the velocity has minimum value. Classical theories such as Boussinesq's eddy viscosity concept and Prandtl's mixing length theory would, on the other hand, indicate a value of zero shear stress on the locus of minimum velocity point. As a matter of fact, the value of shear stress, at a y location corresponding to the locus of minimum velocity, can become as high as 8 to 10 percent of free stream dynamic head as can be seen from these figures. The value of the shear stress on the minimum velocity locus is used as one of the boundary conditions in the theoretical equations in the present method for the calculations of the wake flow and the profile drag of a given airfoil. Hence, the use of Boussinesq's or Prandtl's hypothesis in the present method may lead to erroneous calculation results.

IV.2 Investigations of Fundamental Parameters for Wake Flow

Theoretical equations in Section II contain such terms as (i)

$$\int_0^{K_1} f(\eta)\, d\eta, \quad \int_0^{K_1} f^2(\eta)\, d\eta,$$

(ii) shear integral terms $\int \tau/\rho\, dy$ and shear distribution $\tau(y_8)/\rho$ on the locus of minimum velocity and (iii) integral for pressure distribution across the wake $\int C_p\, dy$, distribution of static pressure on the loci for outer and inner edges of wake and also on the locus of the minimum velocity. In order to solve these theoretical equations for the calculations of flow in the wake and prediction of profile drag of airfoil sections, it is necessary to express the above items by auxiliary equations as functions of either dependent variables or in terms of initial conditions in the vicinity of trailing edge. In this way the number of dependent variables, which are required for the complete specification of flow in the wake, are kept the same as the number of theoretical equations. These auxiliary equations are derived, as shown in the following paragraphs, by the use of dimensional analysis, investigation of generalized parameters and by the use of available results for "similar flows". For this purpose use is also made of experimental measurements obtained during the present investigation.

IV.2.1 Functional Relationships for Velocity Profile Similarity for Wake Flow: Figures IV-17 and IV-18 are the plots of experimental data for similarity of velocity profiles with different similarity parameters. Experimental data used in constructing these similarity curves are for chordwise locations in the wake which are far from the airfoil trailing edge. The same experimental data

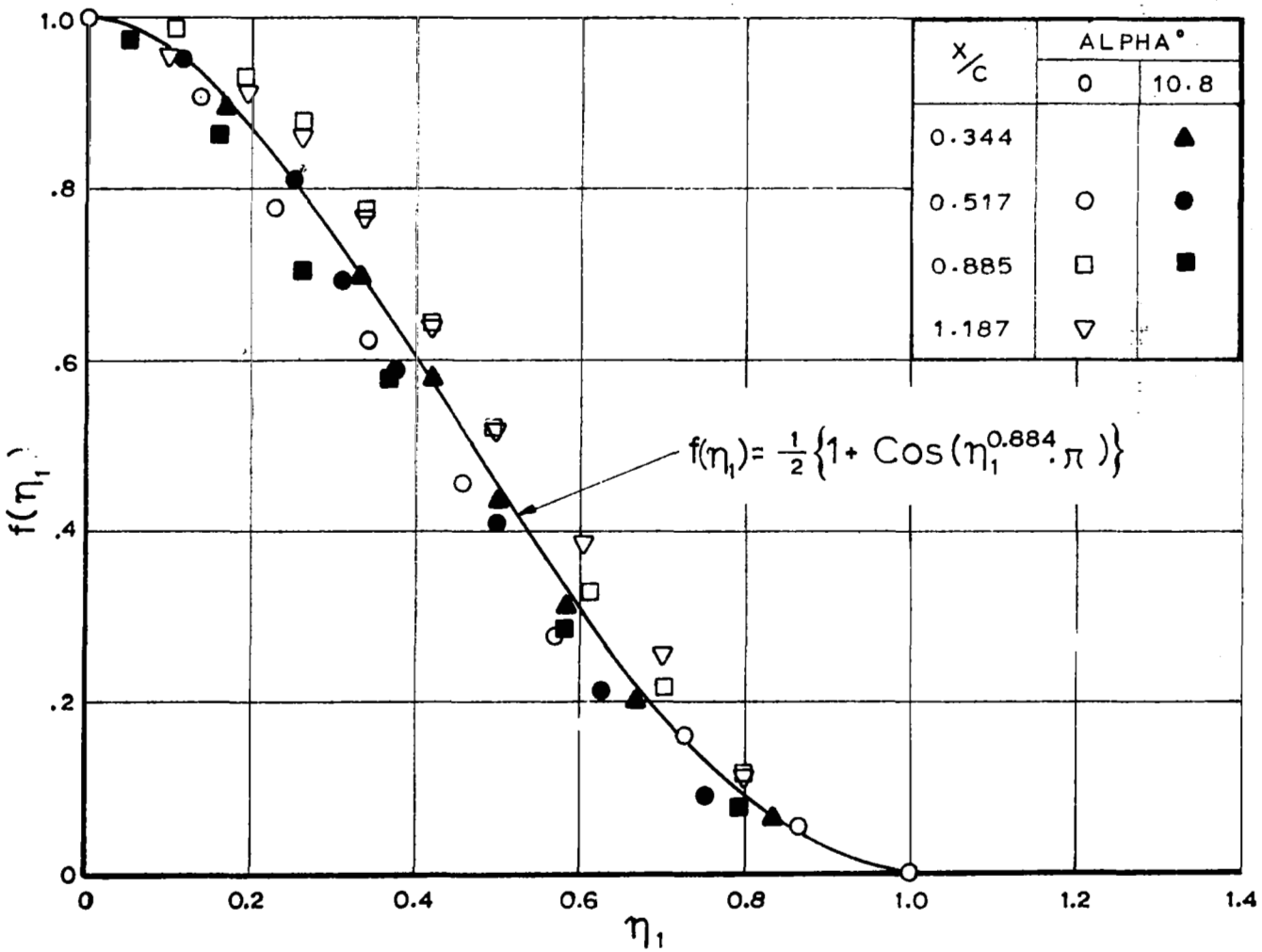

FIGURE IV-17 - VELOCITY PROFILE SIMILARITY (1) IN REGION IV
(FAR FROM AIRFOIL TRAILING EDGE)

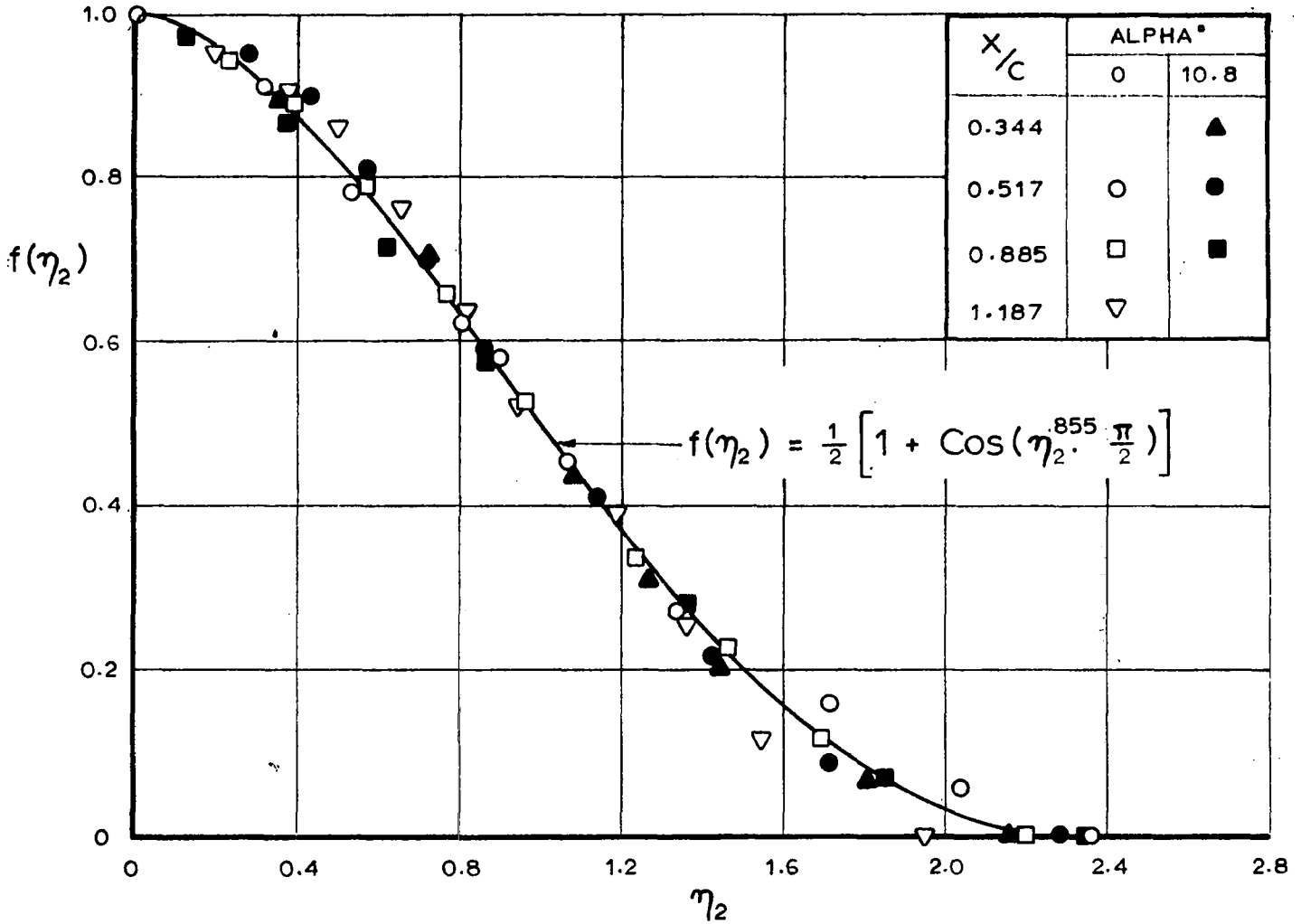

FIGURE IV-18 - VELOCITY PROFILE SIMILARITY (2) IN REGION IV
(FAR FROM AIRFOIL TRAILING EDGE)

for velocity profiles are used in constructing similarity curves of Figures IV-17 and IV-18. Comparison of velocity profile similarity plots of Figures IV-17 and IV-18 indicate that, when similarity parameter shown in Figure IV-18 is used for the purpose of obtaining velocity profile similarity there is less scatter in experimental data than by the use of similarity parameter of Figure IV-17. This fact suggests that similarity parameter of Figure IV-17 is more suitable for true representation of wake flow characteristics at large distance downstream in the wake of single component airfoil with sharp trailing edge. For the purpose of making use of this information about velocity profile similarity, it is necessary to obtain an analytical expression for the relation between similarity parameter η and similarity function $f(\eta)$. The curve which fits the experimental data of Figure IV-17 has the analytical expression of the form given by

$$f_{(\eta_1)} = \frac{1}{2} [1 + \text{Cos } (\eta_1^{0.884} \cdot \pi)]. \qquad \text{(IV-1)}$$

An analytical expression for the curve, which fits the experimental data of Figure IV-18, is given as

$$f_{(\eta_2)} = \frac{1}{2} [1 + \text{Cos } (\eta_2^{0.885} \cdot \frac{\pi}{2})]. \qquad \text{(IV-2)}$$

Equation (IV-1) and (IV-2) show the functional relationships for the similarity parameters for the viscous flow in the wake at chordwise locations far away from the airfoil trailing edge. Similarity plots for velocity profiles for the viscous flow in the wake of airfoil with sharp trailing edge and in the vicinity of airfoil trailing edge are shown in Figures IV-19 and IV-20. Definitions for similarity parameters and variables in Figures IV-19 and IV-20 are similar to those of Figures IV-17 and IV-18, respectively. As seen in Figure IV-19, the scatter of experimental data for wake flow in the neighborhood of trailing edge is larger than corresponding plot for far distance wake flow shown in Figure IV-17; the similar remark can also be made for data shown in Figure IV-18 and IV-20 which are for large and small distances in the wake behind the airfoil trailing edge. An analytical expression for the curve fit of the mean curve shown in Figure IV-19 is given by

$$f_{(\eta_3)} = \frac{1}{2} [1 + \text{Cos } (\eta_3^{0.825} \cdot \frac{\pi}{2})] \qquad \text{(IV-3)}$$

As the scatter in experimental data, shown in Figure IV-20 is larger than corresponding similarity plots of Figure IV-18, three different curve fits are defined by an expression of the following form:

$$f_{(\eta_4)} = \frac{1}{2} [1.0 + \text{Cos } (\eta_4^{P} \cdot \frac{\pi}{2})] \qquad \text{(IV-4)}$$

where, for the curve C_1, P = 1.0,
for the curve C_2, P = 0.755,
and for the curve C_3, P = 0.631.

Various values of powers P can be tried in the theoretical method in order to find out desirable value for better overall correlation with experimental

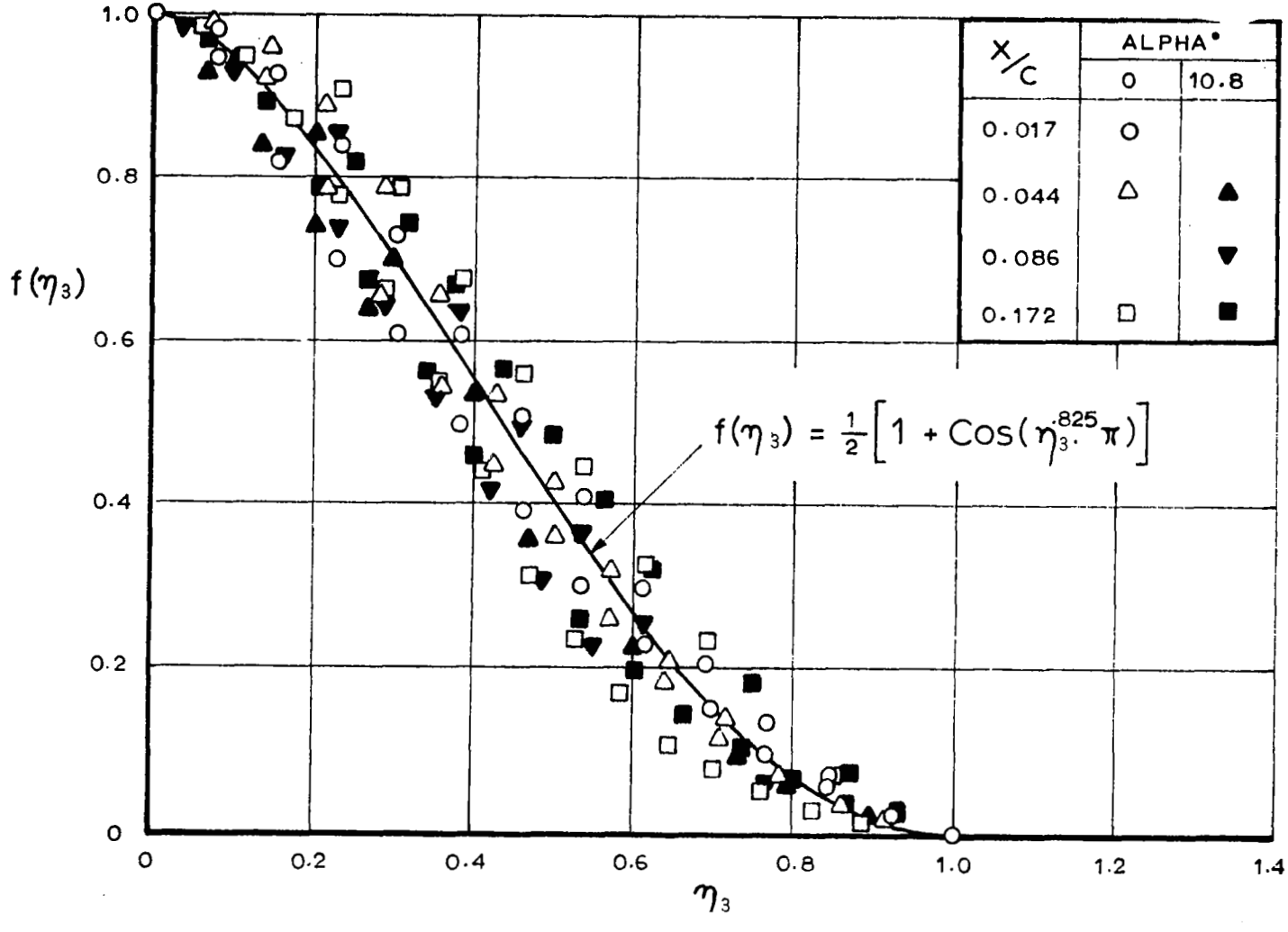

FIGURE IV-19 - VELOCITY PROFILE SIMILARITY IN THE WAKE IN THE VICINITY OF TRAILING EDGE OF SINGLE-COMPONENT AIRFOIL WITH SHARP TRAILING EDGE

data. The reason for the larger scatter in experimental data for similarity curves of Figures IV-19 and IV-20 is that these measurements were performed by the use of total-static pressure probe combination in the region where the circulatory flow may be present. This is due to the mixing of upper and lower surface boundary layer and the airfoil trailing edge thickness — even though it is small it has a finite value. The measurements by the total-static pressure probe, such as shown in Figure III-9, in circulatory flow are not very accurate.

IV.2.2 Generalized Parameters for the Pressure Distribution in the Wake of Single Component Airfoil with Sharp Trailing Edge: Figures IV-21 through IV-24 show the plots of non-dimensional pressure or velocity distribution at upper and lower edges of the wake for angles of attack α of 0.0°, 8.0°, 8.0° (fixed transition) and 10.79°, respectively. Parameter for the non-dimensional pressure at the edges of the wake is defined as

$$\gamma = \frac{\left(\frac{U_e}{U_\infty}\right)_{(x)} - \left(\frac{U_e}{U_\infty}\right)_{T.E.}}{1.0 - \left(\frac{U_e}{U_\infty}\right)_{T.E.}} \qquad \text{(IV-5)}$$

where U_e = velocity at edges of wake
U_∞ = freestream velocity

and subscripts T.E. = values at or in the neighborhood of trailing edge over airfoil surface, and
(x) = chordwise locations in the wake.

Non-dimensional parameter γ was chosen because, as seen from equation (IV-5), its value along the wake will vary from zero at the trailing edge to the value of 1.0 at very far distance from the trailing edge. Experimental data, shown in Figures IV-21, IV-22, IV-23 and IV-24, indicate that when values of γ_U or γ_L are plotted against distance X'/C, measured from the airfoil trailing edge, in the wake then experimental data for upper wake and lower wake arrange nicely to form smooth curves for all angles of attack shown. However, different curves are obtained for upper and lower edges of wake and moreover curves of γ vs. X'/C are different for various angles of attack. Thus, in this form γ vs. X'/C relationship cannot be utilized as an ingredient to the theoretical drag computation method. By the use of physical reasoning and dimensional analysis, a transformed X'/C coordinate for the wake flow was arrived at, such that when γ_U or γ_L is plotted versus transformed coordinate along the wake, then experimental data, for both upper and lower edge of wake and for all angles of attack, arranged on a single curve. This dimensionless transformed X-coordinate is given by the following equation:

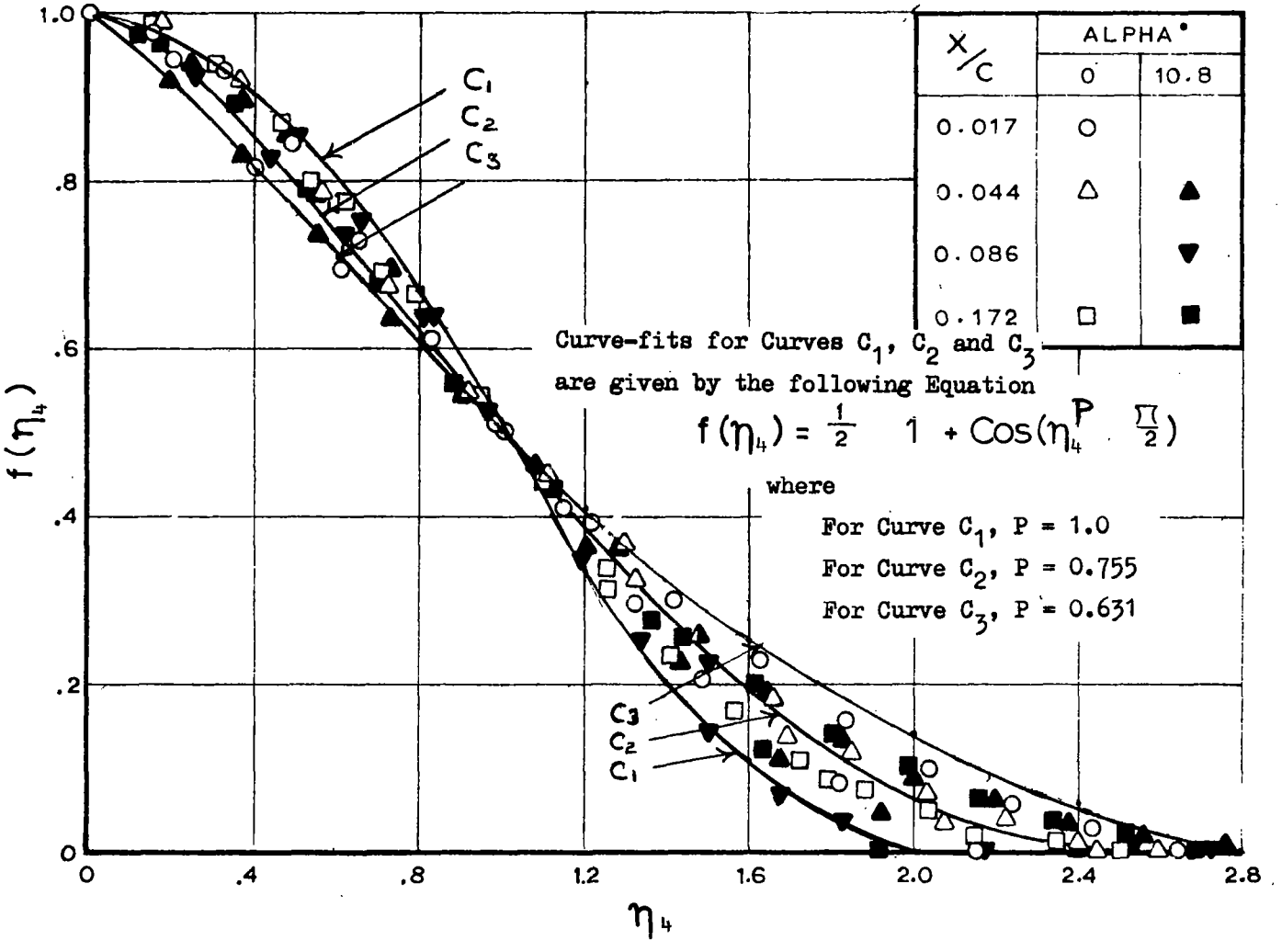

FIGURE IV-20 - VELOCITY PROFILE SIMILARITY IN THE WAKE IN THE NEIGHBORHOOD OF TRAILING EDGE OF SINGLE-COMPONENT AIRFOIL WITH SHARP TRAILING EDGE

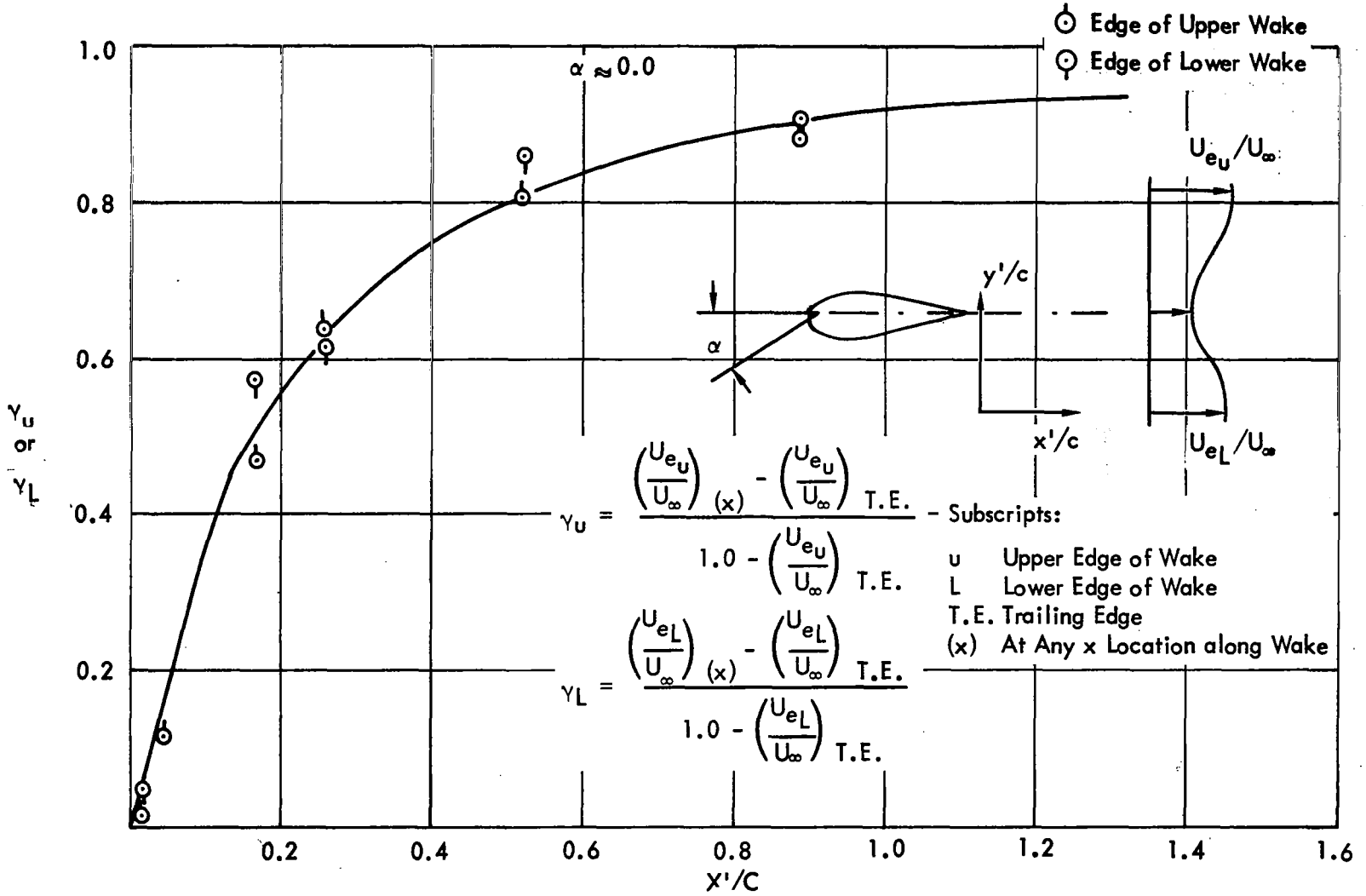

FIGURE IV-21 - NONDIMENSIONAL PRESSURE DISTRIBUTION AT UPPER AND LOWER EDGES OF WAKE FOR $\alpha = 0.0$

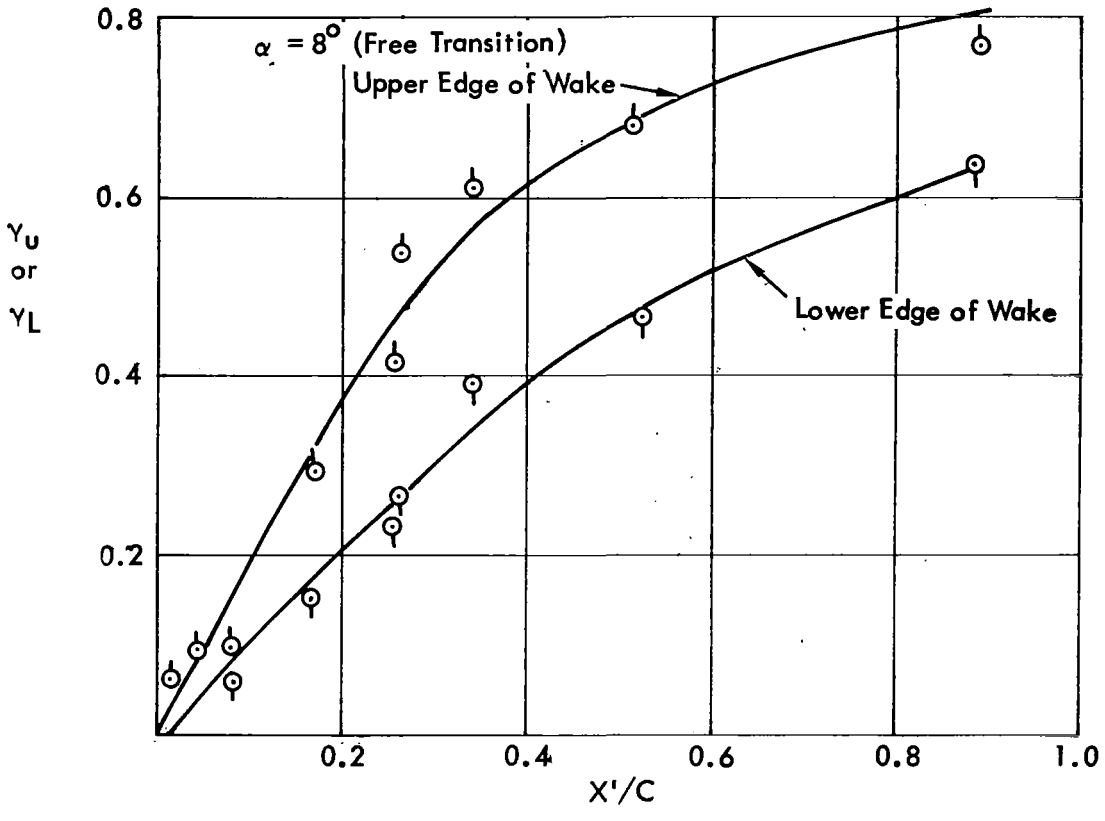

FIGURE IV-22 - NONDIMENSIONAL PRESSURE DISTRIBUTION AT UPPER AND LOWER EDGES OF WAKE FOR $\alpha = 8.0^o$ (FREE TRANSITION)

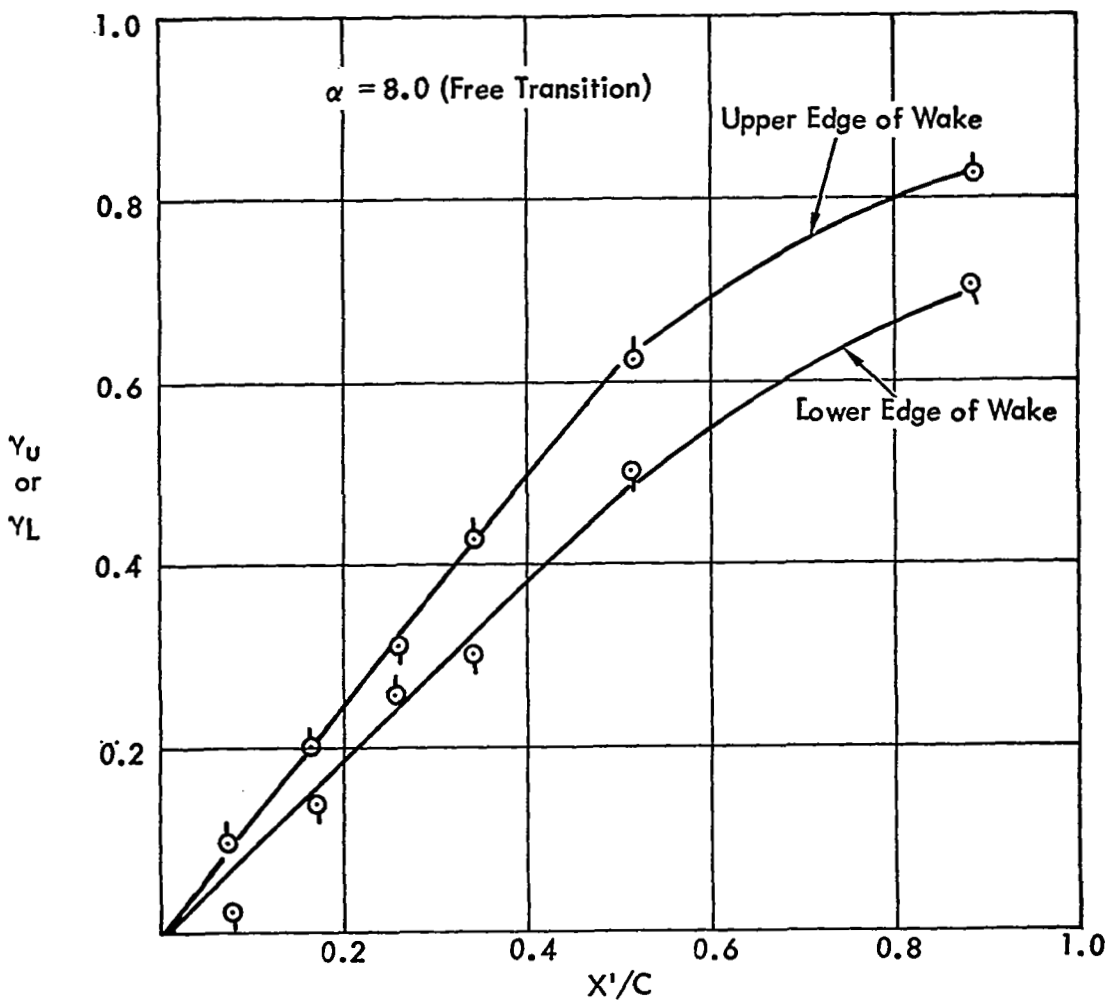

FIGURE IV-23 - NONDIMENSIONAL PRESSURE DISTRIBUTION AT UPPER AND LOWER EDGES OF WAKE AT $\alpha = 8.0^{\circ}$ (FIXED TRANSITION)

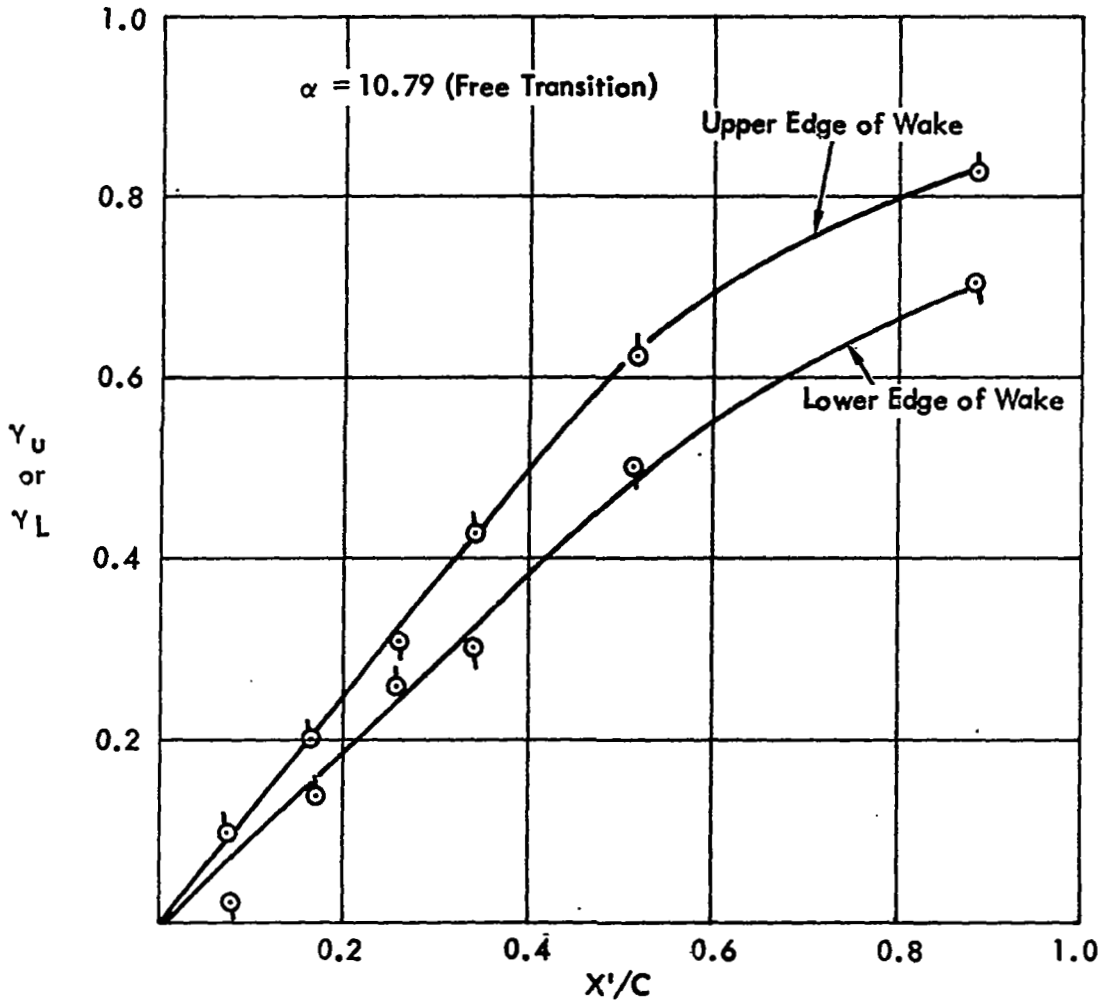

FIGURE IV-24 - NONDIMENSIONAL PRESSURE DISTRIBUTION IN WAKE AT UPPER AND LOWER EDGES AT $\alpha = 10.79^{\circ}$

$$\mathcal{X}_u \text{ or } \mathcal{X}_L = \frac{X'}{C} \cdot \left[1.0 - 12.5 \left\{ \frac{\delta_G}{\delta_u} \right\}^{0.262}_{T.E. \text{ or } L} \cdot \left\{ \left| \frac{\delta_u - \delta_L}{C} \right| \right\}_{T.E.} \right] \qquad \text{(IV-6)}$$

where $\mathcal{X}$ = transformed X-coordinate along the wake

X' = distance along wake measured from the airfoil trailing edge

c = airfoil chord

δ_u = boundary layer thickness at the trailing edge on upper surface of airfoil

δ_L = boundary layer thickness at the trailing edge on lower surface of airfoil

δ_G = greater value of δ_u or δ_L

Figure IV-25 shows the plot of dimensionless pressure distribution at the edges of the wake versus dimensionless transformed coordinate X. This figure shows that all points at different chordwise locations and various angles of attack arrange nicely on a single curve. The functional relationships between parameters γ and X is given by

$$\gamma_{u \text{ or } L} = 1 - \frac{0.132}{(0.363 + X_{u \text{ or } L})^2}$$

Figure IV-26 shows the generalized parametric representation and functional relationship for the pressure distribution on the locus of minimum velocity in the airfoil wake for sharp trailing edge airfoil. The parameters for this universal pressure distribution along the locus of minimum velocity point were arrived from the consideration of the flow behind the backward facing step and from physical reasonings. In this case also, by the choice of proper transformed X-coordinate, experimental points for $C_{Pu_{min}}$ arrange themselves very nicely on a single curve. The functional relationship between the parameters for the pressure along the locus of minimum velocity in the airfoil wake behind the sharp trailing edge airfoil is given by,

$$\frac{C_{Pu_{min}(x)}}{C_{p\ T.E.}} = 0.556\, e^{-.162\beta} + (0.444 + 1.121\beta + 0.285\beta^2)e^{-2\beta} \qquad \text{(IV-8)}$$

where $C_{Pu_{min}(x)}$ = static pressure coefficient along the locus of minimum velocity in wake

$C_{p\ T.E.}$ = pressure coefficient at the trailing edge of airfoil

β = transformed X coordinate for C_p along locus of minimum velocity

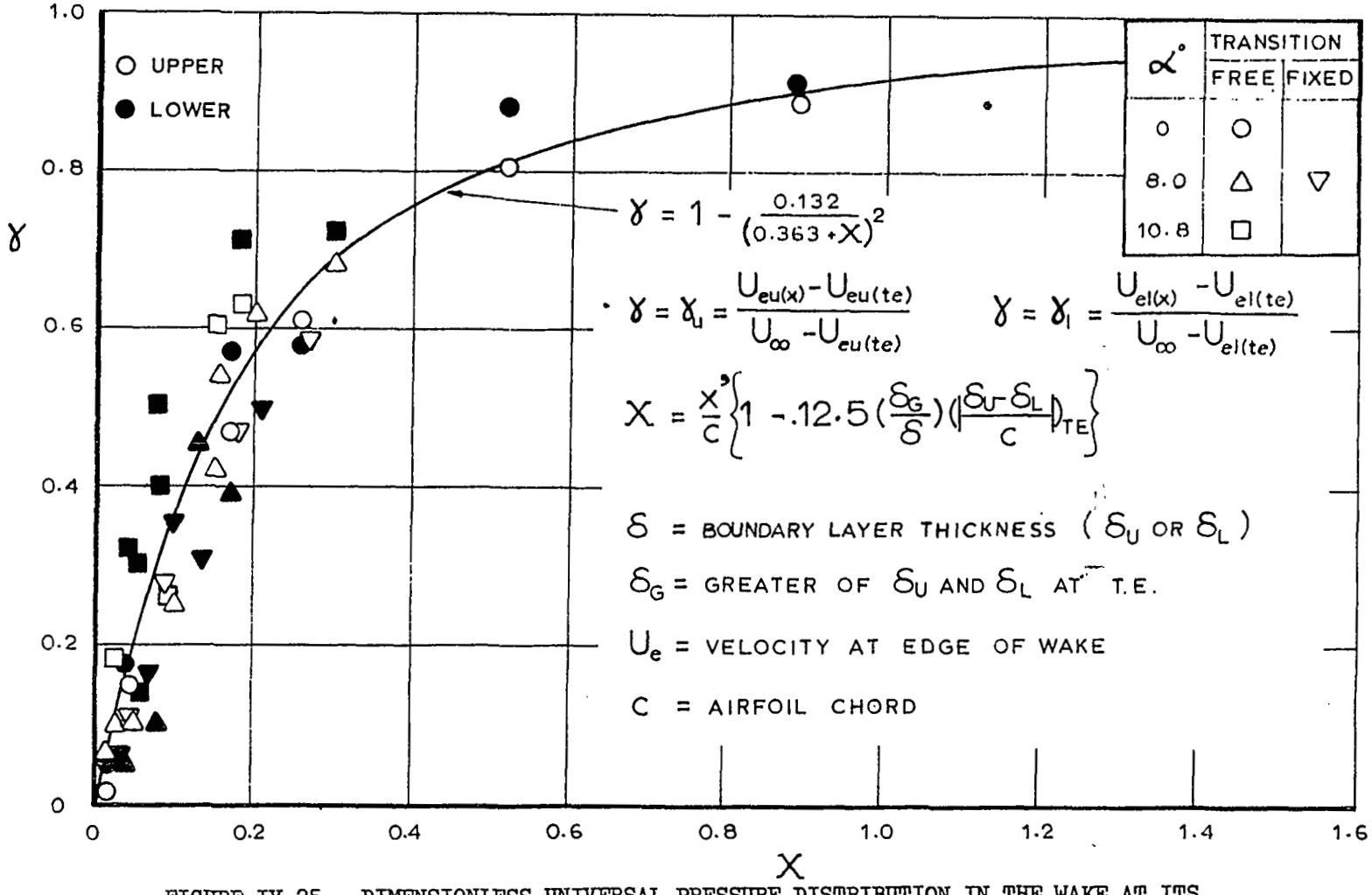

FIGURE IV-25 - DIMENSIONLESS UNIVERSAL PRESSURE DISTRIBUTION IN THE WAKE AT ITS EDGES FOR SINGLE COMPONENT AIRFOIL UP TO INCIPIENT SEPARATION (SHARP T.E. AIRFOILS)

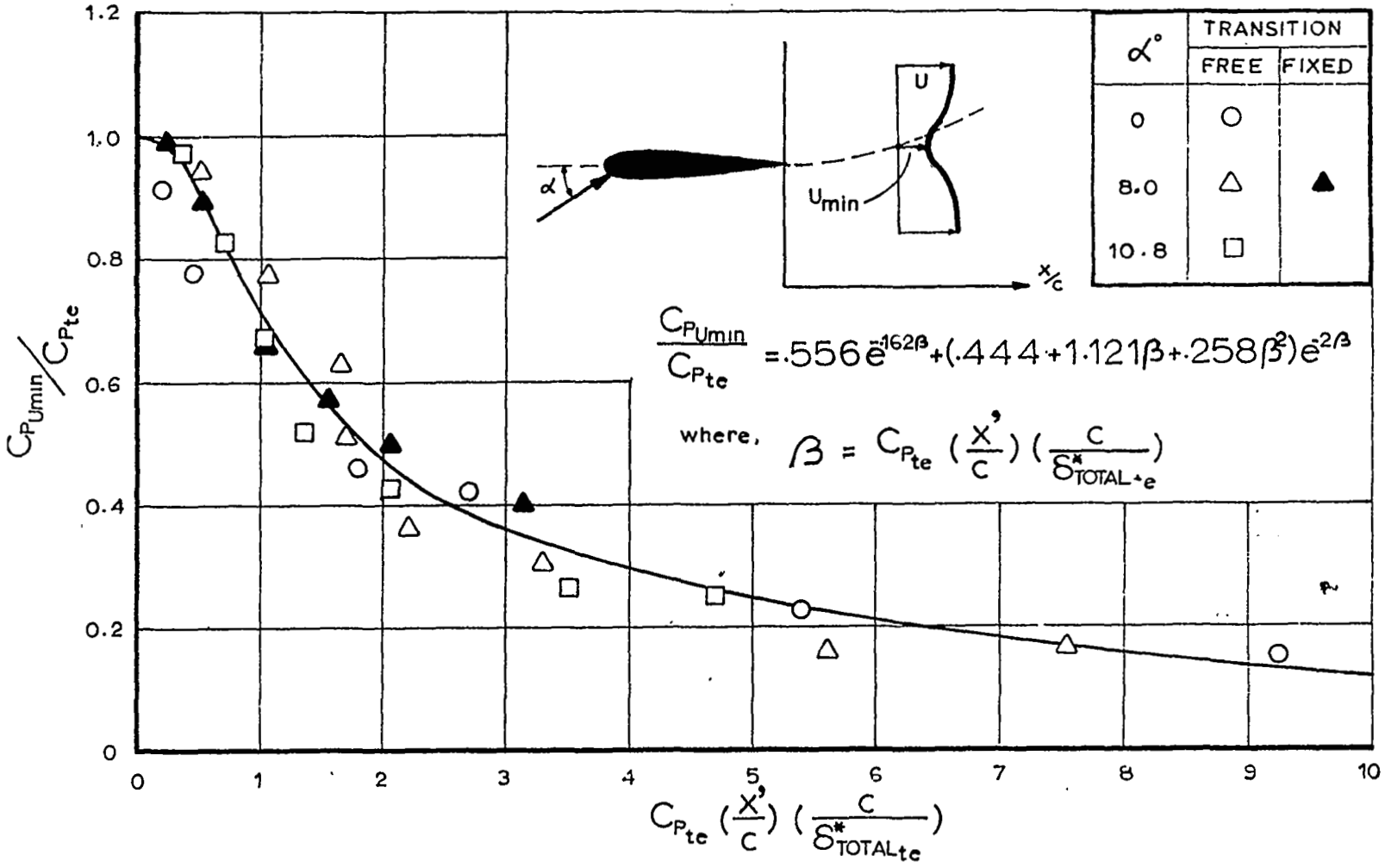

FIGURE IV-26 – VARIATION OF $C_{P_{U_{min}}}$ ALONG THE WAKE OF SINGLE COMPONENT AIRFOIL WITH SHARP TRAILING EDGE

$$\beta = C_{p\ T.E.} \left(\frac{c}{\delta^*_{\text{Total T.E.}}}\right) \times \left(\frac{x}{c}\right)$$

$\delta^*_{\text{Total T.E.}}$ = sum of displacement thickness on upper and lower surface at the trailing edge of the airfoil

x = distance along chordline in wake from airfoil trailing edge

c = airfoil chord.

IV.2.3 Generalized Parametric Representation of Shear Stress at Velocity Minimum: The theoretical integral equations of Section II for the solution of viscous flow in airfoil wake, contained coupling terms involving shear stress at the velocity minimum. It was noted in previous paragraphs that velocity profiles in the airfoil wake were "similar" for proper choice of similarity function and similarity variable. This fact suggests that it is possible to arrive at generalized parameter for the representation of shear at minimum velocity point from Prandtl's new shear stress hypothesis for free jet flows. According to this hypothesis, at any X-location the turbulent shear stress is given by,

$$\tau_{(y)} = K_1 \rho_c b_c U_c \frac{dy}{dy} \qquad \text{(IV-9)}$$

where $\tau(y)$ = shear stress at any y ordinate in viscous layer
b_c = characteristic width of viscous layer
U_c = characteristic velocity in viscous layer
K_1 = constant.

For the upper wake the suitable characteristic width is (nomenclature is shown in Figure IV-27),

$$b_c = (Y_4 - Y_3)_{(x)} \qquad \text{(IV-10)}$$

and the characteristic velocity is

$$U_c = U_{e_{u(x)}} - U_{min(x)} \qquad \text{(IV-11)}$$

For the lower wake, the characteristic width is

$$b = (Y_3 - Y_2)_{(x)} \qquad \text{(IV-12)}$$

and the characteristic velocity is

$$U_c = U_{e_{L(x)}} - U_{min(x)}. \qquad \text{(IV-13)}$$

The locus of the minimum velocity $U_{min(x)}$ is contained in both upper wake and lower wake layers. Assuming that shear at the locus of minimum velocity is proportional to the product of the four quantities given by equations (IV-10), (IV-11), (IV-12) and (IV-13), the following functional representation can be written after non-dimensionalizing,

$$\frac{\tau(y_3)}{\frac{1}{2}\rho U_e^2} = F\left[\frac{(y_4 - y_3)}{(y_4 - y_2)} \cdot \frac{(y_3 - y_2)}{(y_4 - y_2)} \cdot \left\{\frac{U_{e_u(x)}}{U_\infty} - \frac{U_{min(x)}}{U_\infty}\right\} \cdot \left\{\frac{U_{e_L(x)}}{U_\infty} - \frac{U_{min(x)}}{U_\infty}\right\}\right] \qquad \text{(IV-14)}$$

Figure IV-27 shows the functional relationship between the non-dimensional shear on the locus of the minimum velocity and the product of the parameter indicated in equation (IV-14). Experimental data plotted in this figure are obtained during the present studies in the wake of sharp trailing edge test airfoil at various chordwise locations and various angles of attack. Non-dimensional shear $\tau(y_3)/(\frac{1}{2}\rho U_e^2)$ was obtained from the indirect shear measurements from measured experimental velocity profiles and pressure distributions by the aid of the numerical method. The curve fit for the functional relationship of Figure IV-27 is given by

$$\frac{\tau(y_3)}{\frac{1}{2}\rho U_e^2} = -\ 115.2\ \theta^2 \qquad \text{(IV-15)}$$

where $\tau(y_3)$ = shear stress on the locus of minimum velocity

$U_{e(x)}$ = arithmetic mean of velocities at upper and lower edges of wake

and

$$\theta = \left[\frac{(y_4 - y_3)}{(y_4 - y_2)} \ \frac{(y_3 - y_2)}{(y_4 - y_2)} \left\{\frac{U_{e_u(x)}}{U_\infty} - \frac{U_{min(x)}}{U_\infty}\right\}\left\{\frac{U_{e_L(x)}}{U_\infty} - \frac{U_{min(x)}}{U_\infty}\right\}\right]$$

IV.3 Presentation of Correlation Results

Computer program subroutines were developed for the purpose of comparing the results of theoretical computation method, developed under this study, with the experimental data for three airfoil configurations. Input to the computer program consists of initial conditions of boundary layer and pressure quantities on upper and lower surfaces of the airfoil in the vicinity of the trailing edge. Experimentally measured values for these input conditions were used as input to the computer program. Computations for the characteristics of the flow in the wake and profile drag were performed at several angles of attack for the following three airfoils: (i) Joukowski airfoil with thickness ratio t/c of 12 percent, (ii) present sharp trailing edge test airfoil with thickness ratio of 15 percent, and (iii) NACA 63_1-012 airfoil. Results of correlations are discussed in the following paragraphs.

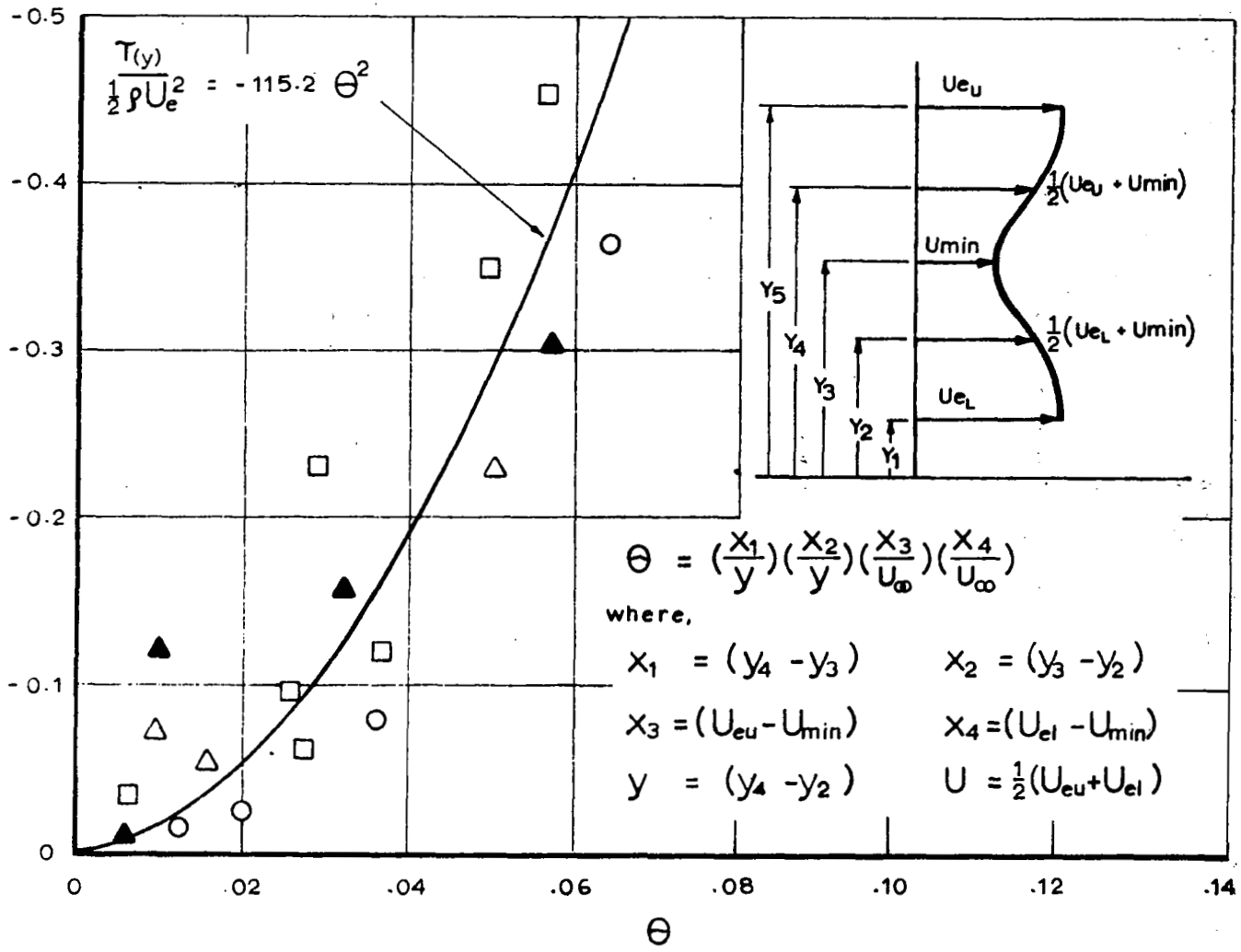

FIGURE IV-27 - PARAMETRIC RELATIONSHIP OF SHEAR STRESS ON THE LOCUS OF MINIMUM VELOCITY ALONG THE WAKE OF SINGLE COMPONENT AIRFOIL

(i) Joukowski Airfoil: Figure IV-28 shows the results of computations for upper and lower edge of velocity profiles in the wake of Joukowski airfoil at zero degree angle of attack. In this figure the locus of minimum velocity, which in this case is a straight line because of symmetrical airfoil at zero angle of attack, is also shown. Experimental data shown plotted in this figure by symbols indicate that good correlation is obtained.

Figure IV-29 shows the plot of experimental measurements (Reference 7) of boundary layer momentum thickness, displacement thickness and the form factor at the trailing edge of Joukowski's airfoil as a function of an angle of attack. This plot shows that at an angle of attack of 6°, the lower surface boundary layer is separated near the trailing edge as indicated by the value of form factor $H_{lower} = 2.15$. At an angle of 9°, both upper and lower surface boundary layer are separated; this is indicated by the values of form factors and also by sudden increase in slope $d\delta^*/d\alpha$ for the upper surface at $\alpha = 9°$. These values of physical boundary layer thickness and pressure coefficient at the trailing edge were input to the profile drag computer program. Values of boundary layer physical thicknesses were computed from experimental momentum thicknesses and form factors by the use of the following equation:

$$\frac{\delta}{\theta} = 0.17 \frac{1 + 0.1\, M_e^2}{[1 - \exp\{-3.5(H-1)\}]} \qquad \text{(IV-16)}$$

Figure IV-30 shows the computed variations of displacement thickness, momentum thickness and form factor in the wake of Joukowski airfoil at an angle of attack $\alpha = 0°$. Figure IV-31 shows the plot of above parameters at an angle of attack $\alpha = 6°$. Experimentally measured values of these parameters, which have been shown plotted in Figure IV-30 and IV-31 as symbols, indicate that good agreement is obtained between computational results and experimental data. Figures IV-32 and IV-33 show the comparisons between results of comptations of velocity profiles and experimental data in the wake of Joukowski airfoil for angles of attack of 0° and 6°, respectively. The above comparison is made at $X'/C = 0.1$, 0.25 and 0.5 in Joukowski airfoil wake and this comparison between computed and experimental velocity profiles indicate that reasonable correlation is obtained.

Figure IV-34 shows the plot of computed values of the profile drag coefficients as a function of an angle of attack and comparison with experimental data. This figure shows that the comparison between computed profile drag values and experimental data is reasonable at angles of attack $\alpha = 0°$, 3° and 6° whereas at $\alpha = 9°$ the comparison between present theoretical computational results and experimental data is not so good. Experimental measurements at airfoil trailing edge, which is shown in Figure IV-29, indicate that at $\alpha = 0°$ and 3° flow separation is absent on airfoil surfaces. Incipient separation exists on airfoil surfaces near the trailing edge in the neighborhood of $\alpha = 6°$ and appreciable flow separation probably exists on airfoil surfaces for angles of attack greater than $\alpha = 6°$ as evidenced from Figure IV-29. The discrepancy in drag between results of computations and experimental drag data for angles of attack greater than 6° can be due to the following two reasons. The initial conditions of boundary layer quantities, which are required as input to computer program were obtained from data of Figure IV-29. These data, which were obtained from Reference 7, were measured by pressure probe and the validity

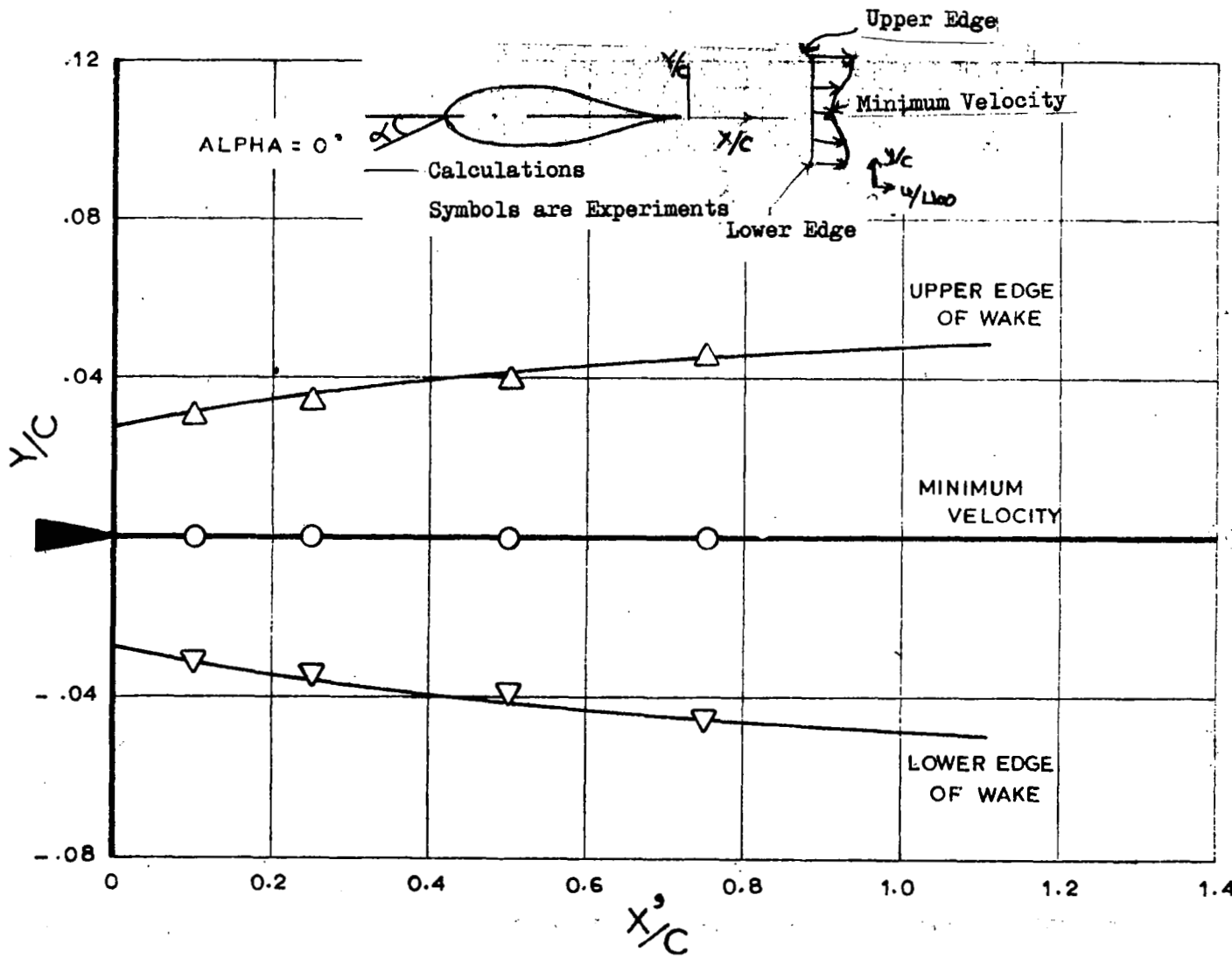

FIGURE IV-28 - LOCI OF VARIOUS EDGES FOR VELOCITY PROFILES IN THE WAKE BEHIND JOUKOWSKI AIRFOIL AT $\alpha = 0°$

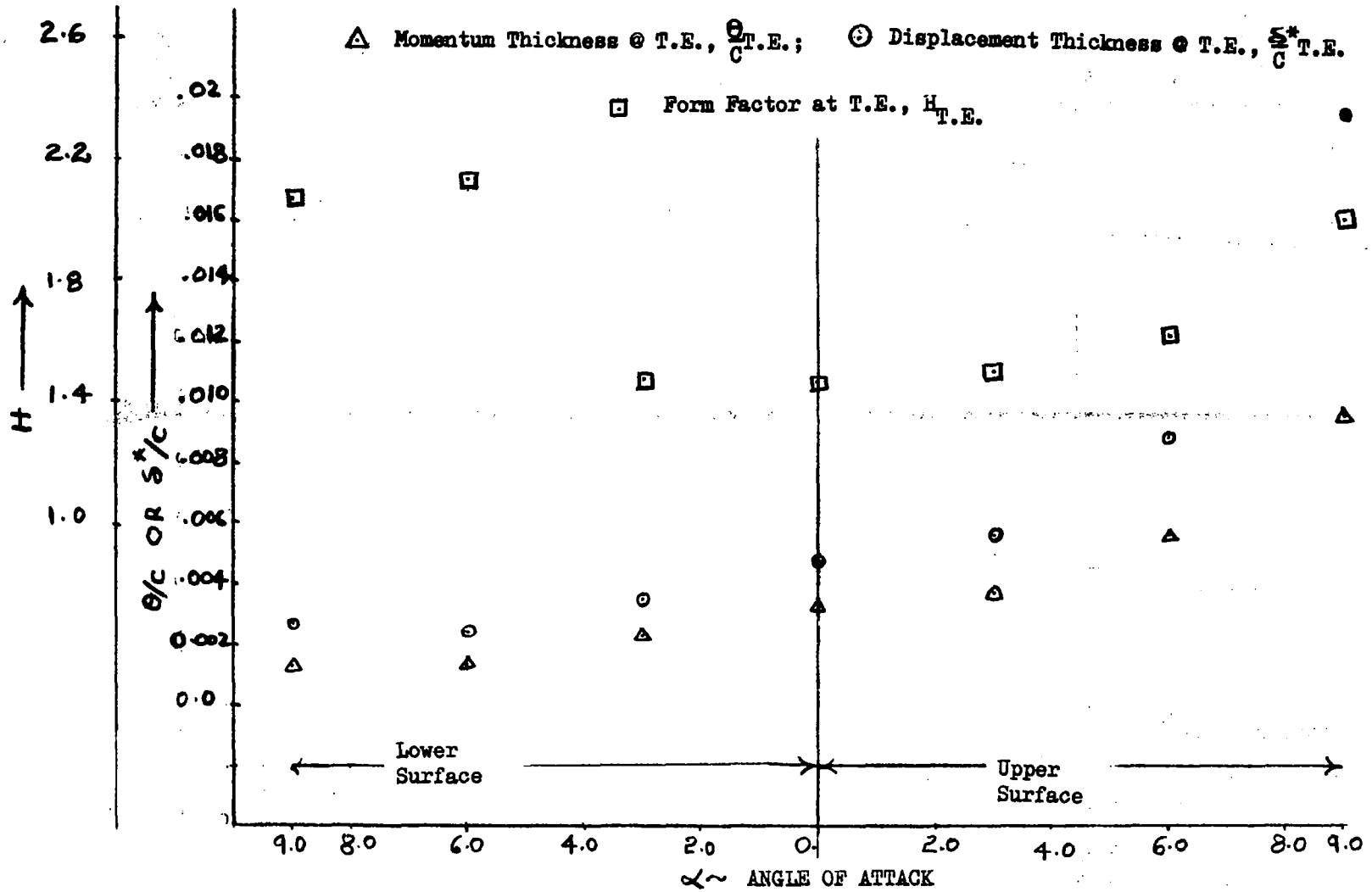

FIGURE IV-29 - VARIATION OF $\frac{\delta^*}{c}$, $\frac{\theta}{c}$ AND FORM FACTOR AT TRAILING EDGE OF JOUKOWSKI AIRFOIL WITH ANGLE OF ATTACK

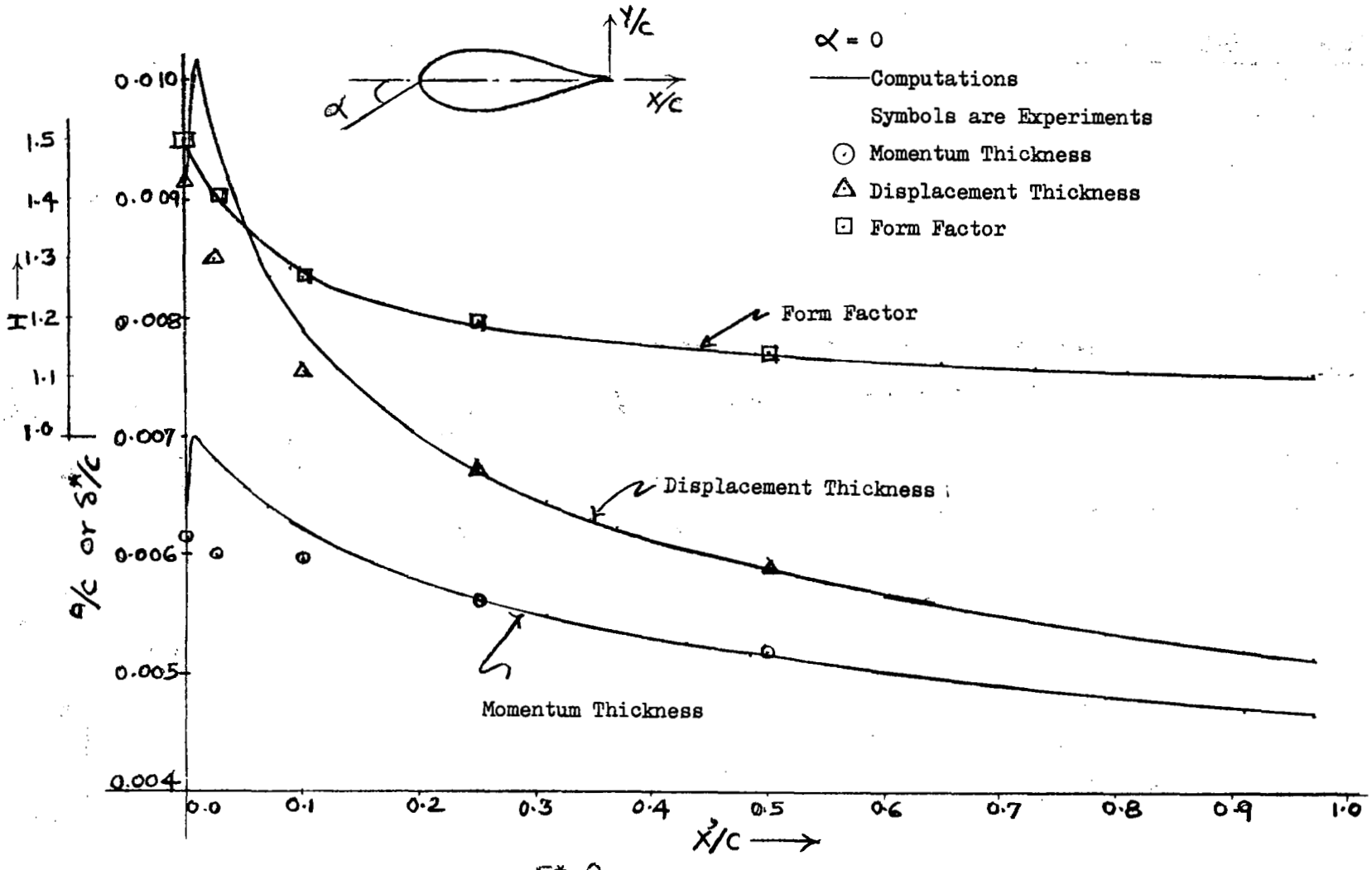

FIGURE IV-30 - VARIATION OF $\frac{\delta_1^*}{c}$, $\frac{\theta}{c}$ AND H IN THE WAKE OF JOUKOWSKI AIRFOIL @ $\alpha = 0°$ AND COMPARISON WITH EXPERIMENTAL DATA

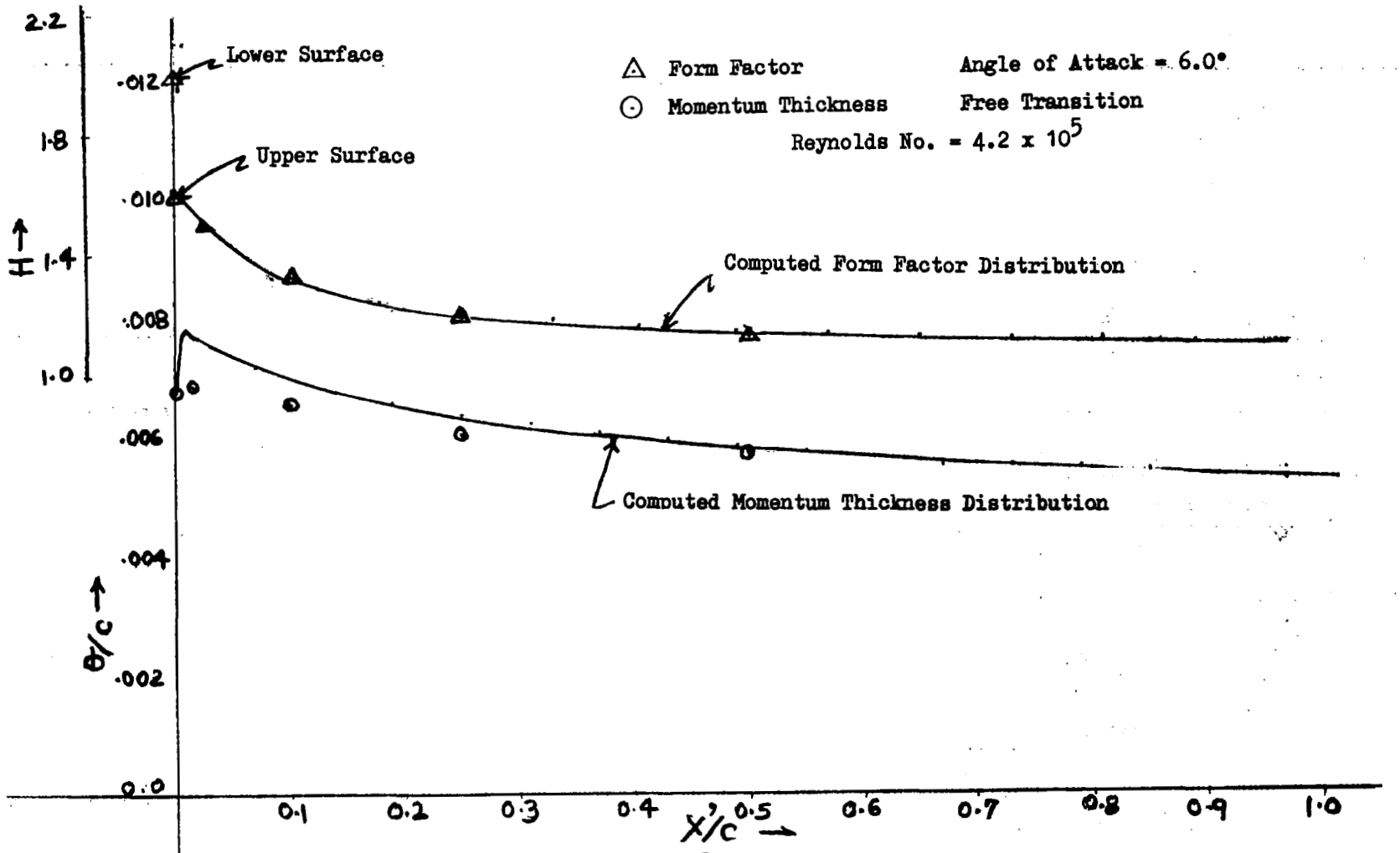

FIGURE IV-31 - COMPUTED VARIATION OF $\frac{\theta}{c}$ AND H IN THE WAKE OF JOUKOWSKI AIRFOIL @ $\alpha = 6°$ AND COMPARISON WITH EXPERIMENTAL DATA

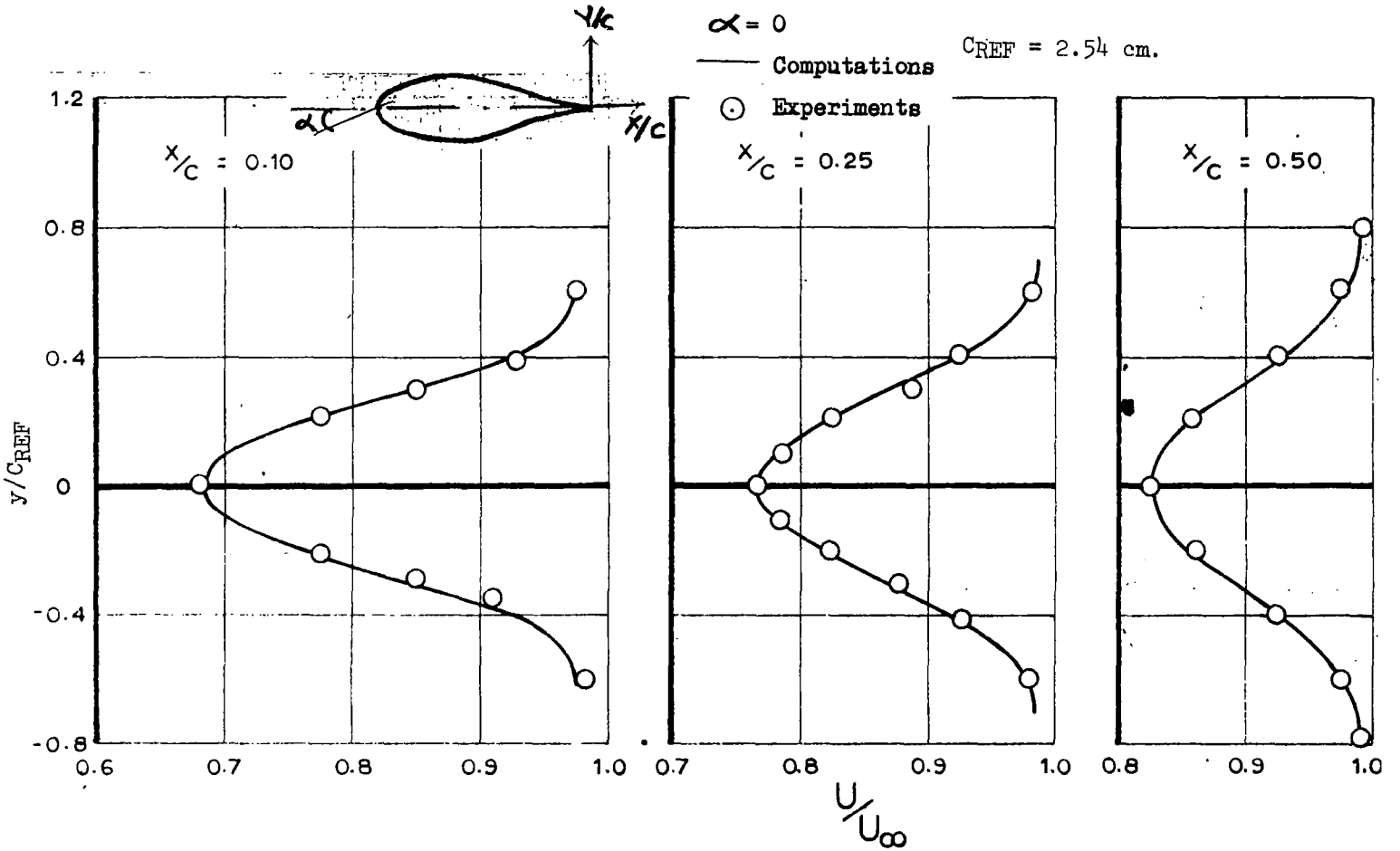

FIGURE IV-32 - COMPUTED VELOCITY PROFILES IN THE WAKE OF JOUKOWSKI AIRFOIL AT α = 0° AND COMPARISON WITH EXPERIMENTAL MEASUREMENTS

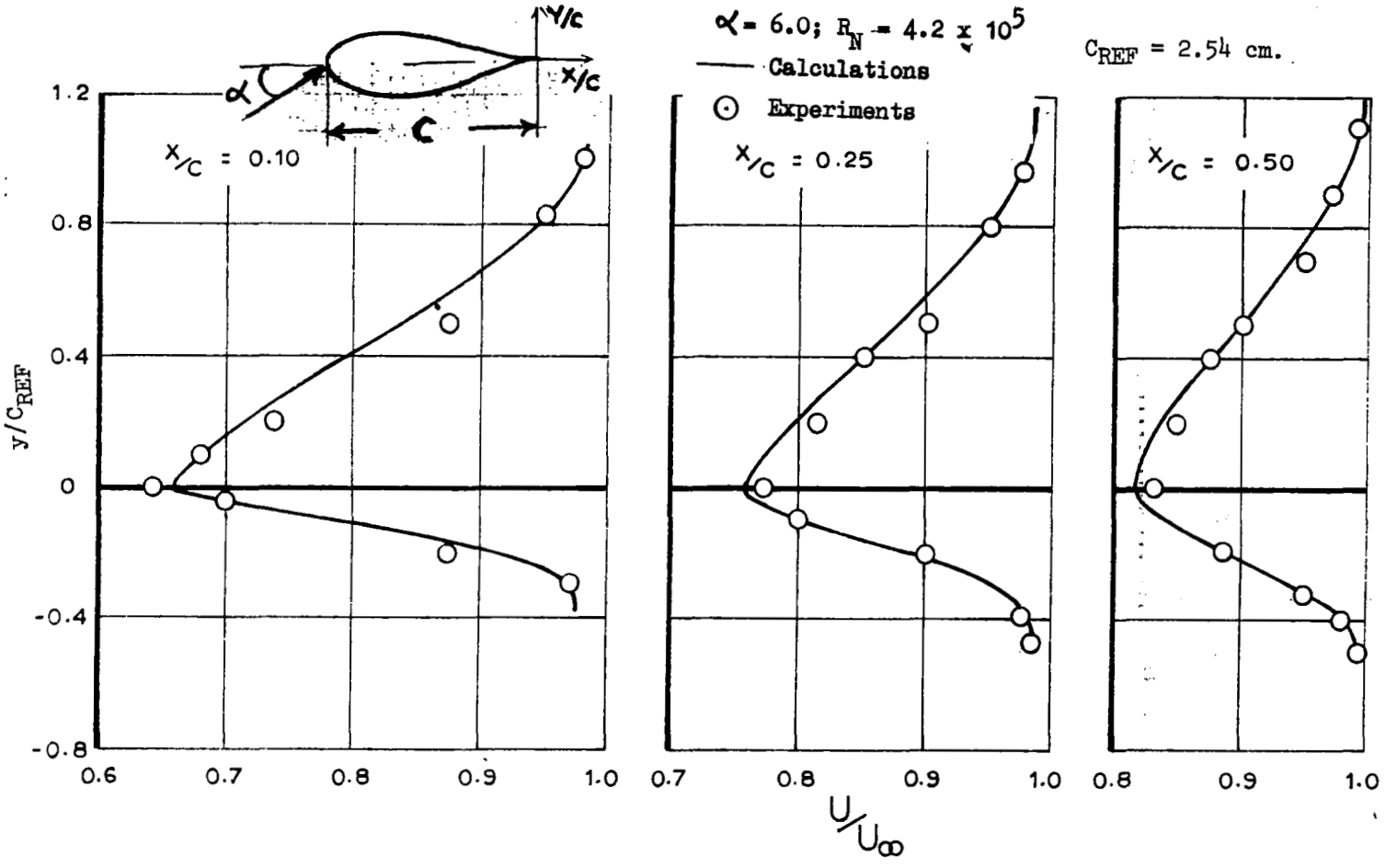

FIGURE IV-33 - COMPUTED VELOCITY PROFILES IN THE WAKE OF JOUKOWSKI AIRFOIL @ α = 6.0° AND COMPARISON WITH EXPERIMENTAL DATA

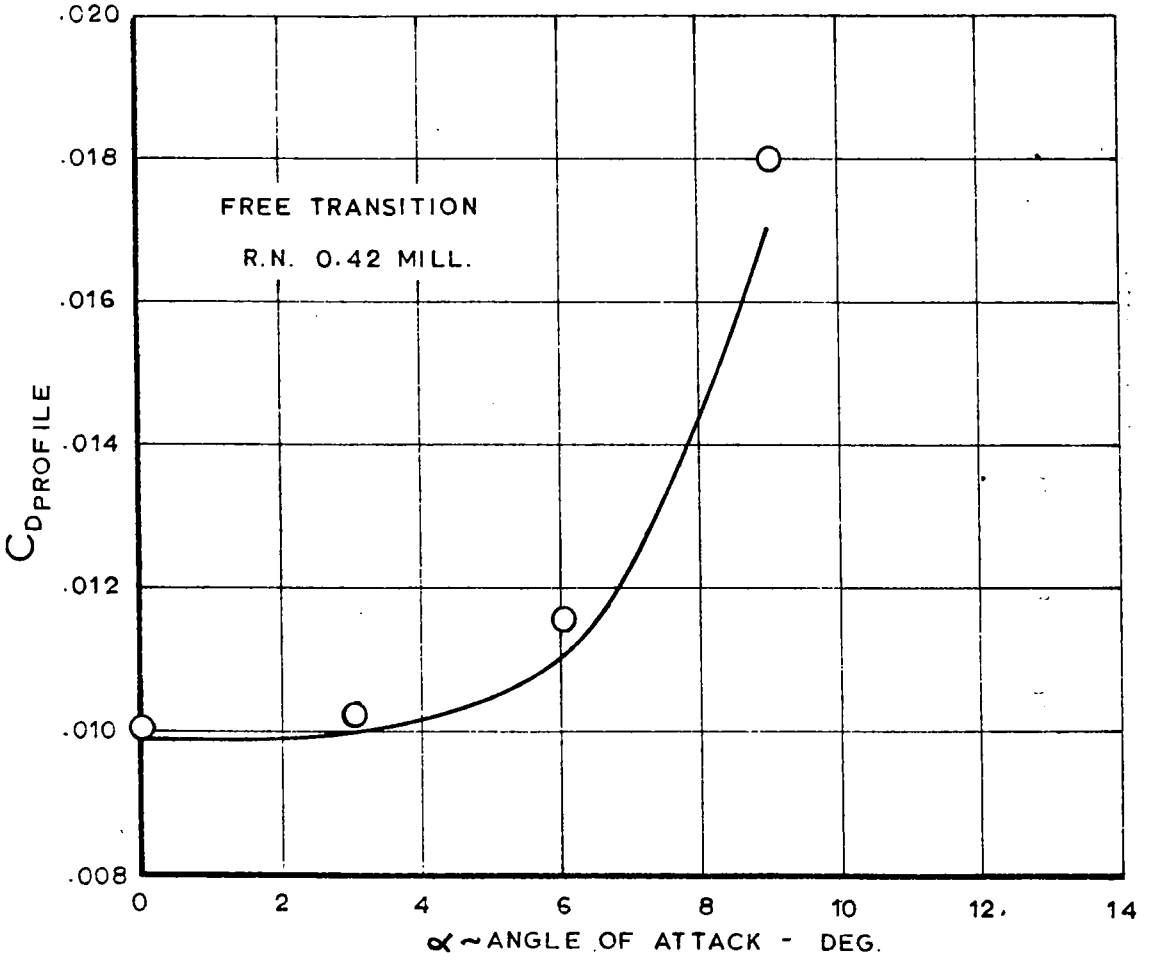

FIGURE IV-34 - COMPUTED VARIATION OF PROFILE DRAG COEFFICIENTS WITH ANGLE OF ATTACK FOR JOUKOWSKI AIRFOIL AND COMPARISON WITH EXPERIMENTAL MEASUREMENTS

of measurements by the pressure probe in the separated boundary layer is questionable. Secondly, the validity of assumptions which were used in deriving theoretical wake flow equations of Section II, when appreciable flow separation exists on airfoil surfaces, is not known at the present time. For the purpose of clarifying the above-mentioned situation, need exists for (i) developing proper experimental techniques for obtaining accurate and reliable measurements in separated flow region and (ii) then making appropriate modifications to the theory for wake flow calculations as are necessary for accurate drag predictions in the presence of flow separation.

(ii) Sharp T.E. Test Airfoil: Figure IV-35 shows the plot of computed characteristic loci at an angle of attack $\alpha = 8°$ and for the case of free transition on the surfaces of the test airfoil. Computed loci are plotted for upper edge of the wake, lower edge of the wake and the locus of minimum velocity for the velocity profiles in the test airfoil wake. Experimental values, which are shown in this figure as symbols, indicate that agreement between computed values for these characteristic points in velocity profiles and experimental data is good. It should be noted that slope of these loci downstream of X'/C of approximately 0.5 become approximately parallel to the free stream direction.

Figures IV-36, IV-37 and IV-38 show the plots of computed values of momentum thickness and form factor distribution in the wake of the test airfoil at angles of attack $\alpha = 0°$, $8°$ (fixed transition) and $10.79°$, respectively. Computed values of momentum thickness distribution is shown plotted for lower half of wake profile and total wake velocity profile; difference between these two momentum thickness distributions is the upper wake momentum thickness. Computational results for form factor distribution in airfoil wake indicate that even though the form factor on the upper and lower surfaces at the trailing edge are vastly different, the values of form factors for upper and lower half of wake velocity profile become identical at a very short distance from the airfoil trailing edge. For this reason only one value of computed form factor distribution for the flow in the wake is shown in Figures IV-36, IV-37 and IV-38. Experimental data for the form factor distributions, which are shown plotted in this figure, are either for lower half wake or upper half wake because measured values of form factors are very nearly equal for either upper or lower wake velocity profile. Figure IV-39 shows the plot of results of calculations of profile drag versus angle of attack for the test airfoil. Experimental data which are shown plotted in this figure indicate that agreement between experiment and theoretical method is reasonable.

(iii) NAC 63_1-012 Airfoil - Results of correlation between computations and experimental data for this airfoil are shown in Figure IV-40. Experimental data shown in this figure are obtained from Reference 5. For the purpose of correlation for this airfoil, measured values of boundary layer quantities on airfoil upper surface at trailing edge were used as input to the profile drag computer program. Boundary layer quantities on the lower surface at the trailing edge of the airfoil which are also required input to the computer program, were obtained from the output of the computer program subroutine for ordinary boundary layer calculation method. Experimental pressure distributions on the lower surface of the airfoils were used as an input for the purpose of calculation of lower surface boundary layer quantities at several angles of attack. In addition, values of experimental pressure at the trailing edge of

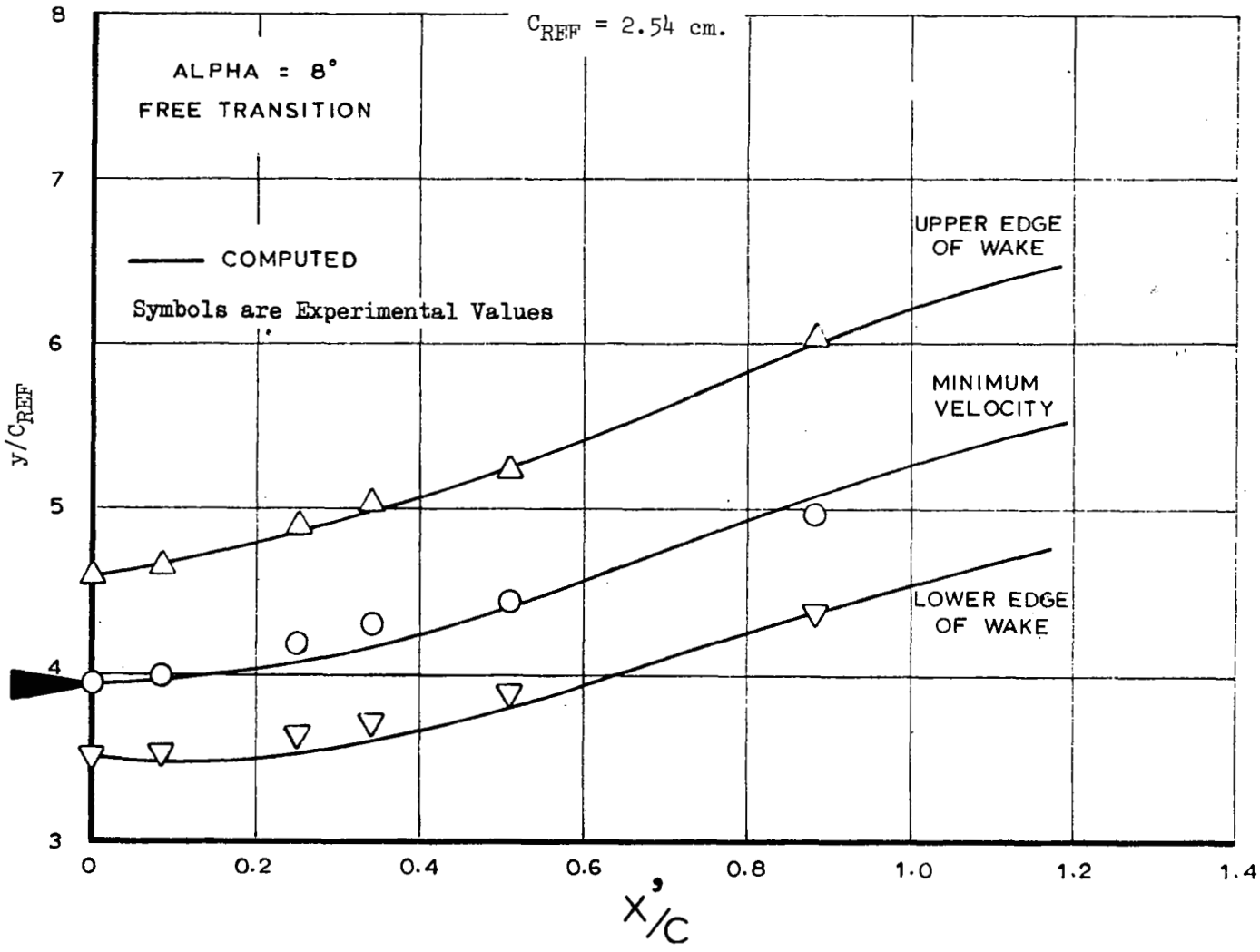

FIGURE IV-35 - COMPARISON OF COMPUTED AND EXPERIMENTAL CHARACTERISTIC LOCI FOR α = 8° (FREE TRANSITION) FOR SHARP T.E. TEST AIRFOIL

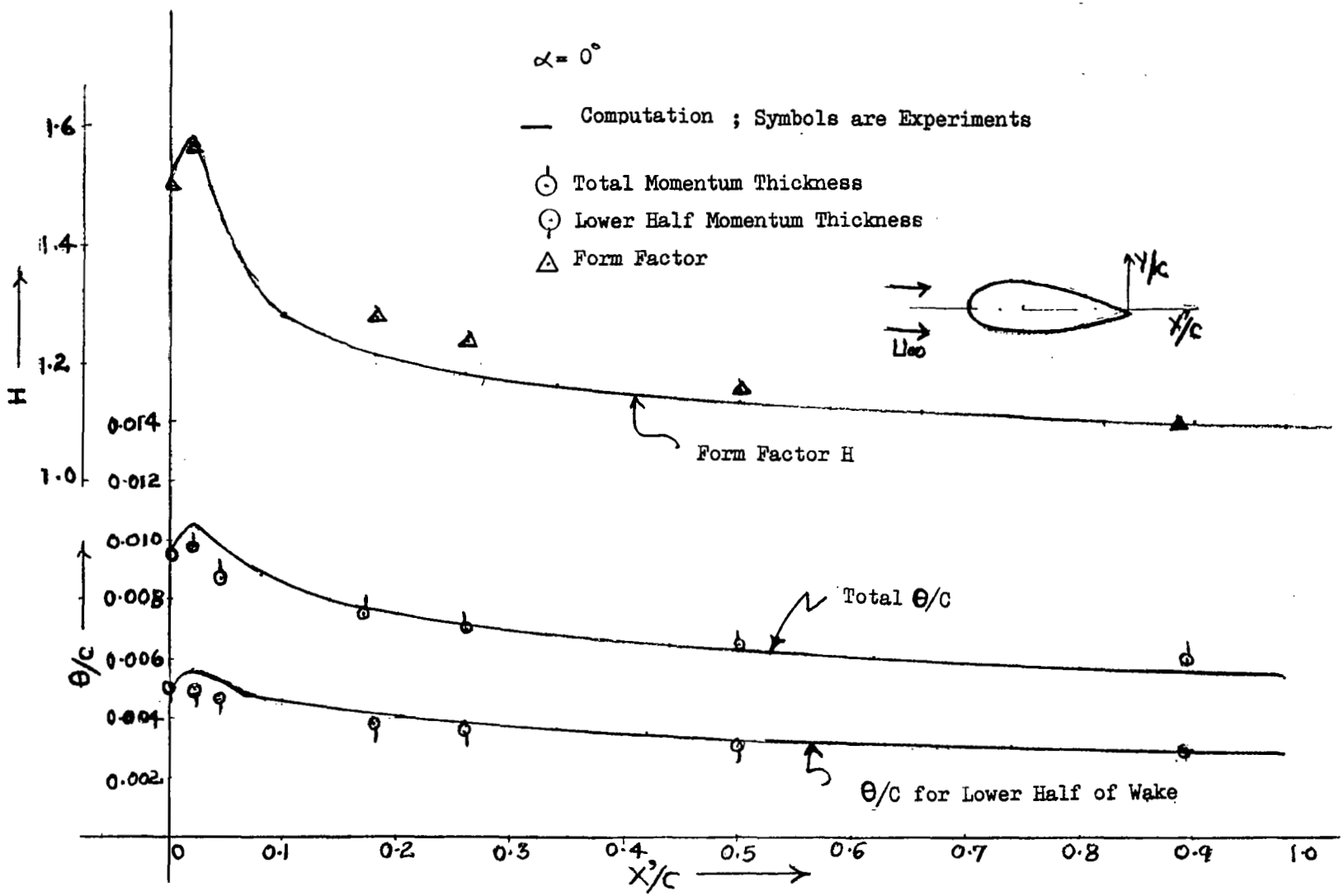

FIGURE IV-36 - COMPUTED VARIATION OF θ/C AND H IN THE WAKE OF SHARP T.E. TEST AIRFOIL @ α = 0° AND COMPARISON WITH EXPERIMENTAL MEASUREMENTS

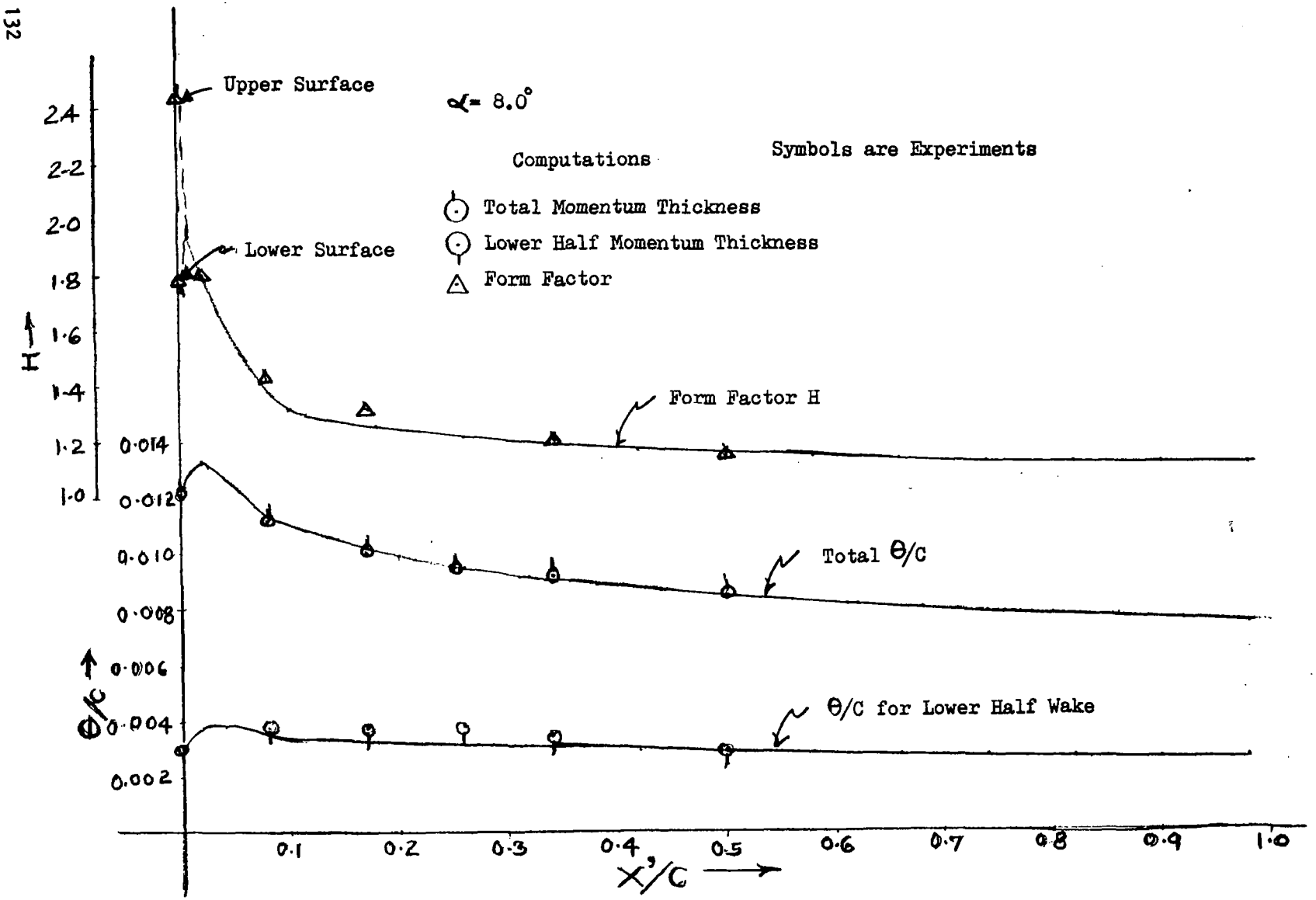

FIGURE IV-37 - COMPUTED DISTRIBUTION OF θ/C AND H IN THE WAKE OF SHARP T.E. TEST AIRFOIL AT $\alpha = 8.0^{\circ}$ (FIXED TRANSITION) AND COMPARISON WITH EXPERIMENTAL DATA

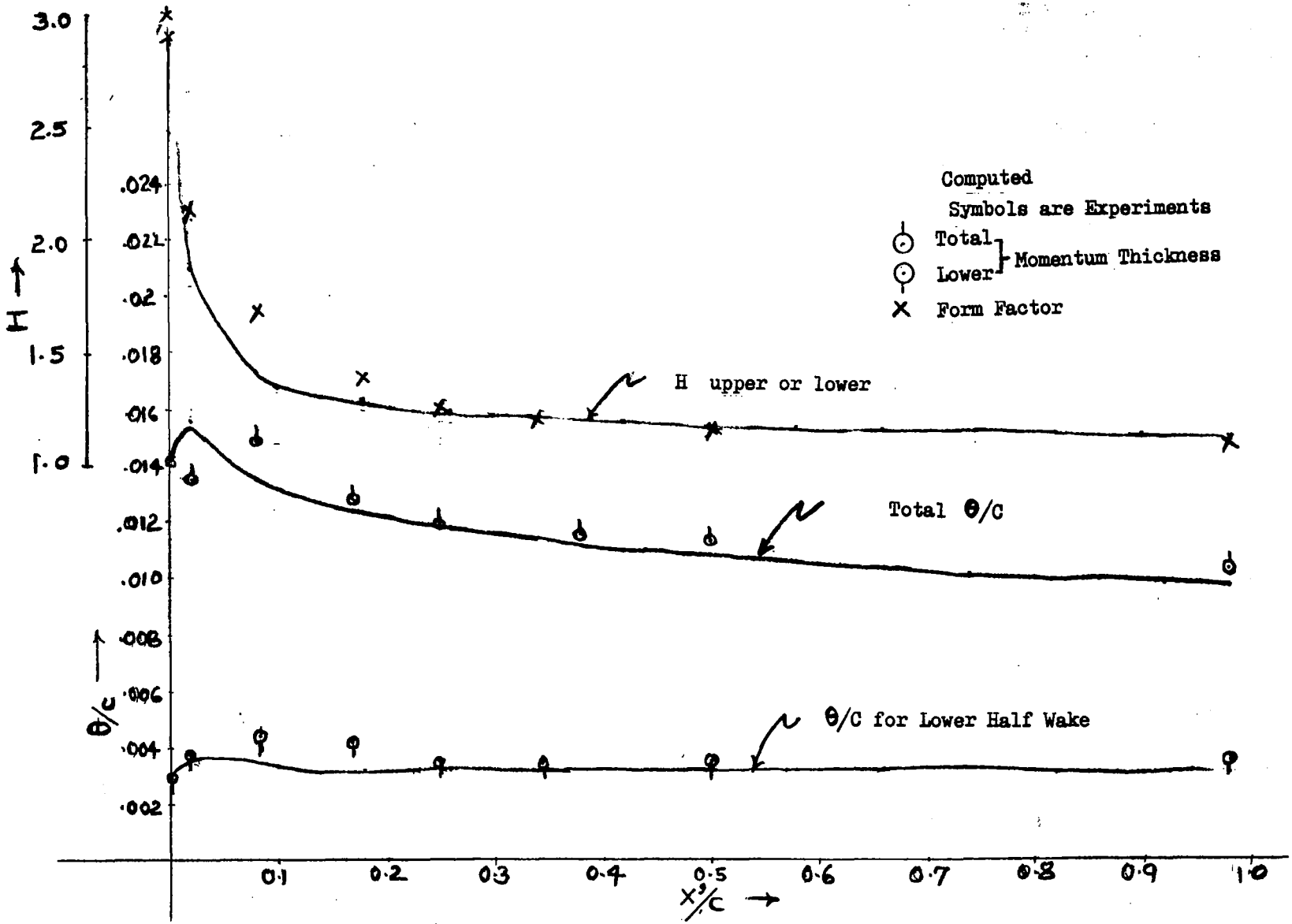

FIGURE IV-38 - MOMENTUM THICKNESS AND FORM FACTOR DISTRIBUTIONS IN THE WAKE OF SHARP T.E. TEST AIRFOIL AT $\alpha = 10.79^{\circ}$ (FREE TRANSITION) AND COMPARISON WITH EXPERIMENTAL DATA

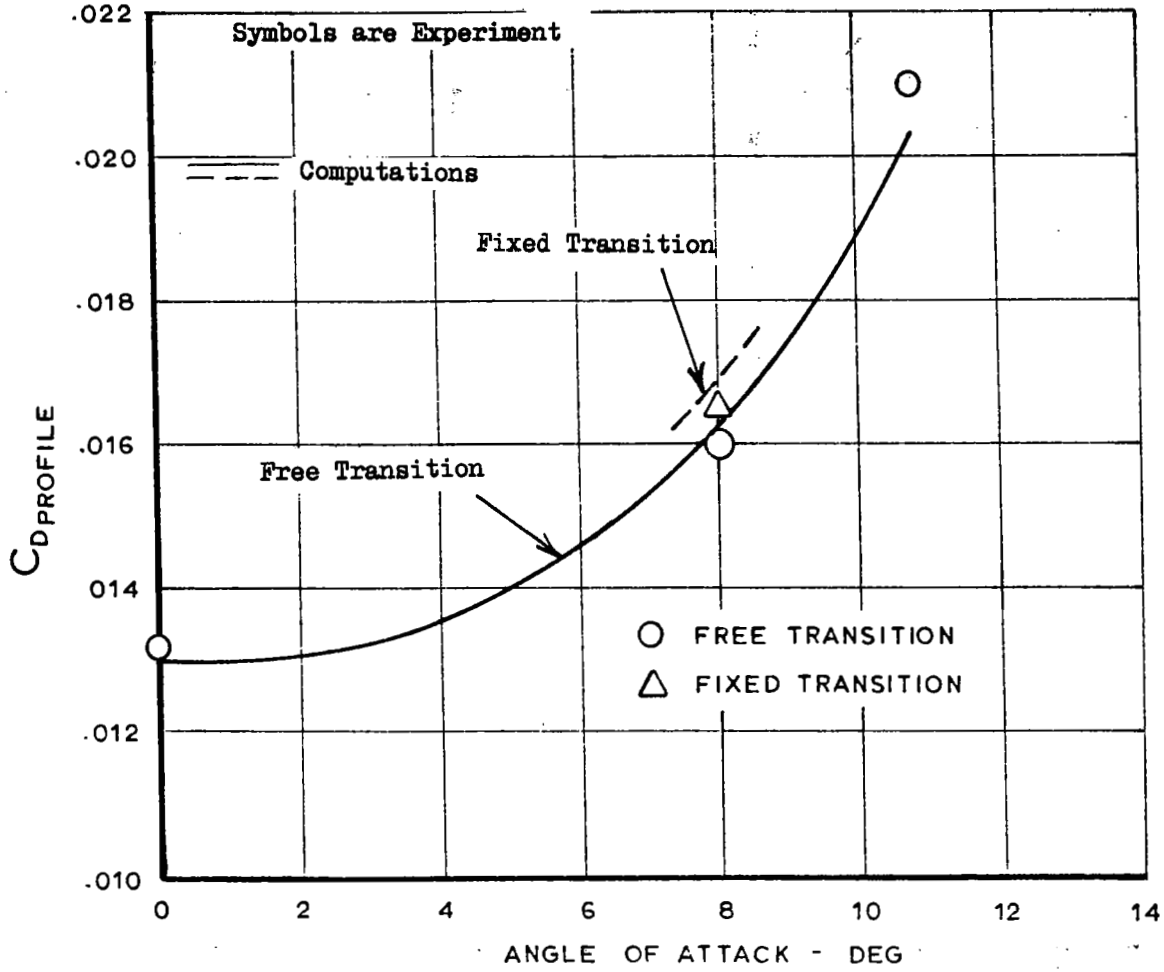

FIGURE IV-39 - COMPARISON OF C_D VS. α BETWEEN THEORETICAL METHOD AND EXPERIMENTAL DATA FOR SHARP T.E. TEST AIRFOIL

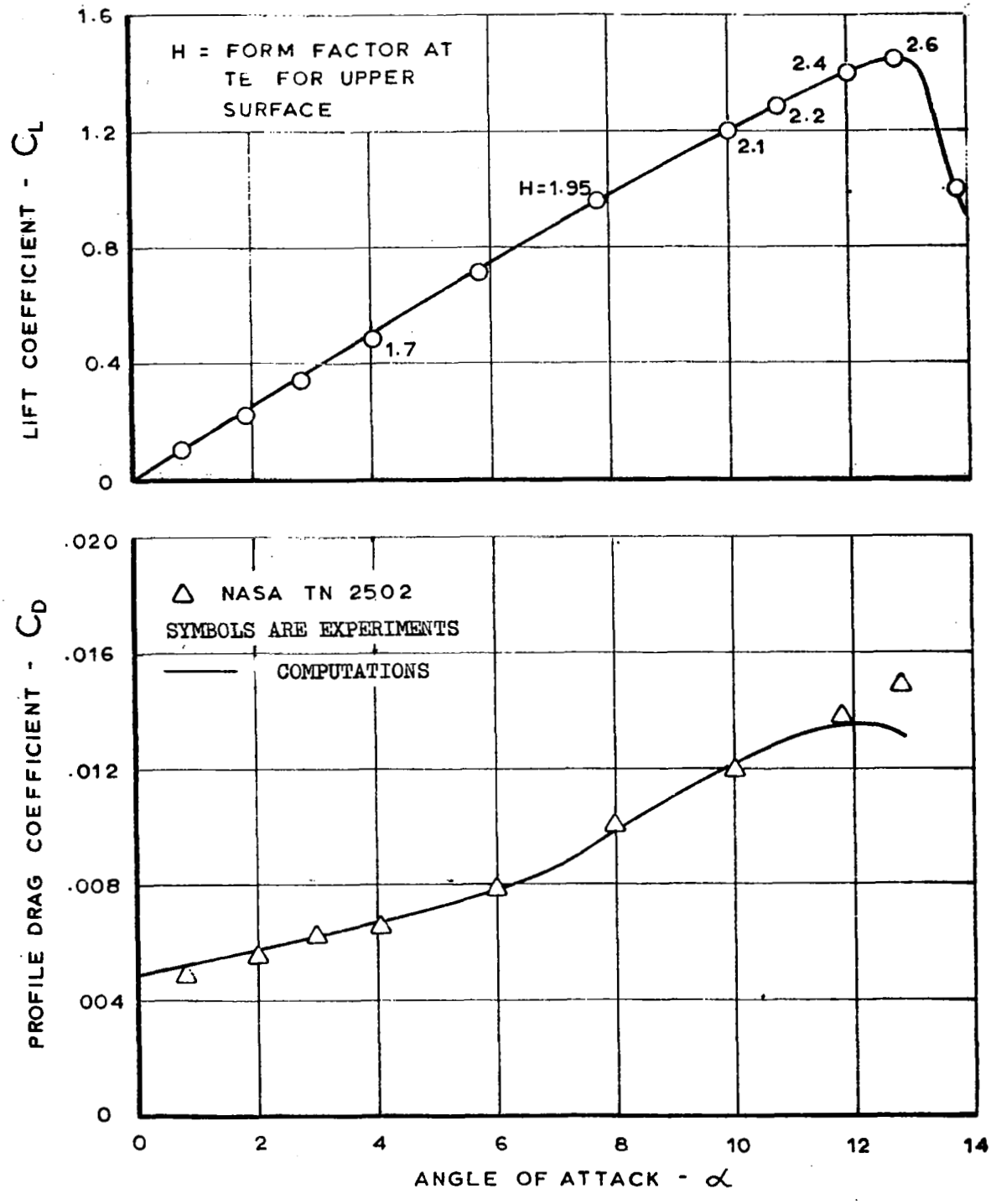

FIGURE IV-40 - PROFILE DRAG CORRELATION FOR NACA 63_1-012 AIRFOIL

the airfoil were used as input to the profile drag computer program subroutines. Figure IV-40 shows the comparison of the results of computations for the profile drag coefficient of NACA 63_1-012 airfoil with experimental data. Plot of experimental C_L vs. α for this airfoil is also shown in this figure; in addition, values of form factor on the upper surface of the airfoil at its trailing edge are noted on this C_L - α curve at several angles of attack. This is done for the purpose of indication of approaching trailing edge separation and also for the purpose of indicating values of angles of attack for which separated flow conditions exist at airfoil trailing edge. The comparison of computed profile drag quantities with experimental data is good as seen from this figure.

V. CONCLUSIONS AND RECOMMENDATIONS

From the theoretical and experimental studies presented in this report it is possible to make the following conclusions and recommendations for the future studies.

V.1 Conclusions

(1) The total-static pressure probe combination, such as used in the present studies, can be used for reliable measurements in viscous flow over airfoil surface when this flow is attached or non-separated. However, the measurements by such a probe, for the flow approaching separation or in separated flow region, are subject to interpretation and hence can be used only in qualitiative sense.

(2) Measurements of velocity profile by the use of hot-wire anemometer technique have been found more reliable, both qualitatively and quantiatively, than similar measurements performed by the use of pressure probe. However, with the present state of the art in hot-wire anemometry technique, measurements of velocity profiles in the region of low values of velocities (less than 30 fps and nominal values of turbulence level) are not very accurate. As the hot-wire anemometer measures only the absolute magnitude of velocity then with the above-mentioned present limitation, it is difficult to determine the separated flow velocity profile with the desired accuracy.

(3) Shear stress profiles for the wake flow have been determined by the use of indirect measurements and these values are used in the parametric form in the present theoretical method. The accuracy of indirect shear measurements for the wake flow in the trailing edge region is questionable because of the existence of the circulatory shear flow in this region. For this reason it is recommended to perform the direct shear measurements by the use of such devices as hot-wire X probe or by the use of Laser Doppler Velocimeter and make comparisons with the present indirect shear measurements.

(4) From the comparison between results of computer program subroutines with experimental data on three airfoil configurations, the following three remarks can be made:

(i) Agreement between computed and experimental velocity profiles for the flow in the wake is quite good for symmetrical wake at large distances from the trailing edge. However, for the unsymmetrical wake and especially in the region of wake near the airfoil trailing edge, the discrepancies exist between the results of computations and experimental measurements. These discrepancies might be due to inaccuracies in measurements or theoretical calculations or both in this region.

(ii) The computed variations of integral quantities in the airfoil wake, such as momentum thickness, displacement thickness and the form factor, agree well with experimental data for distances far from the trailing edge. In the region near the trailing edge, however, discrepancies are observed between the theory and experiments.

(iii) Results of computations of profile drag agree quite well with experimental measurements in the range of values of angles of attack from $\alpha = 0^\circ$ to α corresponding to the occurrence of incipient separation on the upper surface of the airfoil. However, for high values of angles of attack where large region of flow separation is present on the airfoil surface, computed values of the profile drag are not in good agreement with experimental measurements. This discrepancy can be attributed to the breakdown of the assumptions, in case of separated flow, which were used in deriving theoretical equations for the present method.

V.2 Recommendations

(1) For the purpose of establishing the limitations and restrictions of the present method, it is necessary to perform correlations with experimental data for the wake flow and profile drag on several classes of airfoil configurations. Thus performing calculations on supercritical and conventional airfoils of several thickness ratios and camber distributions and at several values of lift coefficients and comparison of computational results with experimental measurements would be very valuable for the purposes of needed refinements for this new method.

(2) This method is developed for sharp trailing edge airfoils and for low subsonic free stream Mach number where the flow can be considered essentially incompressible. However, for the general applicability in the design and development work on wing sections it is recommended that the present method be extended for high subsonic flows and for airfoils with thick trailing edges.

(3) Experimental and theoretical studies are recommended for the refinements of the present method for the purpose of the prediction of profile drag when extensive region of flow separation is present on airfoil surface. Such conditions exist at $C_{L_{MAX}}$ conditions on airfoils exhibiting trailing edge stall.

(4) The basic approach of the theory of the present method is valid for the more important situations of the computation of profile drag for multi-component airfoil sections. Under the present study the validity of this approach is proven for single-component airfoil sections. It is hence recommended that this approach be extended to airfoils with more than one component.

REFERENCES

1. Stevens, W. A.; Goradia, S. H.; and Braden, J. A.: Mathematical Model for Two-Dimensional Multi-Component Airfoils in Viscous Flow. NASA CR-1843, July 1971.

2. Squire, H. B.; and Young, A. D.: The Calculation of the Profile Drag of Aerofoils. ARC Technical Report R&M 1838, November 1937.

3. Tollmien, W.: Berechnung turbulenter Ausbreitungs vorgäng. ZAMM .6, 6, 1926, p. 468.

4. MacMillan, F. A.: Experiments on Pitot-Tubes in Shear Flow. ARC Technical Report R&M 3028, 1957.

5. McCullough, G. B.; and Gault, D. E.: Examples of Three Representative Types of Airfoil Section Stall at Low Speed. NACA TN-2502, September 1951.

6. Preston, J. H.; Sweeting, N. E.; and Cox, D. K.: The Experimental Determination of the Boundary Layer and Wake Characteristics of a Piercy 12/40 Aerofoil with Particular Reference to the Trailing Edge Region. Aerodynamics Division of NPL, Report and Memoranda No. 2013, February 1945.

7. Preston, J. H.; and Sweeting, N. E.: The Experimental Determination of the Boundary Layer and Wake Characteristics of a Simple Joukowski Aerofoil, with Particular Reference to the Trailing Edge Region. ARC Technical Report R&M 1998, March 1943.

8. Young, A. D.; and Winterbottom, N. E.: Note on the Effect of Compressibility on the Profile Drag of Aerofoils at Subsonic Mach Number in the Absence of Shock Wakes. ARC Technical Report R&M 2400, 1950.

9. Goradia, S. H.: Confluent Boundary Layer Flow Development with Arbitrary Pressure Distribution. Ph.D. Thesis, Georgia Institute of Technology, August 1971.

10. Goradia, S. H.; and Bennett, J. A.: Method of Analysis of Two-Dimensional Airfoils in Subsonic Flows with Some Transonic Applications. Work done under ontract with the Army Research Organization, ARO Contract Number DA 31-124-ARO-D-398, July 1966.

11. Betz, A.: Ein Verfahren zur direkten Ermittlung des Profilwiderstandes. ZFM 16y 42, 1925.

APPENDIX A

DETERMINATION OF SIDE WALL BLOWING REQUIREMENTS

It is known that in the case of two-dimensional testing at conditions of high lift, the validity and accuracy of experimental measurements is sometimes questionable because of the existence of boundary layer separation on the test section sidewalls. The presence of the two-dimensional model at moderate and high angles of attack in the wind tunnel test section creates high adverse pressure gradients in the direction of flow on the side walls of the tunnel test section upstream of the leading edge of the model. This high adverse pressure gradient causes the separation of boundary layer on the wind tunnel test section side walls at the juncture of the model with the side walls. Separated boundary layer on the side walls then flows toward the center of the model with the result that the flow pattern on the airfoil model is three-dimensional thus making it impossible to obtain measurements of two-dimensional aerodynamic characteristics of given airfoil model at moderate and high angles of attack. The above-mentioned phenomena has been observed by various investigators at NASA, R.A.E. in England, and at Lockheed-Georgia Company.

The solution of the above problem can be approached by the use of several methods, such as distributed blowing through slits located in the sidewalls at juncture of the model with side walls, distributed suction through pores or slits located upstream of the model or at the juncture of the model with the tunnel side walls, and blowing high energy air through a single slit located at an appropriate distance upstream of the leading edge of the model on both side walls. For the present investigations boundary layer control on wind tunnel side walls was accomplished by blowing the appropriate amount of high energy air through single slits located at approximately one chord length upstream of model leading edge on both side walls. Figure III-8 shows the general layout of the side wall boundary layer control system used in the present investigation. The following paragraphs describe the procedure that was used in determining the appropriate amount of high energy air for various model configurations and angles of attack.

Velocity profiles on the side walls of the tunnel were measured without the presence of the model at locations corresponding to the approximate locations of the trailing edge of the main component and flap. Then, with the model in the tunnel in various configurations and angles of attack, measurements of velocity profiles were made on the side walls of the tunnel at the same locations. These measurements were used to determine blowing requirements. It is necessary that the side wall BLC be just sufficient to prevent boundary layer separation on the side walls. It has to be emphasized that the amount of blowing on the wind tunnel side walls for boundary layer control has to be precise — for example, if there is excess blowing then the value of freestream q_∞ in the test section would be affected. In addition, an excess amount of blowing on wind tunnel walls creates an undesirable pressure field around the two-dimensional model; this is due to the fact that vortices are created due to the rubbing action of low velocity tunnel freestream air with the high velocity blown air. These vortices give rise to tip effects or the effects of finite span on two-dimensional test model. If the amount of blown high energy air on the tunnel side walls is

insufficient then, of course, the boundary layer on the side walls separates. In order to avoid both undesirable effects, the proper value of the pressure ratio P_{ts}, P_{s_s} and the proper geometrical dimensions of the slits are required.

A simplified theoretical equation of the amount of blown air required to suppress boundary layer separation on wind tunnel side walls can be derived as

$$C_{\mu_{required}} = \frac{2}{e}\frac{\Delta\theta_{max}}{c} + \frac{1}{2}\frac{\rho_s}{\rho_\infty}\frac{h_s}{c} \qquad \text{(A-1)}$$

where $\Delta\theta_{max}$ = maximum value of the difference in momentum thickness on wind tunnel side walls in the presence of and absence of model in the test section, inches

c = airfoil chord, inches

e = effectivity factor

h_s = height of blowing slits, inches

ρ_s = density of high energy air in blowing plenum

ρ_∞ = freestream density.

The blowing momentum coefficient C_μ in equation (A-1) is defined as

$$C_\mu = \frac{(\text{mass of blown air}) \cdot (\text{velocity of blown air})}{\frac{1}{2}\rho_\infty U_\infty^2 \ (\text{wing chord}) \cdot (\text{span of model})} \qquad \text{(A-2)}$$

The value for the ratio of velocity of blown air through the blowing slit to the freestream velocity, V_s/U_∞, is approximately by

$$\frac{V_s}{U_\infty} = 2.0\left(\frac{q_\infty}{\rho_\infty}\right)^{1/2}\left[\frac{\gamma}{\gamma-1} \cdot Rg_c\, T_o \left\{1 - \left(\frac{Ps_s}{PT_s}\right)^{0.286}\right\}\right]^{1/2} \qquad \text{(A-3)}$$

where γ = ratio of specific heats for air (1.4)

R = gas constant for air (=53.3)

g_c = gravitational constant (=32.2)

Ps_s = static pressure at the exit of blowing slit, psia

PT_s = plenum air total pressure.

The amoung of C_μ that is available corresponding to a given pressure ratio, Pt_s/Ps_s, is given by the following equation:

$$C_{\mu_{available}} = 2 \left(\frac{\rho_s}{\rho_\infty}\right) \left(\frac{V_s}{U_\infty}\right) \left(\frac{h_s}{c}\right) \left(\frac{K_w}{h_t}\right) \qquad \text{(A-4)}$$

where V_s/U_∞ is given by equation (A-3)

ht = span of the model, inches

= 30 inches for the present tunnel

K_w = width of blowing slit, inches

= 30 inches for the present tunnel

Figure A-1 shows the plot of available C_μ for the unit slot height as a function of pressure ratio Pt_s/Ps_s. Figure A-2 shows the plot of velocity ratio as a function of pressure ratio Pt_s/Ps_s. Figure A-3 shows the plot of effectivity factor as a function of velocity ratio U_{e_1}/V_s. The curve of Figure A-3 is obtained from knowledge of experimental measurements and is empirical. The curves shown in Figures A-1 and A-2 are plots of equations (A-4) and (A-3), respectively; these curves are constructed for freestream dynamic head q_∞ of 60 psf and freestream total temperature of 500°R. By simultaneous use of equation (A-1) and the curves of Figures A-1, A-2, and A-3, a desired value of the pressure ratio of blown high energy air can be calculated by trial and error such that the required C_μ is equal to the C_μ which is available corresponding to a given pressure ratio Pt_s/Ps_s.

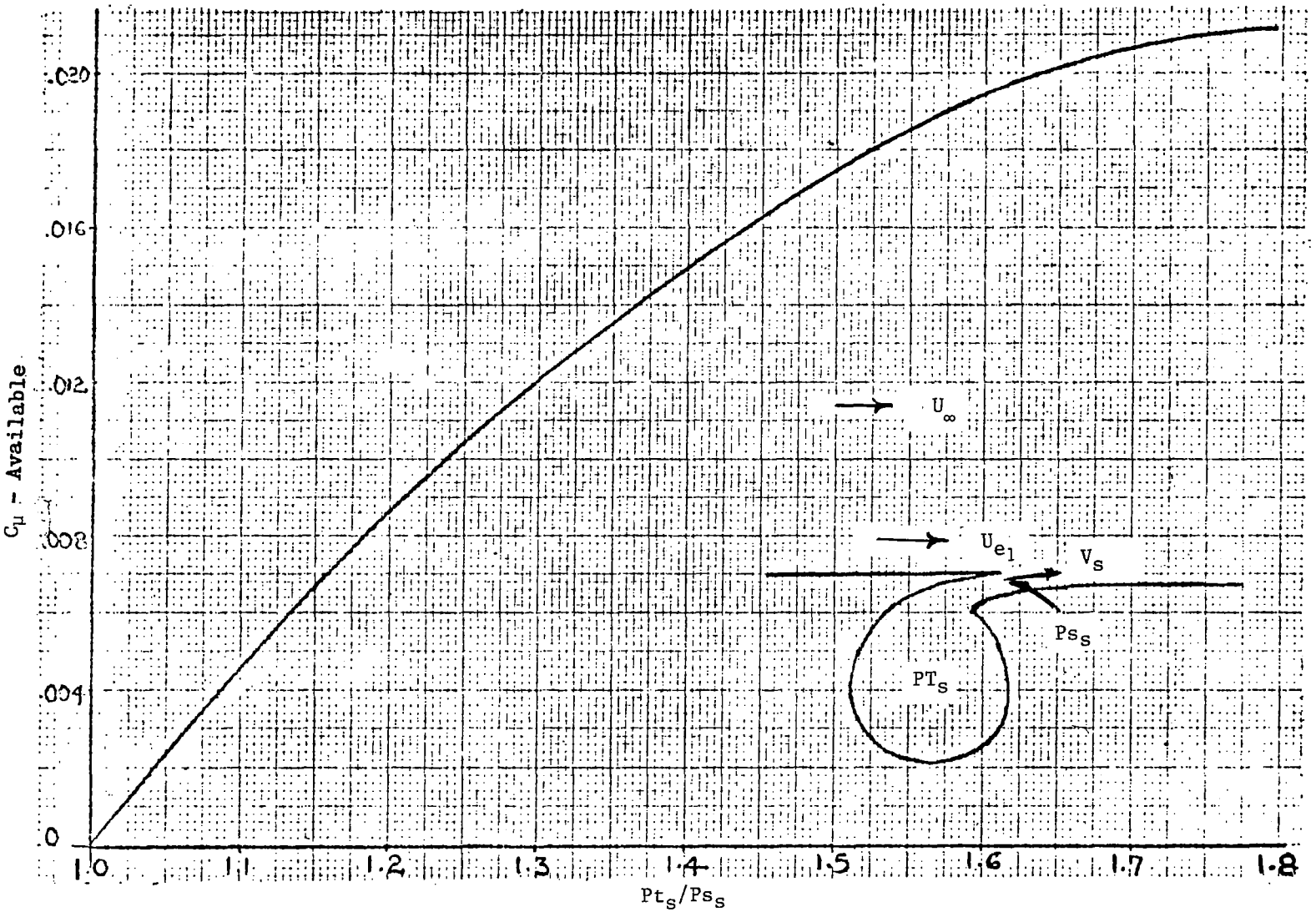

Figure A-1 Wind Tunnel B.L.C. Performance

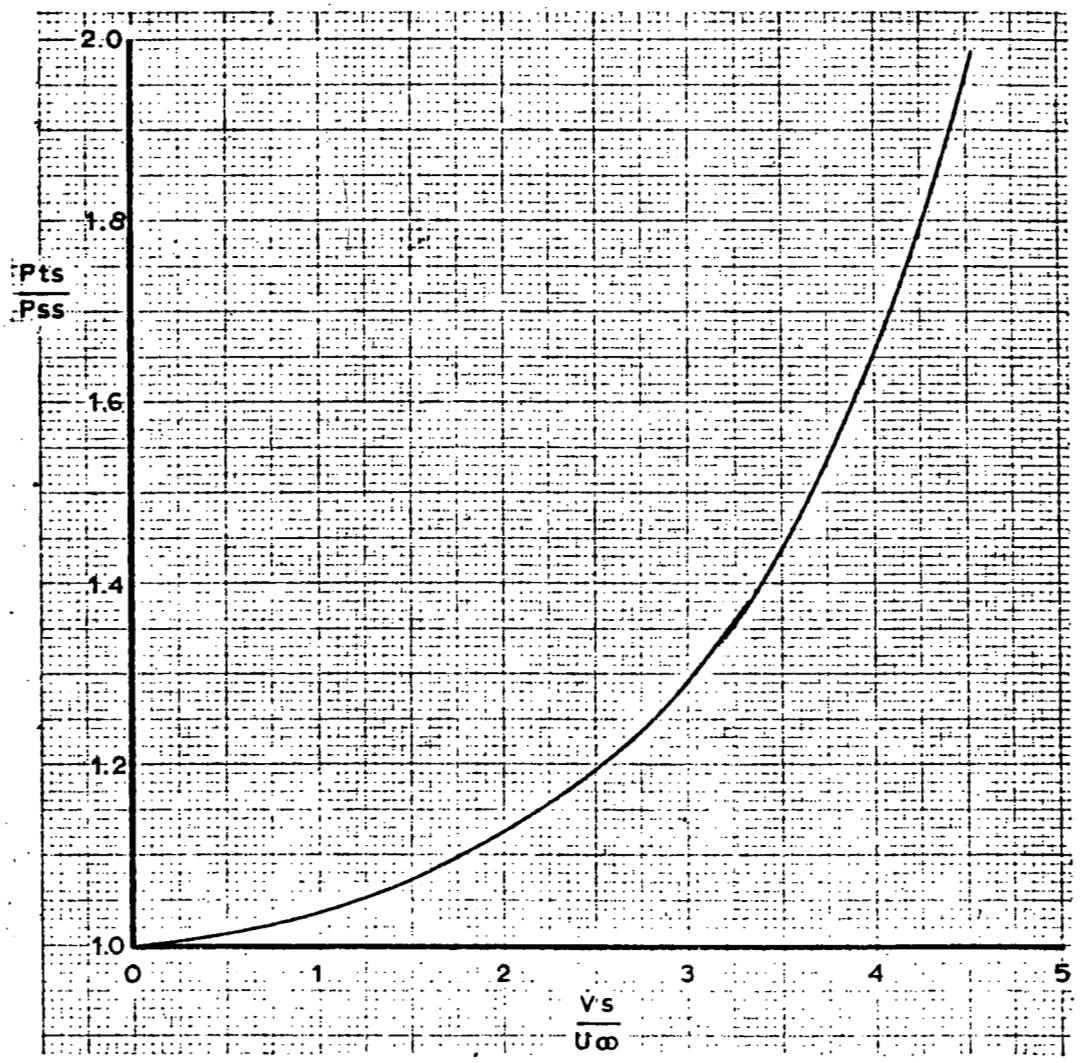

Figure A-2 Velocity Ratio of Blown Air at Slot Exit as a Function of Pressure Ratio

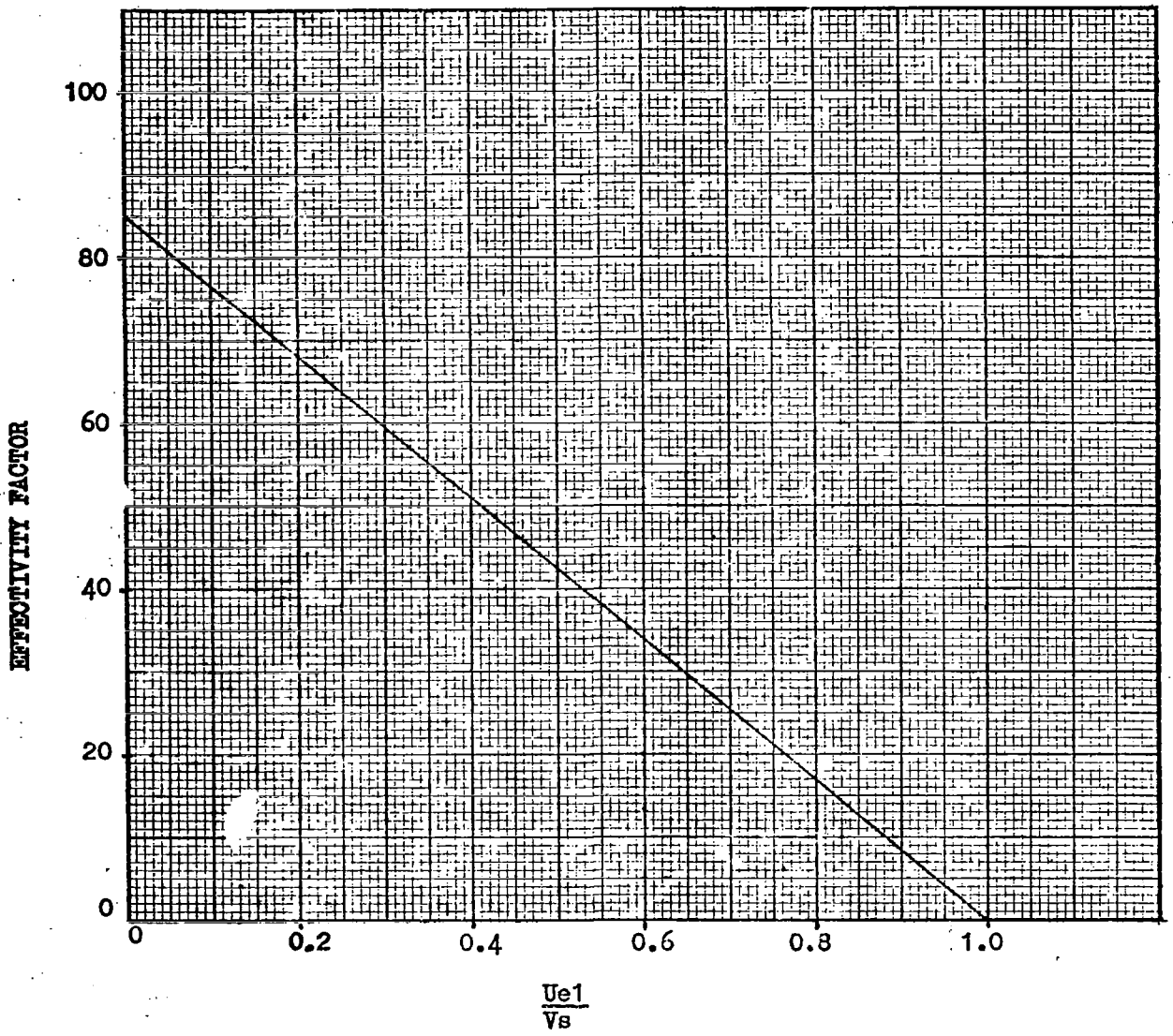

Figure A-3 Effectivity Factor Versus Reciprocal of Velocity Ratio at Exit of Slot of Blowing Plenum

APPENDIX B

ADDITIONAL INSTRUMENTATION

The test section flow conditions and wind tunnel performance data were monitored with conventional instrumentation. Fan speed, clutch current, and tunnel airstream total temperature were displayed on the control console near the speed control potentiometer as shown in Figure B-1. During these tests, atmospheric pressure was measured using a 9-inch diameter Wallace and Tieman absolute pressure gage with reading increments to 0.01 pounds per square inch. Atmospheric pressure was manually input to the data system before each run.

The test section dynamic pressure was set and monitored visually with a 70-inch water manometer connected to pressure orifices located upstream and downstream of the wind tunnel contraction. The manometer reading gave the static pressure drop across the contraction. This reading was related by calibration to the dynamic pressure in the empty test section. The manometer, which is shown in Figure B-2 has provisions for reading the height of the water column to within ±0.001 inch with good repeatability. This manometer was also used to calibrate some of the pressure transducers used during these tests.

The contraction pressures were also read in electrical units using two Statham type PM6TC pressure transducers rated at ±1.0 pound per square inch differential. These transducers can be expected to be accurate to within about 0.5 pounds per square foot in the normal operating range. One transducer was connected to the contraction pressure orifices in parallel with the water manometer and was calibrated versus dynamic pressure in the empty test section. The other was connected to the upstream or high pressure end of the contraction and was calibrated versus test section total pressure. The output of these transducers was transmitted to the data acquisition system for recording and use in data reduction.

The wind tunnel airstream total temperature is measured by a thermistor mounted on a probe in the settling chamber. Temperature information from the probe is displayed on the control console and is transmitted electrically to the data acquisition system. A diagram of the basic wind tunnel instrumentation is shown in Figure B-3.

Static pressures were measured at 41 orifice locations on the model using two Statham model D3-GM scanivalves with two PM-131 pressure transducers. The scanivalves were ganged together and actuated by a single solenoid type stepper. Valve number one contained a transducer rated at 12.5 pounds per square inch and was connected to the orifices on the model upper surface. Valve number two contained a 2.5 pounds per square inch transducer and was connected to the orifices on the lower surface of the model. The output from these transducers was recorded by the data acquisition system for use in computing pressure coefficients, lift coefficients, and local velocities. Figure B-4 shows the scanivalve installation.

Total pressure in the boundary layer control plenums was calibrated versus the pressure in the auxiliary air supply duct between the plenums and the control

valve. The supply duct pressure was displayed on an ordinary 0 to 100 pounds per square inch pressure gage mounted on the control console as shown in Figure B-1.

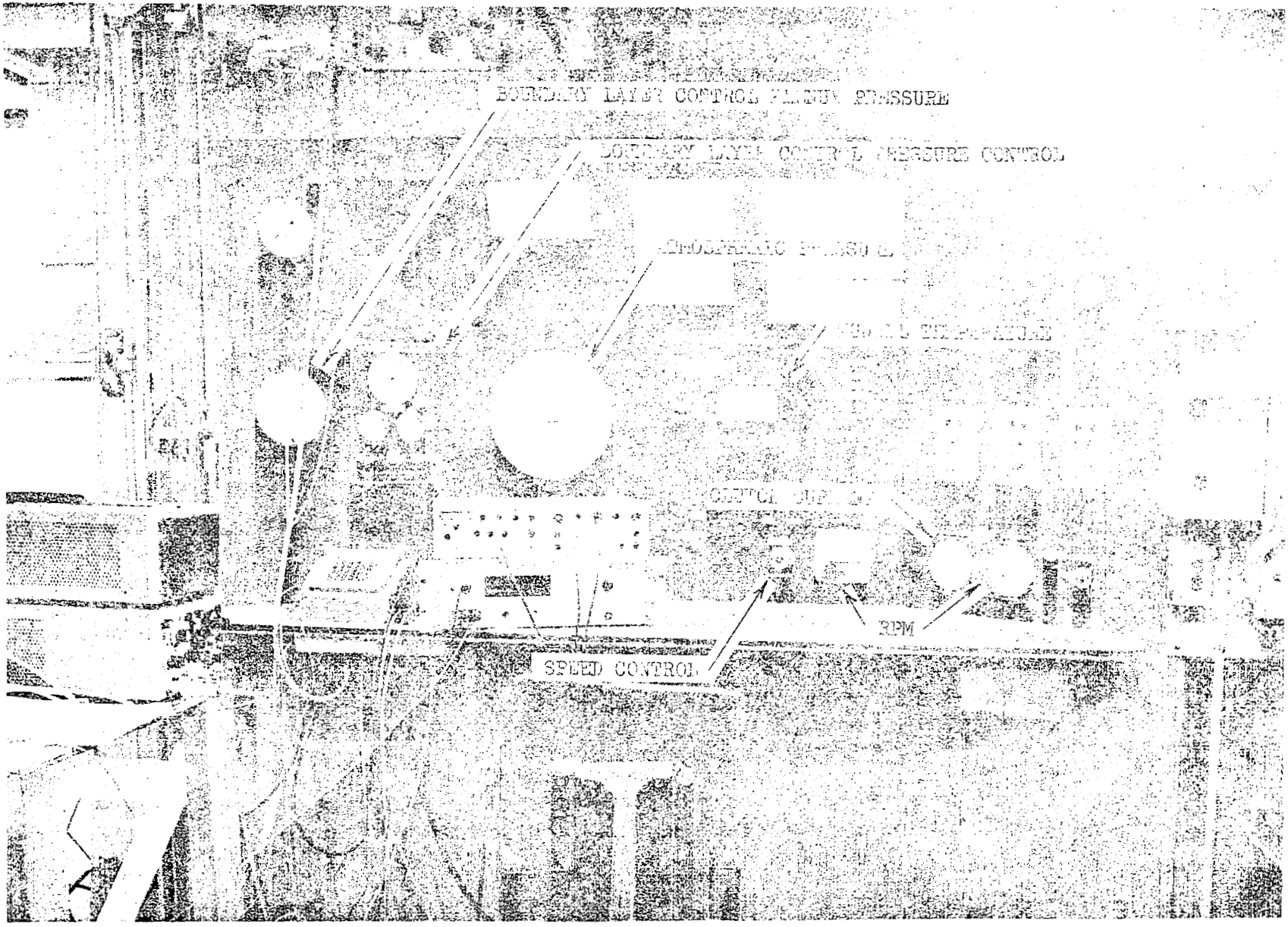

Figure B-1 Wind Tunnel Control Console

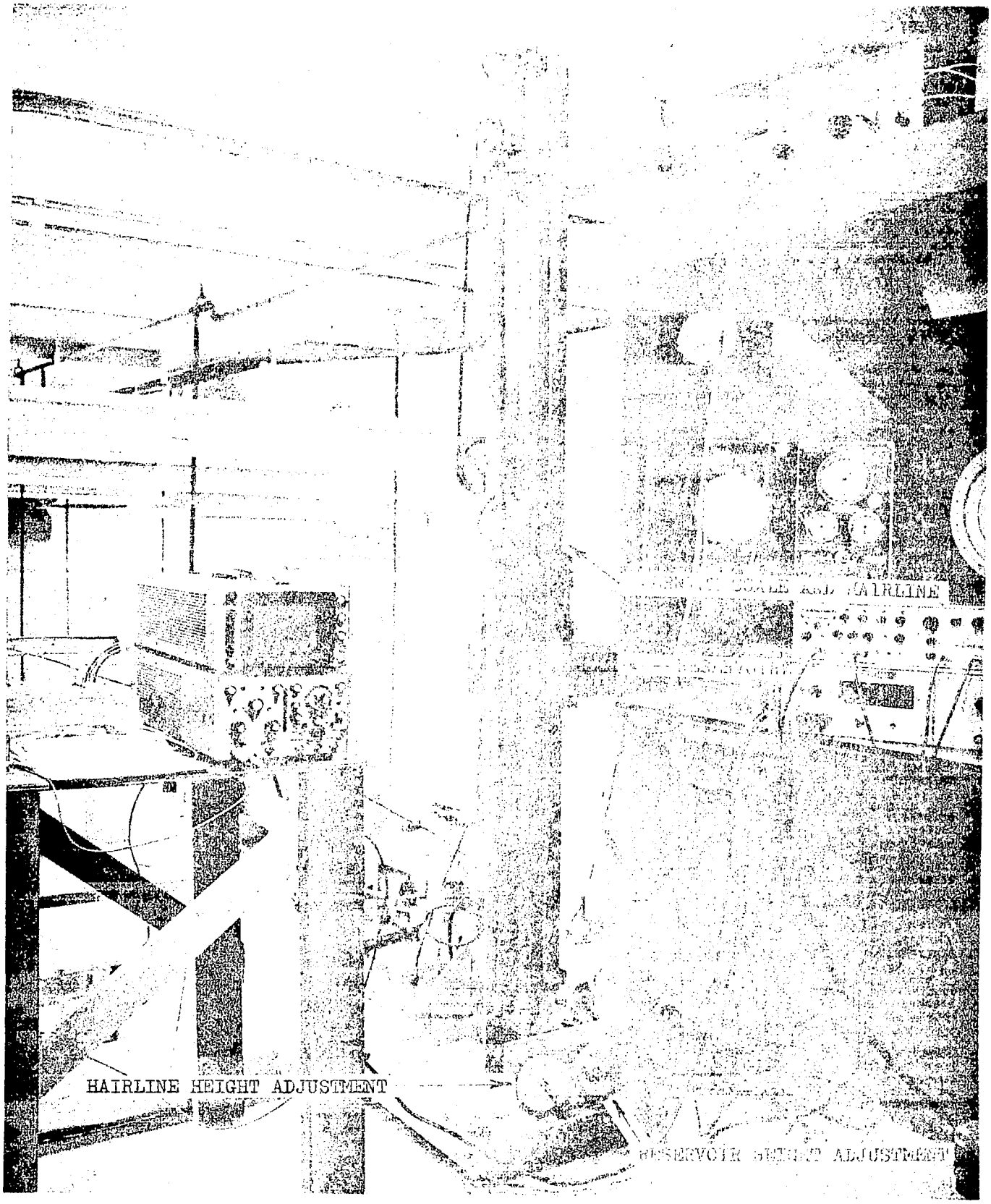

Figure B-2 70-Inch Water Manometer

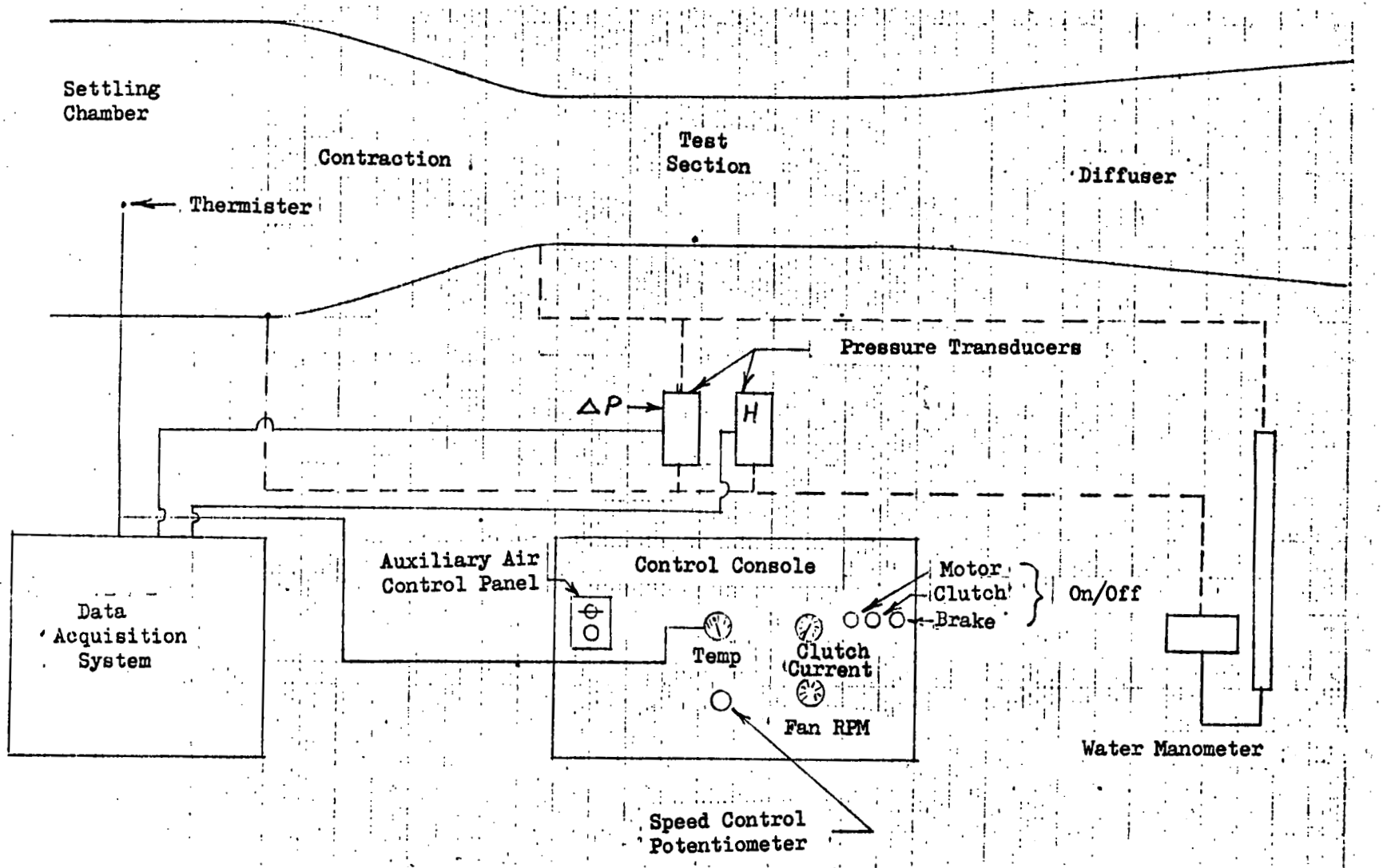

Figure B-3 Wind Tunnel Instrumentation Diagram

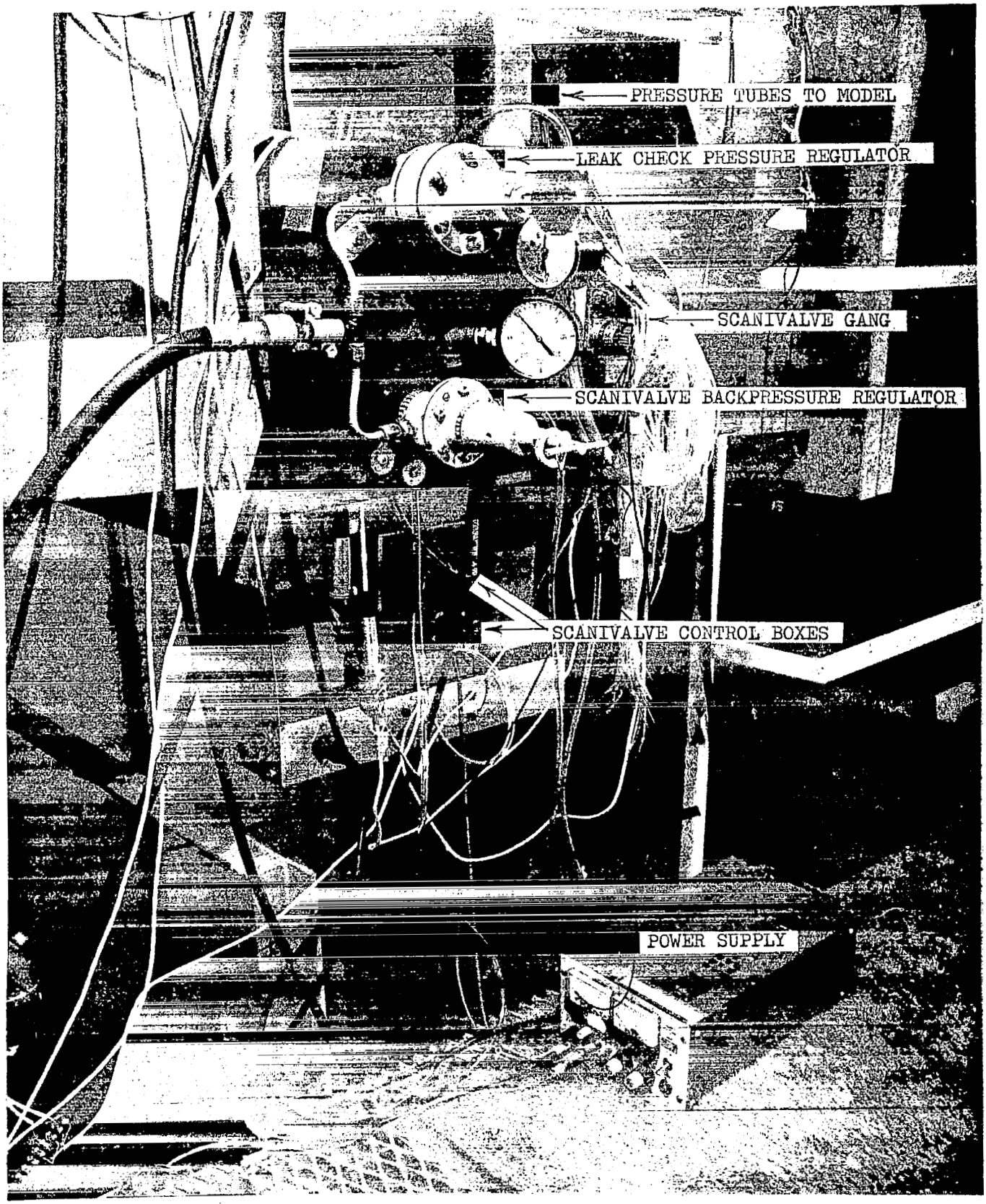

Figure B-4 Scanivalve Installation

APPENDIX C

DATA ACQUISITION SYSTEM

General Description

The data processing system utilized for this contract was set up for two specific purposes, these being the measurement of the static pressure distribution on the surface of the model and the measurement of the velocity profiles within the boundary layer and wake of the model. The measurements were made using a Data Acquisition Unit (D.A.U.) which was controlled by a real-time digital computer which activated scanivalve units for obtaining the static pressure distribution and traversed a pressure or hot wire anemometer probe for the velocity profiles.

The system used for acquiring and reducing the test data is shown in Figure C-1. The heart of the system is a Lockheed Electronics MAC 16 computer. The raw data was made available, in an abbreviated form, on a teletype for on-line monitoring of the test, and in its entirety on paper tape using a high speed punch. Final data reduction was accomplished on a UNIVAC 1106 Central Computing System with remote access terminals.

An additional MAC 16 computer was used in an executive mode to permit time sharing of the main computer. The disc storage associated with this computer was intended to provide the basis of an on-line data reduction capability in conjunction with a UNIVAC 418. During this contract, however, the immediate availability of the remote access terminals made the on-line capability unnecessary.

The Data Acquisition Unit

The data acquisition unit incorporated an analog multiplexer for transmission of measured data and a digital multiplexer for transmission of thumb-wheel switch inputs. One additional analog channel was provided for probe position measurement.

A rotary switch permitted any of the measured data to be monitored on a digital voltmeter during the test. Variable gain amplifiers in all of the analog channels enabled gain levels to be selected that approximated the raw data to engineering units for ease of monitoring of the digital voltmeter and on-line teletype output.

The tunnel conditions of 'q', 'H' and temperature were acquired at each scanivalve position during the static pressure distribution and at each probe position during the boundary layer survey. The thumb-wheel switch inputs included a probe option for choice of no probe, pressure probe or anemometer probe and also a selection of the number of scanivalves and ports to be cycled through the static pressure distribution. Any selection below the maximum

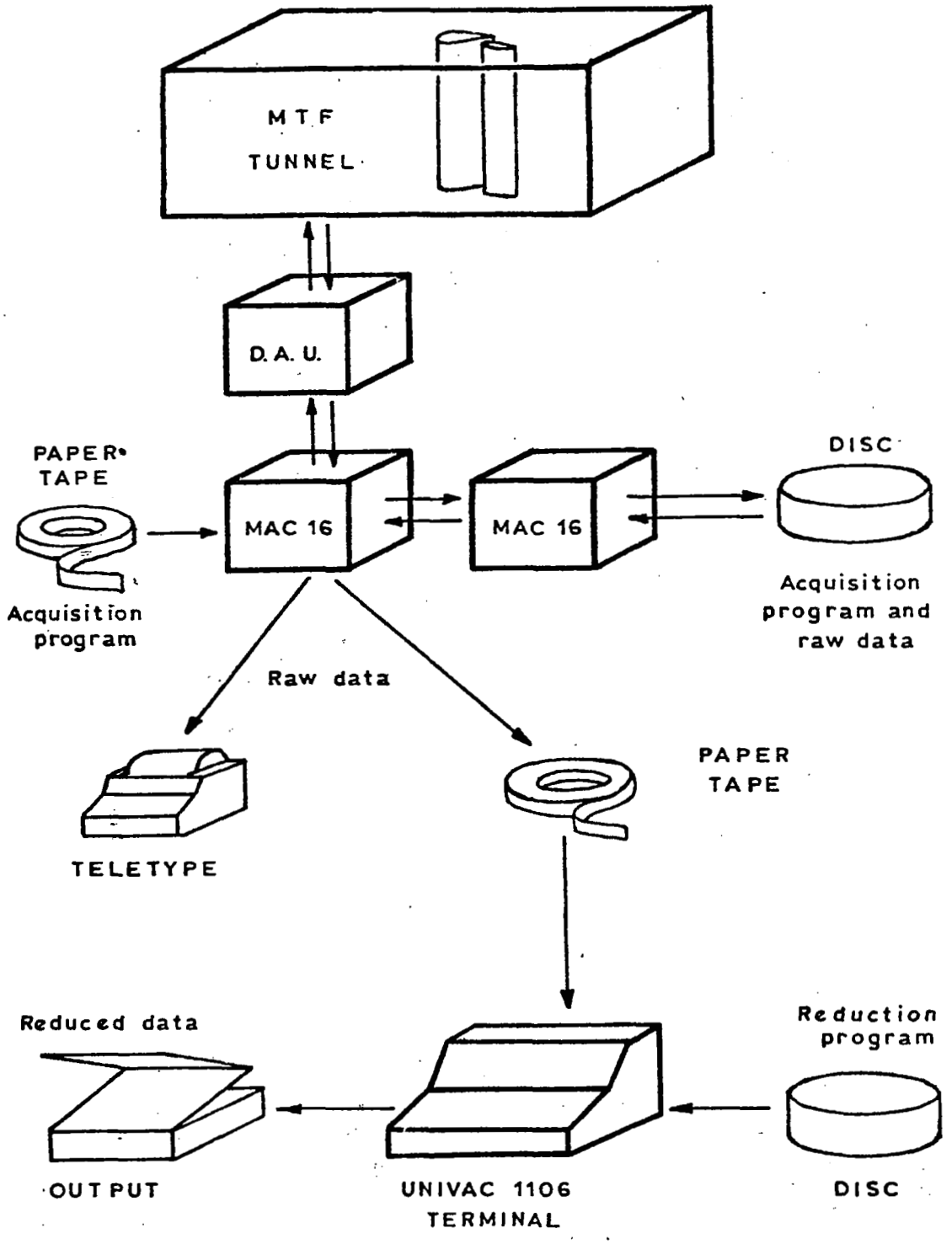

Figure C-1 The Data Acquisition and Reduction System

required (2 scanivalves and 36 ports) inhibited printout of the pressure data during reduction with significant saving in reduction time. This option was exercised when a series of velocity surveys were made with no change of basic configuration, and hence pressure survey, in which case the minimum number of ports was selected that would include the static pressure port at the chordwise location of the velocity survey.

Control of the data acquisition was achieved with one analog channel which activated the probe positioning servo mechanism and one digital channel which stepped and homed the scanivalves and controlled the multiplexing.

*U.S. GOVERNMENT PRINTING OFFICE: 1975 - 635-053/91